Turbostratic Carbon Powder

FINAL REPORT

Reporting Period
September 10, 2003 to July 30, 2004

Report Prepared by
John W. Zondlo
Department of Chemical Engineering
College of Engineering and Mineral Resources
P.O. Box 6102

Report Issued
July 31, 2004

Subcontract No.: 2566-WVU-DOE-0350

Other Contributors

Abha Saddawi, Peter Stansberry and Elliot Kennel
Department of Chemical Engineering
College of Engineering and Mineral Resources
P.O. Box 6102
West Virginia University
Morgantown, WV 26506-6102

DISCLAIMER

Abstract

Fine particulate carbon was created by grinding Solvent Extracted Carbon Ore (SECO), lightly oxidizing it, and heat treating it to various temperatures to produce a dense micropowder. Eight SECO samples were prepared and analyzed via proximate (dry) and elemental analyses, as well as with XRD and SEM. The electrical resistivity of some of the samples was also assessed. Dr. Cooper's group at Lawrence Livermore National Laboratory (LLNL), as well as Dr. Steven Chuang's group at the Department of Chemical Engineering, University of Akron, Akron, OH, were supplied with these SECO samples for testing in their Direct Carbon Fuel Cells (DCFC). It was found that heat-treated samples demonstrated a continuous increase in carbon, and a decrease in volatile matter, nitrogen, hydrogen and sulfur as the heat-treated temperature was raised. The oxygen content jumped significantly following oxidation, and then decreased dramatically upon heat treatment. XRD results indicated some degree of order in the structure of these heat-treated SECO samples, where a higher degree of order was observed for the samples heated at higher temperatures. Carbon foams consisting of coal tar pitch (CTP) combined with one of the oxidized SECO samples were made and assessed for their properties. The SECO/CTP foam sample showed properties consistent with other similar foam samples. The SECO heat-treated to 800 °C and above proved to be a more conductive carbon for use in the fuel cell, and showed favorable performance in LLNL's fuel cell. The University of Akron also reported favorable results for the oxidized SECO. The low ash, low sulfur, and highly conductive character of these samples makes them very attractive for application in the direct carbon fuel cell.

TABLE OF CONTENTS

LIST OF TABLES

LIST OF FIGURES

Executive Summary

This program is focused on the production of a low cost coal-derived turbostratic carbon powder for structural and other applications, and investigates the suitability of such a material for use in a carbon fuel cell, such as that which has been demonstrated by Lawrence Livermore National Laboratory (LLNL). The Direct Carbon Conversion (DCC) process, pioneered by a LLNL team led by Dr. John Cooper, employs a unique fuel cell to produce electric power. The overall cell reaction is combustion of carbon with oxygen (from ambient air) forming carbon dioxide and electricity. Cooper's results at LLNL suggest that the ideal carbon feed for a carbon fuel cell should be a turbostratic carbon with microscopic domain size of 30 nm or smaller, with an ash value less than 0.5%, low VM, a sulfur level between 0.25% to 1.0%, low graphitization, and high electrical conductivity.

Solvent-extracted carbon ore (SECO) was initially suggested due to its low ash and sulfur content, as well as its presumed high friability enabling the production via grinding of extremely small particles. Fine particulate carbon was created by grinding Pilot Plant and lab-scale SECO, where the lab-scale SECO was lightly oxidized and coked to 400 °C, 600 °C 800 °C, 1000 °C, to produce a dense micropowder. The SECO samples were analyzed via proximate (dry) and elemental analyses, as well as with XRD and SEM. The electrical resistivity of some of the samples was also assessed. For testing purposes, Dr. Cooper's group was supplied with these SECO samples as well as cokes prepared from condensed byproducts from other CPCPC projects. Dr. Steven Chuang's group at the Department of Chemical Engineering, University of Akron, Akron, OH, is

also working on the development of a carbon fuel cell and collaborated in evaluating the SECO samples produced by WVU.

Additionally, carbon foams consisting of coal tar pitch (CTP) combined with one of the oxidized SECO samples were made and assessed for their properties. The SECO/CTP foam sample was successfully created and showed properties consistent with other similar foam samples with a crush test value of 12.3 MPa.

WVU Coal Extraction Pilot Plant SECO samples SECO-4 and SECO-6/7 were found to be low in ash and sulfur. However, both samples had a large VM content (~40%) and difficulties were encountered during testing in the fuel cell. Thus, the lab-scale SECO batch was made, where heat treatment resulted in a dramatic decrease of volatile matter. Heat-treated samples also demonstrate a continuous increase in carbon, and a decrease in nitrogen, hydrogen and sulfur. The XRD results show some degree of order in the structure, and data indicate higher order for the samples heated at higher temperatures. All the samples thus produced have domain sizes less than 30 nm, indicating turbostratic carbon. No unusual surface effects due to heat-treatment are evident in the SEM images of the SECO. Resistivity measurements indicated that the higher the heat-treatment temperature, the lower the resistivity of the SECO becomes. Thus, the 800°C or above heat-treated SECO proved to be a more conductive carbon for use in the fuel cell, and showed favorable performance in LLNL's fuel cell. The University of Akron also reported favorable results for the oxidized SECO.

Introduction

This program is focused on the production of a low cost coal-derived turbostratic carbon powder for structural and other applications. This material will differ from carbon black in that it will be a turbostratic carbon with low surface area, as opposed to carbon black, which is usually a high surface area amorphous material. The turbostratic carbon powder, when combined with an appropriate binder pitch, can be used as part of a carbon composite manufacturing process. In addition, such a material can be suitable for use in a carbon fuel cell, such as that which has been demonstrated by Lawrence Livermore National Laboratory (LLNL). The Direct Carbon Conversion (DCC) process, pioneered by a LLNL team led by Dr. John Cooper, employs a unique fuel cell to produce electric power. The overall cell reaction is combustion of carbon with oxygen (from ambient air) forming carbon dioxide and electricity. A schematic diagram of the direct carbon fuel cell concept is shown in Figure 1.

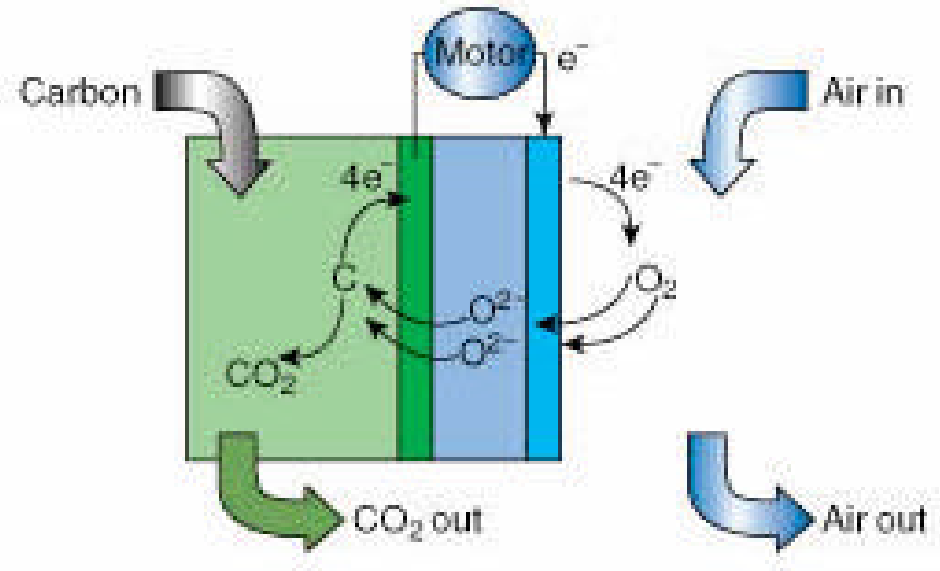

Figure 1. Direct Carbon Conversion Concept (by LLNL)

The reactions involved in this process are as follows[1]:

$C + 2CO_3^{2-} = 3CO_2 + 4e^-$	Anode
$O_2 + 2CO_2 + 4 e^- = 2CO_3^{2-}$	Cathode
$C + O_2 = CO_2$	Overall Reaction
	?G ~32.8 MJ/kg;
	E = 1.02 V at T=800 °C

LLNL results to date have shown that the fuel cell reaction yields 80 percent of the carbon-oxygen combustion energy as electricity[1]. It provides up to 1 kilowatt of power per square meter of cell surface area, which is comparable to other electrochemical systems. Laboratory cells tested at LLNL consist of a nickel anode current collector, a ceramic matrix for containing the molten electrolyte, a nickel screen for reacting the oxygen from the air, and a thermocouple (see Figure 2). The solid carbon fuel is fed as a fine powder to the cell. Currently the cell is operated in the batch mode but continuous operation is possible.

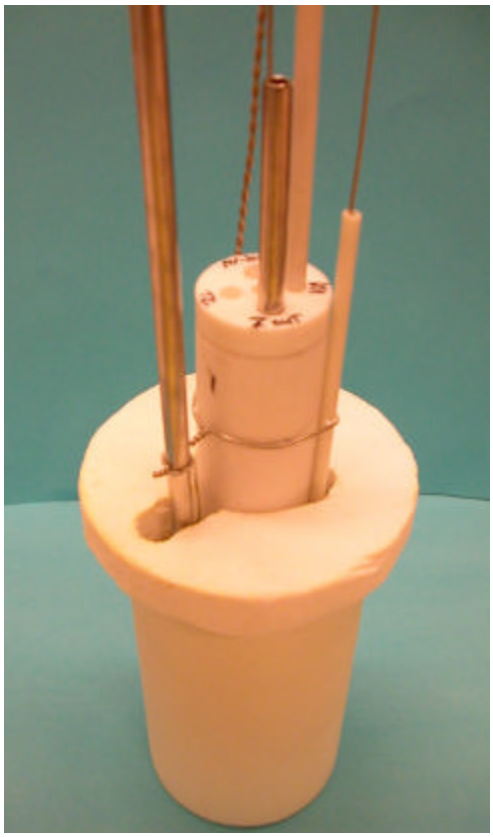

Figure 2. LLNL Fuel Cell (1.8cm^2)

Cooper's results at LLNL suggest that the ideal carbon feed for a carbon fuel cell should be a turbostratic carbon with microscopic domain size of 30 nm or smaller.[1] It also must have an ash value less than 0.5% to prevent excessive contamination of the molten salt electrolyte. Ranging degrees of volatile matter (VM) are of interest, but low VM is preferred. The sulfur level should be between 0.25% to 1.0% so that the metal electrodes are not chemically attacked and degraded excessively. Cooper's results also indicate that the electrochemical performance of the carbon improves with less graphitization as that increases reactivity of the carbon to oxidation. Performance is also enhanced with carbon of increased electrical conductivity which improves performance due to enhanced charge transport.[1]

In this project, the use of solvent-extracted carbon ore (SECO) was evaluated as a feedstock for the direct carbon fuel cell. The SECO was initially suggested due to its low ash and sulfur content, as well as its presumed high friability enabling the production via grinding of extremely small particles. Fine particulate carbon was created by grinding SECO, lightly oxidizing it, and heat-treating it to produce a dense micropowder. Eight SECO samples were prepared and analyzed via proximate (dry) and elemental analyses, as well as with XRD and SEM. The electrical resistivity of some of the samples was also assessed. For testing purposes, Dr. Cooper's group was supplied with these SECO samples as well as cokes prepared from condensed byproducts from other CPCPC projects. Dr. Steven Chuang's group at the Department of Chemical Engineering, University of Akron, Akron, OH, is also working on the development of a carbon fuel cell and collaborated in evaluating the SECO samples produced by WVU.

Additionally, carbon foams consisting of coal tar pitch (CTP) combined with one of the oxidized, heat-treated SECO samples were made and assessed for their properties.

Experimental

A reconfiguration of the Coal Extraction Pilot Plant at West Virginia University was completed in the Fall of 2003. Figure 3 shows an overall view of the pilot plant as it currently is configured. In a typical extraction run, approximately 30 pounds of SECO can be produced.

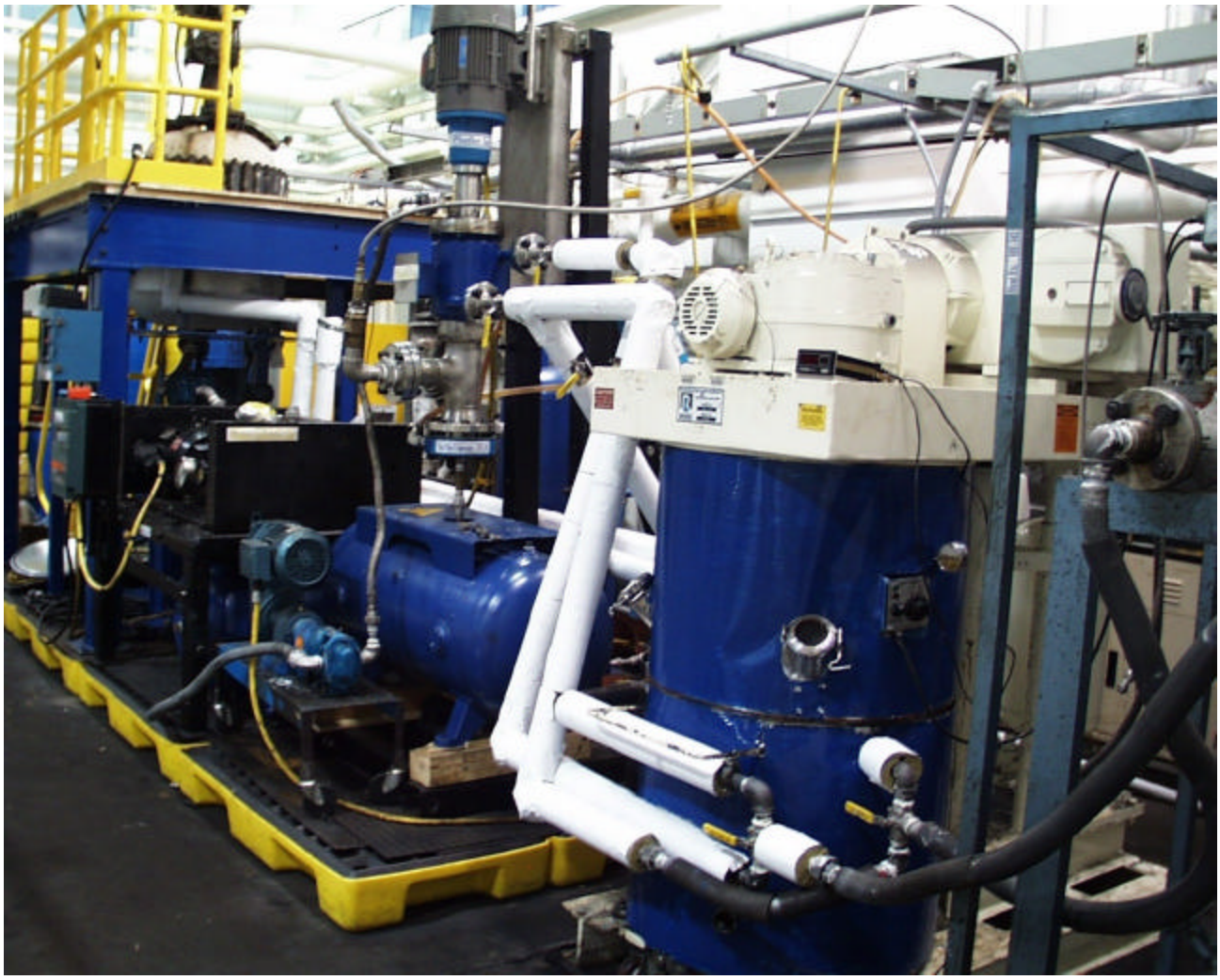

Figure 3. Solvent Extraction Pilot Plant Facility at WVU

Samples from two runs at the pilot plant, SECO-4 and SECO-6/7, were obtained for use in this project. These SECO samples were produced from a raw Kingwood coal

mined in Preston Co., WV. The proximate and elemental analyses for the raw coal are shown in Table 1. The SECO samples were ground to ~200 mesh and were also characterized via proximate and elemental analysis. Results of these tests are shown in Table 1 as well.

Table 1. Proximate and Elemental Analysis Results of raw Kingwood Coal and SECO samples 4, 6/7 made in the WVU Pilot Plant

a) Proximate:	Moisture (wt %)	Volatile Matter (wt %)	Fixed Carbon (wt %)	Ash (wt %)
Raw Kingwood Coal	6.86	30.07	55.03	8.04
SECO-4	0.66	36.73	62.11	0.50
SECO-6/7	2.10	40.60	56.79	0.51
b) Elemental Composition:	C	N	H	S
Raw Kingwood Coal	77.44	1.18	4.95	1.58
SECO-4	83.36	2.78	5.73	0.62
SECO-6/7	80.01	3.86	6.04	0.54

As can be seen from the analysis, these two SECO samples are similar in composition. It should also be noted that the samples are very low in ash and contain only 0.5% sulfur, a considerable reduction from the ash and sulfur in the raw coal. Roughly 30 grams of SECO-4, 6/7 were sent to LLNL for testing and evaluation.

For more efficient operation of the direct carbon fuel cell, it is advantageous to grind the SECO to the micron range. To this end, an ultra sonic grinder (Ultrasonic Processor for Industrial Application, Model UIP2000) was obtained and tested for this purpose. The device was found to reduce the size of smaller particles to about 3 microns. However it was ineffective at reducing large particles of SECO. Thus, conventional grinding, via the ball mill, was still necessary. Figure 4 shows an electronmicrograph of

SECO ground using conventional ball milling equipment. It can be seen that particle sizes on the order of 1µm can easily be obtained.

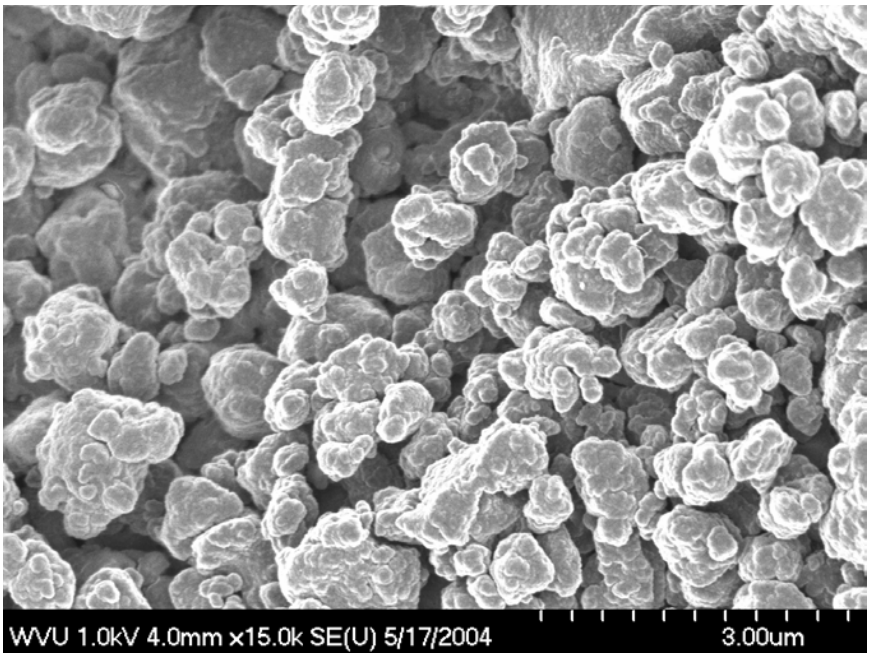

Figure 4. SEM image of ground SECO using a conventional ball mill

Feedback from Dr. Cooper indicated that the high volatile matter content (~40%) created difficulties in testing and determining accurate cell efficiency since some of the fuel left the cell as unburned volatiles. To rectify this problem, another batch of SECO from the same coal was prepared on the lab scale.[2] A block flow-sheet of the process is shown as Figure 5.

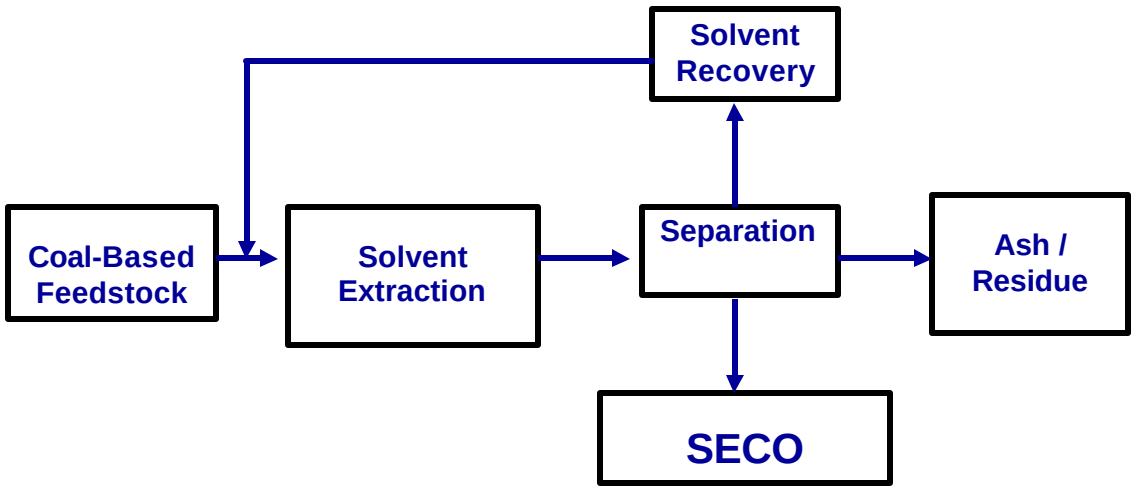

Figure 5. Flowchart of the solvent extraction process for SECO

Kingwood Coal, first air-dried for two days, was ground and vacuum-dried overnight at about 120°C. N-methyl pyrrolidone (NMP) was heated to about 200 °C after which coal was mixed in a ten-to-one solvent-to-coal ratio (10mL of NMP = 1g of coal) while being continuously stirred under nitrogen. This solution was left to reflux for 30 minutes. Following extraction, the solution was cooled and vacuum-filtered. Final evaporation of the NMP in a rotary evaporator precipitated the desired SECO as a solid product.

The resultant SECO was then heat-treated to varying temperatures to drive off some of the volatile matter. However, upon heat-treatment, the raw SECO was found to foam violently and boil out of the vessel. To prevent this, the sample was first partially oxidized at 250 °C for 4 hours in air so that cross-linking could be effected. Following oxidation, the sample was again heat treated, this time with no foaming noted. Four different levels of heat treatment were performed: 4 hours each at 400 °C, 600 °C, 800 °C, 1000°C in an inert atmosphere. These samples were then subjected to elemental and proximate analysis along with evaluation by x-ray diffraction (XRD) and SEM.

The electrical resistivity of the compacted heat treated SECO powders was also assessed by placing the powder in a nonconductive piston/cylinder assembly with electrodes on each end. Figure 6 shows photographs of the resistivity cell.

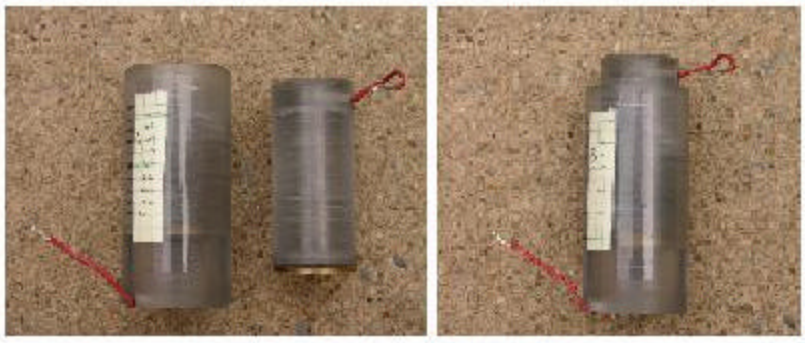

Figure 6. Electrical resistivity cell (WVU)

The resistance measurements were made by placing a known amount of sample in the cell. Electrical contact was made with the sample by means of two polished brass discs placed on either side of the sample bed. The diameter and the height (i.e. distance between the electrodes) of the sample bed was measured. A Keithley Model 2700 DVM was connected to the electrodes and resistance measurements were made as various amounts of weight were placed on the piston so that the powders could be compacted. The weight was increased until no further change in resistance was noted. Unfortunately, for highly conductive powders (like graphite and heat-treated SECO), the lower limit of the ohm meter was reached and further measurements were not possible. Hence reliable data were obtained only for the SECO samples heated to 600 °C and 800 °C. The 1000 °C sample had a resistivity too low for accurate measurement.

Three additional coke samples were prepared by Dr. Stansberry from a related CPCPC project. These samples were cokes made from the by-product coal liquids driven off during preparation of hydrogenated coal extracts. During processing, one of the steps

is a partial distillation to raise the softening point of the desired product. This step produces a volatile stream of by-product hydrocarbons which when coked produces a low-sulfur, low-ash carbon. These recovered liquids were then coked at a rate of 3 °C per minute pausing at 300 °C for 2 hours and then raised the temperature at the same rate to 700 °C. This temperature was held for 2 hours before cooling to room temperature. The entire operation was performed in a covered crucible which was itself immersed in coke breeze to prevent burning. These samples were sent to LLNL. Samples were also sent to Dr. Chuang's group at the University of Akron.

A calcined carbon foam was produced from one of the previously mentioned SECO samples and tested for density, porosity and crush strength. The SECO powder that was oxidized and heat treated to 800 °C was ground to less than 200 mesh and mixed with CTP, which was also ground to under 200 mesh, in a ratio of seven parts coke to 3 parts CTP. The mixed powder was then put into a mold and heated under nitrogen to 500 °C at a rate of 5 °C per minute for 5 hours. Then the sample was calcined at 1000 °C for 5 hours. For comparison, a similar sample was made of only CTP without the addition of the coke. It was heat treated by the identical protocol.

Results and Discussion

Elemental and proximate analyses of the raw coal used in this project, Kingwood coal mined in Preston Co., WV, and WVU Coal Extraction Pilot Plant SECO samples SECO-4 and SECO-6/7 are listed in Table 1. Both SECO samples were low in ash and sulfur. However, due to the samples' large VM content (~40%), difficulties during the testing of the DCFC were experienced and an accurate determination of the cell efficiency was not possible since some of the fuel left the cell as unburned volatiles.

With the goal of decreasing VM and ash content, another lab-scale SECO batch was made (also from Kingwood Coal).[2] To prevent foaming during heat treatment, the samples were first partially oxidized at 250°C for 4 hours in air so that cross-linking could be effected. Following oxidation, the samples were again heat treated, this time with no foaming noted. Four different levels of heat treatment were performed: 4 hours each at 400 °C, 600 °C, 800 °C, and 1000 ºC in an inert atmosphere. The extract and oxidized heat-treated samples were subjected to elemental and proximate analysis. These results are shown in Table 2.

Table 2. Proximate (Dry) and Elemental Analysis of Raw and Heat-Treated SECO (Kingwood) made in the laboratory

Proximate Analysis			VM wt%	FC wt%	Ash wt%
Kingwood Coal			33	58	8.92
SECO Extract			32	67.82	0.18
Oxidized SECO Extract			32.17	67.54	0.29
Oxidized SECO, HT 400°C			28.87	70.90	0.24
Oxidized SECO, HT 600°C			9.05	90.66	0.29
Oxidized SECO, HT 800°C			3.84	95.90	0.27
Oxidized SECO, HT 1000°C			1.78	97.82	0.40
Elemental Analysis	**C**	**N**	**H**	**S**	**O**
Kingwood Coal	77.44	1.18	4.95	1.58	ND
SECO Extract	85.80	1.78	5.83	0.64	3.91
Oxidized SECO Extract	75.50	1.90	3.77	0.65	11.70
Oxidized SECO, HT 400°C	80.37	1.88	3.50	0.64	8.60
Oxidized SECO, HT 600°C	84.24	1.69	2.19	0.61	2.52
Oxidized SECO, HT 800°C	88.75	1.35	0.80	0.56	1.51
Oxidized SECO, HT 1000°C	91.00	1.48	0.34	0.44	ND

Table 3. XRD Analysis of Bench Samples

Sample	2? (002)	2 ? (110)	d(002) (nm)	d(110) (nm)	La (nm)	Lc (nm)
Raw SECO	22.9	81.43	0.3884	0.11819	2.4151	1.126
Ox/SECO	23.21	81.4	0.3832	0.11822	2.7072	1.0678
Ox/SECO 400°C	23.79	81.24	0.374	0.11842	2.3795	1.4925
Ox/SECO 600°C	23.94	81.45	0.3717	0.11816	2.7219	1.832
Ox/SECO 800°C	24.08	79.34	0.3696	0.12077	3.3361	2.2706
Ox/SECO 1000°C	ND	ND	ND	ND	ND	ND
Graphite Sample	26.33	73.83	0.3385	0.12835	27.851	45.118

XRD results can be seen in Table 3 and Figure 7, and a typical SEM image is show in Figure 8.

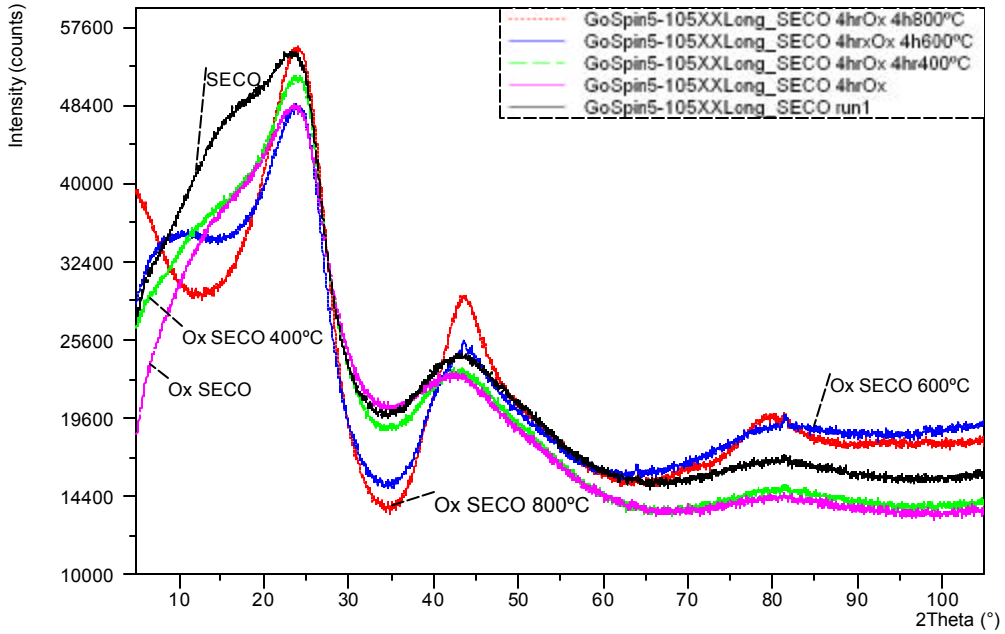

Figure 7. XRD analysis of bench samples

One may note, from the proximate analysis, the heat treatment results in a dramatic decrease in volatile matter. Heat-treated samples also demonstrate a continuous increase in carbon, and a decrease in nitrogen, hydrogen and sulfur. The oxygen content jumps significantly following oxidation, as is expected, and then decreases dramatically upon heat treatment. The XRD results show that the d (002) spacing consistently decreases upon heating to higher temperatures indicating some degree of order in the structure. In addition, the crystallographic domain sizes Lc and La increase steadily as a result of heat treatment. For reference, a sample of graphite was also tested in the XRD for comparison. These data indicate higher order for the samples heated at higher temperature. As can be seen, all the carbons thus produced have domain sizes less than 30 nm, indicating turbostratic, carbons.[4,5]

From the SEM image for the SECO treated at 800 °C, shown as Figure 8, one may see that any unusual effect of heat-treatment is not evident on the surface. The

image resembles that of a friable glassy carbon, and is representative of the other images taken of the Oxidized SECO samples treated at different temperatures.

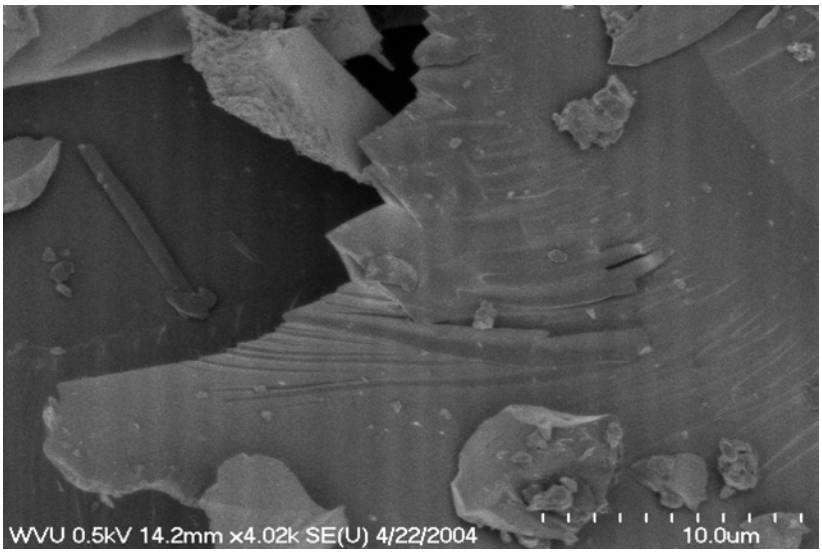

Figure 8. SEM image of oxidized SECO coked to 800 ºC

The electrical resistivity of the compacted heat treated SECO powders was assessed by placing the powder in a nonconductive piston with electrodes on each end. The resistivity was measured with respect to packing weight loaded on top of the piston. The results are listed in Table 4, as well as in Figures 9 and 10. From the results listed in Table 4, one can clearly see that the higher the heat-treatment temperature, the lower the resistivity of the SECO becomes. Thus the 800 °C sample represents one with low VM and resistivity and should perform well in the carbon fuel cell.

Table 4. Electrical Resistivity Measurements of some heat treated SECO samples

Sample Name	Resistivity (Ocm)
Oxidized, Heat-Treated to 400 °C SECO	Too high for accurate measurement
Oxidized, Heat-Treated to 600 °C SECO	$6.1 X10^{6}$
Oxidized, Heat-Treated to 800 °C SECO	29
Oxidized, Heat-Treated to 1000 °C SECO	Too low for accurate measurement

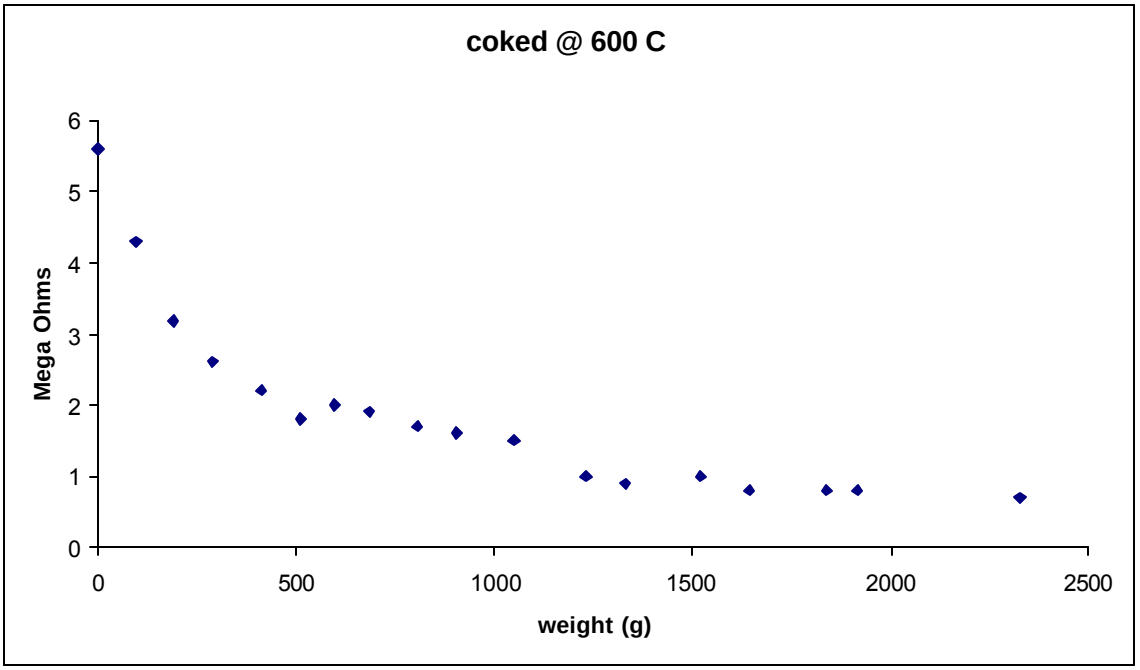

Figure 9. Electrical resistance measurements versus weight loading for Oxidized SECO heat treated to 600 °C

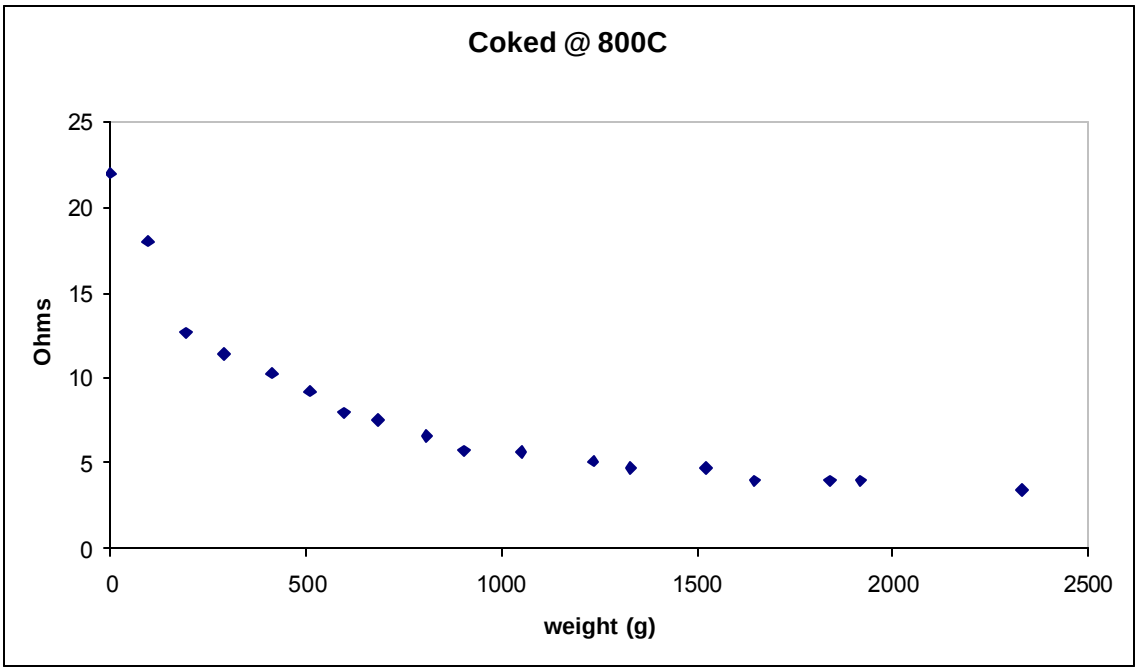

Figure 10. Electrical resistance measurements versus weight loading for Oxidized SECO heat treated to 800 °C

Dr. Cooper's group at LLNL was only able to test two of the samples sent to them by WVU. These two samples were the Oxidized, 400 °C heat-treated SECO and the oxidized, 800°C heat-treated SECO. In the case of the 400°C fuel, the cell voltage was reported to be poor due to sulfur interference with the cathode activation. However, the 800°C sample showed very favorable performance. These results are shown in Figures 11 and 12.

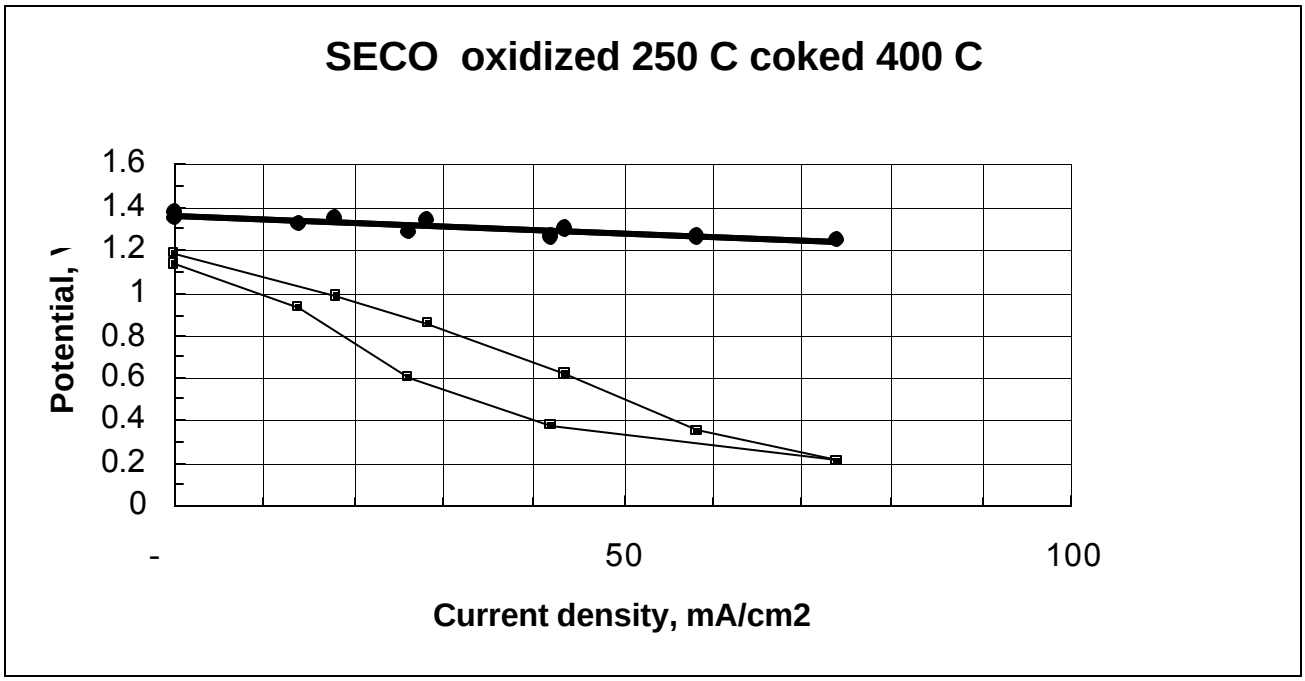

Figure 11. Polarization of Coked Solvent-Derived Sample
In this cell, we attempted to activate cathode in presence of C. The polarization of the carbon (upper trace) was favorable

Vcarbon ° Ecarbon - Eref (Au/ 5/7 air, 2/7 CO2)

Cell voltage was poor because S interfered with cathode activation

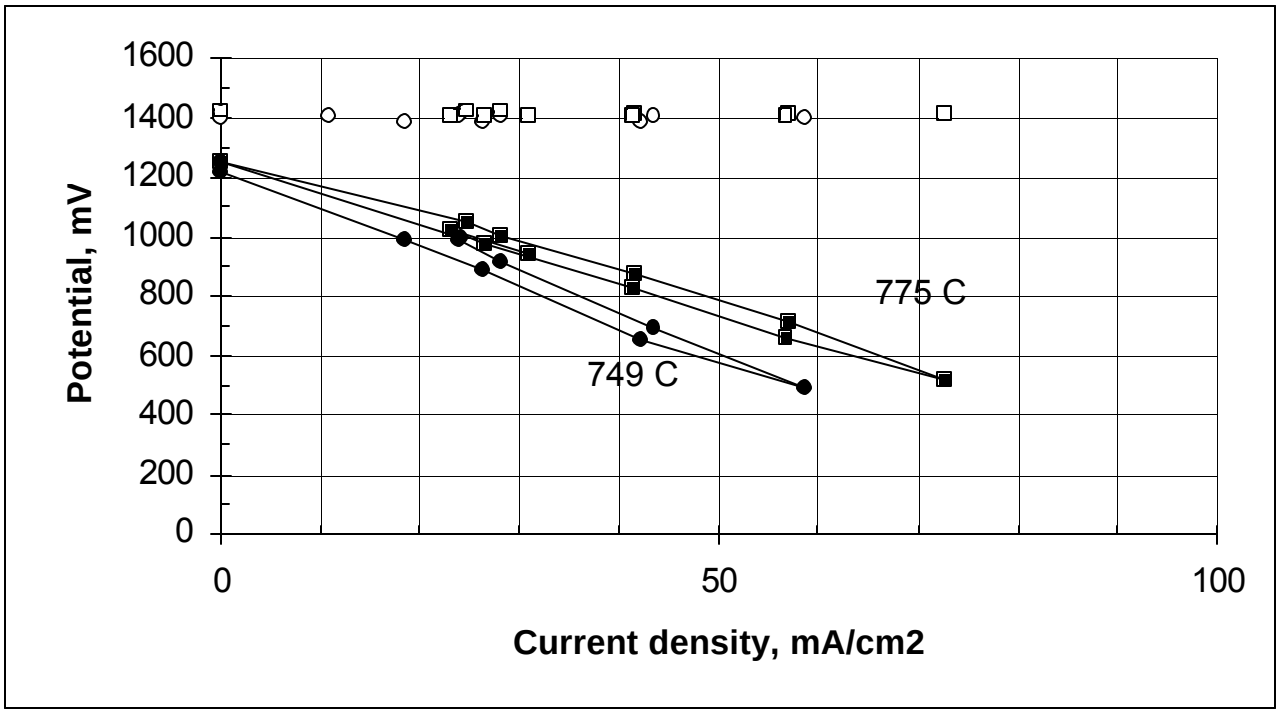

Figure 12. Pre-activation of Nickel Cathode Maximizes Performance of Carbon/Air Cell

- **Sample: WVU low-ash SECO; oxidized 250 °C, coked at 800 °C**
- **Cathode: activated prior to adding carbon to cell**
- **Favorable performance: 0.8 V at ~ 50 mA/cm2**

Dr. Chuang's assessment of the lab-scale SECO was as follows:

> "Your clean coal performed at the same level as Ohio no. 5 coal without producing much ash. The problem is the current density of our fuel cell remains to be very low. The low current density is not due to your clean coal. It is due to the problem inherent to our fuel cell. We are working to improve our fuel cell. Once I get good results, I will let you know immediately."[3]

Finally, Figure 13 shows a photograph of two foam samples produced during this work. The one on the left is a foam made from only CTP and the one on the right is the foam made from the blend of 30% CTP and 70% oxidized SECO which was heat-treated to 800°C. As can be seen, the CTP-only foam was very porous, of low density and of

low strength. In contrast, the SECO/CTP was very dense with much smaller pores and with much greater strength.

Figure 13. Carbon foam produced from SECO powder and CTP (right), and from CTP alone treated under the same conditions (left)

A crush test was conducted on the SECO/CTP foam sample and resulted in a value of 12.3 MPa. The density of the foam was found to be 0.87 g/cm^3 and the porosity was found to be 47%. These results are comparable to other carbon foams produced from a variety of feedstocks at WVU.

Conclusions

Elemental and proximate analyses of WVU Coal Extraction Pilot Plant SECO samples, SECO-4 and SECO-6/7, showed that the samples were low in ash and sulfur. However, a significant reduction in the VM content was needed in order to minimize difficulties during the testing of the DCFC. With the goal of decreasing the VM, and minimizing ash, a lab-scale SECO batch was successfully made from Kingwood Coal. This SECO was partially oxidized to prevent foaming during the heat-treatment process which was conducted at four different temperature levels (400, 600, 800, 1000 °C). Heat treatment resulted in a dramatic decrease in volatile matter. Heat-treated samples also demonstrated a continuous increase in carbon, and a decrease in nitrogen, hydrogen and sulfur. The oxygen content jumped significantly following oxidation, as was expected, and then decreased dramatically upon heat treatment.

XRD results indicated some degree of order in the structure of these heat-treated SECO samples. A higher degree of order as indicated by both the d-spacing and L values was observed for the samples heated at higher temperatures. All the carbons thus produced had domain sizes less than 30 nm, indicating turbostratic carbons.

Electrical resistivity measurements showed that the higher the heat-treatment temperature, the lower the resistivity of the SECO becomes. Thus, with the oxidized SECO heat-treated to 800°C or above, a more conductive carbon is obtained. Unfortunately, an accurate value for the resistivity of the 1000 °C heat-treated sample was not possible with the equipment available in the laboratory.

A SECO/CTP foam sample was successfully created and showed properties consistent with other similar foam samples.

The oxidized, 800 °C heat-treated SECO showed favorable performance in LLNL's fuel cell. The lab-scale SECO was also shown to perform well according to Dr. Chuang's findings. The low ash character of these samples makes them very attractive for application in the direct carbon fuel cell. Further work is this direction will be pursued in the future.

REFERENCES

1. N.J. Cherepy, R. Krueger, K.J. Fiet, A.f. Jankowski, J.F. Cooper, "Direct Conversion of Carbon Fuels in a Molten Carbonate Fuel Cell," (Journal of the Electrochemical Society February 25, 2004)
2. K. Renganathan, J.W. Zondlo, E.A. Mintz, P. Kneisl, A.H. Stiller, "Preparation of an Ultra-Low Ash Coal Extract under Mild Conditions," (Fuel Processing Technology, 18 (1988) 273-278)
3. Personal communication between Dr. Steven S.C. Chuang at the University of Akron and Dr. John W. Zondlo at West Virginia University.
4. Norio Iwashita, Chong Rae Park, Hiroyuki Fujimoto, Minoru Shiraishi, Michio Inagaki, "Specification for a standard procedure of X-ray diffraction measurements on carbon materials," (Carbon 42 (2004) 701-714)
5. "Standard Test Method for Determination of Crystallite Size (Lc) of Calcined Petrolium Coke by X-ray Diffraction," (ASTM Designation: D 5187 – 91 (Reapproved 1997))
6. Ron Walker, "Direct Carbon Fuel Cells: Assessment of the ir Potential as Solid Carbon Fuel Based Power Generation Systems," (Ron Wolk, Wolk Integrated Technical Services, San Jose, CA, (Report to Directors' Review Committee April 9, 2004; Report No. UCRL-SR-203880))

LIST OF ACRONYMS AND ABBREVIATIONS

LLNL:	Lawrence Livermore National Laboratory
DCC:	Direct Carbon Conversion
VM:	Volatile Matter
SECO:	Solvent-Extracted Carbon Ore
XRD:	X-ray diffraction
SEM:	Scanning Electron Microscopy
VM:	Volatile Matter
CTP:	Coal Tar Pitch
NMP:	N-methyl pyrrolidone
DCFC:	Direct Carbon Fuel Cell
WVU:	West Virginia University

CONSORTIUM FOR PREMIUM CARBON PRODUCTS FROM COAL

Pitch Derived Fiber Reinforced Fly Ash Concrete

Subcontract No. 2565-UK-DOE-0350

FINAL REPORT
for Period 1 July 2003 through 30 June 2004

by

University of Kentucky
Center for Applied Energy Research

August 2004

Disclaimer

ABSTRACT

The results of Laboratory and supporting technical assessments conducted under DOE Subcontract No. 2565-UK-DOE-0350 are reported for the period July 1, 2003 to June 30, 2004. This contract is with the University of Kentucky Research Foundation, which supports work with the University of Kentucky Center for Applied Energy Research, Koppers Industries. The work involves the production of bulk carbon fiber fabricated from a range of pitch precursors using a centrifugal melt spinning (CMS) process, production of concrete mixtures that utilize coal combustion fly ash as a pozzolan and utilization/assessment of bulk carbon fiber reinforcement in concretes.

TABLE OF CONTENTS

EXECUTIVE SUMMARY

This report describes the methods and results for the evaluation of CMS carbon fibers as a reinforcement in fly ash concrete and mortar composites. Preliminary work on modifying and then commissioning a CMS fiber production unit was carried out. This involved re-design of the pitch feed system and the addition of a cyclone fiber collection system.

The main focus of the experimental study was to assess common performance improvements associated with the addition of fiber reinforcement in concrete. Test specimen sizes were maintained at a relatively small scale to facilitate ease of storage, handling, and testing. Quantitative tests performed on concrete and fiber composite concrete specimens included: indirect tensile strength; unconfined compressive strength; modulus of elasticity; and a brief study on nuclear shielding. Tests performed on mortar composites included: drying shrinkage; flexural strength properties; and thermal conductivity. Additional investigations and studies to determine air content, admixture demand, and workability effects on wet and hardened concrete, mortar, and cement paste were also performed.

1. SECTION ONE

UNIVERSITY OF KENTUCKY
CENTER FOR APPLIED ENERGY RESEARCH

INTRODUCTION

This project is the integration of two developing areas in value-added products derived from coal. The first area is the production of low cost discontinuous carbon fiber from coal derived pitch, the second, utilization of recovered coal combustion fly ash in concrete. In this project, pitch was fabricated into discontinuous carbon fiber and used as reinforcement in fly ash concretes and mortars. The addition of pitch derived fiber to fly ash concrete should maintain stress transfer capability across a matrix crack to improve toughness, impact resistance and fatigue endurance in fly ash concrete.

Since the 1930s, the benefits of using pulverized coal combustion fly ash as a concrete admixture have been recognized in the U.S. [Davis et al., 1937]. With the advent of more stringent environmental regulations such as the Clean Air Act, large amounts of high-quality fly ash became available in the late 1960's and early 1970's [ACI, 2000]. Using fly ash as a partial replacement for Portland cement not only improves the “workability” of fresh concrete, but also improves long-term strength and durability. In a Portland cement-water system fly ash behaves as a pozzolan, which is defined as a glassy silicate or aluminosilicate that does not possess cementitious properties when mixed with water, but will react with aqueous calcium hydroxide at ordinary temperatures to form a cement [ACI, 2000]. Replacing a portion of Portland cement with a high quality fly ash reduces the amount of calcium hydroxide that is responsible for secondary destructive reactions in concrete such as sulfation, while simultaneously increasing the formation of calcium aluminosilicate hydrate gels, which serve as “binders” in concrete. Consuming the calcium hydroxide in the interstitial pore waters to form additional cement thus imparts many structural benefits to the concrete including greater compressive strength, lower permeability and increased durability. A reduction in permeability is particularly important for prevention of corrosion in reinforcing steel.

In addition to the structural benefits imparted to concrete by the addition of fly ash and carbon fiber, the replacement of Portland cement with coal combustion fly ash can indirectly lower the amount of CO_2 emitted to the atmosphere. The production of Portland cement is the third largest man-made source of CO_2 emissions. As a rule of thumb, the production of one ton of Portland

cement releases one ton of CO_2 to the atmosphere. In the conterminous United States alone there were approximately 89 million metric tons of cement manufactured in 2002 [USGS, 2003]. Thus, an important environmental benefit can be realized by replacing more Portland cement in concrete with fly ash. This benefit occurs because the CO_2 emission that occurs when fly ash is produced is caused by electricity, not fly ash, production, there is also far more fly ash produced than is utilized. In other words, increasing the use of fly ash in concrete will not cause additional fly ash to be produced to meet demand. In fact, when the improvements in concrete strength and durability are factored in, there may not be a more effective and unobtrusive technology for CO_2 reduction. Therefore, in addition to determining the performance of the coal derived pitch fibers in concrete, a goal of this project will be to design the pitch fiber reinforced concrete mixes to maximize the proportion of fly ash that can be added to the concrete while also achieving a high synergistic performance with the fibers (i.e. increasing the paste volume to better accommodate the fibers).

Corrosion of steel in concrete has lead to a significant amount of effort aimed at finding alternative ways of reinforcing concrete. One possibility is to reinforce concrete with randomly distributed fibers such that fibers maintain the stress transfer capability across a matrix crack, and in turn, improve the toughness, impact resistance, and fatigue endurance of concrete [Bentur and Mindess, 1990]. Various applications such as slabs on grade, bridge decks, and tunnel linings, where steel is provided mainly to combat secondary stresses, the use of fiber is proven to be practical and cost-effective [Bantha et. al., 1995].

Concrete contains a significant volume fraction of coarse aggregate larger than 5 mm, and consequently a much smaller paste (cement and water) volume fraction available to accommodate the fibers. Therefore, the maximum fiber content without excessive mixture stiffening and loss of workability is rather small, often less than 1%, and usually not more than 2% by volume of mixture. Rigorous mechanical mixing is usually needed to blend the fibers with coarse and fine aggregates, cement, and filler materials present. Fly ash, slag, or silica fume are used to increase the paste volume fraction and facilitate accommodation of fibers. Steel fibers are most commonly used, but fibrillated polypropylene, and monofilament forms of polypropylene, polyethylene, polyvinyl alcohol and polyacrylonitrile can also be incorporated

into concrete by mechanical mixing, or in some cases by dry-process shotcreting [Johnston, 2001].

Coal derived pitch carbon fiber may be a viable performance and cost alternative to traditional concrete fiber reinforcements. The carbon fibers produced for this project will be fabricated from isotropic pitch, supplied by Koppers Industries. Fibers will be formed using a novel technique, Centrifugal Melt Spinning (CMS), previously developed at the University of Kentucky Center for Applied Energy Research. The CMS process is capable of producing fibers from feedstocks containing significant quantities of solids, offering the potential for utilizing low cost feedstocks and reduced processing economics. Furthermore, regardless of the purity of the pitch feedstock, the high throughput of the CMS process makes it eminently suitable for producing large quantities of material in bulk fiber applications like concrete reinforcements.

CMS generates discontinuous fiber in the form of large fiber mats. CMS fibers have characteristic variations in diameter over the length of fiber, they also tend to be curved. These features do not necessarily detract from their performance in bulk filler applications and in fact may actually enhance adhesion of the fiber in the matrix. Variations in fiber geometry cause the matrix to "lock" around the fiber more effectively, allowing more effective stress transfer from the matrix to the fiber without allowing the fiber to slip within the matrix.

Literature Review

Zhang et al. (2002) uses a fiber-reinforced strip of mortar in concrete slabs in hopes of replacing typical jointing in concrete slabs. The idea is to localize cracking in the strip. They use 1.5 % by volume of polyethylene fibers E = 120 Gpa, tensile strength = 2700 Mpa, diameter = 0.038 mm, and length = 19.05 mm. Strain hardening was observed after first crack. The composite strains at 5% as opposed to 0.02% for regular concrete. Fiber composite mix proportions were cement = 1, sand = 0.5, water = 0.32, superplasticizer = 0.02, methyl cellulose = 0.0007, and antifoamer = 0.0005. Slabs were broken in uniaxial tension in a MTS 810 material testing system at 3, 7, 14, 21, and 28 days. Stress / strain and tensile strengths were reported.

Zollo states that ASTM C1018 is the typically accepted test for strength and toughness, but mentions that post cracking testing may be better. It reduces the sudden energy release associated with typical failure tests. For a flexure test, the specimen is placed between two steel plates and loaded in flexure to a specified deflection where the specimen is beginning to fail by cracking. The steel plates are then removed and the specimen is tested by itself to a chosen deformation, and load deformation relationships are obtained. An example of a 4"x4"x14" specimen in a four-point loading was given. Value added applications mentioned include low fiber volume, 0.5 vol%. Slab on grade and composite deck applications were given because of improved serviceability such as durability and toughness. Cast in place and precast applications include dam, bridge deck, mine, tunnel, canal, and reservoir lining, security and utility vaults, caisson, pile and pile cap foundation elements, slope stabilization, highway and airport slabs and many others. Typical applications are for crack control and utilize the energy-absorbing capabilities of fibers.

Tatro used steel fiber reinforcement in concrete composites with large size (1.5") aggregate. 3 types of steel fibers were used. Properties are as follows: yield strength = 170, 140, and 55 ksi, length = 60, 76, 19 mm, diameter = 0.8, 0.8, 0.4 mm, fibers had hooked ends, corrugated shape or were smooth. Beams were tested for fatigue and in flexure (ASTM C1018) and load deflection were curves plotted. Cylinders were tested for compressive strength and impact resistance. Impact testing was performed on 2 5/8" thick specimens sawed from 6" cylinder cross-sections by dropping a 10.5 lb weight from a height of 18in. The number of blows to first crack and ultimate failure (deformation to 6 3/8") were recorded for impact testing. Cylinder mix fiber content varied and beam fiber contents were 80 lbs/cyd for hooked and corrugated and 200 lbs/cyd for smooth. Flexural toughness, impact resistance, and fatigue properties were improved. Cylinder mix proportions were: Cement = 637 and 575 lb/cyd, water = 255 and 230 lb/cyd, 1.5" coarse aggr. = 778 and 709 lb/cyd, ¾" coarse aggr. = 1246 and 1162 lb/cyd, fine aggr. = 1091 and 1354 lb/cyd. Fatigue specimen mix proportions were: Cement = 597 lb/cyd, water = 229 lb/cyd, 1.5" coarse aggr. = 707 lb/cyd, ¾" coarse aggr. = 1157 lb/cyd, fine aggr. = 1348 lb/cyd. Entrained air was kept at 5%.

ACI suggests that section thickness may be reduced by use of fibers. ASTM C1116 is standard spec. for fiber reinforced concrete and ASTM A820 covers steel fibers. They recommend mix proportions as follows: cement = 500-900 lb/cyd, w/c =0.35-0.50, percent fine to coarse aggr. = 45-55, air content 4-6, smooth fiber = 0.3-0.8 vol%, deformed fiber = 0.6-1.6 vol%. Slab joints should be sawed 1/3 to ½ way through slabs to prevent random cracking elsewhere in the slab due to increased performance of the FRC at the joint.

Uomoto et al. mentions applications for FRC such as prestressed concrete, anchors for slope stabilization, and in special structures such as high speed motor railway tracks, MRI units of hospitals, and repair and rehabilitation works.

Zhang and Li (2001) state that Mangat and Azari (1988) performed shrinkage tests on steel fiber reinforced concrete and mortar beams with dimensions of 100x100x500mm. The specimens were cured at 20C at a relative humidity of 55%. The shrinkage was measured with an extensometer with regular measurements up to 120 or 520 days of age. The concrete mix proportions by weight were 1:2.5:1.25:0.58 (cement:sand:stone:water) and the mortar proportions by weight were 1:2.75:0:0.58 (cement:sand:stone:water). Three fiber types were used: hooked, crimped, and smooth extract. The fiber contents varied from 0 to 3%, fiber radius = 0.2-0.57mm, E = 210 Gpa, L = 22.5-48.7, depending upon the fiber type. Shrinkage vs. age was reported. FRC showed less shrinkage after about 50 days.

Zhang (2003) also states that Mangat et al. (1985) measured creep of FRC beams with smooth and hooked steel fibers. The mix was the same as mentioned above. The specimen was placed in a creep rig and loaded to a stress/ strength ratio of 0.3 and 0.55 respectively. The load was kept constant for 90 days and the creep measured with an extensometer. Creep strain versus time was reported. The FRC demonstrated less creep strain.

Bischoff performed axial tension tests on 100x100x1100mm concrete beams reinforced with a central 15 or 20 M steel bar and steel fiber. The FRC mix consisted of Cement = 450 kg/m^3, coarse aggr. = 764 kg/m^3, fine aggr. = 928 kg/m^3, water = 188 kg/m^3, 60kg/m^3. It appears that some of the coarse aggregate was taken out to accommodate the steel fiber and keep the

yield at 1 m^3. Specimens were moist cured for 7 days the air-dried for 64 or 65 days until testing. Stress strain and crack spacing and widths were reported.

In a run through of some of the remaining abstracts, the same tests keep surfacing as mentioned in the summaries above, ASTM C1018, compression, tension and impact resistance as well as shear tests and shrinking and cracking. The tests seem to result in improved characteristics, especially toughness, when performed on FRC. Resistance to wear heat and corrosion was noted with carbon fibers. Fiber volumes are consistent from 0 to 2 or 3%. The main applications that are continuously mentioned are slabs. Repair and rehabilitation are also mentioned as well as use of fibers in shotcrete.

It is suggested that fiber length should exceed the maximum aggregate size in the matrix (Blood, 1970; Tatro, 1985). Fibers currently marketed for use in concrete are rarely shorter than 15 mm or longer than 65 mm. Guidelines for water-cement ratio, cement content and fine/total aggregate contents for mechanically mixed steel fiber-reinforced concrete have been developed (ACI Committee 544, 1993). The process has been utilized primarily with steel fibers at fiber contents up to 20% by volume (Lankard, 1986; Bayasi and Zheng, 1997).

Task 1.0 Fabrication of CMS Carbon Fiber

Further to the work completed under a previous CPCPC Project and described in, “Production of Bulk Carbon Fibers and Activated Carbon Fibers via Centrifugal Melt Spinning” Final Report, March 2002 through June 2003 Subcontract No. 2191-UK-DOE-0350, the CMS processor was modified. Modifications included the addition of cyclone fiber collection system that dramatically reduced the amount of damage and breakage of the green fibers during production. The extruder feed system was also rebuilt using a slightly smaller i/d extruder bore, to improve the precision and consistency of the feed rate delivery to the spin head. The entire CMS unit was also skid mounted. CMS process modifications are shown below in Figure 1.

Figure 1 – Skid mounted CMS with cyclone collection system.

Koppers Industries Inc supplied two coal tar pitches, one low QI low softening point pitch (Stickney pitch) and one high QI high softening point pitch (Clairton pitch). As reported previously, "Production of Bulk Carbon Fibers and Activated Carbon Fibers via Centrifugal Melt Spinning" Final Report, March 2002 through June 2003 Subcontract No. 2191-UK-DOE-0350, the high QI Clairton pitch was successfully converted into CMS fiber mats. However, carbon fibers produced from this feedstock showed lower tensile strength and elastic modulus compared to other fibers produced from lower QI feedstocks. To produce fiber concrete composites that fully exploit the properties of the fiber reinforcement, CMS fibers were produced from the low QI Stickney pitch. However, before the Stickney pitch could be converted into CMS fibers its softening point was increased so that CMS fibers could be thermally processed to CMS carbon fibers.

Air blowing was used to increase the softening point of the Clairton pitch from 110 ^{o}C to 250 ^{o}C. The air blowing process can be described as follows. The pitch was heated to 300 ^{o}C while air flowing at approximately 1 L/min was bubbled through the pitch. Air blowing was performed in batches of approximately 2.5 kg of pitch for 12-17 h. Samples of pitch were removed and their softening points measured during the treatment.

After a desired softening point of 250 ^{o}C was reached, the pitch was allowed to cool and then crushed to a particle size of < 2 mm. The crushed pitch was transferred to the CMS extruder feed system and the molten pitch fabricated into discontinuous fiber mats and collected by the cyclone collection system. Approximately 2 kg of CMS fibers was produced during each spinning run. The green fibers were then processed to carbon fibers in two steps. The first step was oxidative stabilization. Green fiber mats were heated in air at 5 ^{o}C/min to 180 ^{o}C, then at 0.1 ^{o}C/min to 320 ^{o}C and held for 3 h. The cross-linking reactions that occur during stabilization are exothermic, hence the very slow heating rate was necessary to prevent the fiber mats from overheating and igniting during stabilization. The stabilized fiber mats were then carbonized by heating at 20 ^{o}C/min to 1000 ^{o}C in nitrogen. During the course of this project approximately 10 kg of CMS pitch derived carbon fiber was produced. Table 1 shows fiber processing for CMS fibers derived from Stickney pitch.

Table 1 – Data summary for processing of Stickney pitch fibers.

Pitch	Stabilization				Carbonization			Carbon Yield (%)
	Rate (^{o}C/min)	Linear Shrink (%)	Weight Change (%)	Status	Linear Shrink (%)	Weight Change (%)	Status	
Stickney	0.1	n/a	4.2	3	n/a	28.1	3	76.1
Status: 0 = melted, 1 = stuck, 2 = slightly stuck, 3 = OK. *n/a = not applicable.*								

The discontinuous fiber mat nature of CMS fibers makes assessment of their physical properties difficult. To determine approximations of tensile strength and elastic modulus of fibers derived from Stickney pitch, continuous filaments where melt spun using a ¼" Wayne Yellow Jacket bench top extruder. Continuous filaments were spun from a 330 μ die and the filaments wound onto a rotating drum. By controlling the extruders screw speed and the speed of the wind up drum the diameter of the resultant filaments can be controlled. Continuous filaments were cut of the wind up drum as fiber tows and processed to carbon fibers using the same methods described above. The mechanical properties of the continuous filaments were measured according to ASTM D3379 using an MTS Qtest tensile tester, Table 2.

Table 2 – Mechanical properties of Stickney pitch derived continuous filament carbon fibers.

Diameter (μm)	25.3
Tensile Strength (MPa)	408
Modulus (Gpa)	32

Figure 3 shows an example of CMS fibers produced from Koppers Stickney pitch. Inspection of Figure 3 shows the typical characteristics of CMS fibers. The fibers have variable diameter, are curved and may be tapered along the axis. A small batch (~500g) of CMS fibers were treated with boiling nitric acid for 2 hours. The nitric acid treatment was used to modify the surface

functionality of the fibers. These acid treated fibers were used for different investigations described below.

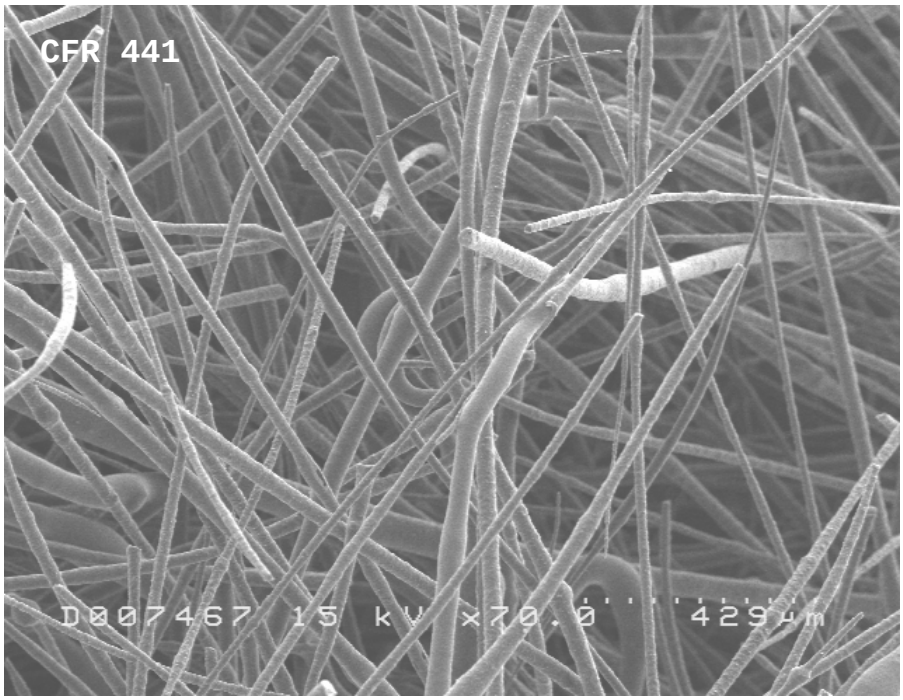

Figure 3 – CMS fiber produced from Stickney pitch.

Task 2.0/3.0 Fly Ash Concrete Test Specimens/Fabrication of fiber reinforced concrete

CMS carbon fibers were evaluated as reinforcements in both concrete and mortar mixes. The concrete mix design chosen for this project was the Class AAA mix, outlined in the Kentucky Transportation Cabinet (KYTC) Standard Specifications for Road and Bridge Construction 2000 Edition. The AAA mix was an ideal candidate for the addition of CMS carbon fibers. The mix produces a high performance concrete primarily utilized for bridge deck construction. However, because of its high cement content use of the AAA mix has for the most part been discontinued by the KYTC due to problems with shrinkage and cracking during curing. The addition of CMS carbon fiber should not only further improve the concrete strength but may also help control shrinkage during curing. Mortar mixes matched those outlined in ASTM standards C596 (for shrinkage specimens) and C109 (for flexure specimens).

A 20% by weight replacement of flyash for cement was used in all concrete and mortar mixes. Fiber contents of 0.1, 1.0, and 2.0% by volume were chosen to span typical ranges found in literature. A volume of sand, equal to the volume of fiber used, was removed in all mixes to maintain a constant yield. The concrete mix designs are presented in Table 3.

Table 3 - Class AAA Concrete Mix Proportions

		AAA Mix							
		Control		**0.1% Fiber**		**1% Fiber**		**2% Fiber**	
	SG (cc/g)	**wt (kg)**	**vol (m^3)**	**wt (kg)**	**vol (m^3)**	**wt (kg)**	**vol (m^3)**	**Wt (kg)**	**vol (m^3)**
Cement	3.2	325.6	0.1	325.6	0.1	325.6	0.1	325.6	0.1
Fly Ash	2.4	81.4	0.0	81.4	0.0	81.4	0.0	81.4	0.0
Water	1.0	162.8	0.2	162.8	0.2	162.8	0.2	162.8	0.2
Sand	2.6	673.2	0.3	670.6	0.3	646.9	0.2	620.6	0.2
Gravel	2.7	1029.0	0.4	1029.0	0.4	1029.0	0.4	1029.0	0.4
Fiber	1.8	0.0	0.0	1.8	0.0	18.0	0.0	36.0	0.0
Air	-	0.0	0.1	0.0	0.1	0.0	0.1	0.0	0.1
Total		**2272.0**	**1.0**	**2271.2**	**1.0**	**2263.7**	**1.0**	**2255.4**	**1.0**

The coarse concrete aggregate consisted of crushed limestone (No. 57 and No.8 size), and the fine aggregate comprised washed river sand. Admixtures used included an air-entraining admixture (AEA) as well as mid- and high-range water reducing admixtures. It should be noted that the high range plasticizer was only used in the 2 % fiber mixes. The fly ash was obtained from a central Kentucky power plant, and meets C 618 requirements for use as a pozzolanic admixture in concrete. The sand used for mortar strength and shrinkage testing comprised ASTM standard (graded) Ottawa sand, whereas that used for mortar air entrainment tests comprised ASTM 20-30 sand.

Concrete was prepared in a portable concrete mixer with a capacity of 2.3 m^3. Fibers were added to the wet concrete using two methods: 1) dispersion of the fibers into a slurry using a 4 L blender and adding the slurry to the mix, or 2) separation and distribution of the fibers into the mix by hand. All aggregates, water, and plasticizers were charged into the mixer and tumbled slowly for approximately 10 min to free the fine particles that had adhered to the surface of the coarse aggregate. The cement, ash, and AEA was then charged into the mixer and mixed at full speed for approximately 2 min, allowed to set for approximately 4 min, while the sides of the mixer were scraped down, and then mixed for an additional 2 min at full speed. Mortars were mixed with a 4.7 L (5 qt) stand mixer in accordance with ASTM C 305.

Workability, Air Entrainment and Admixture Demand

Investigations were performed to determine the effect that CMS fibers had on entrained air content and workability of concrete and mortar. All water contents and admixtures dosages were held constant, unless otherwise noted. Concrete workability and air content was determined using the methods outlined in ASTM C 143 and ASTM C 231, respectively. Mortar workability and air content was determined by using the methods outlined in ASTM C109 and ASTM C185, respectively. Table 4 and 5 present the workability and air data for concrete and mortar mixes.

Table 4 – AAA concrete mixes air content and workability

	Slump (in)	Air (%)
Control	7	6
0.1% Fiber	6.5	6.5
1% Fiber	5	9
1% Fiber **	nd	9

****** Note: No air entraining admixture used in this mix

Inspection of Tables 4 and 5 reveals that the addition of CMS fibers reduced the workability and flow of the mortar and concrete mixes. This is to be expected given that any alteration or addition to a standard concrete or mortar mix will affect the workability. Table 5 also shows a slight increase in air content for the 1% fiber mortar mix. Additional tests were performed to determine the origin or source of the additional air observed for the fiber mortar mixes.

Table 5 – Mortar workability and air content

	Flow (%)	Mortar Air (%)
Control	86	18
0.1% Fiber	44	19
1% Fiber	32	20

A modified version of Dodson's foam index test (modified by Boral Material Technologies) and Ultraviolet-Visible (UV-Vis) spectroscopy were used to quantify adsorption of the air entraining admixtures (AEAs) by the carbon fibers. The foam index is essentially a titration where the endpoint is indicated by the formation of a stable foam on the surface of an aqueous cement-air entrainment admixture mixture. The test is performed by blending the materials together and adding aliquots of the air entrainment admixture (AEA) are added and the mixture re-blended. The solution surface is inspected after each aliquot addition until a stable foam is observed (defined as an unbroken foam covering the entire surface). The larger the volume of AEA added indicates higher adsorption of AEA by the CMS fiber. Tests were performed using two different

AEA's, abietic acid and sodium laural sulfate on cement-fly ash mixtures with and without CMS fibers. The results from the foam index tests are presented in Table 6.

Table 6 – Modified foam index test results

	Abietic Acid, sodium salt	**Sodium Laural Sulfate**
Cement	2.2	3.2
Cement + Fibers	2.2	2.8
Cement + Acid Treated Fibers	2.5	3.3

In the UV-Vis spectroscopy experiments, different mixtures of Portland cement, fly ash, carbon fibers, water, and AEAs were prepared. After mixing for 5 min the aqueous mixture was filtered through a 0.45 micron filter and the solutions AEA concentration measured. Abietic acid (5.9%) and sodium dodecylbenzosulfonate (NaDDBS) were used as model compounds representing two classes of commercial concrete AEAs. The results of UV-Vis tests results for CMS fibers and nitric acid treated fibers are presented in Tables 7 and 8.

Table 7 – Adsorption of AEA by CMS fibers

	ppm remaining in solution	
	Abietic Acid	**NaDDBS**
Standard Solution	1945	1100
Cement Only	1434	NA
Cement and Flyash	1759	367
Cement, Flyash and Fibers	1609	344

Table 8 – Adsorption of AEA by CMS fibers treated with nitric acid

	ppm remaining in solution	
	Abietic Acid	**NaDDBS**
Standard Solution	1200	1299
Cement Only	NA	454
Cement and Flyash	1184	413
Cement, Flyash and Fibers	931	440

The results for the modified foam index and UV-vis tests show that the CMS fibers do not have any affinity for the AEAs. This also indicates that any additional air observed in fiber concrete and mortar mixes is likely due to air trapped within agglomerates of CMS fibers.

For concretes to resist the effects of freezing and thawing there must be sufficient air voids in the cured concrete. It is generally considered that the maximum distance from any point in the cement paste to the periphery of an air void should be 0.20 mm or less. This distance is referred to as the spacing factor (L). The spacing factor (L) was measured using optical microscopy analysis of polished cross sections of concrete fiber composites, Table 9. Inspection of Table 9 shows that the spacing factor (L) to be below the desired value of 0.20 mm, hence the concrete fiber composites should not be adversely affected by freeze/thaw conditions.

Table 9 – Optical microscopy results for air and fiber content

Sample	**Air Content (%)**	**Fiber Content (%)**	**L (spacing factor)**
No fiber	7.64	0	0.16
0.1% Fiber	5.84	0.24	0.18
1% Fiber	8.23	0.97	0.15

Task 4.0 Evaluation of fiber reinforced concrete

Mechanical Properties

All specimens were cast according to American Society for Testing Materials (ASTM) accepted practices and cured submerged in water at a controlled temperature of 23^{o}C, Figure 4. Cylindrical concrete specimens, with dimensions of 76x152 millimeters (3 in X 6 in), were cast and cured in accordance with ASTM C 192. Strength parameters are to be tested after 29, 57 and 113 days of curing. Compressive strength and elastic modulus data will be obtained following the procedures outlined in ASTM C 39 / C 39M-99 and C 469-94, respectively, and tensile strength will be determined through the indirect split cylinder method outlined in ASTM C 496-96. The results of the concrete cylinder testing can be seen in Tables 10, 11, 12 and 13.

Figure 4 – Curing of concrete test specimens.

Addition of CMS fibers to concrete and mortar composites appears to have little if no effect on the tensile, compressive, and flexural strength of the specimens over the relatively short time span of this project. However, closer inspection of the data does show a small trend toward improved strength of the fiber composites, above the control specimens, in the long term. This is particularly evident for the 1 vol% fiber content specimens, Table 13, where this sample showed slightly higher tensile and compressive strength after 29 days of curing compared to the standard concrete, Table 10. It should also be noted that the fibers for these composite concretes were dispersed into the concrete by hand before being mechanically mixed. This procedure involved "teasing" the fibers apart into smaller agglomerates rather than adding the fibers as one large mat. Addition of the fibers as smaller agglomerates should have reduced excessive shortening of the fiber during mechanically mixing and indeed these composites did show moderately improved strength. Unfortunately, due to the time constraint of the project, longer term curing and strength measurements could not be completed.

Table 10 – AAA concrete standard cylinder test results

Curing Time (days)	Tensile Strength (MPa)	Compressive Strength (MPa)	Elastic Modulus (MPa)
29	4.7	35.5	15169
57	4.5	36.5	16893
113	5.2	46.4	18237

Table 11 – AAA concrete containing 0.1 vol% fiber cylinder test results (mechanically dispersed)

Curing Time (days)	Tensile Strength (MPa)	Compressive Strength (MPa)	Elastic Modulus (MPa)
29	4.5	36.5	15169
57	4.8	37.6	16962

Table 12 – AAA concrete containing 1.0 vol% fiber cylinder results (mechanically dispersed)

Curing Time (days)	Tensile Strength (MPa)	Compressive Strength (MPa)	Elastic Modulus (MPa)
29	4.4	31.0	12917
57	4.8	33.5	14893

Table 13 – AAA concrete containing 1.0 vol% fiber cylinder results (hand dispersed)

Curing Time (days)	Tensile Strength (MPa)	Compressive Strength (MPa)	Avg. Elastic Modulus (MPa)
29	5.1	38.5	15031

The flexural strength of fiber composite mortars was also assessed. Mortar bars with dimensions of 25 x 25 x 305 mm were cast with CMS fibers added in loadings of 0.1, 1 and 2 vol%, nitric acid treated fibers were also cast into fiber mortar composites. The specimens were cured at 23 ^{o}C and 100 % humidity for periods up to 61 days. Specimens were sawn into 152 mm lengths and tested via three-point bending on an MTS Q-test instrument. Mortar bars were tested across a span of 89 mm with a point load applied to the center of the sample and a constant cross head speed of 0.1 mm/min. The results of the flexural testing are presented in Tables 14, 15, 16, 17, and 18.

Table 14 – Standard mortar bar flexural test results

Curing Time (days)	Peak Flexural Strength (MPa)	Strain at Break (%)	Flexural Modulus (MPa)
28	6.8	0.18	3820
56	6.9	0.18	3873

Table 15 – 0.1 vol% CMS fiber mortar bar flexural test results

Curing Time (days)	Peak Flexural Strength (MPa)	Strain at Break (%)	Flexural Modulus (MPa)
28	6.1	0.16	3813
61	6.5	0.17	3980

Table 16 – 1 vol% CMS fiber mortar bar flexural test results

Curing Time (days)	Peak Flexural Strength (MPa)	Strain at Break (%)	Flexural Modulus (MPa)
28	5.8	0.17	3375
57	7.1	0.19	3753

Table 17 – 2 vol% CMS fiber mortar bar flexural test results

Curing Time (days)	Peak Flexural Strength (MPa)	Strain at Break (%)	Flexural Modulus (MPa)
28	4.8	0.16	3308
56	5.8	0.15	3871

Table 18 – 1 vol% nitric acid treated CMS fiber mortar bar flexural test results

Curing Time (days)	Peak Flexural Strength (MPa)	Strain at Break (%)	Flexural Modulus (MPa)
28	5.7	0.15	3897

Inspection of the above data shows that the addition of CMS fibers at varying loadings did not significantly increase or decrease the flexural strength of the mortars. Closer examination of the composite concretes and mortars was performed to determine why addition of CMS fibers had no impact on mechanical properties.

The fracture surfaces of composite concrete and mortars were examined under optical microscopy, Figure 5 and 6. Inspection of the fracture showed that the majority of CMS fibers were well dispersed within the matrix, however, there was evidence of small fiber agglomerates in both concretes and mortars. Evidence of fracture bridging by the fibers was also noted, Figure 7. However, the length of fibers within the composites was well below the desired lengths identified in the literature (see Introduction). Although fiber length was not quantified, generally fibers less than 10 mm were observed.

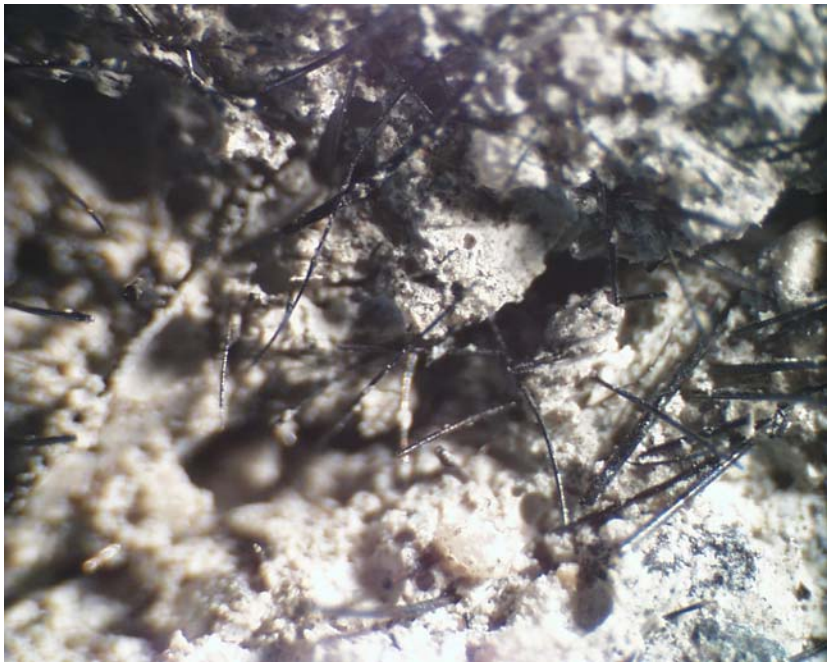

Figure 5 – Composite concrete fracture surface

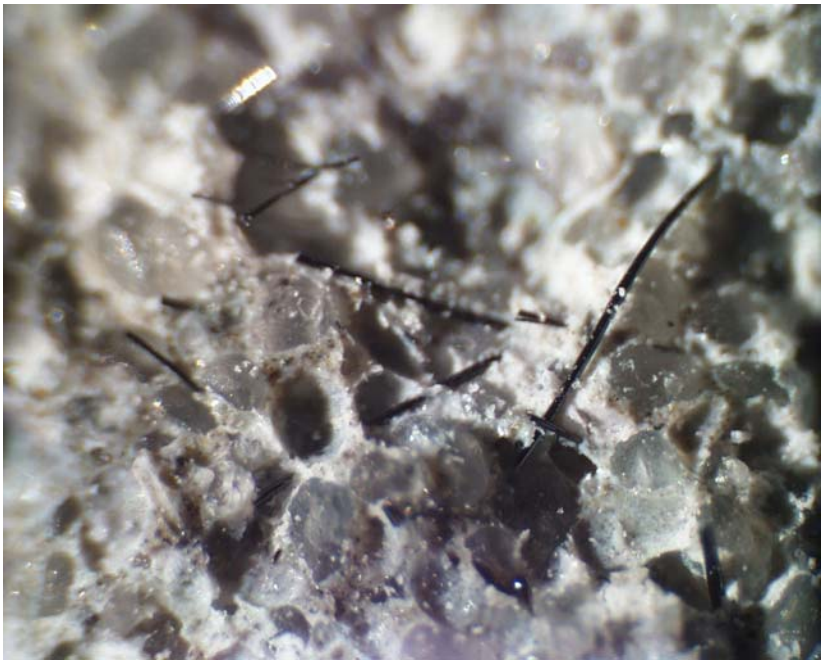

Figure 6 – Composite mortar fracture surface

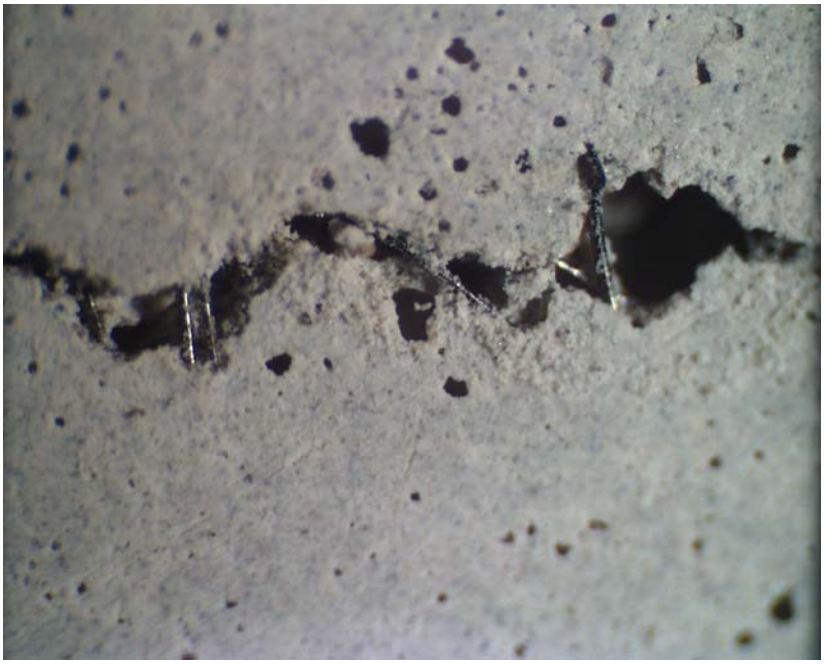

Figure 7 – Bridging of concrete composite fracture by CMS fibers

The lack of mechanical property enhancement by the CMS fibers can be attributed to two factors. The first was the short length of the fibers. Indeed, this was partly confirmed by the results obtained for tensile strength of composite concretes prepared by hand dispersing the fibers prior to mechanical mixing, Table 13. The strength results for these composites showed slight improvements over the mechanically dispersed fiber composites. The second was the small agglomerates of fibers in the composites. The presence of such agglomerated fibers was not primarily responsible for the absence of improved mechanical properties, as the results did not show large decreases in the mechanical properties. However, these small agglomerates of fibers were a source of trapped macroscopic air pockets within the mix, causing these agglomerated fibers to act as weak aggregates. This would have lead to an overall weakening of the composite and effectively canceling out any synergistic reinforcing effects the fiber may have had. This problem had been identified previously [Chung, 1992] where increases in the air content of fiber reinforced concretes was observed. Results shown in Table 4, support this hypothesis, where 1 vol% fiber concrete mix showed 9% air content without the addition of an AEA. Furthermore, data presented in Table 6, 7 and 8 show that the fibers themselves have no significant demand for AEAs.

Mortar Shrinkage Tests

Specimens for drying shrinkage experiments were cast, cured, stored, and tested in accordance with ASTM C 596, with the exception of curing conditions, Figure 8. The ambient humidity was approximately 55-60%, but was not rigorously controlled at that level. However, the humidity was monitored using a data logger and both the control and fiber mortar bars were prepared at the same time and exposed to identical curing conditions. Plots of shrinkage versus dry storage time for standard and fiber mortar composites with varying fiber contents are presented in Figures 9, 10 and 11.

Figure 8 – Curing of CMS fiber composite mortar bars for shrinkage tests

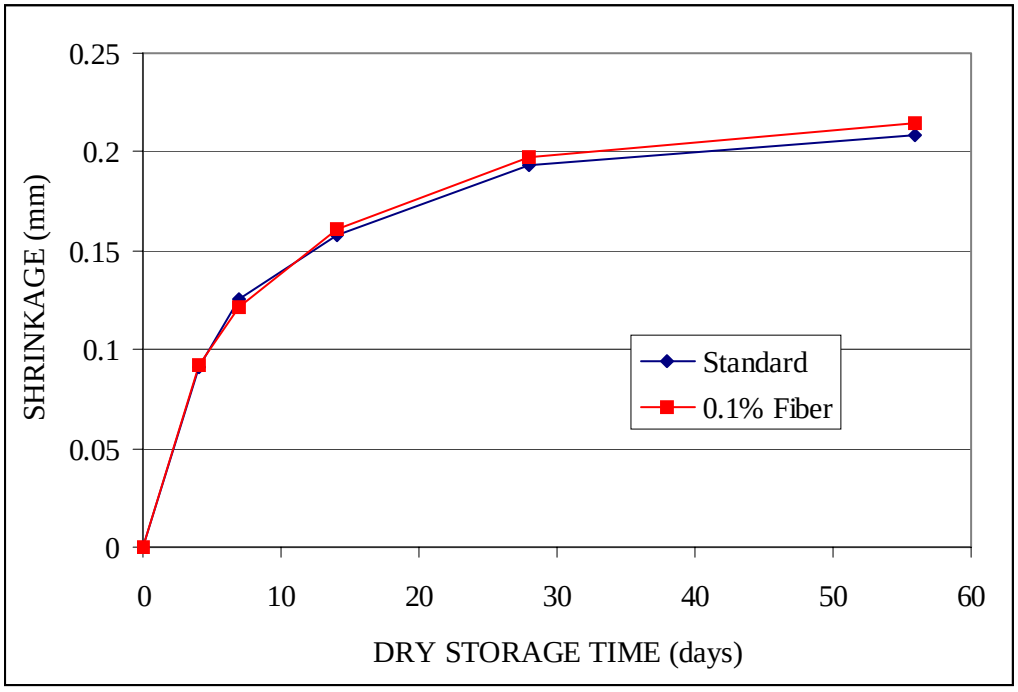

Figure 9 – Drying shrinkage vs. storage time for standard and 0.1% fiber mortar bars

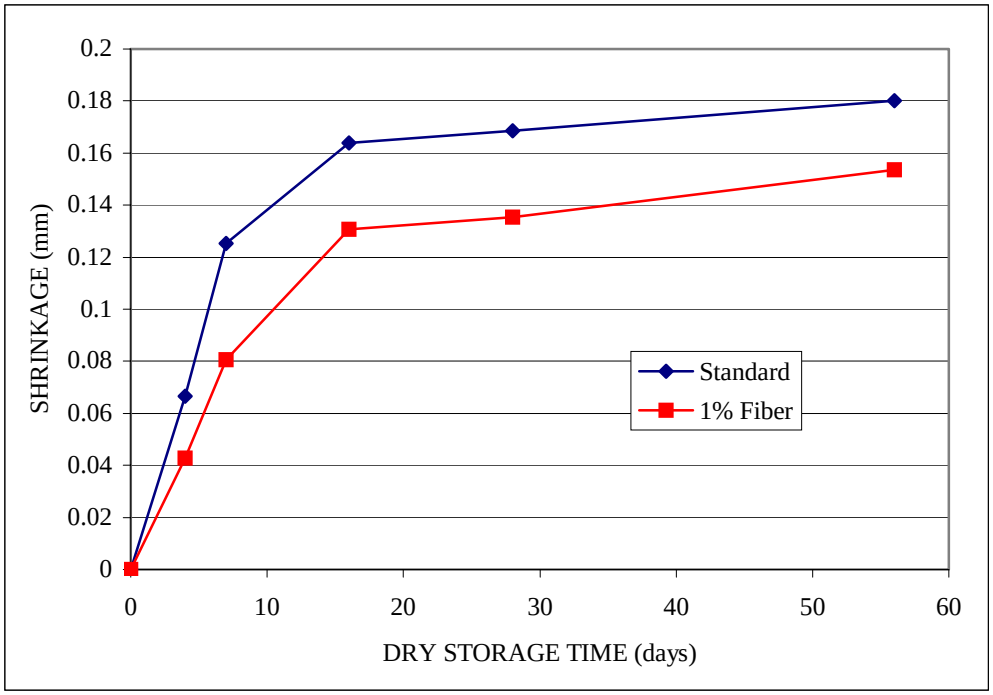

Figure 10 - Drying shrinkage vs. storage time for standard and 1% fiber mortar bars

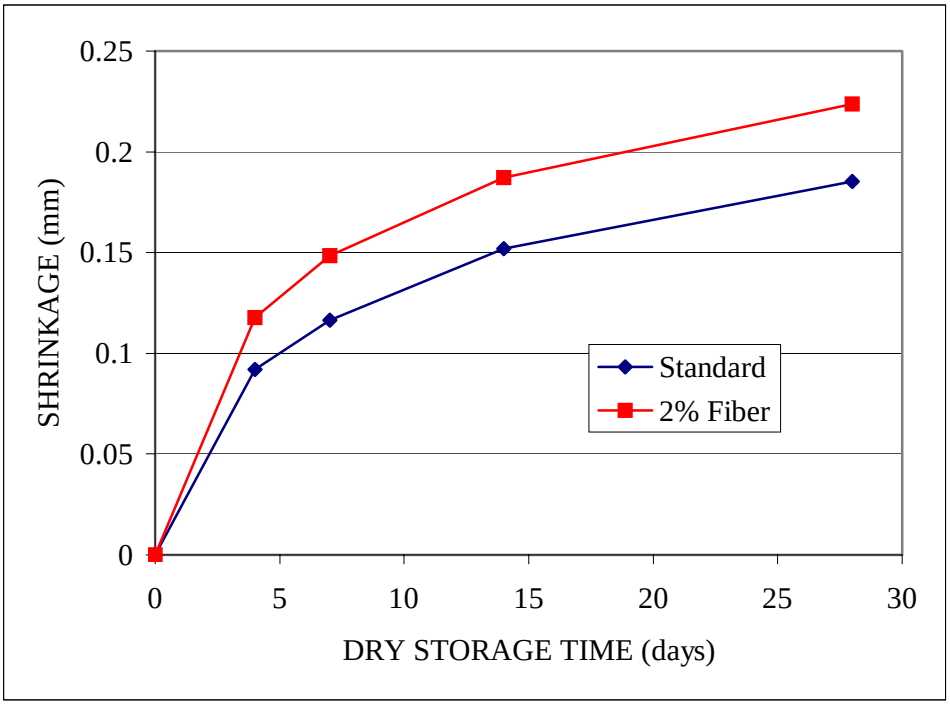

Figure 11 - Drying shrinkage vs. storage time for standard and 2% fiber mortar bars

The addition of CMS had a significant effect on the drying shrinkage of composite mortars, showing approximately 36 % less mortar shrinkage for the addition of 1 vol% CMS fiber. The marked reduction in mortar shrinkage is quite significant. As discussed above, many high performance concrete mixes have been discontinued because of excessive shrinkage and cracking problems. The results attained during this work show that mortar shrinkage can be significantly reduced by the addition of CMS fibers.

Task 5.0 Full Scale Field Test / Test Specimen

The research proposal for this project described the production of a $2m^3$ concrete pour for field testing evaluation. Unfortunately due to the time constraints of this project a full scale test was not completed. The time required to fabricate and process the necessary quantity of CMS fibers, as well, as, the time required to study the properties and characteristics of a large scale test specimen during curing was beyond the time available for this project. In place of the large scale field test, two additional studies on CMS fiber concrete composites were performed.

Nuclear Shielding

A brief investigation into the nuclear radiation abatement capability of carbon fiber reinforced concrete composites was performed. Concrete composites produced with carbon fiber reinforcement might offer some degree of shielding to nuclear radiation. A control concrete slab and a slab containing 2 vol% CMS fibers were cast. Each slab measured 406 mm in diameter and 152 mm thick, Figure 12 and 13 and both cured under identical conditions. Water content of each slab was held constant; this included accounting for an approximate 114 wt% absorption of water by the carbon fibers. A 16 mm diameter hole was cast through the depth of each slab to be used for density and moisture measurements.

The nuclear shielding tests were performed with a Surface Moisture-Density Gauge, manufactured by Troxler Electronic Laboratories Inc., as a radiation source. The gauge contains a ^{137}Cs point source to emit gamma radiation through a sample, a detector quantifies the intensity of the gamma radiation emitted through the sample. The intensity reading is correlated to the density of the specimen. A lower number of gamma photons reaching the detector indicates higher scattering/absorption of photons within the test specimen, resulting in a higher density measurement. Moisture within the slab was also measured with the Troxler gauge. Moisture content is measured using 40mCi Am and ^{241}Be sources to emit neutrons. Neutrons are "thermalized" or slowed by water molecules in the sample. A ^{3}He detector measures the flow of neutrons through the sample, this measurement is directly proportional to the moisture content of the slab. The density and moisture content of the slabs were measured at 17 days curing age.

The results of these measurements along with calculated theoretical densities are presented in Table 19.

Figure 12 – Concrete slab for nuclear shielding tests

Figure 13 – CMS fiber concrete composite slab for nuclear shielding tests

Table 19 – Density and moisture data for concrete and CMS concrete composites

	Control Slab	2 vol% Fiber Slab
Measured Density (kg/m3)	2148.1	2002.3
Calculated Density (kg/m3)	2184.9	2066.4
Measured Moisture (%)	6.0	7.9

Thermal Conductivity

Generally concretes and mortars are insulating materials, however, the addition of CMS fibers to mortar mixes may affect the thermal conductivity of the material. A brief investigation to determine the difference in thermal conductivity of mortar and fiber mortar composites was performed. The thermal conductivity of fiber mortar composites was determined by measurement of the thermal diffusivity at ambient temperature. Thermal conductivity cannot be measured directly. However, thermal diffusivity can be measured directly and is directly proportional to thermal conductivity. Samples of fiber mortar composites measuring 10 mm x 8 mm were cut and then coated with graphite. Thermal diffusivity measurements were performed with Netzsch Instruments Laser Flash Apparatus LFA 427. Thermal diffusivity measurement involves pulsing the sample with a laser and measuring the radiated heat emitted through the sample. Thermal diffusivity measurements were performed at ambient temperature, under an atmosphere of flowing Ar, laser voltage was 450 V and pulse width 0.8 ms. The results shown in Table 20 are mean values for 5 shots per sample. Inspection of the data reveals that the addition of CMS fibers did not significantly alter the thermal diffusivity of the mortar.

Table 20 – Thermal diffusivity data for mortar and CMS fiber composite mortar

Sample	Mean Thermal Diffusivity (mm2/s)	Standard Deviation (mm2/s)
Control Mortar	1.570	0.044
2 vol% CMS Fiber Mortar	1.606	0.047

Conclusions

The results obtained during the course of this project support the following conclusions:

- The addition of CMS carbon fibers decreased the workability of concrete and mortar mixes.
- CMS carbon fibers did show any affinity for adsorption of air entraining admixtures (AEAs) in the concrete and mortar mixes. Optical microscopy studies showed that CMS fiber composite concretes had sufficient air contents to resist the detrimental effects of freeze/thaw conditions.
- Addition of CMS fibers to concrete and mortars did not significantly decrease or increase the mechanical properties of concretes or mortars compared to control concrete and mortar mixes. This was attributed to the following:
    - Although the majority of the CMS fibers were dispersed, majority of these fibers were too short, <10mm, to be effective in bridging fractures and failures in the matrix.
    - The presence of small fiber agglomerates increased the air content of the fiber, effectively negating any potential improvements in strength.
- Addition of CMS fibers where shown to be effective in controlling concrete shrinkage during curing. This result is significant, as many high performance concrete mixtures (such as the AAA mix studied here) suffer from excessive shrinkage and premature cracking during cure and significant effort is required to control the rate of shrinkage for these concretes.

References

ACI Committee 544, (1993), Guide for Specifying, Proportioning, Mixing, Placing and Finishing SFRC, MCP-5, Report ACI 544.3r, 10pp.

American Concrete Institute (ACI), *Manual of Concrete Practice: Part 1*, 116R-90, pp. 116R-1 to 116R-68, 2000.

Banthia, N, M. Al-Asaly, and S. Ma. (1995). "Behavior of Concrete Slabs Reinforced with Fiber-reinforced Plastic Grids", Journal of Materials in Civil Engineering, Nov., 1995, 252-257.

Bentur, A. and Midness, S. (1990). Fiber Reinforced Cementitious Composites, Elsevier Applied Science, New York, N.Y.

Bischoff, P. H. (2003). "Tension Stiffening and Cracking of Steel Fiber-Reinforced Concrete" Journal *of Materials in Civil Engineering*., March/April 2003, 174-182.

Blood, G.W. (1970), Material Science Thesis, University of Calgary.

Bayasi, Ziad, Jack Zeng, (1997), "Flexural Behavior of Slurry Infiltrated Mat Concrete (SIMCON)", Journal of Materials in Civil Engineering, Nov, 1997, 194-199.

Chung, D D L (1992), Carbon Fiber Reinforced Concrete, Strategic Highway Research Program, National Research Council, Washington DC, 1992.

Davis, R.E., Carlson, R.W., Kelly, J.W. and Davis, H.E., Properties of Cements and Concretes Containing Fly Ash, *Journal of the American Concrete Institute*, Vol. 33, pp. 577-612.

Johnston, Colin D. (2001). Fiber-Reinforced Cements and Concretes, Gordon and Breach Science Publisher, Canmet, Ottawa, Ontario Canada.

Kentucky Transportation Cabinet. *Standard Specifications for Road and Bridge Construction* (2000).

Lancard, D.R., (1986), Steel Fiber Concrete, (Ed. Shah and Skarendahl), Elsevier, pp. 200-217
Tatro, S.B.,(1985), Master's Thesis, Purdue University, Lafayette, Indiana, U.S.A.

Tatro, S. B., (1986). "The Effect of Steel Fibers on the Toughness Properties of Large Aggregate Concrete." Purdue University, Joint Highway Research Project, 1986.

United States Geological Survey (USGS), *Mineral Commodities Summaries: Cement*, http://usgs.gov, January 2003Annual Book of ASTM Standards (2000).
Uomoto, T., Mutsuyoshi, H., Katsuki, F., Misra, S. (2002). " Use of fiber reinforced polymer as reinforcing material for concrete." *Journal of Materials in Civil Engineering*., May/June 2002, 191-210.

Zhang, J., Li, V. C. (2001). "Influences of fibers on drying shrinkage of fiber reinforced cementitious composite" *Journal of Engineering Mechanics*., January 2001, 37-44.

Zhang, J.,(2003). "Modeling of the influence of fibers on creep of fiber reinforced cementitious composite" *Composites Science and Technology*., Vol. 63, 2003, 1877-1884.

Zhang, J., Li, V. C., Nowak, A. S., and Wang, S. (2002). "Introducing Ductile Strip for Durability Enhancement of Concrete Slabs." *Journal of Materials in Civil Engineering*., May/June 2002, 253-260.

Zollo, R. F., (1995). "Fiber Reinforced Concrete: and Overview after 30 Years of Development." *Cement and Concrete Composites*., Elsevier 1997, 107-122.

DEVELOPMENT OF ANTHRACITE-BASED CARBON CATALYSTS

Final Report

Report Period: March 1, 2003-February 28, 2004

Principal Investigator: Dr. John W. Larsen and
Dr. Harold H. Schobert
Author: Francelys Medina
Report Issue: October 2004

Internal Agreement No.,
For Award No.: DE-FC26-98FT40350

The Energy Institute
Penn State University
C 211 CUL
University Park, PA 16802

ABSTRACT

An exploratory study has been made of the kinetics of the carbon-catalyzed reduction of nitrobenzene to aniline by hydrazine and the carbon-catalyzed decomposition of hydrazine in refluxing *iso*-propyl alcohol. The reactions are thermodynamically highly feasible, but do not proceed at measurable rates in homogeneous solutions. The catalytic mechanism for the nitrobenzene reduction by hydrazine was previously proposed to be adsorption of the reactants on the surface of the carbon followed by electron transfer.[1] The principal goal of this project was to provide additional information on the catalytic mechanisms of these reactions. The ultimate goal of this program at The Energy Institute is to develop carbon catalysts for existing commercial reactions and for new reactions. This requires a better understanding of how different carbons catalyze reactions so that carbon catalysts can be developed in the most efficient and expeditious manner.

Various commercial carbons, with widely differing physicochemical properties, were characterized and their catalytic activity for both reactions was investigated. The carbon samples studied included activated carbons, carbon blacks, non-activated charcoals and graphite. The reactions were followed by measuring the production of gases as a function of time using a gas burette. All of the carbon samples brought about easily detectable rates of hydrazine decomposition and nitrobenzene reduction by hydrazine. The reaction rates were proportional to the catalyst concentration, increased with surface area, and were independent of the stirring conditions, providing evidence that both reactions may be surface-controlled. However, the nitrobenzene reduction may

be, in part, controlled by pore diffusion as determined by the almost linear relationship between the initial reaction rates and the external surface area and pore volume of the carbon catalysts.

For both reactions, the catalytic activity of carbon catalysts was found to vary linearly with the surface area (of carbon blacks in the case of the nitrobenzene reduction) and bulk oxygen content at low oxygen content. The surface area dependence can be separated into two different straight lines corresponding to acidic and basic carbons, which was proposed as due to the presence of two different types of oxygen surface groups affecting the adsorption of hydrazine and nitrobenzene.

The kinetics of the hydrazine decomposition reaction exhibited a change of reaction order from first order at low concentrations of hydrazine to zero order at high concentrations. The observed kinetics have been explained by postulating a Langmuir adsorption process is involved in the slow step of the reaction, in which the hydrazine molecules are nondissociatively adsorbed on the carbon surface. A subsequent reaction between liquid-phase hydrazine molecules and hydrazine molecules adsorbed on the carbon surface, followed by a reaction between two adsorbed diimide molecules, leads to the final products.

The kinetics of the nitrobenzene reduction by hydrazine were complicated by the simultaneous decomposition of hydrazine. The observed kinetics for the nitrobenzene reduction exhibited a pronounced order change from a fractional positive value at low nitrobenzene concentrations to a fractional negative order at high nitrobenzene concentrations. This behavior has been explained by deriving the overall rate equation on the assumption that the rate-determining step is the reaction between an adsorbed

nitrobenzene molecule and an adsorbed hydrazine molecule, according to a Langmuir-Hinshelwood model.

Table of Contents

List of Figures

List of Tables

Chapter 1.

Introduction

Carbons are known to catalyze a wide range of reactions.[2-11] For several reactions, catalytic mechanisms have been investigated. We are continuing the investigation of the mechanism of the carbon-catalyzed reduction of nitrobenzene by hydrazine and the carbon-catalyzed decomposition of hydrazine in *iso*propanol. Earlier studies[1,12] indicated that these reactions may proceed by adsorption of the reacting species at the carbon surface followed by electron transfer—a mechanism originally proposed by Spiro for other reactions catalyzed by carbons and noble metals.[13] If this reaction pathway is common, it raises the possibility of replacing expensive and environmentally troublesome metal catalysts with carbon in some processes.

Carbons are attractive as catalysts because of their low cost, environmental acceptability, reasonably high electrical conductivity, relatively low chemical and electrochemical reactivity, and easily reproducible and controllable surface chemistry. Current market price for a carbon black is about 30 ¢/lb.[14] Carbon poses little risk of environmental contamination and is generally considered non-toxic with only minor effects to the respiratory and cardiovascular systems. In fact, carbon does not appear on any of the lists of hazardous or toxic substances.[15] Carbon may display the electronic properties of metal, semiconductor, or insulators, and often has electrical conductivity comparable to common metals.[16] At ordinary temperatures, carbon is one of the most chemically inactive of the elements due to its high tendency to form covalent bonds.[16] Carbon possesses only a rather limited area of thermodynamic stability, but both oxidation and reduction of carbons are extremely slow reactions (electrochemically

irreversible) and cannot actually be brought about under normal conditions of temperature and pressure.[17]

In addition, carbon is suitable as a catalyst because of its availability in a wide variety of physical structures, ranging from highly oriented pyrolytic graphite to amorphous carbon black and activated carbon. In between the two extremes of highly graphitic and amorphous carbons, there is a host of carbons with a wide range of differing and reasonably well-defined morphologies (e.g. small particles, fibers, large solid blocks, etc.) and physicochemical, chemical, electrical and thermal properties. These materials are obtained by the use of different precursors, manufacturing processes, and subsequent treatment steps.[16] For instance, heat treatment at progressively higher temperatures produces carbons with physicochemical properties that start with amorphous carbon and end with graphitized carbon.

A perusal of the literature shows the diversity of reactions catalyzed by carbons. Carbon is used commercially to catalyze the formation of phosgene and sulfuryl chloride.[18] Carbon as a catalyst for other industrially useful reactions represents a potential new market for premium carbon products. These catalysts could be cheaper and more environmentally acceptable than traditional, heavy-metal, supported catalysts. To intelligently select reactions that might be catalyzed by carbons, the mechanisms by which carbon catalyzes reactions must be understood. However, there is no published summary of the mechanisms of carbon catalysis.

The objective of this thesis is to further explore the catalytic mechanisms of two carbon-catalyzed reactions for which there exists some mechanistic information in the literature: the reduction of nitrobenzene to aniline by hydrazine[1] and the decomposition

of hydrazine.[12] In doing so, we attempt to understand the fundamentals of carbon as catalyst in order to develop the knowledge to design carbon catalysts for existing commercial reactions.

1.1. Hypotheses of this project

The hypothesis of this research is that carbon may catalyze the nitrobenzene reduction by hydrazine and the hydrazine decomposition reactions by the same mechanisms that occur with some metals.

Chapter 2. Literature Review

2.1. Heterogeneous catalysis

A catalyst is a substance that increases the rate at which a chemical system attains equilibrium without itself undergoing an irreversible chemical change.[19] In other words, the primary result of catalysis is to enhance the reaction rate and sometimes to yield the desired products with high selectivity. To do so, the catalyst has to reduce the activation barrier of the rate-determining step. The type of catalysis where the catalyst exists in a different phase from the reactant molecules (usually as a solid in contact with either gaseous reactants or with reactants in a liquid solution) is known as **heterogeneous catalysis**.

The sequence of elementary steps by which a reaction proceeds is known as its reaction mechanism. If a reaction proceeds by a multistep mechanism (stepwise reaction) one of the steps may be much slower than the others and so be the rate-determining step. The rate-determining step governs the rate law for the overall process.

Heterogeneous catalysis must involve interaction between the surface and at least one of the reactants. In general, if the reaction

$$A + B \rightarrow C + D$$

occurs at the surface of a catalyst, several pieces of information are required before it is possible to understand or unravel the mechanism.[19] These may include the following:

1. Are both A and/or B molecules adsorbed at the catalyst surface? Will A displace B or vice versa?

2. If both A and B are adsorbed, what are their relative surface concentrations?
3. Are there changes taking place in A and B if they are adsorbed? What is the nature of the bond between the catalyst and the adsorbed species?
4. What is the nature of the surface intermediates?
5. What features of the catalyst are the important ones that make it catalytically active?
6. Do the products influence the reaction in any way?
7. What is the rate-determining step in the catalytic process?

Obtaining these key pieces of information requires studying the kinetics of the reaction. In general, studies of reaction mechanism begin with a study of the reaction kinetics. In this study, we want to explore questions (5) and (7).

A heterogeneous catalytic process involves five distinct steps:[20]

- mass transport of reactant(s) to the catalytic surface from the bulk solution;
- adsorption of the reactant(s) on the surface;
- chemical reaction at the surface, which involves the chemical rearrangement (bond breaking, bond, formation, molecular rearrangement) of the adsorbed reaction intermediates;
- desorption of product(s) from the surface; and
- mass transport of product(s) away from the surface into the bulk solution.

Any of these steps could be the rate-determining step in a catalytic process. However, the processes of adsorption or desorption are *usually* too fast to be rate-

determining steps in solution catalysis.[20] In addition, the majority of reactions in liquid solutions are not diffusion-controlled; instead only a small fraction of encounters lead to reaction. We will show that the reduction of nitrobenzene to aniline by hydrazine and the decomposition of hydrazine are surface-controlled reactions, i.e., the rate-determining step involves the reaction on the surface of an adsorbed reactant or of a derived species. The terms "surface-controlled reaction" and "surface reaction" will be used interchangeably throughout this thesis.

2.1.1. Rates of surface reactions

In a kinetic experiment, the change in the amount of a reactant or product with time is measured to learn the rate law. The discussion that follows is mainly based on that of Spiro's review on heterogeneous catalysis of solution reactions.[20] Consider the elementary reaction of the form

$$a\mathrm{A} + b\mathrm{B} \rightarrow c\mathrm{C} + d\mathrm{D} \tag{2.1}$$

where a, b,…are the coefficients in the balanced chemical equation and A, B,…are the chemical species. If the reaction takes places in a closed, isothermal system, the **reaction rate** may be defined as the time derivative of the extent of reaction,

$$R = -\frac{1}{a}\frac{dn_a}{dt} = -\frac{1}{b}\frac{dn_b}{dt} = \frac{1}{c}\frac{dn_c}{dt} = \frac{1}{d}\frac{dn_d}{dt} \tag{2.2}$$

where n_i is the amount (in moles) of species i. The reaction rate defined in this way is independent of the particular reactant or product chosen, so no ambiguity arises if any of the terms in this expression is taken to be the rate of the reaction. Equation (2.2) may be used even when there are volume changes during the reaction or two or more phases are

present. It should be noted that the reaction rate as defined by Eq. (2.2) is an extensive quantity, but in fundamental reaction kinetics, an intensive reaction rate is needed. In this case, Eq. (2.2) is divided by a reference variable that may affect concentration through means other than destruction of reactant or creation of product. In closed homogeneous systems, volume is the most important variable of this kind.[*] In dealing with heterogeneous systems, the mass of the solid, as well as the surface area of the solid, may be taken as the reference variable but with certain caution because the dependence of the reaction rate on the mass or surface area of the catalysts may not be straightforward. Besides, the active surface area of the catalyst is seldom known precisely. Since we are dealing with initial rates in this thesis, we will use Eq. (2.2) as the reaction rate divided by the total volume of solution, which is either constant or changes by a negligible amount at the beginning of the reaction even for concentrated solutions.

The rate of a reaction may be expressed in the form of an empirically determined equation called the **rate law** of the reaction

$$R = k[\mathrm{A}]^{\alpha}[\mathrm{B}]^{\beta}... \tag{2.3}$$

where the brackets [ ] represent concentration (customarily molar) and α, β…are constants, known as the **orders** of the reaction with respect to A, B…The overall reaction order, *n*, is equal to the sum of the individual orders. The proportionality constant *k* in the rate law is referred as the **rate constant**. *It is important to note that the reaction orders are not necessarily determined by the stoichiometric coefficients of the balanced*

---

[*] If the volume is constant during the reaction, the reaction rate may be expressed in terms of the change of the concentration (for diluted solutions) of one of the reactants or products.

chemical equation, except in the special case of an elementary reaction[†]*, so the reaction orders must be determined in kinetic experiments.* In addition, although there are some heterogeneous reactions which exhibit simple orders of reaction, for example the copper-catalyzed hydrogenation of ethylene at high temperatures, the majority of surface reactions cannot be assigned a simple order.[19]

One can determine the rate law for a reaction by using the solution of the differential rate equations (integration method), and comparing the time evolution of the concentrations of the reacting species (or an equivalent quantity that expresses the extent of the reaction) predicted by the possible rate laws with the experimental data. Laidler[21] refers to the order determined from the integration method as the order with respect to time. The integration method is useful for providing accurate rate constants if the order of a reaction has been well established. However, the method creates prejudice in favor of integral or half-integral orders.[21] The rate law can also be determined by observing the effect of changing initial reactant concentrations on the initial rate of the reaction (differential method). The order determined in this way is referred to as the order with respect to concentration. This procedure, dealing with initial rates, avoids or minimizes the effects of complicating factors (e.g., interference by products, sintering or poisoning of the catalyst, etc.) contributing to the change in the reaction rate. A full discussion of the kinetic methods and their advantages and disadvantages can be found in Laidler.[21]

In addition to its variation with reactant concentration at the surface, the rate of a surface reaction varies with the surface area of the catalyst. The surface area determines

---

[†] An elementary reaction is a reaction that occurs in a single step, with no experimentally detectable reaction intermediates.

the number of active sites for adsorption and catalysis. In a constant volume system, the number of molecules reacting in unit time is proportional to the number of collisions with the surface. Thus the reaction rate will vary directly with the area of the catalyst surface.[19]

A problem in the kinetics of heterogeneous reactions is the difference in dimensionality of a molecule in solution and on a surface, and the inclusion of adsorption onto a surface in the kinetic treatment. This problem is handled by the use of adsorption isotherms. Before considering each type of surface reactions, it is important to introduce the concept of adsorption since the extent of adsorption has a profound effect on the rate of a heterogeneous reaction.

2.1.2. Adsorption isotherms

Adsorption refers to the binding of molecules to a surface. In practice, not all the molecules bound to a catalyst surface are reactive. Besides, various impurities may be adsorbed at the surface, and these may occupy potential reaction sites and block the reaction. The places where adsorbed molecules may become reactive are called **active sites**. The number of active sites per unit amount of catalyst depends on the nature of the catalyst, on its method of preparation, and on its treatment before use.

The most common isotherm equations used to describe adsorption are those by Langmuir and Freundlich, which represent reasonably well the adsorption from dilute solutions. Both Langmuir and Freundlich isotherms are applicable to chemisorption and physisorption processes.[22] Adsorption isotherms of nitrobenzene from its aqueous

solutions on activated carbons and carbon blacks appear to be of the Type I or Langmuir variety.[23,24]

Three important assumptions are made in the derivation of the Langmuir adsorption isotherm. These are as follows:[19]

(1) the species are adsorbed in definite, localized sites in a monolayer;

(2) adsorption involves one and only one adsorbed molecule per site;

(3) the energy of an adsorbed molecule is the same at any site and is unaffected by adsorption on neighboring sites, i.e. the heat of adsorption is independent of surface coverage.

Deviations from the Langmuir equations are often observed. This may be because the surface is not uniform, and also there may be interactions between adsorbed molecules. Another reason for deviations from the Langmuir isotherm is that there may be adsorption in more than one layer, that is, multilayer adsorption. When such deviations occur, the adsorption results can sometimes be fitted to an empirical adsorption isotherm due to Freundlich.

The Freundlich isotherm is an empirical relationship between concentration and surface coverage. However, it can be derived theoretically if the following assumptions are made:[19]

(1) the heat of adsorption falls exponentially as the coverage is increased;

(2) the decrease in heat is due to surface heterogeneity, rather than to repulsive forces between adjacently adsorbed species.

(a) Langmuir isotherm without dissociation

A brief derivation of the Langmuir adsorption isotherm is as follows. If θ is the

fraction of surface which is covered by a molecule, then (1 – θ) is the fraction which is bare. Let us assume that [a] is the concentration of the adsorbing species in solution and k_a and k_{-a} are the kinetics rate constants for adsorption and desorption respectively. Then for adsorption without dissociation to cover a single surface site, the rate of adsorption is

$$v_a = k_a[a](1-\theta) \tag{2.4}$$

Desorption involves one adsorbed species and the rate is

$$v_{-a} = k_{-a}\theta \tag{2.5}$$

At equilibrium the rates are equal, so that

$$k_a[a](1-\theta) = k_{-a}\theta,$$

$$\frac{\theta}{1-\theta} = \frac{k_a}{k_{-a}}[a] = K_a[a],$$

and

$$\theta = \frac{K_a[a]}{1+K_a[a]} \tag{2.6}$$

where $K_a = k_a/k_{-a}$, is an equilibrium constant for the adsorption-desorption process.

The variation of θ with [a] is the following:

(a) at low concentrations [a] is small and $K_a[a] << 1$, so

$$\theta = K_a[a], \tag{2.7}$$

the fraction of surface covered being proportional to the concentration of the reactant;

(b) at high concentrations [a] is large and $K_a[a] >> 1$, so

$$\theta \approx 1, \tag{2.8}$$

and the fraction of surface covered is independent of the concentration of the reactant. At intermediate concentrations the fraction of surface covered is proportional to the

concentration of the reactant to some power between one and zero.

(b) Langmuir isotherm with dissociation

Langmuir's derivation of the isotherm for adsorption with dissociation to cover two surface sites is as follows. The rate of adsorption is

$$v_1 = k_1[a](1-\theta)^2 \tag{2.9}$$

Desorption involves two adsorbed species and the rate is

$$v_{-1} = k_{-1}\theta^2 \tag{2.10}$$

At equilibrium the rates are equal, so that

$$k_1[a](1-\theta)^2 = k_{-1}\theta^2,$$

$$\frac{\theta}{1-\theta} = \left(\frac{k_1}{k_{-1}}[a]\right)^{\frac{1}{2}} = K_a^{\frac{1}{2}}[a]^{\frac{1}{2}},$$

and

$$\theta = \frac{K_a^{\frac{1}{2}}[a]^{\frac{1}{2}}}{1+K_a^{\frac{1}{2}}[a]^{\frac{1}{2}}} \tag{2.11}$$

The variation of θ with $[a]$ is the following:

(a) at low concentrations $[a]$ is small and $K_a^{\frac{1}{2}}[a]^{\frac{1}{2}} << 1$, so

$$\theta = K_a^{\frac{1}{2}}[a]^{\frac{1}{2}}, \tag{2.12}$$

the fraction being proportional to the square root of the concentration of the reactant;

(b) at high concentrations $[a]$ is large and $K_a^{\frac{1}{2}}[a]^{\frac{1}{2}} >> 1$, so

$$\theta \approx 1, \tag{2.13}$$

and the fraction of surface covered is independent of the concentration of the reactant. At

intermediate concentrations the fraction of surface covered is proportional to the concentration of the reactant to some power between ½ and zero.

(c) Freundlich isotherm (nonlinear adsorption)

According to this adsorption equation due to Freundlich,[21] the amount of a substance adsorbed is related to the concentration by the equation,

$$\theta = K_a [a]^m \tag{2.14}$$

where K_a and m are empirical constants. This equation does not give saturation of the surface; the amount adsorbed keeps increasing as $[a]$ increases. If Eq.(2.14) applies, a plot of $\log_{10} x$ versus $\log_{10} [a]$ gives a straight line of slope m.

2.1.3. Kinetics of heterogeneous reactions

(a) Unimolecular reactions

In a unimolecular surface reaction, one molecule of a single reactant species is adsorbed and reacts on the surface. This type of surface reaction is usually treated in terms of the Langmuir adsorption isotherm as follows. The rate R of a heterogeneous reaction is proportional to the fraction of surface which is covered, i.e.

$$R = k\theta = \frac{kK_a[a]}{1 + K_a[a]} \tag{2.15}$$

for adsorption without dissociation and,

$$R = k\theta = \frac{kK_a^{\frac{1}{2}}[a]^{\frac{1}{2}}}{1 + K_a^{\frac{1}{2}}[a]^{\frac{1}{2}}} \tag{2.16}$$

for adsorption with dissociation. Here, k is the rate constant defined earlier in this chapter.

The dependence of rate on [a], shown in Figure 2.1, is exactly the same as that given by the Langmuir isotherm.

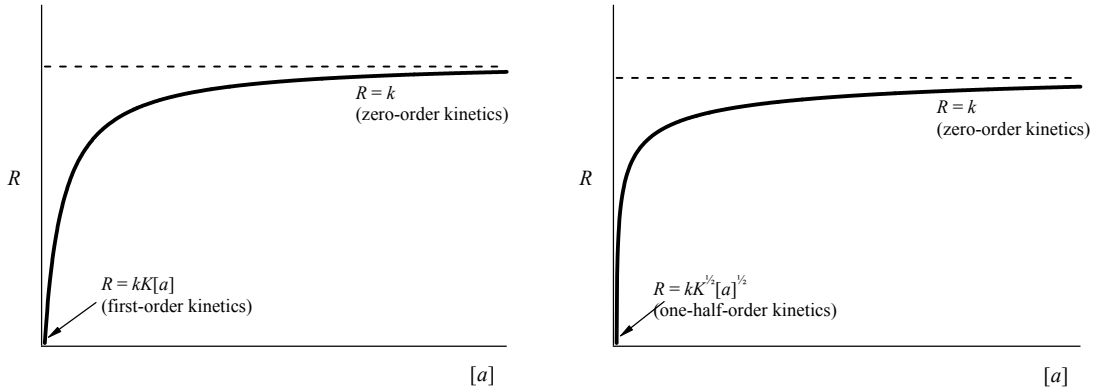

Figure 2.1. Variation of rate with concentration for unimolecular reactions with nondissociative adsorption (*left*) and dissociative adsorption (*right*).

Suppose now that the adsorption of a reactant A is the rate-determining step, the *net* rate of adsorption will be the difference between the rate of adsorption of A and its rate of desorption. Applying the notion of Langmuir we can write[25] the rate of adsorption of A,

$$R = \frac{k_a[a]}{1 + K_a[a]} \tag{2.17}$$

(b) Bimolecular reactions

(i) Langmuir-Hinshelwood mechanism

In a Langmuir-Hinshelwood mechanism, the reaction occurs between two adsorbed molecules, as shown in Figure 2.2. Suppose that the fraction of surface covered by molecules of type A is θ_a and that the fraction covered by B is θ_b. The bare fraction is

$1-\theta_a-\theta_b$. If both substances are adsorbed without dissociation, the rates of adsorption of *a* and *b* are

$$v_a = k_a[a](1-\theta_a-\theta_b) \tag{2.18}$$

and

$$v_b = k_b[b](1-\theta_a-\theta_b) \tag{2.19}$$

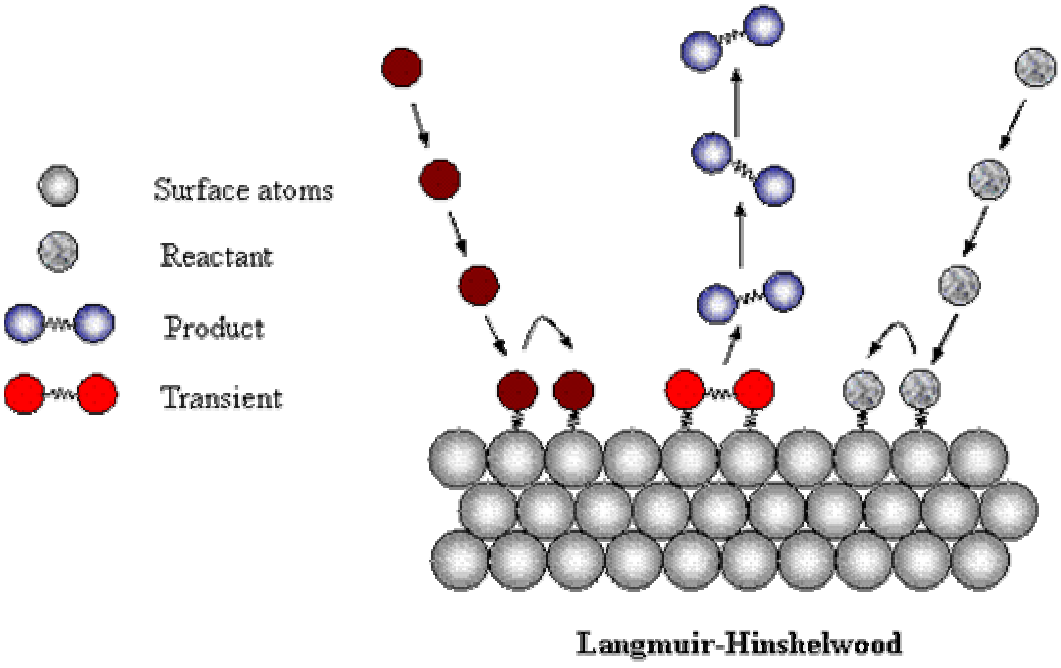

Figure 2.2. Graphic illustration of the Langmuir-Hinshelwood mechanism, where the reactants are equilibrated on the surface prior to reaction.

The rates of desorption are

$$v_{-a} = k_{-a}\theta_a \tag{2.20}$$

$$v_{-b} = k_{-b}\theta_b \tag{2.21}$$

Equating Eqs. (2.18) and (2.20) leads to

$$\frac{\theta_a}{1-\theta_a-\theta_b} = K_a[a] \tag{2.22}$$

where $K_a = k_a/k_{-a}$. From Eqs. (2.19) and (2.21) it follows that

$$\frac{\theta_b}{1-\theta_a-\theta_b} = K_b[b] \tag{2.23}$$

where $K_b = k_b/k_{-b}$. Equations (2.22) and (2.23) are two simultaneous equations that can be solved to give, for the fractions covered by *a* and *b*, respectively,

$$\theta_a = \frac{K_a[a]}{1+K_a[a]+K_b[b]} \tag{2.24}$$

$$\theta_b = \frac{K_b[b]}{1+K_a[a]+K_b[b]} \tag{2.25}$$

This simple derivation requires that a number of assumptions are met: (a) each adsorption site accommodates only one molecule; (b) molecules are adsorbed without dissociation; (c) all sites are energetically equal (i.e., the adsorption enthalpy is independent of coverage).

A clear consequence of the first assumption follows from Eqs. (2.24) and (2.25), that is, that the fraction of the surface covered by one substance is reduced if the amount of the other substance is increased. This is because the molecules of A and B are competing with one another for limited number of surface sites, and we speak of competitive adsorption.

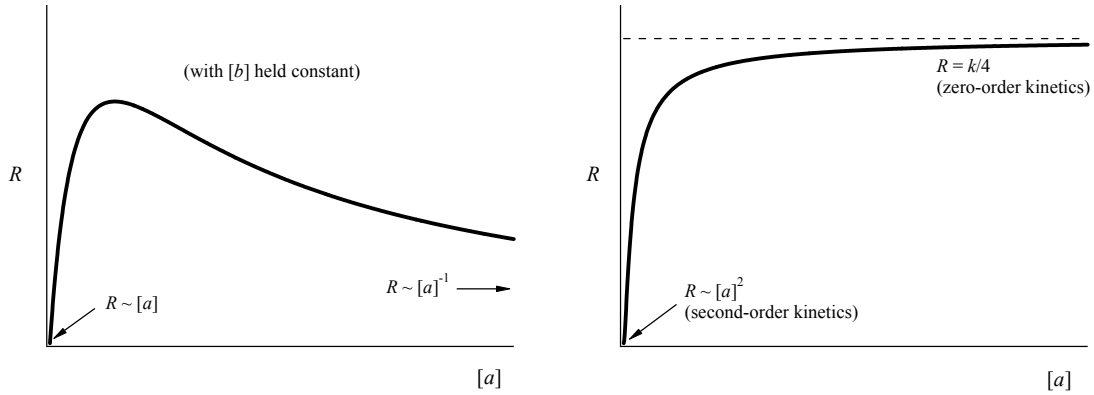

Figure 2.3. Variation of rate with concentration for a bimolecular reaction occurring by a Langmuir-Hinshelwood mechanism between two different molecules (*left*) and two molecules of the same type (*right*).

In the Langmuir-Hinshelwood mechanism, the rate is proportional to the fractions of the reacting molecules A and B that are adsorbed. The reaction rate is therefore

$$R = k\theta_a\theta_b = \frac{kK_aK_b[a][b]}{(1+K_a[a]+K_b[b])^2} \tag{2.26}$$

where k is the rate constant of the reduction reaction. If [b] is held constant and [a] is varied, the rate varies in accordance with Figure 2.3(a):

(a) at sufficiently low concentrations [a] and [b] are small, $K_a[a] << 1$ and $K_b[b] << 1$, so

$$R = kK_aK_b[a][b] \tag{2.27}$$

The reaction is therefore second order, being first order in both A and B.

(b) at high concentrations [b] is large and $K_b[b] >> 1$, so

$$R = \frac{kK_a[a]}{K_b[b]} \tag{2.28}$$

The rate is now inversely proportional to [b], and the order with respect to B is -1.

(c) the rate is maximum when $\theta_a = \theta_b$, i.e., when $[a] = \frac{K_b}{K_a}[b]$.

If both A and B are the same reactants, the rate equation for the Langmuir-Hinshelwood mechanism is therefore

$$R = \frac{kK_a^2[a]^2}{(1+2K_a[a])^2} \tag{2.29}$$

The kinetics become second-order and zero-order at low and high concentrations, respectively, as shown in Figure 2.3(b).

(ii) Eley-Rideal mechanism

In an Eley-Rideal mechanism, the reaction occurs between an adsorbed B molecule and a molecule of A in the liquid phase, as shown in Figure 2.4. The rate is proportional to the fraction of surface covered by B and to the concentration of A in solution:

$$R = k\theta_b[a] = \frac{kK_b[a][b]}{1+K_a[a]+K_b[b]} \tag{2.30}$$

Note that adsorbed A molecules do not enter directly into reaction, but they reduce the rate by occupying surface that might otherwise be occupied by B molecules.

If both A and B are the same reactants, the rate equation for the Eley-Rideal mechanism is therefore

$$R = \frac{kK_a[a]^2}{1+2K_a[a]} \tag{2.31}$$

The kinetics become second-order and first-order at low and high concentrations, respectively, as shown in Figure 2.5(a). For like molecules, the rate varies with concentration in the manner shown in Figure 2.5(b).

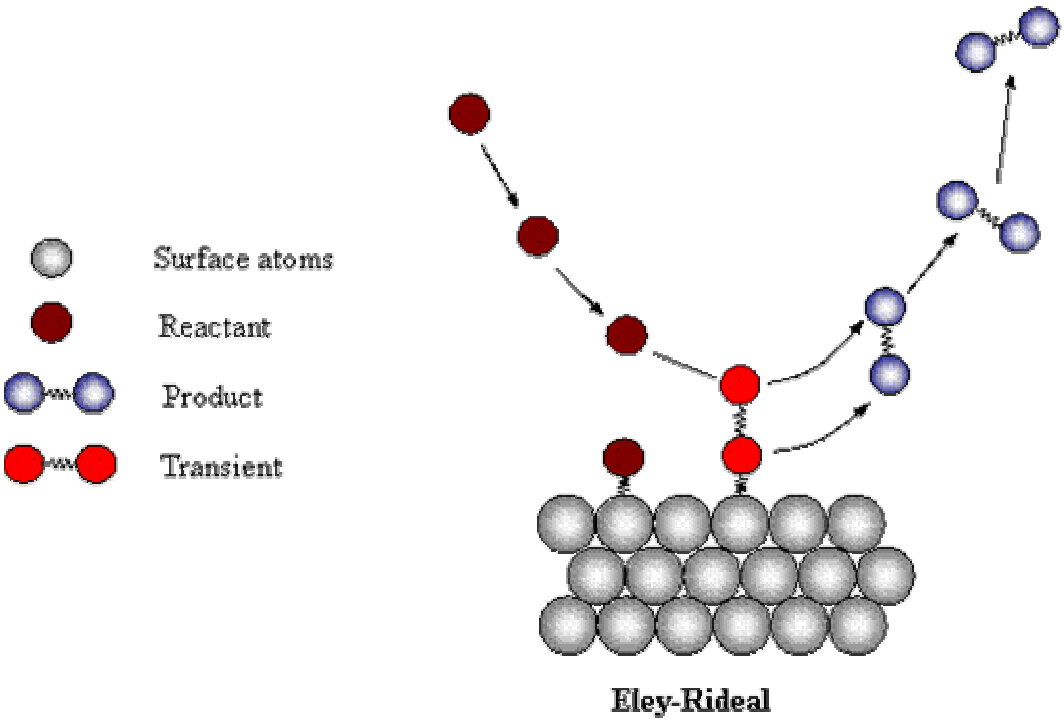

Figure 2.4. Graphic illustration of the Eley-Rideal mechanism, where an adsorbed species reacts by a direct collision with a liquid-phase species.

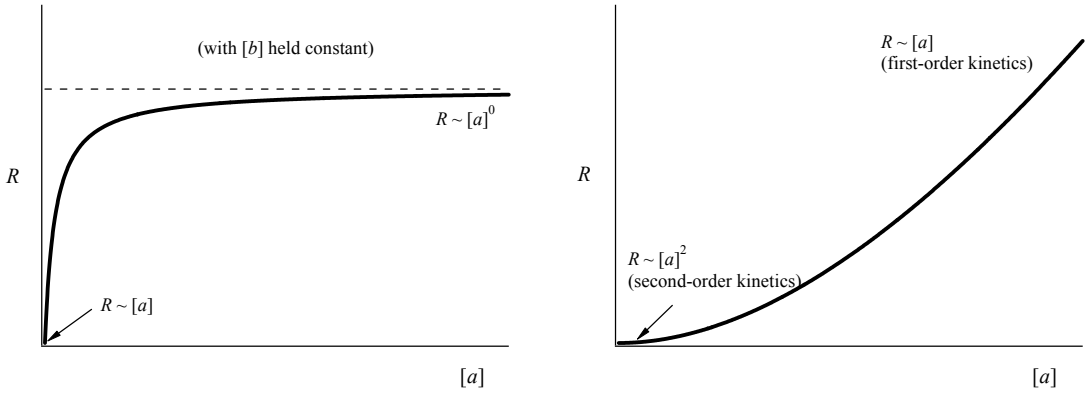

Figure 2.5. Variation of rate with concentration for a bimolecular process occurring by an Eley-Rideal mechanism between two different molecules (*left*) and two molecules of the same type (*right*).

The third category of bimolecular surface reactions is peculiar to redox reactions catalyzed by metals and semiconductors. The discussion of this mechanism, known as the

electrochemical mechanism, is postponed for later in this chapter.

2.2. Carbon as a catalyst

Carbon catalyses a variety of liquid-phase reactions including decomposition, polymerization, halogenation, substitution, isomerization, hydrocracking, and redox reactions.[2-11] There is neither a comprehensive list of reactions known to be carbon-catalyzed, nor a codified list of the mechanisms for carbon-catalyzed reactions. The literature on carbon-catalyzed reactions is fragmented, with many single reports scattered in the literature.

The earliest review on carbon catalysis seems to be the monograph by Hassler,[3] in which an incomplete list of reactions catalyzed by activated charcoal is presented. No space is devoted to catalytic mechanisms in that review. The reviews by Coughlin[4,5] and Weiss[2] deal with an arbitrarily selected group of reactions and attempt to describe most catalytic properties of carbon in terms of electronic effects of metals, semiconductors or insulators. No serious attempt was made to sample the patent literature. In the article by Tripathi and Ramachandran,[7] reactions catalyzed by carbon were reviewed for the effect of surface area, pore size and nature of surface complexes. Trimm[6] also briefly discussed carbon-catalyzed reactions in terms of the surface groups present on the carbon materials. Jüntgen and Kühl[8] summarized briefly the role of activated carbon catalysts in environmentally relevant reactions and correlated catalytic activity to the physical properties of the carbon catalyst. Kalra *et al*.[9] presented the status of investigations on an arbitrary group of carbon-catalyzed reactions. A more recent review deals with a group of

carbon-catalyzed reactions in solution.[10] The monograph by Radovic and Rodriguez-Reinoso[11] devoted little space to carbon catalysts. None of these reviews is exhaustive and none attempts a general understanding of the mechanisms by which carbons catalyze reactions.

Several examples of reactions known to be catalyzed by carbons are presented next. The reactions have been selected to provide a breadth of examples:

1) Isomerization reactions: α-methyl mono-olefin and straight-chain olefins (e.g., 2-methyl-1-butene, 2-methyl-1-pentene, and 1-pentene),[26-28] oximes,[29,30] optically active 1,1'-binaphthyl and disubstituted derivatives,[31-33] optical isomers of *tris*(ethylenediamine)-cobalt(III) ion $[Co(en)_3]^{3+}$,[34-39] optically active unsymmetrical facial bis[di(2-aminoethyl)sulfide]-cobalt(III) ion $(-)_D$-$[Co(daes)_2]^{3+}$,[40,41] *tris*(propylenediamide)-cobalt(III) ion $[Co(pn)_3]^{3+}$,[42] (ethylenediamide)tetraacetato-cobalt(III) Co(EDTA),[43] and $[Pt(en)_3]^{4+}$.[44]

2) Substitution (solvolysis) reactions: 2,2'-binaphthyl methyl phosphate ester of 1,1'-bi-2-naphthol,[45] methyl acetate to acetic acid,[46] ethyl acetate,[47] benzyl acetate,[20] alkyl halides (e.g. ethyl iodide) by metallic nitrates (e.g., $AgNO_3$),[48,49] and compounds of cobalt or chromium ions coordinated to nitrogen atoms (e.g. cobaltammine).[50-54]

3) Oxidative hydrogenation and dehydrogenation reactions: conversion of ethylbenzene to styrene,[55-62] conversion of primary alcohols (e.g., 2-propanol and butan-2-ol) to acetals,[63-66] conversion of cyclohexanol to cyclohexene, cyclohexanone, and phenol,[67] and conversion of aliphatic and aromatic carboxylic acids and carboxylic acid anhydrides with CCl_4 to the corresponding acid chlorides.[68-70]

4) Oxidation-reduction reactions: oxidation of hydrogen sulfide by oxygen,[71-77]

oxidation of sulfur dioxide,[78-82] reduction of nitric oxide,[83-87] oxidation of fluorene to fluorenone,[88] oxidation of *o*-xylene to phthalic anhydride,[89-92] oxidation of olefinic compounds (e.g., cyclohexene),[93] oxidation of hydrochloric acid,[94] oxidation of aqueous oxalic acid,[95-98] oxidation of *n*-hexane,[99] and reduction of nitroaromatic compounds.[1]

5) Decomposition reactions: hydrogen peroxide,[100-110] peracids, peracid salts and alkyl hydroperoxides,[111] 1,2-dicholoethane,[112-114] benzoyl peroxide,[105,115,116] nitrogen dioxide,[117] and hydrazine compounds.[12]

6) Polymerization reactions: methyl olefins (e.g. 2-methyl-propene and isobutene),[26] methyl methacrylate,[118] N-vinylcarbazole,[119,120] isobutyl vinyl ether,[121] α-methylstyrene,[122] and N-vinyl-2-pyrrolidone.[123]

7) Halogenation and dehalogenation reactions: production of phosphene[124-126] and sulfuryl chloride,[127] chlorination of toluene and benzene,[128,129] conversion of chloride into hydrochloric acid,[130,131] hydrodehalogenation of halogenated aromatic compounds (e.g. 9-bromophenanthrene, 1-chloronaphthalene, 1-bromonaphthalene, 4-chlorobiphenyl),[132] dehydrochlorination of 1,1,2,2,-tetrachloroethane to trichloroethylene,[133] and synthesis of hydrobromic acid[134-141] and hydrogen iodide.[142]

8) Hydrocracking reactions: degradation of polyethylene to aromatic hydrocarbons, [143]cracking of Decalin, *n*-hexadecane, paraffin wax, and *iso*propylbenzene,[144] and bond cleavage of 4-(1-naphthylmethyl)bibenzyl.[145-147]

9) Exchange reactions: hydrogen-deuterium exchange,[148,149] and ortho-para hydrogen exchange.[150,151]

10) Other reactions: Friedel-Crafts acylation of aromatic compounds (e.g. anisole, toluene and *o*-xylene) with acyl halides,[152] Kemp elimination,[153] Menschutkin reaction,[154]

alkylation of imidazole[155] and dealkylation of polymethylbenzene (e.g. toluene to benzene).[156]

It is obvious from the forgoing list that carbons are versatile catalysts capable of effectively increasing the rate of a broad range of reaction types. It seems likely that in doing so, a variety of reaction mechanisms are involved. Our concern here is with a pair of reactions in which the carbon-catalyzed reactions seems to be similar to metal-catalyzed reactions. There are important industrial uses to carbon catalysts. For example, the synthesis of phosgene and sulfuryl chloride is performed over activated carbons.[3] With increasing awareness of the problem of air and water pollution by industrial wastes, carbonaceous materials are finding new applications in the removal of a wide spectrum of unwanted chemical species. In these applications, carbons initiate conversions of pollutants to less toxic or nontoxic chemical species. For example, the oxidation of SO_2, NO, H_2S are industrial processes for the simultaneous removal of these species, especially from flue gases downstream of an SO_2 scrubbing process.[8]

Few fundamental studies have been published on the mechanisms of most of these catalytic reactions and the nature of the active sites is usually unknown. In general, many of the catalytic properties of carbon can be understood in terms of textural properties (e.g. surface area, pore shape and pore size), structure, electronic behavior, and surface chemistry, which in turn, depend on treatment and preparation. In many instances, these considerations suggest how selecting and pretreating a carbon might enhance its activity, capacity, and selectivity as a catalyst or adsorbent. To mention a few examples, the decompositions of hydrogen peroxide[110] and nitrous oxide[117] were suggested to be controlled by the presence of surface complexes. On the other hand, the microporosity of

carbons has been suggested to be very important in the catalyzed oxidation of hydrogen sulfide.[72,73]

One problem which will emerge in the consideration of carbons as catalysts is that of impurities in the carbon. Traces of impurities may have a large effect on the catalytic behavior of a given carbon. For instance, Cariaso and Walker[74] found that impurities in the carbon could also have a strong influence on the carbon-catalyzed oxidation of hydrogen sulfide.

Catalytic reactions involve adsorption of one or more reactants on the carbon surface. The course and extent of such reactions, therefore, are often found to be related to surface complexes already present on the carbon surface. The most common groups on the surface of carbons involve oxygen. The importance of surface complexes in the behavior of carbons has been reflected in several surveys of the field.[105,157-160] A real problem here involves the difficulty in quantifying accurately these functional groups on the carbon surface, so the exact catalytic role of carbon surface is often open to considerable question.

Although the state-of-the-art for carbon as a catalyst is not as well developed as for carbon-supported catalysts, it is clear that the future will be promising once it is understood that carbon offers unparalleled flexibility in tailoring catalyst properties to specific needs. However, the future growth of the use of carbon materials in catalysis will depend on the better understanding of the role of carbon surface chemistry and the clear identification of the catalytically active sites for given reactions, which can then be exploited in the design of truly unique catalysts.

2.2.1. Catalysis by carbons of redox reactions

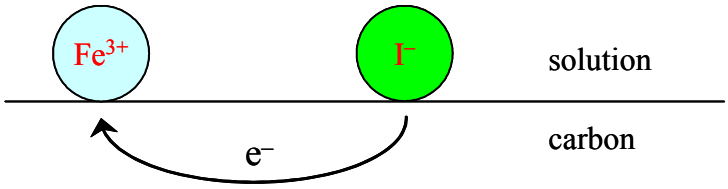

Figure 2.6. Catalytic mechanism of electron transfer through the carbon for the reaction between Fe(III) and iodine ions (Adapted from Spiro[10]).

An electrochemical mechanism was proposed to account for the widespread catalysis by carbons of redox reactions in solution.[13] In this mechanism both reactants sit on the surface, not necessarily on adjacent sites, and the electrons are transferred from the reducing to the oxidizing species through the solid catalyst, as depicted in Figure 2.6. The catalyst acts simply as an adsorbent and a conductor of electrons. This mechanism is important because it is a common catalytic mechanism of noble metal catalysts and perhaps they can be replaced for some uses by carbons.[20]

In the electrochemical model the reaction is split into its component half-reactions. In the presence of both couples the catalyst adopts an appropriate "mixture" or "mixed" potential (a potential of zero net current) at which the rate (i.e., the current) of both half-reactions is the same. The rate is identical to that at which electrons are transferred through the carbon and it is therefore also the rate at which the carbon catalyzes the overall heterogeneous reaction. From the electrochemical point of view, the cathodic current due to one couple must equal the anodic current of the other couple at the carbon surface at the mixture potential. The catalytic rate equation can thus be derived from the electrochemical theory. It is worth noting that the rate constant is no longer independent of concentration, unlike the case of other bimolecular surface reactions.[20]

One typical example of a carbon-catalyzed redox reaction is the reaction of Fe(III) and iodine ions.[13] The initial heterogeneous rates at 25 ºC can be represented by the equation

$$R = k \cdot m\left[\mathrm{Fe}^{3+}\right]^{0.87}\left[\mathrm{I}^{-}\right]^{0.51} \tag{2.32}$$

where m is the mass of the carbon. One could easily misunderstand this outcome as indicative of a Langmuir-Hinshelwood mechanism with two reactants adsorbed next to each other by Freundlich isotherms, a warning against too facile an interpretation of the observed rate law.

2.3. Reduction of nitrobenzene by hydrazine

The transformation of a nitroaromatic compound to the corresponding aromatic amine is an important synthetic and industrial process. For instance, the reduction of nitrobenzene is used on a large scale today for the production of aniline—an important feedstock for manufacturing polyurethane foams, dyes, rubber, pesticides, drugs, photographic chemicals, varnishes and explosives. The reduction of nitroaromatic compounds is also significant for hazardous waste treatment.[161] This transformation can be accomplished by using a variety of reducing agents which have been reviewed and discussed extensively.[162] Hydrazine as a reducing agent for the conversion of nitroaromatic compounds to aromatic amines has been investigated.[163] The hydrazine reduction of nitrobenzene follows the overall reaction:

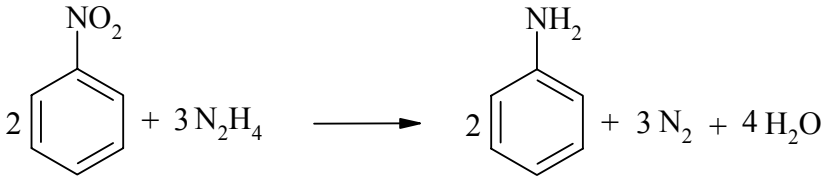

$$\Delta H_f^\circ = -151\,\text{kcal/mol}\,C_6H_5NO_2 \qquad (2.33)$$

Hydrazine is an attractive reducing reagent for the reaction because the reduction is clean and complete. The by-products from the catalyzed hydrazine reduction, nitrogen and water, are easily separated from the aromatic amine and are not environmentally hazardous.

Table 2–1. Selected studies of catalyzed nitrobenzene reduction by hydrazine

Catalyst	Nitrobenzene moles	Hydrazine equivalents	Time (hrs)	*T* (ºC)	Yield (%)
Zn-Cu (2 g):[164]					
prepared	0.01	4	2	25	86
commercial	0.01	4	2	25	7
Fe-Cu-$(NH_2)_2H_2O$[164]	0.01	4	2	25	71
Cu-$(NH_2)_2H_2O$[164]	0.01	4	2	25	42
Montmorillonite (3 g)[165]	0.01	6.25	3	78	85
Graphite (3 g)[166]	0.01	2	2	78	95
$NaNO_3$-C[167]	0.01	6	2	78	87
Oxidized C (3 g)[168]	0.24	5.25	4		80

This reaction is a thermodynamically favored process. The enthalpy change for the reaction is calculated to be –151 kcal/mol $C_6H_5NO_2$ at 25 ºC. In spite of the strongly

favorable thermodynamics, this reaction does not occur in uncatalyzed homogeneous solution. In fact, the first reported reduction of nitrobenzene with hydrazine hydrate, carried out in 1893 by Rothenburg[169] in the absence of a catalyst, achieved very low yields.

Nitrobenzene, as well as other nitro compounds, is reduced with great specificity and efficiency using hydrazine and a catalyst.[163] Table 2–1 compares the reduction of nitrobenzene by hydrazine over some selected catalysts. Metal catalysts used for the hydrazine reduction of nitroaromatic compounds include platinum, palladium, ruthenium, and Raney nickel, among others.[163] Endrey and Reilly[170] observed the catalytic action of carbon black on the reduction of nitroaromatic compounds. In 1985 it was reported that graphite, in large amounts, is an effective catalyst for the reduction of aromatic nitro groups by hydrazine in refluxing ethanol.[166] One advantage over conventional methods is the elimination of use of expensive metals and improvements on reaction conditions as well as yield. The reduction has also been reported on carbon activated with $FeCl_3$ or by the presence of nitrate ion.[167,171] Oxidized carbons have also been used as catalysts and the reported yields are lower than those obtained with graphite.[168] More recent reports showed that the reduction of nitroaromatic compounds by hydrazine is catalyzed by carbon blacks (e.g. Black Pearls L) and graphite.[1] The reaction was optimized to provide complete conversion to the amine without the formation of side products.

2.3.1. Stepwise reaction pathway

The reduction of nitrobenzene may proceed in a stepwise fashion through a

nitrosobenzene and β-phenylhydroxylamine intermediates.[163]

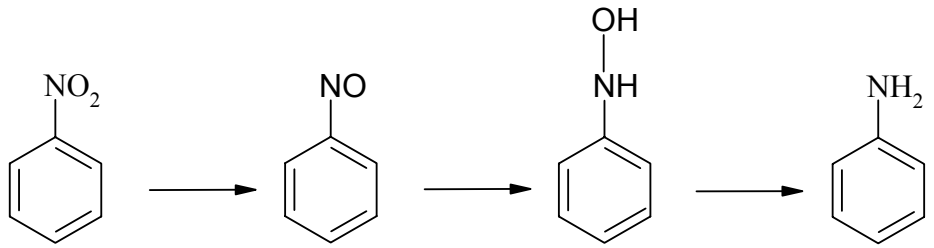

For example, during the reduction of nitrobenzene by hydrazine catalyzed by palladium on charcoal, nitrosobenzene was postulated but not observed.[172] It is possible that once formed the nitrosobenzene is rapidly transformed to the β-phenylhydroxylamine. This pathway has been supported by isolation of a phenylhydroxylamine and formation of coupled products (azobenzene and azoxybenzene), which are attributed to the reaction of nitrosobenzene and/or phenylhydroxylamine intermediates.[172] The reaction may stop with the formation of coupled products or the coupled products may be further reduced, depending on the pH of the solution.[173] Formation of phenyltriazine as an intermediate has been suggested for the Raney nickel catalyzed nitrobenzene reduction by hydrazine hydrate, but there is no evidence to support triazine formation.[174]

2.3.2. Electrochemical mechanism

The nitrobenzene reduction by hydrazine may proceed by redox reactions, comparable to an electrochemical reaction.[20] The electrochemical reduction of nitrobenzene to phenylhydroxylamine proceeds in a single four-electron overall process at all pH values.[173]

$$C_6H_5NO_2 + 3H_2O + 4e^- \rightarrow C_6H_5NHOH + 4OH^- \qquad (2.34)$$

In basic solutions, aniline has been observed to form at various electrodes along with azoxybenzene, azobenzene, and hydrazobenzene.[175-177]

The electrochemical oxidation of hydrazine in alkaline aqueous solutions is represented by the overall equation[178]

$$N_2H_4 + 4OH^- \rightarrow N_2 + 4H_2O + 4e^- \quad E° = +1.16\,\text{V vs. NHE} \quad (2.35)$$

Mostly, one oxidation peak is found, corresponding to the four-electron process to yield nitrogen as the final product. This reaction was proposed to proceed via sequential oxidation steps involving the formation of either the ion $N_2H_3^+$ or the radicals N_2H_3 and N_2H_2, among other intermediates.[178]

Larsen *et al.*[1] provided evidence that the carbon-catalyzed reduction of nitrobenzene by hydrazine occurs by Spiro's electron transfer mechanism. If correct, this mechanism is important for two reasons. First, noble metals catalyze many reactions by this mechanism; these metals can in principle be replaced by an appropriate carbon that acts by the same mechanism. Second, there is a possibility that this behavior can be generalized to other reactions.

The most compelling evidence for this mechanism in carbon-catalyzed reduction of nitroaromatic compounds can be summarized briefly. The identification of phenylhydroxylamine by NMR during the reduction reaction indicated that the initial nitro group reduction is a four-electron process. Hydrazine can act as a two-electron reducing agent and the intermediate formed in the two-electron process (diimide HN=NH) has been observed in this reaction. If hydrazine (two-electron reducer) is to react with a nitroaromatic compound requiring four electrons in the first step, a ternary complex of two hydrazine molecules and one nitroaromatic molecule is required. This is

highly improbable. Carbons catalyze the reaction by adsorbing both hydrazine and nitroaromatic molecules and by allowing the necessary electron flow to occur. This raises the possibility that carbons will be effective catalysts for many reactions in which the number of electrons required for the oxidation and reduction steps is not matched. There is a conflict between the trapping of diimide (a two-electron intermediate) and the normal four-electron kinetics of the hydrazine in carbons in base solutions. Careful kinetics can resolve this issue.

As we move towards a more complete understanding of this reaction mechanism, we are moving towards exciting possibilities, not only the possibility of replacing metal catalysts by carbons, but also the possibility of developing new reactions catalyzed by carbons.

2.4. Decomposition of hydrazine

The decomposition of hydrazine may occur during the hydrazine reduction of a nitroaromatic compound because many catalysts that are used for the reduction are also effective for hydrazine decomposition.[179] The decomposition of hydrazine is an important industrial reaction because of hydrazine's use as a monopropellant rocket fuel. Indeed, the consumption of hydrazine as high-energy fuel dominated the market through the 1960's. The transient decomposition of liquid hydrazine in a space vehicle forms a high-temperature gas mixture ejecting from the nozzle of the thruster to change the flight orbit or to regulate the flight attitude of the space vehicle.[180] The use of hydrazine in satellite attitude control is due to the low activation energy of its decomposition and the high

exothermicity of this reaction.[179]

Hydrazine, both in alkaline and in acid solutions, is capable of undergoing thermal decomposition.[181] In the absence of hydrogen, the decomposition proceeds mainly through

$$3N_2H_4 \rightarrow 4NH_3 + N_2 \qquad (2.36)$$

Under ordinary circumstances this reaction does not take place readily, even though it is thermodynamically favored. The free energy change of this reaction was calculated to be –64.3 kJ/mol at 25 ºC.

Table 2–2. Relevant studies on heterogeneous decomposition of hydrazine in the liquid phase.

Author(s)	Catalyst	*T* (K)	Condition(s)	Stoichiometry‡
Audrieth and Jolly[182]	Raney Ni	274-327	Liquid	(2.36)&(2.39)
Sayer[183-186]	Ir on Al_2O_3	273-327	15-100% H_2O	(2.36)
	Rh on Al_2O_3			(2.38)
Davis and Sayer[187]	20 % Rh on Al_2O_3	273-323	0-100% H_2O	(2.38)
Sayer[188]	20% Ru on Al_2O_3	273-323	0-100% H_2O	(2.36)&(2.38)
Sayer[189]	20% Pd on Al_2O_3	273-327	1.2-3.1 *M* H_2O	(2.38)
	20% Pt on Al_2O_3			
Larsen *et al*.[12]	Carbon	355	*Iso*propanol solution	(2.36)

With a variety of catalysts such as noble metals, hydrazine decomposition does

‡ The stoichiometry of the reaction is determined by Eqs. (2.36)-(2.39).

take place readily in accordance with the above equation.[179] In addition to molecular nitrogen and ammonia, hydrogen was also observed as product of the catalytic decomposition of hydrazine, and at least three other equations can be used to describe the heterogeneous decomposition of hydrazine:[179]

$$3N_2H_4 \rightarrow 2NH_3 + 2N_2 + 3H_2 \quad (2.37)$$

$$2N_2H_4 \rightarrow 2NH_3 + N_2 + H_2 \quad (2.38)$$

$$N_2H_4 \rightarrow N_2 + 2H_2 \quad (2.39)$$

These reactions may take place simultaneously or preferentially. In general, the composition of the gases liberated will depend upon the nature of the catalysts employed and the reaction conditions.[179] For example, a product gas composition corresponding to Eq. (2.38) was found by using platinum black as a catalyst. Upon addition of alkali, the gas composition approached that expected for Eq. (2.37).[190,191] Other investigations did not yield any detectable amount of hydrogen, which supports Eq. (2.36).[192] Apparently, Eq. (2.36) describes the overall reaction when hydrazine decomposition proceeds at lower temperatures, while the reaction described by Eq. (2.38) becomes evident only at higher temperatures.[179] Table 2–2 gives a group of relevant publications devoted to the study of heterogeneous hydrazine decomposition in the liquid phase.

Vitvitskaya and Grabovskaya[193] first observed the catalytic decomposition of hydrazine on AG-3 activated carbon. Larsen *et al.*[12] reported the carbon-catalyzed decomposition of hydrazine during the study of the carbon-catalyzed reduction of nitroaromatic compounds by hydrazine.

2.4.1. Nondissociative bimolecular mechanism

Sayer[185] proposed the following mechanism for hydrazine decomposition in aqueous solution on Shell 405 catalyst:

$$N_2H_{4(aq)} \rightarrow N_2H_{4(ads)} \quad (2.40)$$

$$N_2H_{4(ads)} + N_2H_{4(aq)} \rightarrow N_2H_{2(ads)} + 2NH_3 \quad (2.41)$$

$$2N_2H_{2(ads)} \rightarrow N_2H_{4(ads)} + N_{2(g)} \quad (2.42)$$

$$N_2H_{2(ads)} \rightarrow H_{2(g)} + N_{2(g)} \quad (2.43)$$

The hydrazine molecule may be adsorbed on the surface through the two lone pairs of electrons. An adsorbed hydrazine molecule transfers two hydrogen atoms to another hydrazine molecule in solution to cleave the N-N bond and form two molecules of ammonia and an adsorbed *cis*-diimide (N_2H_2) on the surface. The diimide then reacts by either one of two possible mechanisms. The first mechanism involves the disproportionation reaction with neighboring diimide forming nitrogen that then desorbs and one molecule of hydrazine, which remains adsorbed on the surface. The second mechanism for the decomposition of diimide occurs if diimide adsorbed on the surface cannot find an adjacent diimide to react with, so the diimide molecule decomposes directly to nitrogen and hydrogen. The diimide disproportionation to hydrazine is well established and is a significant complication in the use of diimide to reduce double bonds.[194]

Sayer's suggestions are consistent with isotope studies of hydrazine decomposition using ^{15}N-labeled hydrazine.[185] In these studies, the nitrogen produced consisted only of ^{15}N-^{15}N or ^{14}N-^{14}N, indicating that the N-N bond of the hydrazine

remained intact during the decomposition reaction.

2.4.2. Dissociative bimolecular mechanism

Fouché *el al*.[195] proposed the mechanism illustrated below based on their kinetic studies on iridium-alumina catalysts:

$$N_2H_{4(aq)} \rightarrow N_2H_{4(ads)} \quad (2.44)$$

$$2N_2H_{4(ads)} \rightarrow 2NH_3 + 2NH_{(ads)} \quad (2.45)$$

$$2NH_{(ads)} \rightarrow N_2H_{2(ads)} \quad (2.46)$$

$$N_2H_{4(ads)} + N_2H_{2(ads)} \rightarrow N_{2(g)} + 2NH_3 \quad (2.47)$$

Diimide is assumed as an intermediate in the decomposition of hydrazine. However, the mechanism through N-N bond splitting proposed by Fouché *el al*. is not supported by isotope studies.

2.4.3. Electrochemical mechanism

Spiro and Ravnö[196] first proposed that hydrazine decomposition may proceed by redox reactions in acid or neutral solutions, where the metal catalyst acts simply as an electron-conductor. Hydrazine decomposition could take place by a redox reaction in basic solutions as well. The standard redox potentials for half reactions involving hydrazine have been calculated[181]

$$N_2H_4 + 4OH^- \rightarrow N_2 + 4H_2O + 4e^- \quad E° = +1.16\,\text{V vs. NHE} \quad (2.48)$$

$$N_2H_4 + 2H_2O + 2e^- \rightarrow 2NH_3 + 2OH^- \quad E° = +0.15\,\text{V vs. NHE} \quad (2.49)$$

The overall reaction is spontaneous (E^o = + 1.31 V vs. NHE).

Chapter 3.

Experimental Techniques

3.1. Carbonaceous Samples

A variety of carbonaceous materials were examined as catalysts. They included:

a) Carbon blacks: Monarch 1000, Monarch 1300, Regal 400R, Vulcan XC-72 R, Black Pearls 2000, and Mogul L (Cabot Corporation).

b) Activated carbons: Nuchar SN-20, Nuchar SA-20, Nuchar SA, and Nuchar WV-A 900 (MeadWestvaco Corporation). Darco G60 and Norit SX2 (Norit Americas, Inc.)

c) Charcoals: Coconut (Fisher Scientific, Inc.) and Bone (Ebonex Corporation)

d) Natural graphite (Fisher Scientific, Inc.)

Carbon black[197] is a very fine particulate form of elemental carbon, consisting of well-developed planes of carbon atoms (graphene sheets) stacked roughly parallel to one another, but randomly in orientation with respect to adjacent layers to form spherical particles, which in turn form structures or aggregates. All carbon blacks are produced either by incomplete combustion or thermal decomposition (vapor-phase pyrolysis) of a hydrocarbon feedstock, such as heavy petroleum distillates and residual oils, coal-tar products, natural gas and acetylene. The carbon blacks used here (all from Cabot Corporation) are oil-furnace blacks that exhibit a rather wide range of particle aggregation in which carbon particles are fused into grape-like clusters and/or reticulate

chains or branches. Of all carbon blacks used in this study, Black Pearls 2000 has the highest structure or particle aggregation (average structure level) as determined by the dibutyl phthalate absorption number (330 cc/100 g), as shown in Table 3–1. Carbon blacks from Cabot Corporation are produced by subjecting heavy residual oil feedstock to extremely high temperatures (> 1500 °C) in a carefully controlled combustion process.

Table 3–1. Selected properties of carbon blacks[198]

Carbon black	pH	DBP Oil Absorption (cc/100 g)	Particle size (nm)
Monarch 1300	2.5	100	13
Monarch 1000	3.0	110	16
Mogul L	3.0	62	24
Regal 400R	4.0	71	25
Black Pearls 2000	8.6	330	12
Vulcan XC-72R	8.5	192	30

Activated carbons,[3,199] another form of amorphous carbon, consist of a twisted network of defective layers or stacks of graphene sheets that are less regularly organized than in carbon blacks, and cross-linked by aliphatic bridging groups. They are produced by a process called “activation” where a number of naturally occurring and synthetic carbon-containing substances (coal, peat, wood, nutshells, coconut husks, animal bones, etc.) are first carbonized. The carbon so produced (charcoal) is then washed with acid to remove impurities and "activated" by heating in steam at 600–900 °C or in air. Due to the activation process, the carbon layer planes are separated by micropores, most of which

are slit-shaped. Depending on the precursor, there may also exist a large fraction of the pore volume in meso- and macropores. Activated carbons from MeadWestvasco Corporation are manufactured from hardwood, so they are inherently low in extractable minerals and lower in moisture than other carbons.

Charcoal[16] is the raw material used to produce activated carbon. It contains other organic residues, is much less porous, and has a lower surface area than activated carbons. The relevant properties of these carbons are summarized in Table 3–2 and Table 3–3.

Table 3–2. Selected compositional properties of carbon samples used

				% Elemental analysis (dry basis)				
Carbon	**Type**	**Source**	**% Ash**	**C**	**H**	**N**	**S**	**O**
Graphite		Fisher	1.43	98.85	~ 0	0.07	0.05	~ 0
Coconut charcoal	Charcoal	EM Science	5.38	92.01	0.04	0.55	0.14	1.89
Bone charcoal	Charcoal	Ebonex	83.83	13.66	0.32	0.69	0.06	1.44
Nuchar SA	Activated	Westvaco	4.26	89.60	1.67	0.48	0.02	3.97
Nuchar SA-20	Activated	Westvaco	3.81	89.78	1.86	0.46	0.01	4.08
Nuchar SN-20	Activated	Westvaco	5.62	88.25	1.44	0.40	0.01	4.28
Nuchar WV-A 900	Activated	Westvaco	3.59	89.99	1.75	0.48	0.01	4.18
Norit SX2	Activated	Norit	3.95	93.66	0.04	0.84	0.18	1.34
Darco G60	Activated	Norit	4.76	92.38	0.08	0.72	0.18	1.87
Mogul L	Black	Cabot	0.34	96.13	0.09	0.25	0.95	2.25
Regal 400R	Black	Cabot	0.17	97.76	~ 0	0.35	0.91	0.81
Black Pearls 2000	Black	Cabot	0.47	96.68	0.10	0.46	1.58	1.18
Monarch 1300	Black	Cabot	0.50	94.27	0.11	0.28	0.64	4.20
Monarch 1000	Black	Cabot	~ 0	94.54	0.06	0.39	0.93	4.08
Vulcan XC-72R	Black	Cabot	0.31	99.06	~ 0	0.39	0.62	~ 0

3.1.1. Characterization and Techniques

The BET surface areas, *S*, were determined by N_2 physisorption at 77 K using a Quantachrome Autosorb 1 analyzer (Table 3–3). Prior to the adsorption experiments, samples were outgassed at 150 ºC for 10 hrs. The BET equation was used to calculate the apparent surface area from nitrogen adsorption data in the range $0.1 < P/P_0 < 0.3$.[200] The experimental error associated with these measurements was in the order of ± 10 m^2/g, as determined from the standard deviation of three independent trials.

The external surface area or non-microporous surface, S_{ext}, was determined with the deBoer *t*-method using nitrogen adsorption isotherms in the range $0.2 < P/P_0 < 0.5$. This surface corresponds essentially to the walls of the meso- and macropores in activated carbons. The determination of the external surface using deBoer *t*-method is a standard technique for carbon blacks.[200] For activated carbons other methods, also involving the adsorption isotherm, are more realistic.[201] However, the various techniques used for the determination of the external surface of activated carbons are fairly consistent and produce an overall scatter of 10–15%, which has been interpreted as due to possible errors inherent to the individual techniques.[202] Other textural parameters were evaluated from nitrogen adsorption isotherms: the total pore volume, V_p (amount of N_2 adsorbed at a relative pressure of $P/P_0 = 0.99$), and the mean pore radius, *r* (estimated from the equation $r = 2V_p/S$).[200]

Elemental analysis of the carbon samples was carried out with a LECO CHN-600 elemental analyzer, a LECO SC-132 sulfur determinator and a LECO MAC-400 proximate analyzer. The method consists in the determination of the moisture, volatile

matter, and ash yield using the LECO MAC-400 proximate analyzer. Moisture content is determined by establishing the loss in weight of a sample when heated between 104–110ºC. This quantity is used for calculating other analytical results to a dry basis. Ash yield is determined by weighting the residue remaining after burning the sample between 700–750ºC in the presence of air. Volatile matter is determined by establishing the loss in weight resulting from heating a sample at ~ 950ºC. The total sulfur content, and the total carbon, hydrogen and nitrogen contents are determined using the LECO SC-132 sulfur determinator and the LECO CHN-600 elemental analyzer, respectively. C, H, and S are measured by infrared absorption while N is determined by thermal conductivity. The experimental error associated with the elemental analysis is ~ ± 2%.

Table 3–3. Selected textural properties of carbon samples used

Carbon	Type	S (m^2/g)	S_{ext} (m^2/g)	V_p (cm^3/g)	r (nm)
Graphite		11	8.8	0.043	7.77
Coconut charcoal	Charcoal	934	41	0.527	1.13
Bone charcoal	Charcoal	112	109	0.231	4.13
Nuchar SA	Activated	1350	382	1.060	1.57
Nuchar SA-20	Activated	1342	355	1.211	1.81
Nuchar SN-20	Activated	1193	340	1.008	1.67
Nuchar WV-A 900	Activated	1403	374	1.134	1.62
Norit SX2	Activated	750	171	0.639	1.70
Darco G60	Activated	655	173	0.577	1.76
Mogul L	Black	148	148	0.796	10.75
Regal 400R	Black	96	96	0.745	15.52
Black Pearls 2000	Black	1448	447	3.268	4.52
Monarch 1000	Black	350	289	1.088	6.21
Monarch 1300	Black	494	301	0.867	3.51
Vulcan XC-72R	Black	229	102	0.685	5.98

The bulk oxygen content is determined by weight difference. Therefore, it is

expected that this quantity carries a propagated error from the determination of the content of the other quantities involved in its calculation. The pH values at 24 ºC of the "as received" carbon samples were determined according to the ASTM method D1512, and using a pH meter (Beckman Φ240) with a precision of ± 0.01.

3.2. Kinetic Measurements

The reduction of nitrobenzene (99.5 vol%, Fischer Scientific, Inc.) by hydrazine (98.5 vol%, Alfa Aesar, Co.) using carbon catalysts was studied. All compounds were used as received. The reactions were conducted in refluxing[§] *iso*propyl alcohol (Fisher Scientific, Inc.), which was also used as received. The reaction is then conducted at the normal boiling point of *iso*propanol (~ 82 ºC). *Iso*propanol was chosen as the solvent because it is inexpensive and environmentally sound. In addition, the aromatic amines are readily isolated from *iso*propanol due to its low boiling point.

The experimental setup for kinetic measurements is shown in Figure 3.1. A three neck 100 mL round bottom flask with 24/40 joints was used with a reflux condenser connected to a gas burette, a 30 mL pressure-balanced addition funnel, and a thermometer. The gas burette was composed of two 1L volume calibrated addition funnels connected together at their bottoms with Tygon® tubing. The amount of gas produced as a function of time was measured using the gas burette at a constant pressure

---

[§] Refluxing is the simplest and most convenient way to control the temperature of the reaction mixture by using a reaction solvent that has a boiling point within the desired temperature range for the reaction.

of 1 atm. This is achieved by adjusting the level of the manometric liquid (water), changing the height of the burette. The gas volume is measured with an experimental error ± 5 mL, and each experiment was performed at least three times from which deviations of the experimental data (i.e., gas volume at a particular time) were determined to be less than 5%.

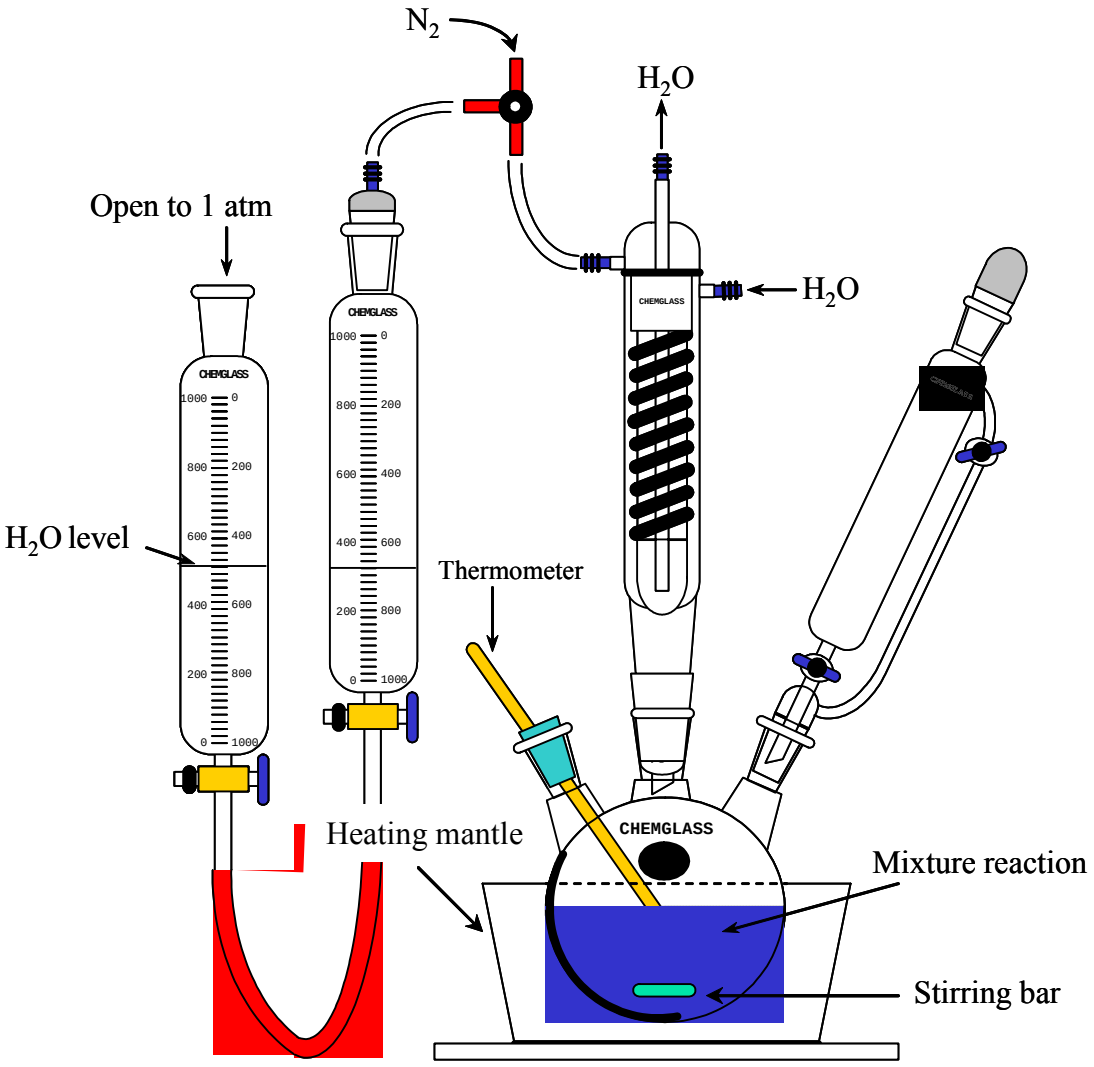

Figure 3.1. Schematic diagram of the experimental setup used to follow the reaction kinetics of the nitrobenzene reduction and hydrazine decomposition.

The standard procedure used for the nitrobenzene reduction follows. All reactions were carried out in a hood and care was taken to ensure safety when working with

hydrazine. The carbon catalyst was added to a solution of nitrobenzene and *iso*propanol in the round bottom flask. A magnetic stir bar and a magnetic stir plate were used to mix the reactants. Hydrazine was placed in the addition funnel. Nitrogen was passed through the system from the top of the reflux condenser for 20 minutes before the ground glass stopper was placed on the addition funnel. All of the ground glass joints were thoroughly greased to insure a tight seal. After the system has been purged with nitrogen, the flask was heated using an electric heating mantle controlled with a variable power controller. The system was brought to reflux and connected to the gas measuring apparatus. When the system was stable, determined by no change in gas volume for at least 30 minutes, the reaction was initiated by the addition of hydrazine to the refluxing mixture of the compound and carbon in *iso*propanol. The reaction was followed by measuring the volume of water displaced from the gas burette at atmospheric pressure.

In a typical experiment, 0.017 moles of nitrobenzene, 0.025 moles of hydrazine, 0.70 g of carbon material and 25 mL of *iso*propanol was charged into the measuring apparatus. The mixture was refluxed until the produced gas volume remained constant. When the reaction was complete, the product mixture was filtered by suction filtration to remove the carbon catalyst.

The decomposition of hydrazine on several carbonaceous catalysts was also examined. The procedure and apparatus were the same as for the reduction of nitrobenzene, except that the nitrobenzene was not included. In addition, 20 mL of *iso*propanol was used to increase the initial concentration of hydrazine with a subsequent increase of the reaction kinetics.

Measurement of the amount of gas produced from the reaction as a function of

time was used to determine a rate of reaction. The rate of gas production is approximately equal to the rate of nitrobenzene reduction if the rate of hydrazine decomposition is slow compared to the reduction rate and the adsorption equilibrium is established instantaneously.

Chapter 4.

Carbon-catalyzed decomposition of hydrazine

4.1. Kinetics of the reaction

Figure 4.1 shows plots of gas volume versus time for refluxing solutions of hydrazine in *iso*propanol to which the indicated carbon had been added. The gas evolution plots show simple time dependence. In the absence of added carbon, hydrazine solutions are stable under the reaction conditions. The production of gas upon addition of carbons to otherwise stable hydrazine solutions demonstrates carbon-catalyzed decomposition. All of the carbons catalyze the reaction to different extents. Based on the amount of gas produced at a given time, we found that graphite is the least effective catalyst and Nuchar WV-A 900 is the most effective catalyst (see Table 4–1).

Nitrogen and ammonia are the only decomposition products according to previous studies by Larsen *et al.*[12] on Black Pearls L (carbon black). The decomposition of hydrazine on a supported iridium catalyst (the Shell 405 catalyst) was also shown to yield nitrogen and ammonia, and the overall reaction is represented by Eq. (2.36).[183] If the overall reaction over carbon catalysts follows Eq. (2.36), the total gas volume expected (V_C) from 0.025 moles of hydrazine used is about 1050 mL if ammonia is in the gas phase or V_C = 210 mL if ammonia remains totally dissolved in *iso*propanol and the water in the gas burette. For some carbons, the observed gas volumes are somewhat larger than the amount of N_2 expected. For example, as shown in Figure 4.2, the amount of gas

produced in the presence of Nuchar WV-A 900 was on the order of 430 mL; twice the amount of N_2 gas expected.

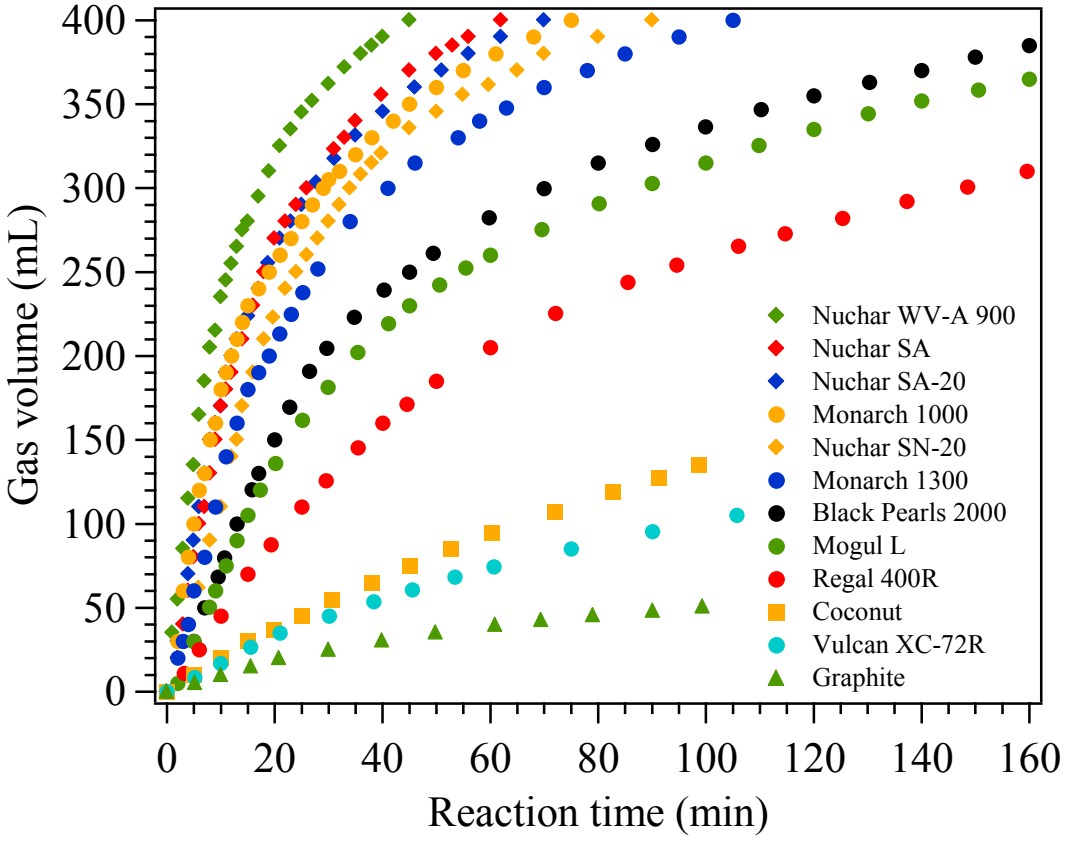

Figure 4.1. Gas evolution from hydrazine decomposition in refluxing *iso*propanol catalyzed by carbons.

There are three possibilities for gases in addition to nitrogen. One is ammonia. Ammonia produced in the decomposition reaction is first dissolved in *iso*propanol, so initially only nitrogen is expected to be produced. At 80 ºC, ~400 mL of ammonia dissolve in 1L of *iso*prpanol.[203] After *iso*propanol saturation with ammonia, the reaction proceeds with the production of both nitrogen and ammonia in the gas phase. However, the solubility of ammonia in water is quite high. At 24 ºC, 692 mL of ammonia gas dissolves in 1 mL of water.[204] Therefore, ammonia produced in the gas phase, after

*iso*propanol saturation, is expected to dissolve quickly in the water of the gas burette.

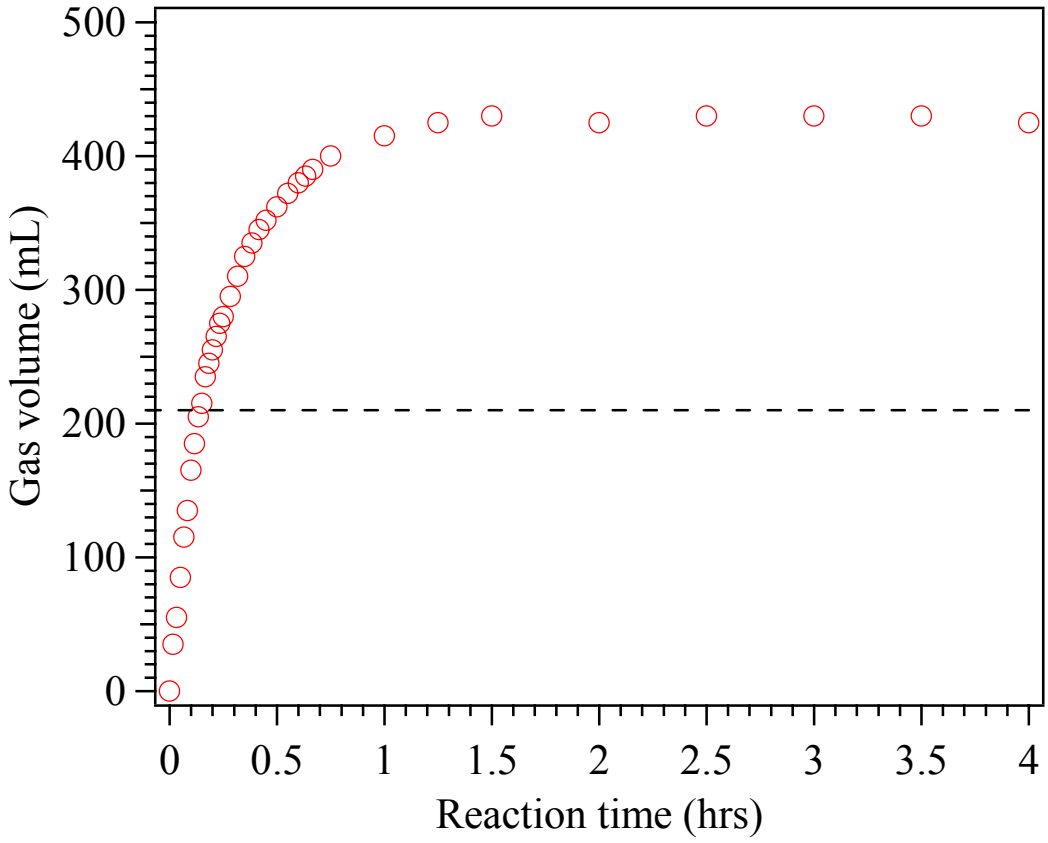

Figure 4.2. Gas evolution from hydrazine decomposition in refluxing *iso*propanol catalyzed by Nuchar WV-A 900 (activated carbon).

The second possibility for the additional gas produced is hydrogen, if the reaction is proceeding by pathways in addition to Eq. (2.36). However, the absence of hydrogen was demonstrated for Black Pearls L using GC techniques.[12]

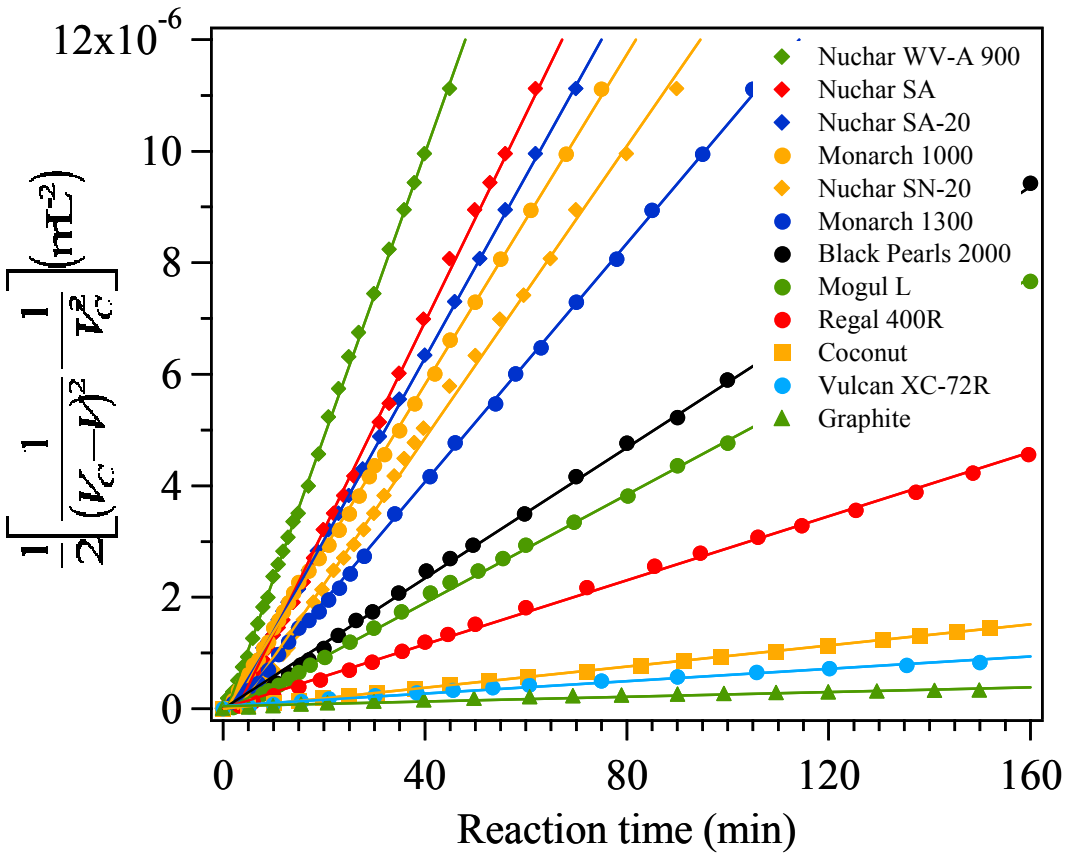

Figure 4.3. Third-order plots for the decomposition of hydrazine in the presence of several carbon catalysts (V is the gas volume at time t, and V_C is the calculated final gas volume using the stoichiometry of Eq (2.36). Solid lines are linear fits to the data.

The third possible explanation for the extra amount of gas produced is that a simultaneous reaction is taken place which is also contributing to the production of gases. Szymanski and Rychlicki[64,65] reported that oxidized carbon and its metal cation-substituted forms catalyze the decomposition of *iso*propanol vapors. Dehydration of *iso*propyl alcohol vapor to propene and *iso*propyl ether, and dehydrogenation to acetone were observed in the temperature range 100º–190 ºC. The authors also found that the presence of adsorbed metal cations enhances the dehydrogenation activity at the expense of the total dehydration activity.[64] It was suggested that dehydrogenation activity requires the simultaneous presence on the carbon surface of acidic and basic Lewis sites, while

dehydration activity results from the presence of carboxylic acid groups of varying strength. This is consistent with the very low or no catalytic activity exhibited by ordinary (non-oxidized) activated carbons, which are basic carbons. Systematic studies are needed on the decomposition of *iso*propanol in the liquid phase over commercial carbons. So far, we have found no clear indication that this reaction is occurring during the decomposition of hydrazine.

To avoid the complications introduced by possible side reactions and ammonia in the gas phase, initial rates were used to analyze the reaction kinetics. At the beginning of the reaction, neither side reactions nor ammonia will contribute to the reaction rate. Surprisingly, the data were found to fit very well a third-order reaction in hydrazine, as shown in Figure 4.3. This is an interesting finding since termolecular reactions are very rare in heterogeneous catalysis. For instance, only one example third-order carbon-catalyzed reaction could be found in the literature: the racemization of *tris*(ethylenediamine)-cobalt(III) ion $[Co(en)_3]^{3+}$ by iodide in the presence of a carbon black.[38] On the other hand, the electrochemical oxidation of hydrazine on glassy carbon electrodes in acetonitrile[205,206] shows a third-order behavior where one-third of the hydrazine molecules are oxidized to N_2H_2 and the other two-thirds act as proton acceptors, but this not a reasonable mechanism for the hydrazine decomposition where there is no oxidative driving force.

Table 4–1. Kinetic parameters for the decomposition of hydrazine on different carbons

Carbon sample	$R \times 10^8$ (mol cm $^{-3}$ s^{-1})	V_{30} (mL)	% dec (30 min)
Graphite	0.069	25	2.5
Coconut	0.312	54	5.4
Nuchar SA	6.138	320	32.0
Nuchar SA-20	5.373	316	31.6
Nuchar SN-20	4.314	280	28.0
Nuchar WV-A 900	8.107	362	36.2
Mogul L	1.599	181	18.1
Regal 400R	0.947	126	12.6
Black Pearls 2000	1.949	205	20.5
Monarch 1000	4.872	305	30.5
Monarch 1300	5.223	260	26.0
Vulcan XC-72R	0.183	45	4.5

Several kinetic parameters were measured for each carbon catalyst; these are (1) the initial rate of reaction, R, (2) volume of gas evolved up to t = 30 min, V_{30}, and (3) percent decomposition at t = 30 min, (%dec = $V_{30}/V_C \times 100$). The results are colleted in Table 4–1. The varying initial rates (0.069–8.107)$\times 10^{-8}$ mol cm^{-3} s^{-1}, as shown in Table 4–1, also confirm the diversity of activity of the carbon catalysts. These differences could be associated with individual differences in the physicochemical properties of the carbon. This issue will be explored later in this chapter. Unfortunately, due to the differences in the reaction conditions employed (i.e., temperature, initial concentrations, etc.), we cannot compare the reaction rates obtained in this study with those in previous studies on metal catalysts.

4.2. Effect of impurities

Many of the carbon catalysts used in this study contain mineral matter, so it was necessary to determine whether any of the catalytic activity is due to the presence of minerals. Evidence that mineral matter plays no role in this reaction is provided by the scattered data in Figure 4.4, where the initial rate of the reaction is plotted as a function of the ash yield. As shown in this figure, carbon blacks with little or no ash yield (~0-0.5%) exhibit wide changes in the initial rates. For instance, the initial rate of the reaction on Monarch 1000 (~0% ash yield) is a factor of ~20 higher than that on Vulcan XC-72R (0.31% ash yield). Also, note the scattering of the data and the wide range of initial rate changes for carbons with ash yield over 3% with high surface area. This is the scattering observed for carbons with medium and low surface area. In addition, the highest initial rates are observed for carbons with high oxygen content. The relationship between the initial rates of the reaction and the oxygen content of the carbons will be discussed later in section 4.6.

Further evidence that the observed reaction is not due to minerals comes for the absence of catalysis by ash. On combustion, most of the carbons used yield some ash (see Table 3–2). Ash is the product of a variety of thermally driven reactions of mineral matter that occur while the carbonaceous portion of the carbon sample is undergoing combustion. Therefore, the composition of ash should resemble that of the oxidized portion of the mineral matter. Ash residue consists of silicates and aluminosilicates of alkali, alkaline earth and other metals such as iron. Some minerals will be oxidized, so the absence of catalytic activity by ash is not definitive. One experiment was carried out to detect the

possible role of mineral matter, by igniting an activated carbon (Nuchar SA, 4.26% ash yield) at 900 °C followed by the determination of the catalytic activity of the ash formed. We observed no detectable catalytic action when 0.3 g of ash was used, i.e., gas was not produced. This amount of ash is 10 times higher than that collected from the combustion of 0.7 g of carbon—the amount of carbon employed to produce the plots in Figure 4.1.

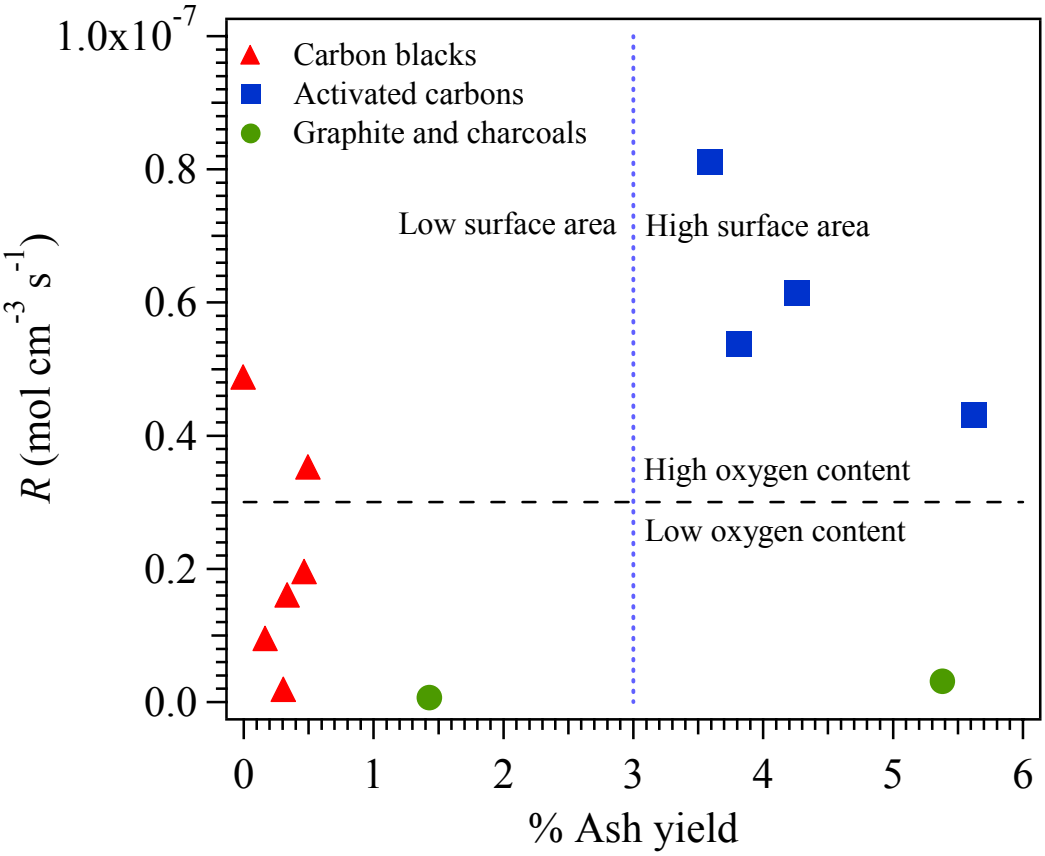

Figure 4.4. Effect of ash yield of carbon catalyst on the initial rate of hydrazine decomposition.

4.3. Variation of rate with mass of catalyst and stirring

The chemical reaction at the surface is likely to be rate-determining in heterogeneous catalysis of solution reactions.[20] It is clearly an essential part of a kinetic

investigation to ascertain whether any other factors (e.g., adsorption, desorption, diffusion) influence the rate of the overall catalytic process. Two main diagnostic criteria have been employed for this purpose:[20]

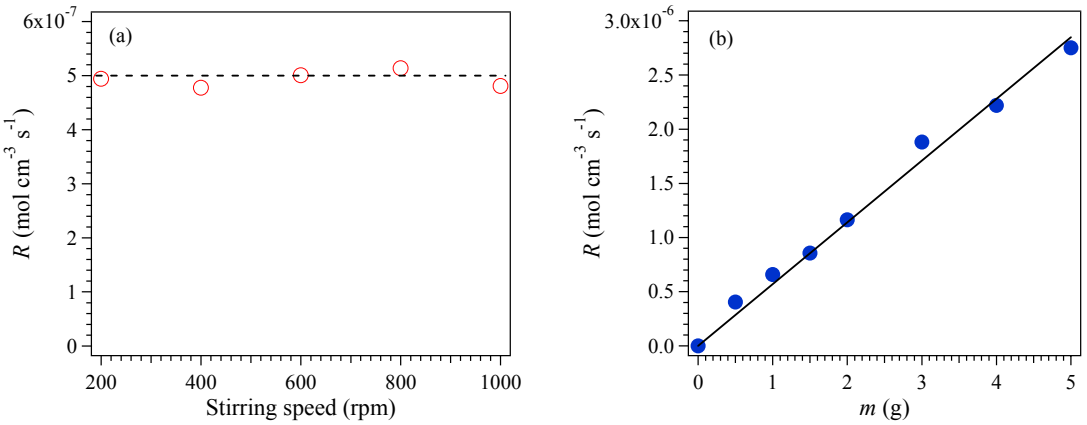

Figure 4.5. Effect of stirring (*left*) and carbon mass (*right*) on the initial rate of hydrazine decomposition over Nuchar SA activated carbon. Solid line is a linear fit of the the data and dashed line is a guide to the eye.

(1) Variation of stirring

More effective agitation of the solution around the solid catalyst does not affect surface-controlled processes but markedly increases external diffusion rates. Figure 4.5(a) illustrates how the overall reaction rate responds to increased agitation of the solution. The constant reaction rate over the experimental range of stirring speed indicates that the carbon-catalyzed hydrazine decomposition is NOT a diffusion-limited reaction but a surface-controlled reaction.

(2) Variation of catalyst area

The catalytic rate is usually directly proportional to the total surface area for reactions controlled by surface kinetics. This is clearly understood if one considers that the reaction rate is directly proportional to the frequency of effective collisions between

reactants. If the molecules can collide only at a surface then more molecules can collide per unit of time when there is a higher number of available catalytic active sites, which in turn, is determined by the surface area of the catalyst. For a given catalyst preparation, when not only surface heterogeneity but also particle size distribution is expected to be uniform from sample to sample, the most appropriate way to change the surface area is by changing the amount of catalyst used. Thus, for surface reactions, the reaction rates are usually directly proportional to the mass of catalyst. Figure 4.5(b) shows that the initial rate of hydrazine decomposition is indeed directly proportional to the amount of carbon used.

4.4. Effect of hydrazine concentration

The variations of the initial rate of carbon-catalyzed hydrazine decomposition with hydrazine concentration [N_2H_4] are shown in Figure 4.6 and Figure 4.7. As the hydrazine concentration is increased the reaction rate increased to saturation, i.e., the reaction rate did not change as the concentration varied. The reaction rate R and the concentration of hydrazine [N_2H_4] may be related by an expression of the form $R = k[N_2H_4]^n$, where k is a rate constant and n is the order of reaction. Writing this equation in the form $\log_{10} R = \log_{10} k + n \log_{10}[N_2H_4]$, we may plot the data in Figure 4.6 and Figure 4.7 in the form of $\log_{10} R$ with respect to $\log_{10}$ [N_2H_4] as in the insert to these figures. Linear fittings of these plots show that at hydrazine concentrations up to ~ 2 M the rate of decomposition is almost proportional to the concentration, the value of n being in the range 0.90-0.95 (i.e., $n \sim 1$). Above ~ 2 M the value of n falls, becoming zero for

high concentrations.

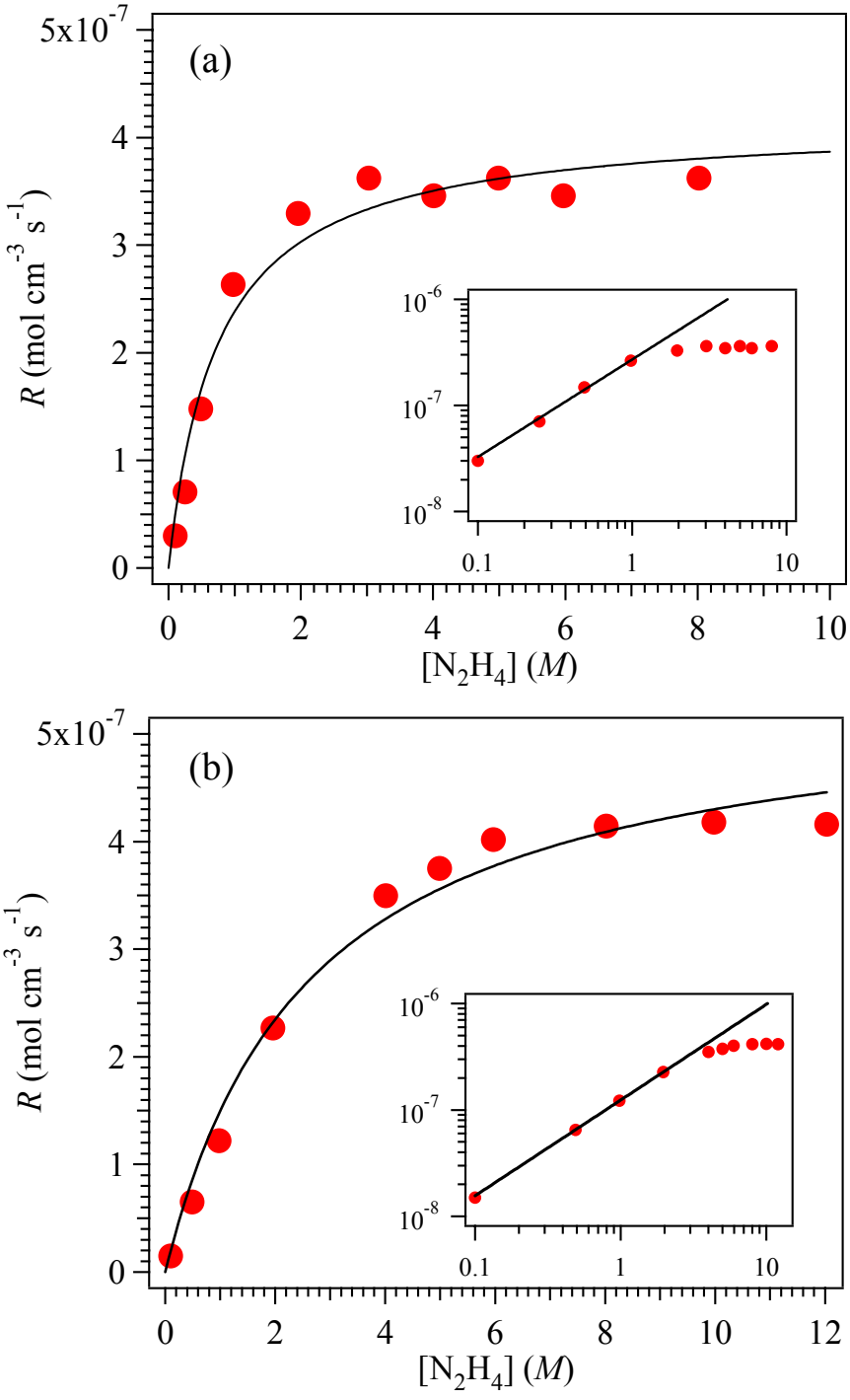

Figure 4.6. Effect of hydrazine concentration on the initial reaction rate of decomposition over carbon blacks: (a) Black Pearls 2000 and (b) Mogul L. Solid line is a fit of the data to Eq. (2.17). The insert shows the log-log plots of the same data with a linear fit at low hydrazine concentrations.

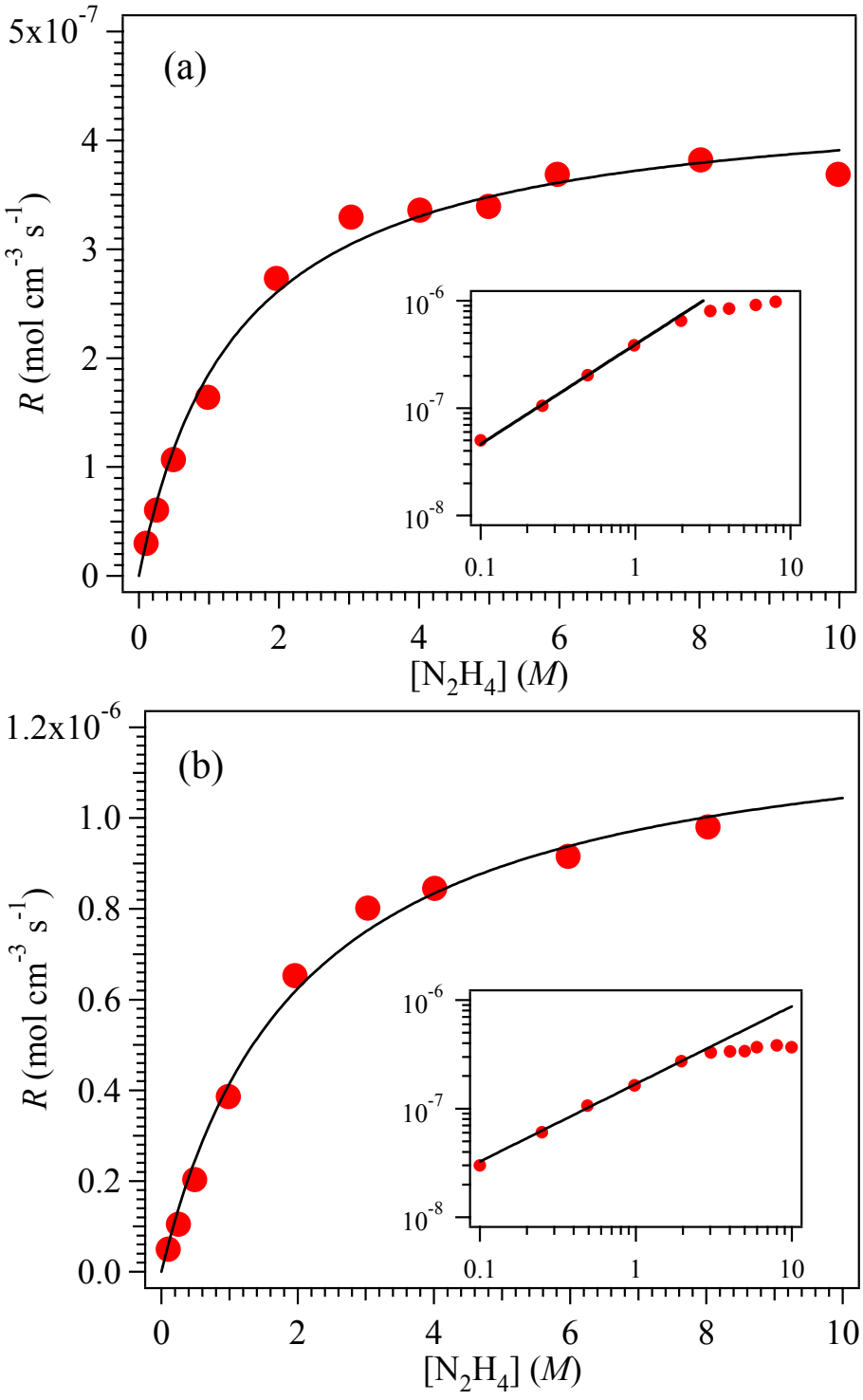

Figure 4.7. Effect of hydrazine concentration on the initial reaction rate of decomposition over activated carbons: (a) Darco G60 and (b) Nuchar SA. Solid line is a fit of the data to Eq. (2.17). The insert shows the log-log plots of the same data with a linear fit at low hydrazine concentrations.

Similar results were obtained in kinetic studies of the decomposition of hydrazine over a supported rhodium catalyst by Davis and Sayer,[186,187] and over platinum catalyst by Sayer.[189] In those cases, however, the authors found that the rate of decomposition is almost proportional to the square root of the hydrazine concentration, i.e, $n \sim 0.5$. According to the authors "the way in which the kinetics change with respect to hydrazine concentration indicates that the [dissociative] adsorption of hydrazine [in the form of amine radicals] on the catalyst surface is involved in the slow step of the reaction." It is worth noting that, unlike the case of carbons, hydrogen is a product of the hydrazine decomposition on rhodium and platinum catalysts.

Here, the relationships of reaction rates to concentrations as shown in Figure 4.6 and Figure 4.7 are commonly found in heterogeneous catalysis when the rate-controlling step of the surface reaction is either the (non-dissociative or molecular) adsorption of the reactant on the catalyst surface or the reaction of the adsorbed species on the surface (unimolecular surface reaction, cf. Figure 2.1).[21] It is difficult to envision a mechanism in which a single hydrazine molecule decomposes to form the products, so we discarded a unimolecular surface reaction as a possibility to explain the kinetic results.

The data are best fit by Eq. (2.17) which is based on the non-dissociative adsorption of hydrazine. The curve fittings were performed using Igor Pro (WaveMetrics, Inc.) Igor Pro is an integrated program for visualizing, analyzing, transforming and presenting data. The reader is referred to Appendix C for details on the curve fitting procedure. The best values for the fitting parameter are shown in Table 4–2. Unfortunately, hydrazine adsorption isotherm could not be measured due to its decomposition. However, it is not surprising that our data can be fitted with a Langmuir

isotherm since hydrazine adsorption on metals (see section 4.6) has been proposed to be a chemisorption process.

Table 4–2. Best fit parameter values achieved with Eq. (2.17)

Carbon	$k_a \times 10^7$ (s^{-1})	K_a (mol^{-1} cm^3)
Black Pearls 2000	5.59	1.344
Mogul L	3.19	0.381
Darco G60	2.07	0.715
Nuchar SA	6.20	0.494

Cosser and Tompkins[207] postulated a dual-plane mechanism to explain the decomposition of hydrazine on different surfaces. They suggested that (i) on more active surfaces where N_2H_4 is dissociatively adsorbed as amide radicals, only H_2 and N_2 will be produced, and (ii) on weakly adsorbing surfaces, dissociative chemisorption of N_2H_4 should be absent and decomposition will occur yielding only NH_3 and N_2. Our kinetic results are in agreement with this postulate, i.e., hydrazine is shown to non-dissociatively chemisorb on carbons and its decomposition produces only N_2 and NH_3.

4.5. Reaction mechanism

The observed kinetics of the decomposition of hydrazine in liquid solutions over carbon catalysts may then be explained by assuming that nondissociative adsorption of hydrazine is the initial step and applying this to the Langmuir adsorption isotherm to derive the overall rate equation. Based on the evidence, we suggest that a scheme

analogous to Sayer's mechanism,[185] with all of the diimide disproportionating to N_2 and hydrazine, is a strong possibility to explain the kinetics of the hydrazine decomposition over carbon catalysts. In this mechanism, the surface reaction occurs between one adsorbed hydrazine molecule and one hydrazine molecule in the liquid phase. In this reaction, the adsorbed hydrazine transfers two hydrogen atoms to the solution hydrazine molecule, to cleave the N-N bond and form two molecules of ammonia and an adsorbed diimide molecule. From stereochemical considerations, the adsorbed diimide exists in the *cis* form due to the abstraction of two *cis* hydrogen atoms by the solution hydrazine molecule. The *cis*-diimide may then disproportionate by reacting with a neighboring diimide, which re-arranges with bonds breaking and reforming to produce nitrogen, which is desorbed, and one molecule of hydrazine, which remains adsorbed on the surface. The desorption of nitrogen leaves a vacancy to be filled by another hydrazine molecule on adsorption. Sayer's mechanism is outlined below:

$$N_2H_{4(aq)} \rightarrow N_2H_{4(ads)}$$

$$N_2H_{4(ads)} + N_2H_{4(aq)} \rightarrow N_2H_{2(ads)} + 2NH_3$$

$$2N_2H_{2(ads)} \rightarrow N_2H_{4(ads)} + N_{2(g)}$$

This mechanism was proposed by Sayer[185] to explain the kinetics of the decomposition of liquid hydrazine on a supported iridium catalyst (Shell 405 catalyst), which also follows the stoichiometry of Eq. (2.36), as in the case of carbon catalysts. According to the authors "The observed first order kinetics over the range 15-100% hydrazine may be explained by the rate controlling step being either the attack by a solution hydrazine molecule on the adsorbed hydrazine molecule…or the adsorption of a hydrazine molecule to fill the vacancy left by the desorption of the nitrogen molecule."

We proposed that, in the case of hydrazine decomposition on carbon catalysts, the rate controlling step is the chemisorption of hydrazine molecules. Thus, in this reaction, the behavior of carbons and metal catalysts seems to be similar.

4.6. Dependence of the catalytic decomposition on carbon properties

Since the catalytic decomposition is a heterogeneous reaction, the available carbon surface is expected to play an important role in the catalysis. We found a correlation between the total surface area of carbon blacks and the initial rates for the reaction, as shown in Figure 4.8. No clear correlation could be established with the use of non-activated and activated carbons. The data in Figure 4.8 show that the initial rate of hydrazine decomposition is directly proportional to the surface area of the carbon blacks. This observation is consistent with the hypothesis that higher surface area carbons contain a relatively higher concentration of active sites for the reaction. Two distinct linear curves with different slopes fitted the data in Figure 4.8. The high-slope curve fitted the data for acidic carbons and the low-slope curve fitted the data for basic carbons. Since the pH characteristic of the carbons is a measure of the total acidic and basic character of the myriad of various functional groups present on carbon surfaces, the trend of the data shown in Figure 4.8 indicates that not only the surface area is relevant for the reaction but also the nature of the surface groups present on the carbon surface. We will discuss the effect of surface functional groups later in this section. Let us first concentrate our attention on the observed change in initial rate with pH and surface area.

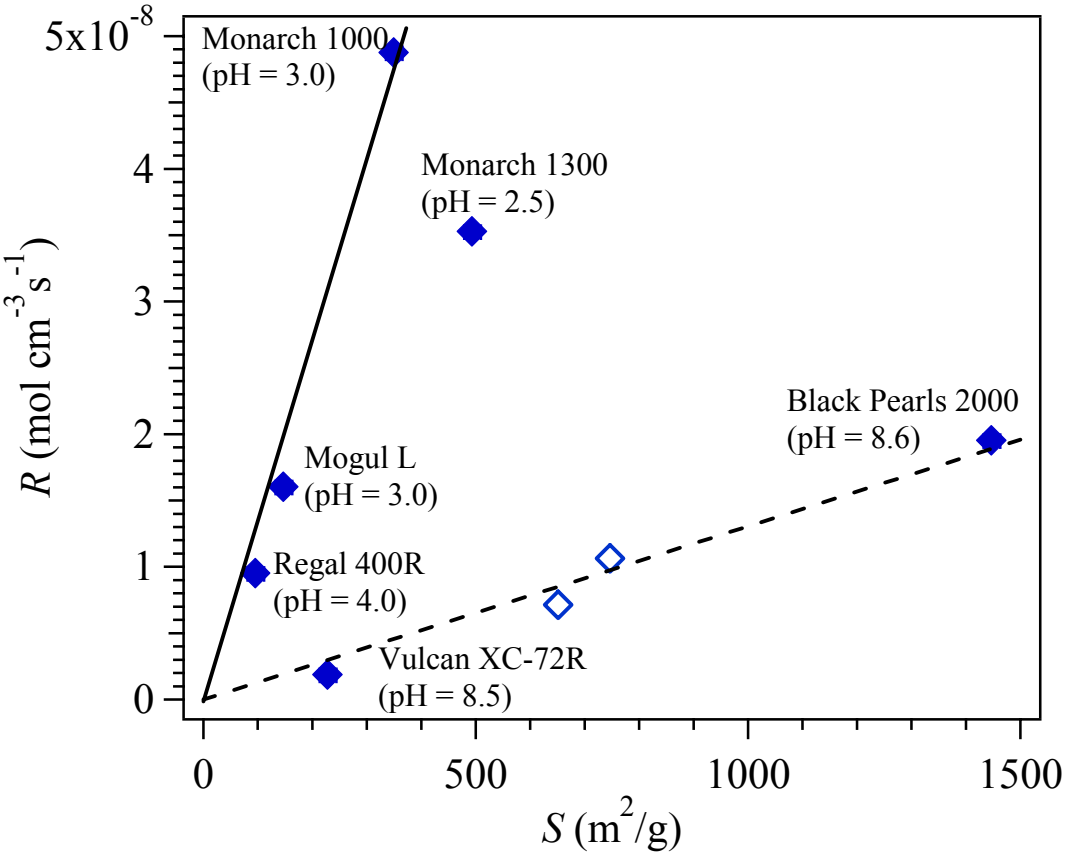

Figure 4.8. Influence of surface area of various carbon blacks on the rate of hydrazine decomposition. Number in parenthesis is the pH of the corresponding carbon. Lines indicate the trend of the data. Data for two activated carbons (open symbols) are included for comparison purposes only.

The pH change for basic carbon blacks is ~ 0 (from Vulcan XC-72R to Black Pearls 2000), and the change in reaction rate is ΔR ~ 0.8% per unit area. A similar change in reaction rate is observed for a pH change of ~ 1.5 (from Regal 400R to Monarch 1300) and for no pH change at all (from Mogul L to Monarch 1000) on acidic carbon blacks. These results suggest that the change in initial rate for these carbons is entirely due to a change in total surface area, but not to a pH change.

The high-slope curve in Figure 4.8 indicates that the reaction rate is enhanced by the presence of surface groups with a much stronger acid character. The acidity of carbon

blacks is generally attributed to the presence of chemisorbed oxygen.[105] The oxygen content of the furnace blacks is probably picked up by the carbon during the various treatments such as pulverizing, pelleting, drying or storage.[208] In particular, the acidic furnace blacks from Cabot Corporation have been further treated *via* an oxidative post production process to increase the amount of chemisorbed oxygen groups present.[198]

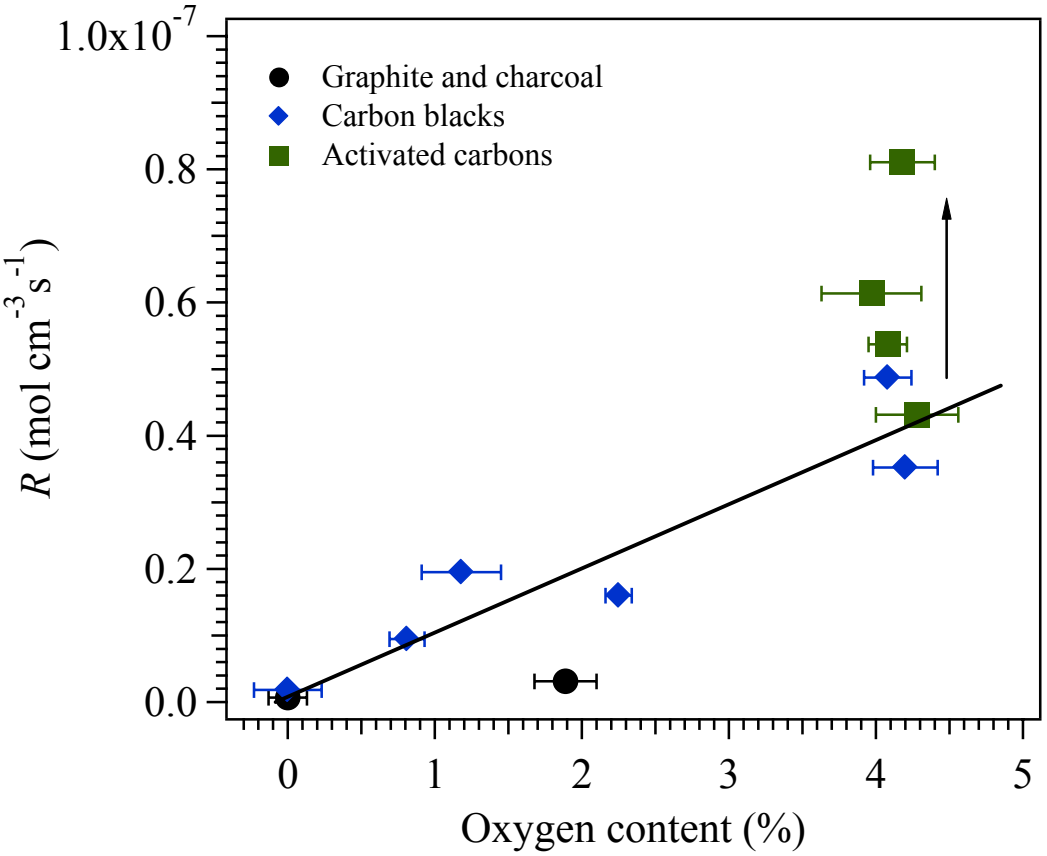

Figure 4.9. Influence of oxygen concentration on the rate of the carbon-catalyzed hydrazine decomposition. Solid line indicates the trend of the data.

To further understand the effect of oxygen functionality on the rate of hydrazine decomposition, we plotted the initial rate of decomposition as a function of the total oxygen content of carbons. The results in Figure 4.9 indicate that the initial rate increases with an increase in the total oxygen content of the carbon catalyst. Most of the data for

carbon blacks, non-activated carbons and graphite in Figure 4.9 could be accommodated on a straight line, but the initial rate varies by a factor of 2 for activated carbons with similar oxygen content. It is possible that the activation procedure of these carbons introduces a variable concentration of different acidic groups or that the change in rate is due to a change in the total surface area. Because the total bulk oxygen content is plotted, no information is available as to the importance of different functional groups on the rate of hydrazine decomposition.

Since the slow step of the reaction was proposed to be the adsorption process of hydrazine on the carbon surface, it is expected that acidic surface groups affect the reaction rate by enhancing the adsorption of hydrazine. The hydrazine molecule exits predominantly in the *gauche* form.[179] It was theorized that the two lone electron pairs (electron pairs which are not involved with bonding to other atoms) in hydrazine interact with unfilled orbitals in the early stages of adsorption and chemisorption of hydrazine on metals.[179] Here, the lone electron pairs of hydrazine may establish a bond to the carbon surface by interacting with partially unfilled π bands. These bands are formed by the overlapping of the p_z-orbital with those from neighboring carbon atoms, in a sideways manner, to form the distributed π-bonds that reside above and below each graphite sheet. It is documented in the literature[23] that heterogeneous oxygen groups chemically bound on the edges can attract and localize the electrons of the basal planes, hence, removing them from the π electron system and forming partially positive "islands" in the basal planes. This effect may improve the adsorption of hydrazine on acidic carbons and enhance the catalytic action of these carbons. Molecular simulations of adsorption of hydrazine on graphene sheets either positive or negatively charged could help to

understand this better.

Chapter 5.

Nitrobenzene reduction to aniline by hydrazine

5.1. Kinetics of the reaction

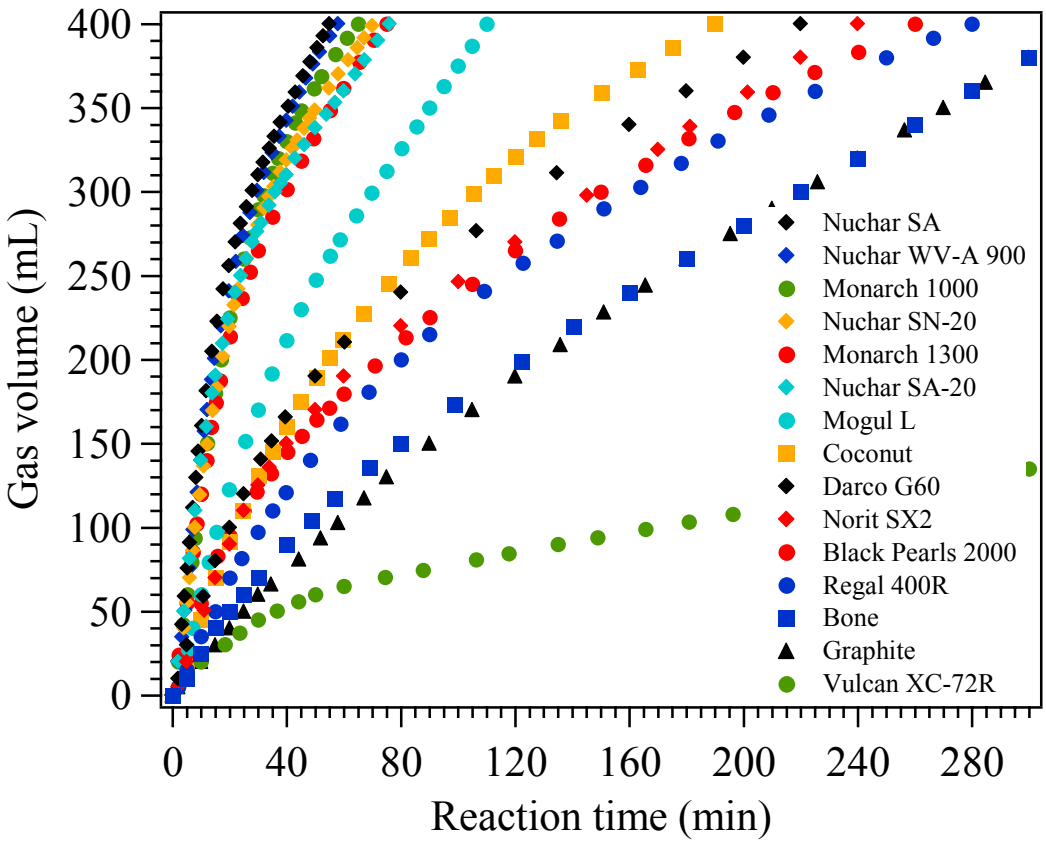

Figure 5.1. Gas evolution from the reduction of nitrobenzene by hydrazine in refluxing *iso*propanol, in the presence of several carbon materials.

The results for nitrobenzene reduction by hydrazine in the presence of different carbons are shown in Figure 5.1, plotted as gas volume evolution vs. time. The gas evolution plots show simple time dependence. In the absence of carbon, no reaction was

observed. The production of gases upon addition of carbons to the reactants demonstrates that the carbons tested catalyze the nitrobenzene reduction by hydrazine with different activities.

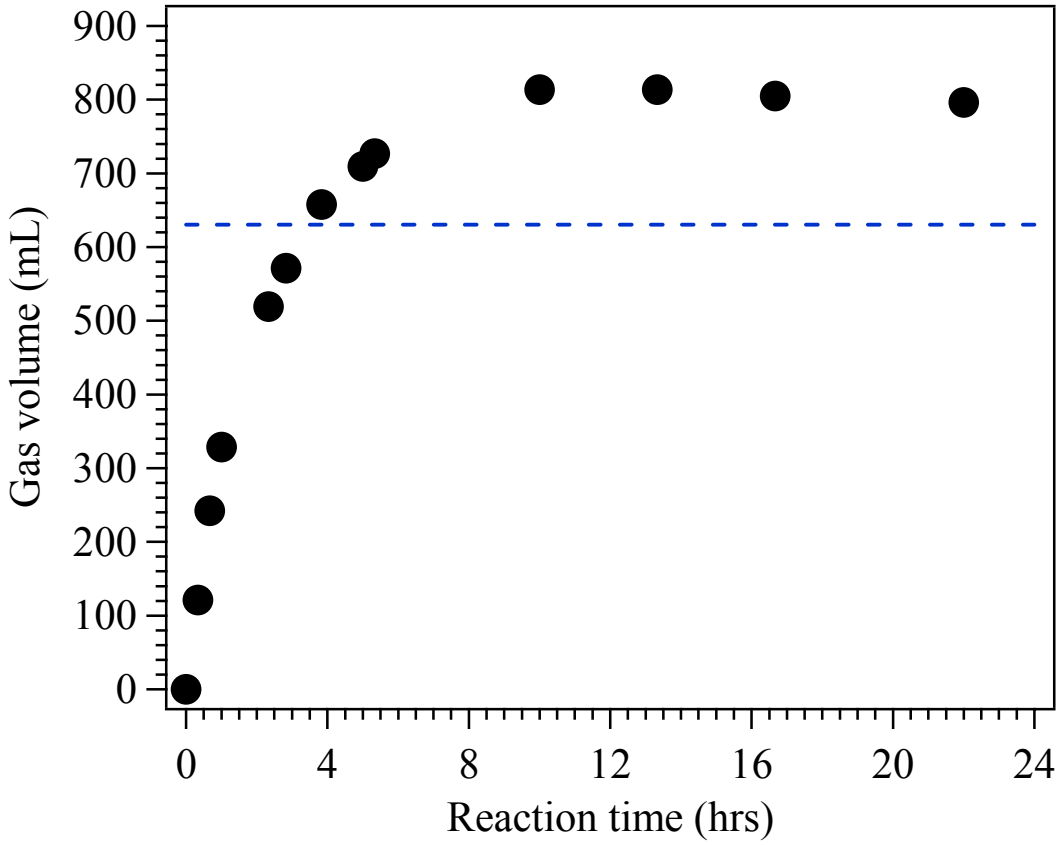

Figure 5.2. Gas evolution from the reduction of nitrobenzene by hydrazine in refluxing *iso*propanol, catalyzed by graphite.

If the overall reaction for the nitrobenzene reduction follows Eq. (2.33), the total nitrogen gas volume expected is about V_C = 630 mL using 0.017 mol of nitrobenzene (see Appendix B). Therefore, based on the amount of gas produced at a given time, we found that Vulcan XC-72R (carbon black) is the least effective catalyst and Nuchar SA (activated carbon) is the most effective catalyst.

Unfortunately, two reactions are occurring simultaneously and this complicates the data analysis of the carbon-catalyzed gas formation. The reactions are given by Eqs. (2.33) and (2.36). For a stoichiometric reaction mixture, we found that certain amount of nitrobenzene is still left in solution, even in the cases where almost the total expected amount of gas is produced. In addition, for some carbons, the observed gas volumes are somewhat larger than the amount of N_2 expected. For example, as shown in Figure 5.2, the amount of gas produced in the presence of graphite was in the order of 800 mL; about 26% higher than the amount of N_2 gas expected.

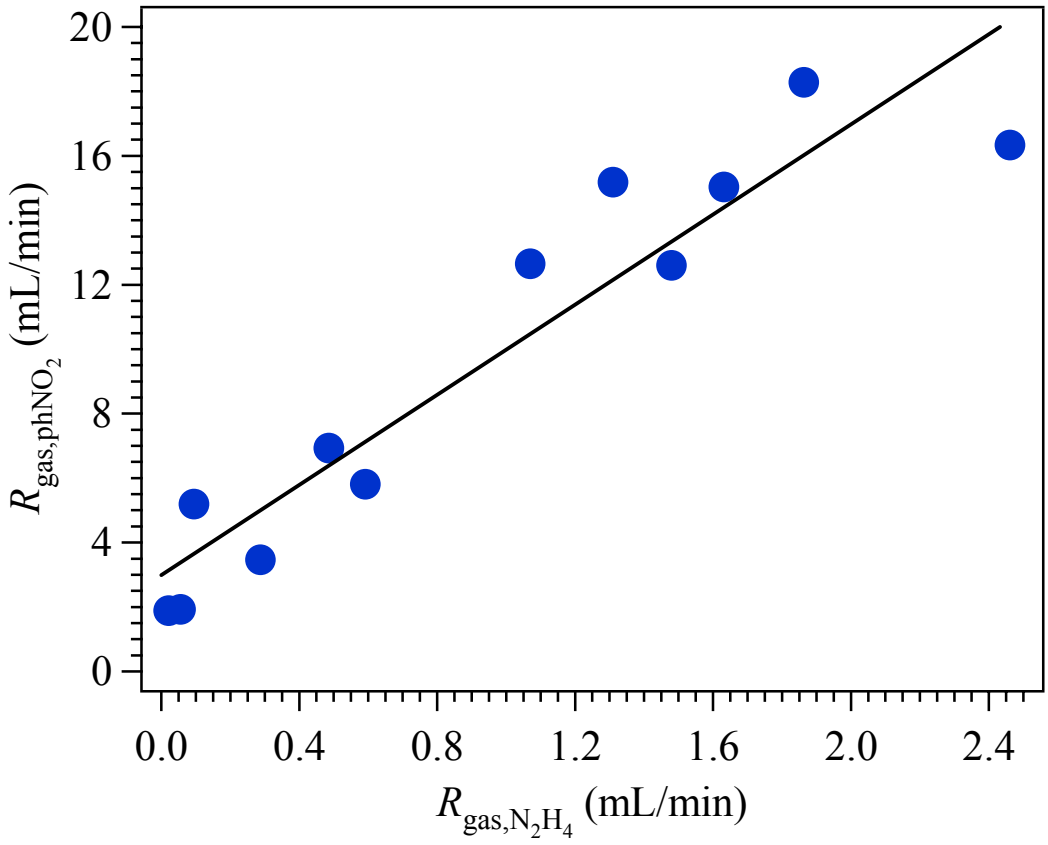

Figure 5.3. Comparison between the initial rates of gas production in the nitrobenzene reduction ($R_{gas,phNO_2}$) and in the hydrazine decomposition (R_{gas,N_2H_4}) reactions on several carbons.

We believe that these effects are due to complications introduced by the carbon-

catalyzed decomposition of hydrazine. However, Figure 5.3 shows that the initial rate of gas production due to hydrazine decomposition is at least 10 times lower than the initial rate of gas production in the nitrobenzene reduction. The data in Figure 5.3 were taken using the same initial amount (0.025 moles) and initial concentration of hydrazine (1 *M*) for both reactions, the hydrazine decomposition and the reduction of nitrobenzene. The hydrazine decomposition may become faster as the two reactions proceed. As explained in the previous chapter and later in this chapter, both the hydrazine decomposition and the reduction of nitrobenzene are surface reactions, where the reactants adsorb competitively on the carbon surface. Since nitrobenzene is first added to the solution of carbon and *iso*propanol, then nitrobenzene molecules are first adsorbed on the carbon surface and promote the reduction reaction at the beginning of the overall reaction. Later in the reaction, nitrobenzene molecules must compete with hydrazine molecules for a limited number of surface sites. If hydrazine molecules adsorb more easily than nitrobenzene molecules on a carbon surface, then the hydrazine decomposition reaction is favorable.

Figure 5.4 shows first-order and second-order plots for the reduction of nitrobenzene on different carbons. The kinetics of the reaction are complex as evidenced by deviations from either first-order or second-order behavior for most of the carbons. This is not surprising for a heterogeneous reaction. Control experiments where nitrobenzene and hydrazine are added together to the reactor showed that this behavior was not due to any progressive deactivation of catalyst by standing with nitrobenzene in *iso*propanol.

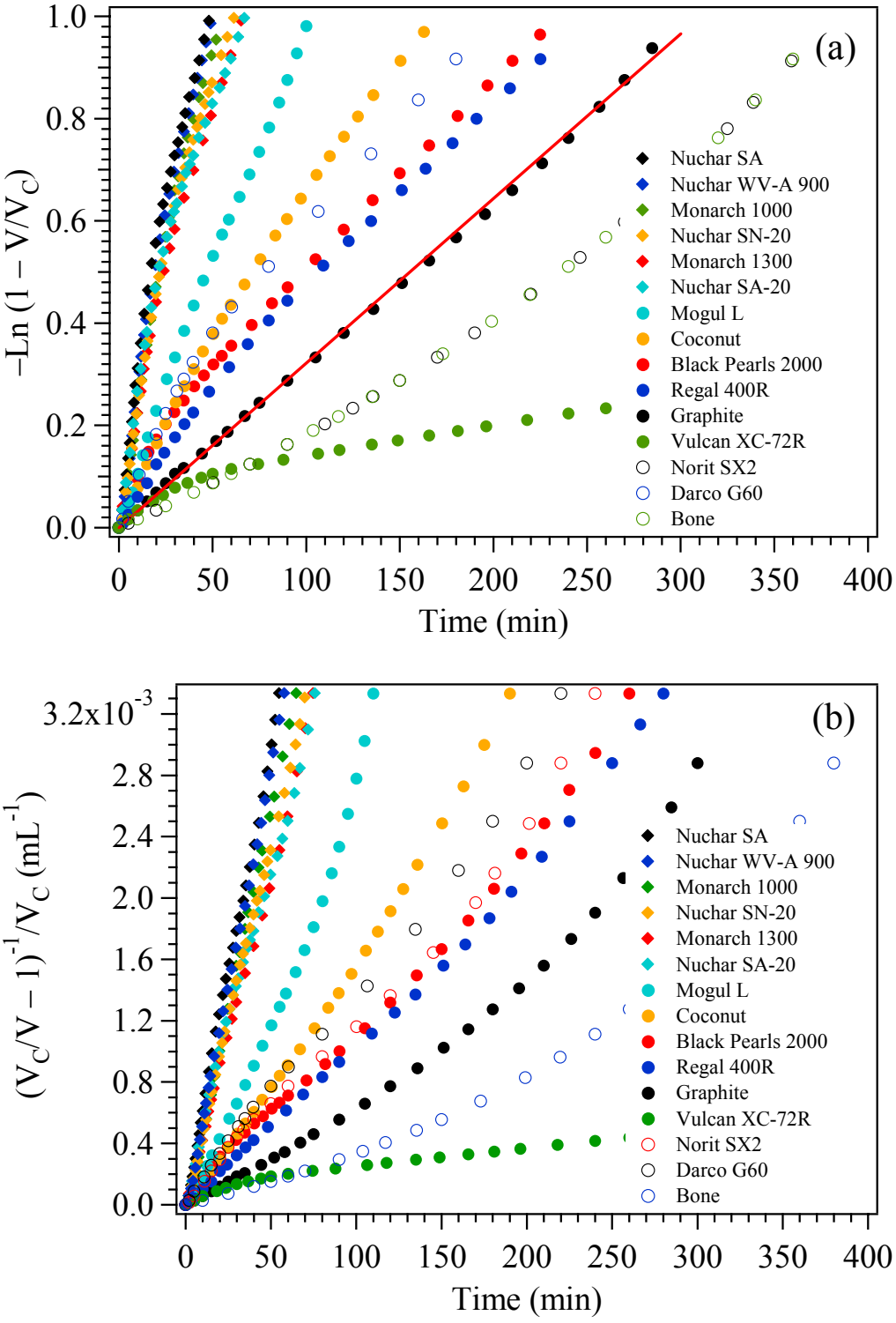

Figure 5.4. First-order (*top*) and second-order (*bottom*) plots for the reduction of nitrobenzene by hydrazine in the presence of various carbon samples.

In any case, we will analyze the kinetics of this reaction using initial rates as determined by initial slopes of the gas evolution plots (see Appendix B). This way we minimize the effect of factors (e.g., interference by products, sintering or poisoning of the catalyst) contributing to the change in the reaction rate other than the changes in concentrations of reactants as the reaction proceeds.

5.2. Effect of impurities

As in the case of the hydrazine decomposition reaction, we performed an experiment to determine the catalytic activity due to the presence of mineral matter in the carbon catalysts. We direct the reader's attention to that section for additional details. In this experiment, no detectable catalytic activity was found when ash was used as a catalyst instead of the carbon. Figure 5.5 shows a plot of the rate of reduction as a function of the ash yield of the carbon catalyst. The lack of a correlation also indicates that mineral matter may play a minor or no role in this reaction. Note that bone charcoal (not shown in Figure 5.5 for clarity) which yields ~83% ash has the same behavior and initial rate (see Figure 5.1) than graphite with ~1.5% ash yield.

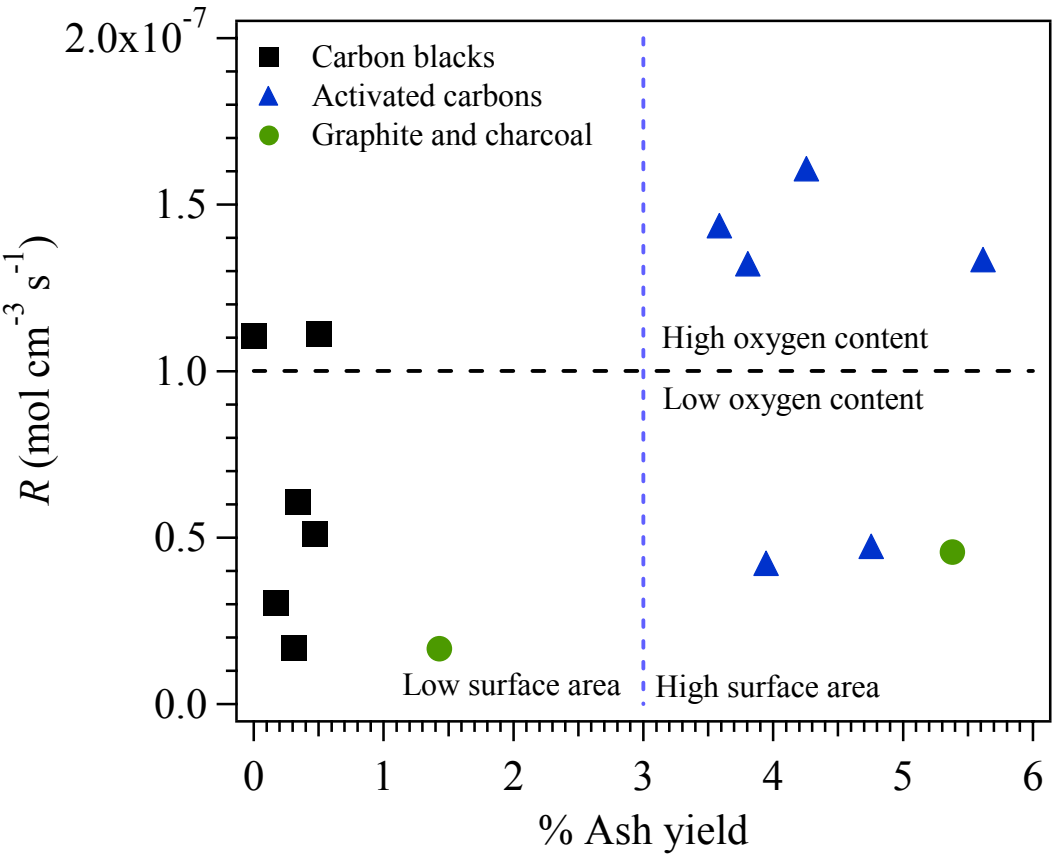

Figure 5.5. Effect of ash yield of carbon catalyst on the rate of nitrobenzene reduction.

5.3. Variation of rate with mass of catalyst and stirring

The initial rate of nitrobenzene reduction as a function of the amount of carbon was found to increase linearly with an increase in the mass of catalyst from 0 to 5 g. The functional dependence shown in Figure 5.6(b) is typical of heterogeneous reactions. The rate of gas production was also found to be independent on the stirring rates as shown in Figure 5.6(a), suggesting that the reaction is NOT mass transport limited.

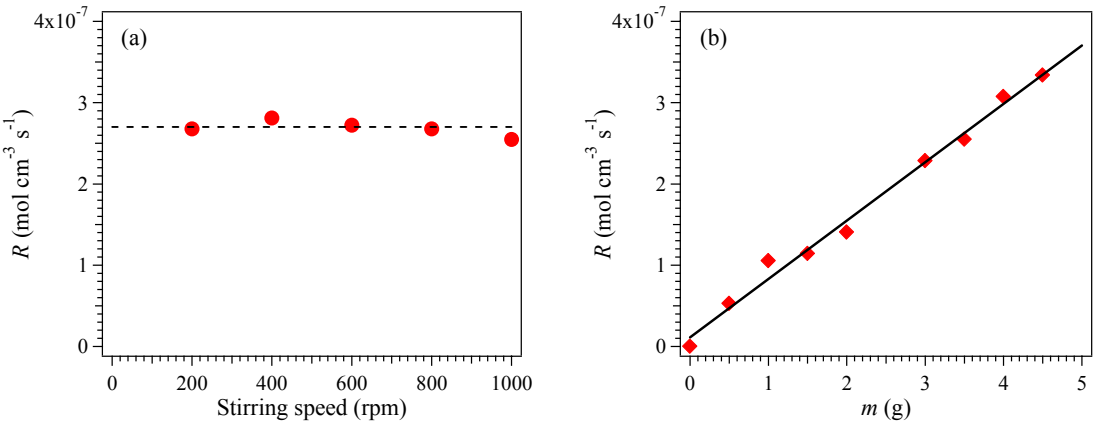

Figure 5.6. Effect of stirring (*left*) and carbon mass (*right*) on the rate of nitrobenzene reduction by hydrazine over coconut charcoal. Solid line is a linear fit of the data and dashed line is a guide to the eye.

5.4. Effect of nitrobenzene concentration

The activity of Black Pearls 2000 (carbon black) and Nuchar SA (activated carbon) was determined for a series of nitrobenzene-hydrazine mixtures ranging from 0.25 to 12 *M* with respect to nitrobenzene at a constant hydrazine concentration of 1 *M*. These data are shown graphically in Figure 5.7. As the nitrobenzene concentration is increased the rate first increases, then passes through a maximum, and finally decreases. The explanation of the fall off in the rate at high concentrations is that one reactant displaces the other from the surface as its concentration is increased. The maximum rate corresponds to the existence of the optimum number of hydrazine and nitrobenzene molecules on the carbon surface.

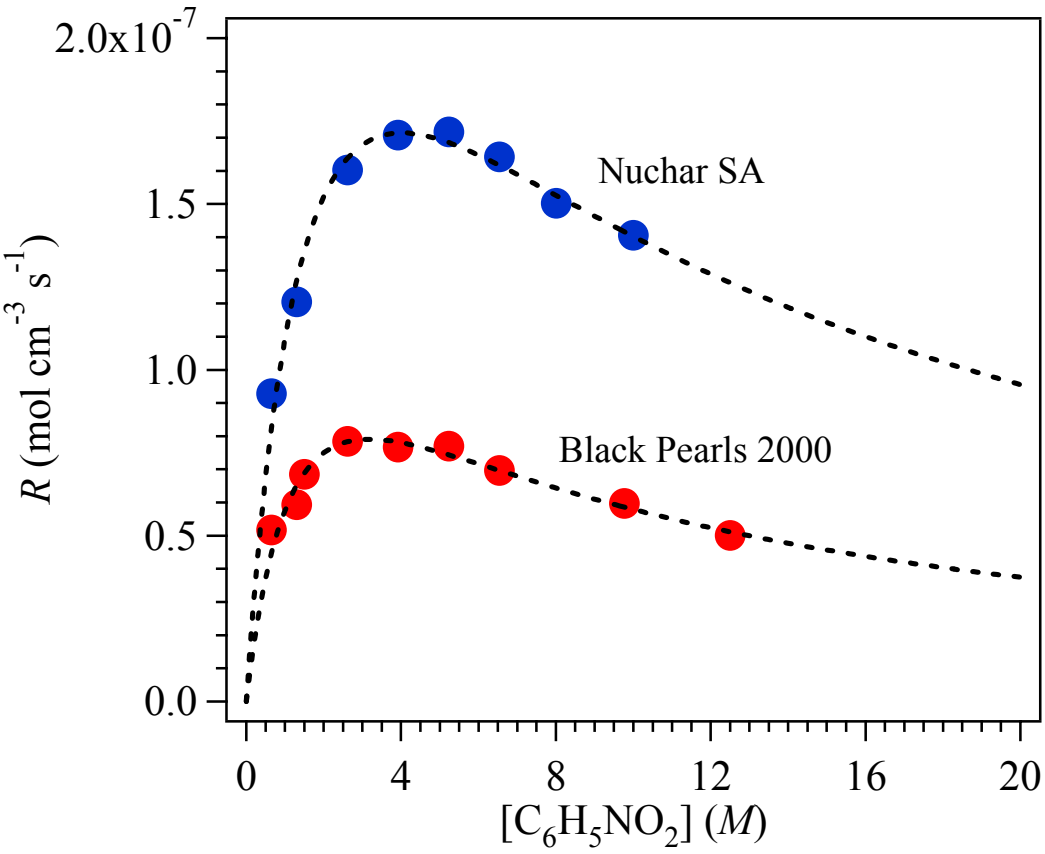

Figure 5.7. Effect of nitrobenzene concentration on the rate of reduction over Black Pearls 2000 (carbon black) and Nuchar SA (activated carbon). Dashed lines are fit of the data to Eq. (2.26).

The relationship of the rate of reaction to concentration as shown in Figure 5.7 is commonly found in heterogeneous reactions when the rate-controlling step is the reaction between two adsorbed molecules, according to a Langmuir-Hinshelwood mechanism (see Figure 2.3(a)).[21] Dashed lines in Figure 5.7 represent fits of the data to the corresponding rate law equation for a Langmuir-Hinshelwood mechanism, Eq. (2.26). As can be seen, excellent fits of the data can be obtained with the use of this equation. The best fit parameters are shown in Table 5–1. Note that the equilibrium adsorption-desorption constants for hydrazine (K_a) and nitrobenzene (K_b) are approximately equal for a particular carbon.

Table 5–1. Best fit parameter values achieved with Eq. (2.26)

Carbon	$k\times10^{6}$ (mol cm^{-3} s^{-1})	$K_a\times10^{-3}$ (mol cm^{-3})	$K_b\times10^{-3}$ (mol cm^{-3})
Nuchar SA	2.76	0.331	0.330
Black Pearls 2000	1.09	0.444	0.411

The observed kinetics of the nitrobenzene reduction by hydrazine in liquid solutions over carbon catalysts may therefore be explained by assuming that the slow step is the reaction between two adsorbed molecules on the carbon surface.

Our kinetic results for the reduction of nitrobenzene may also be explained by quite a different mechanism: the electrochemical mechanism. Catalysis occurs by the electrochemical mechanism if both couples are electrochemically reversible on the catalyst or, should one or even both couples be electrochemically irreversible, if the difference in their Nernst potentials is sufficiently large.[196] The electrochemical oxidation of hydrazine on carbon electrodes is an irreversible 4-electron process (to N_2) in aqueous solutions[209] and methanolic solutions[210] but a reversible 2-electron process (to N_2H_2) in acetronitrile solutions.[205,210] The difference seems to come from the presence or absence of polarized oxygen-containing groups in the electrolyte solution, which can affect the stability of diimide and other intermediates.[206] The electrochemical reduction of nitrobenzene on carbon electrodes is a reversible 4-electron process to phenylhydroxylamine in basic aqueous, alcoholic or mixed aqueous-organic media.[211,212] Phenylhydroxylamine was identified by NMR during the chemical reduction of nitrobenzene by hydrazine over carbon catalysts.[1] Unfortunately, not enough electrochemical data are available on carbon electrodes for a qualitative test of the

electrochemical mechanism.

Larsen *et al.*[1] concluded that a strong evidence for the applicability electrochemical mechanism to the carbon-catalyzed reduction of nitrobenzene by hydrazine was the observation of an electrical potential in an emf cell, where a carbon electrode was immersed in a solution of hydrazine and an identical carbon electrode was immersed in a solution of nitrobenzene. The presence of *this* voltage is irrelevant for a test of the electrochemical mechanism. First, the catalytic potential taken up by a carbon catalyst in the presence of *both couples* (hydrazine-nitrogen and nitrobenzene-phenylhydroxylamine) should be equal to the electrochemically-determined mixture potential at equal anodic and cathodic currents, in order for an electrochemical mechanism to be applicable to a redox reaction.[213] Second, a catalytic potential in the presence of *only* either hydrazine or nitrobenzene can be due to many factors, the most promising candidate being the adsorption of these compounds on the carbon surface.

Adsorption on a metal surface is always accompanied by a change in the distribution of the local electronic states on the substrate atoms.[214] Changes can also occur in the atomic arrangement and—from the thermodynamic viewpoint—in the surface energy. The nature and magnitude of the surface redistribution of electrons are largely dependent on the electronegativity of the adsorbed species and of the metal atoms, but also on the surface symmetry and the shape of the orbitals involved. It is also easy to imagine that when a foreign atom or molecule is adsorbed, the electron density around it will be modified and this will lead to the appearance of an electric dipole. Thus, an electric field is induced on the metal due to the distribution of electric charges near the metal surface as well as the creation of random electric dipoles upon adsorption. One

should expect that chemisorption of hydrazine molecules will have a stronger effect than the physisorption of nitrobenzene on the carbon surface. Indeed, the potential difference between both carbon electrodes was reported to drop steadily to a constant potential in a time period comparable to that required for the complete decomposition of hydrazine over the carbon electrode.[1]

Further evidence for our interpretation on the origin of the potential measured by Larsen *et al*.[1] is provided by the investigations of the noncurrent potentials (with respect to a reference electrode) in hydrazine solutions on several metal electrodes.[215-218] The potential of a metal electrode was usually found to be more positive than the standard potential of reaction in Eq. (2.35), and dependent upon the nature of the metal, the condition of the surface, and the electrode rotation.[218] The noncurrent potential was also found to be more positive than the standard potential of water electrolysis reaction

$$2H_2O + 2e^- \rightarrow H_2 + 2OH^- \quad E° = -0.828\,V \qquad (5.1)$$

so it is very unlikely that the potential of the electrode represents a mixture potential of reactions in Eqs. (2.35) and (5.1). It was concluded that the potential of an electrode in hydrazine solution without current is determined by adsorption processes, and the magnitude of this potential depends on the polarity of the bonds between the dissociative chemisorption products and the surface.[218]

The fact that an alternative explanation exits for previous results of Larsen *et al*. does not mean that the original conclusion from those authors was wrong, but that it was not the only possibility.

5.5. Dependence of catalytic reduction on carbon properties

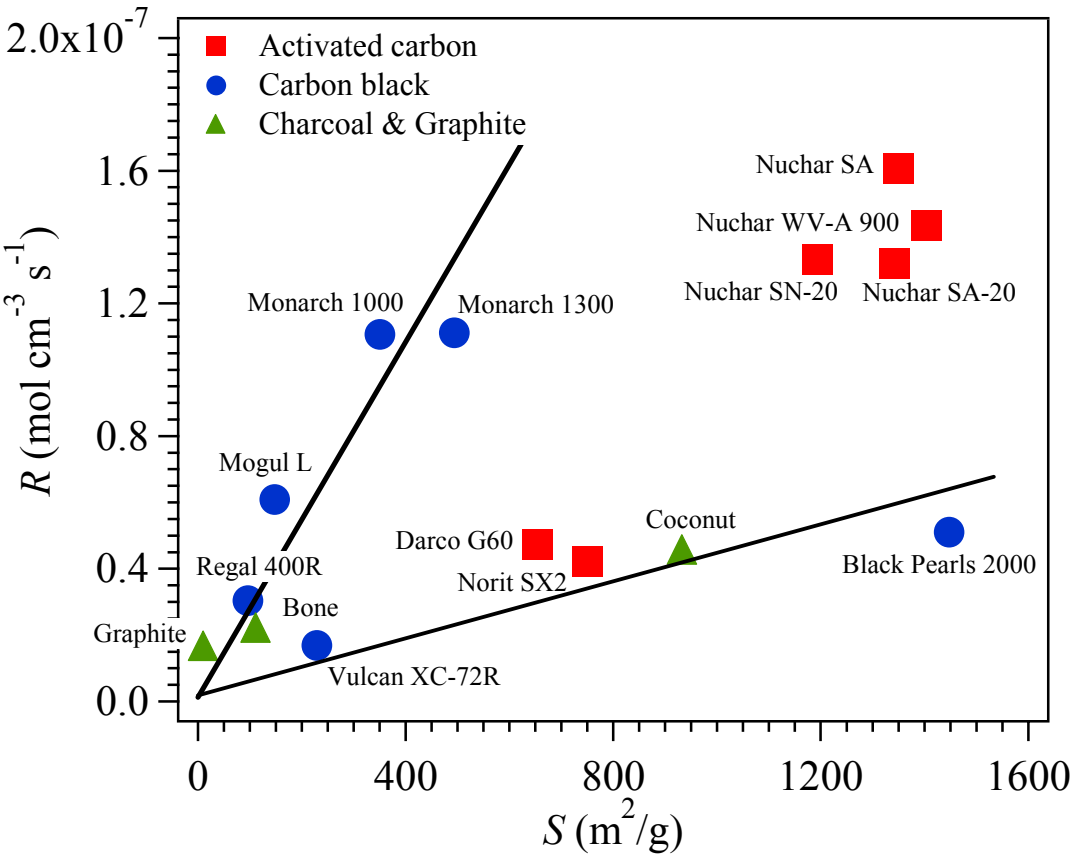

Figure 5.8. Influence of surface area of various carbons on the rate of nitrobenzene reduction. Solid lines indicate the trend of the data.

The observed catalytic activity for the reduction of nitrobenzene by hydrazine as a function of the surface area of the carbon catalyst is shown in Figure 5.8. Despite the scatter in the data, the trend in this figure suggests that the nitrobenzene reduction rate increases with the surface area. At first glance, this is in agreement with the generalized hypothesis that higher surface area carbons contain a relatively higher concentration of active sites for the carbon-catalyzed reaction. The typical active sites for carbon-catalyzed reactions are basal planes of the graphitic crystallites of carbons, edge sites,

surface functional groups, etc. [2-11]

We notice in Figure 5.8 a clear separation between the trends observed for neutral and basic carbons and acidic carbon blacks. A series of acidic activated carbons is grouped together in the higher surface area and higher initial rate region. The fact that the data for basic carbons fall on the same linear curve suggests that carbon structure plays no dominant role in the catalysis. These observations also indicate that surface area is not the only factor which determines the initial rate of the reaction. Aggarwal *et al*.[24] also found that nitrobenzene adsorption depends upon surface area but there is no direct relationship between the maximum amounts of nitrobenzene adsorbed and the surface area of carbon, and concluded that surface area is not the only factor which determines the adsorption of nitrobenzene.

The data in Figure 5.8 also indicate that the rate of the reaction is enhanced by the presence of surface groups with a much stronger acid character. For instance, the reaction rate is increased by ~ 370% for a pH change of ~1.5 in the acidic range. We already discussed the effect of surface acidity on the adsorption of hydrazine. The adsorption equilibrium for nitrobenzene on carbons is also dependent, to a large extent, on the chemistry of the carbon surface.[23,24] Heterogeneous oxygen groups have been reported in the literature to play an important role in the process. Aggarwal *et al*.[24] reported that nitrobenzene adsorption on activated carbons increased on degassing but decreased on oxidation. The maximum adsorption in case of a sample degassed at 600ºC and a subsequent decrease at higher degassing temperature was explained on the basis of the existence of two types of carbon-oxygen surface structures.[199] The carbon sample degassed at 600ºC is devoid of a larger portion of its CO_2-yielding complexes (carboxylic

acid or lactonic groups) but still retains a large proportion of its CO-yielding complexes (quinonic groups), while a carbon sample degassed at 1000ºC is almost free of any of these surface complexes. It thus appears that the presence of acidic CO_2-yielding complexes tends to suppress the adsorption, while emergence of CO-yielding complexes as the dominating oxygen complex enhances its adsorption capacity for nitrobenzene. Following the idea of Aggarwal *et al*., we propose that two different types of acidic groups, one in carbon blacks and another in activated carbons, are responsible for the behavior observed between these two groups of carbons in Figure 5.8.

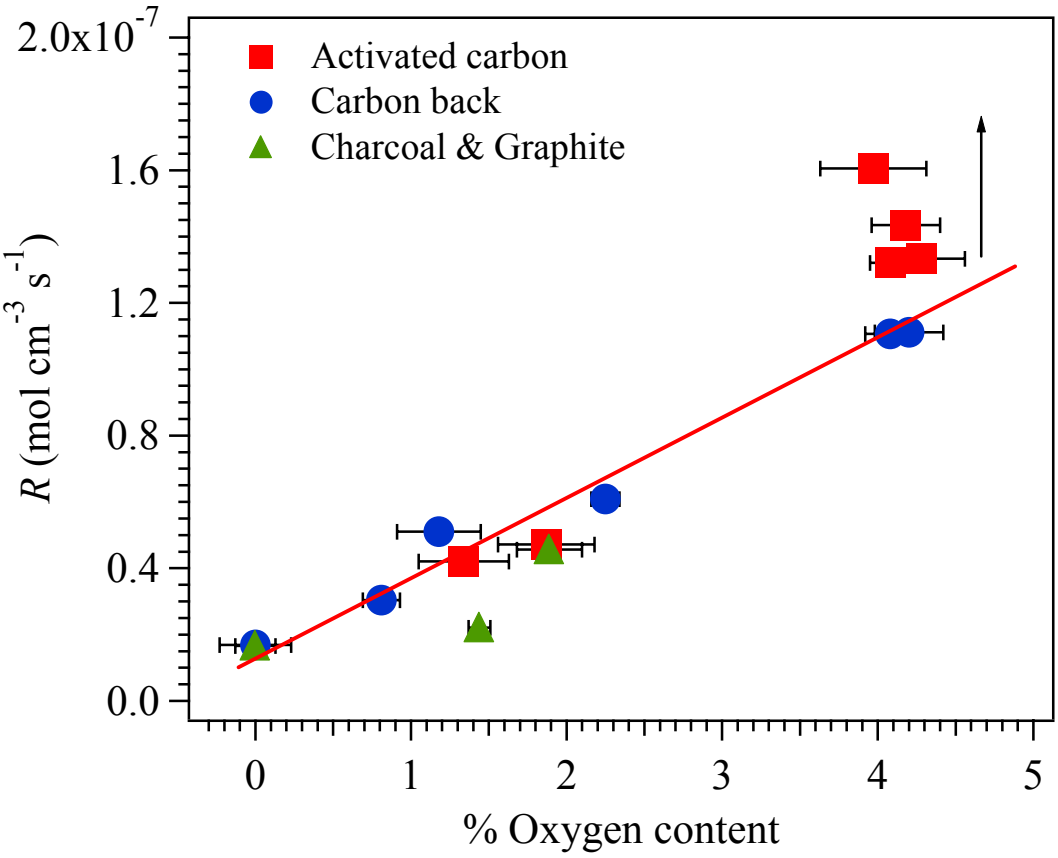

Figure 5.9. Influence of oxygen concentration of various carbon catalysts on the rate of nitrobenzene reduction. Solid line indicates the trend of the data.

Figure 5.9 shows the effect of oxygen concentration on the rate of nitrobenzene reduction. The results demonstrate that the rate of nitrobenzene reduction increases with increasing total oxygen content of the catalyzing carbon. Because the total oxygen content is plotted, no information is available about the relative importance of different oxygen functional groups. The fact that the reaction rate differs considerably for activated carbons with similar oxygen contents indicates that not all of the oxygen functional groups are equally important to this reaction. It is possible that the concentration of acidic CO-yielding complexes increases in these activated carbons without a significant change of the total oxygen content.

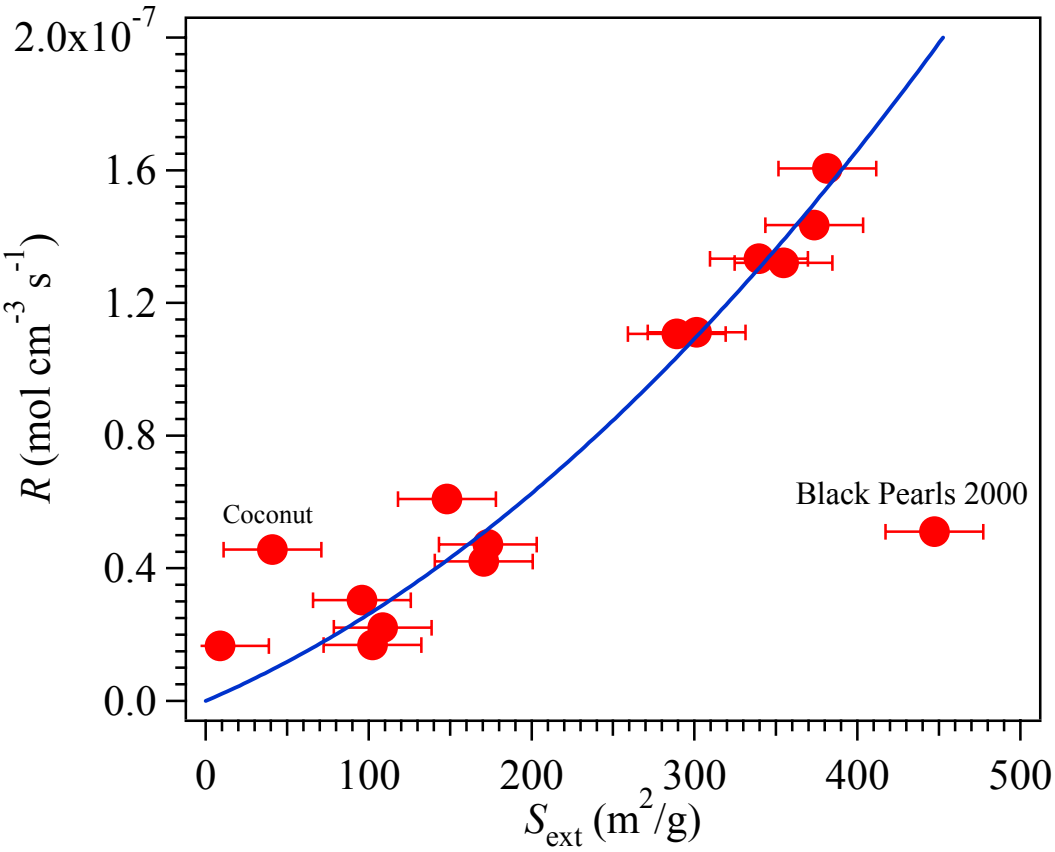

Figure 5.10. Influence of the external surface area of various carbons on the rate of nitrobenzene reduction. Solid line indicates the trend of the data.

It is tempting to suggest that due to the relatively high accessibility of the carbon blacks and ground graphite surfaces (little intraparticle microposity), the whole of their surfaces can be wetted and available for reaction. If this hypothesis is extended to include the activated carbon surfaces and carbon blacks (with high BET surface areas), then it implies that only part of their surface area is available for reaction involving a large molecule such as nitrobenzene and small pores. This hypothesis is reasonable, since most of this surface area is internal microposity. Figure 5.10 displays the initial rate as a function of the external surface area of the carbon catalyst with wide variation in surface area ranging from ~ 10 to 500 m^2/g. It is seen that the initial reaction rate and the external surface area are almost directly proportional, except for a few data points. A relationship of this type is usually observed when the reaction is controlled by external diffusion of the reactants. However, more effective agitation of the solution around the solid catalysts is expected to markedly increase external diffusion rates; an effect not seen in Figure 4.5(a). The catalytic rate is also proportional to the external surface area of the catalyst when a narrow pore structure limits the reaction rate and the reaction is in the pore (or internal) diffusion regime, which is little influenced by stirring.[20] In this case, if the reactant diffuses slowly but reacts rapidly, conversion to product will occur near the pore entrances and the interior of the pores will play no role in the catalysis. It is possible that the nitrobenzene reduction reaction is, in part, limited by pore diffusion. Further tests are needed to prove this hypothesis.

The pore volume per unit mass (V_p) (a measure of the particle porosity) is also a parameter which is important and is implicitly contained in relations of the rate of pore diffusion.[20] When the reaction rate is controlled by pore diffusion, it is either directly

proportional or proportional to the square root of the pore volume. However, Figure 5.11 shows the initial rate of the nitrobenzene reduction increases in a superlinear fashion with the pore volume of the catalyzing carbon, except for a few carbons.

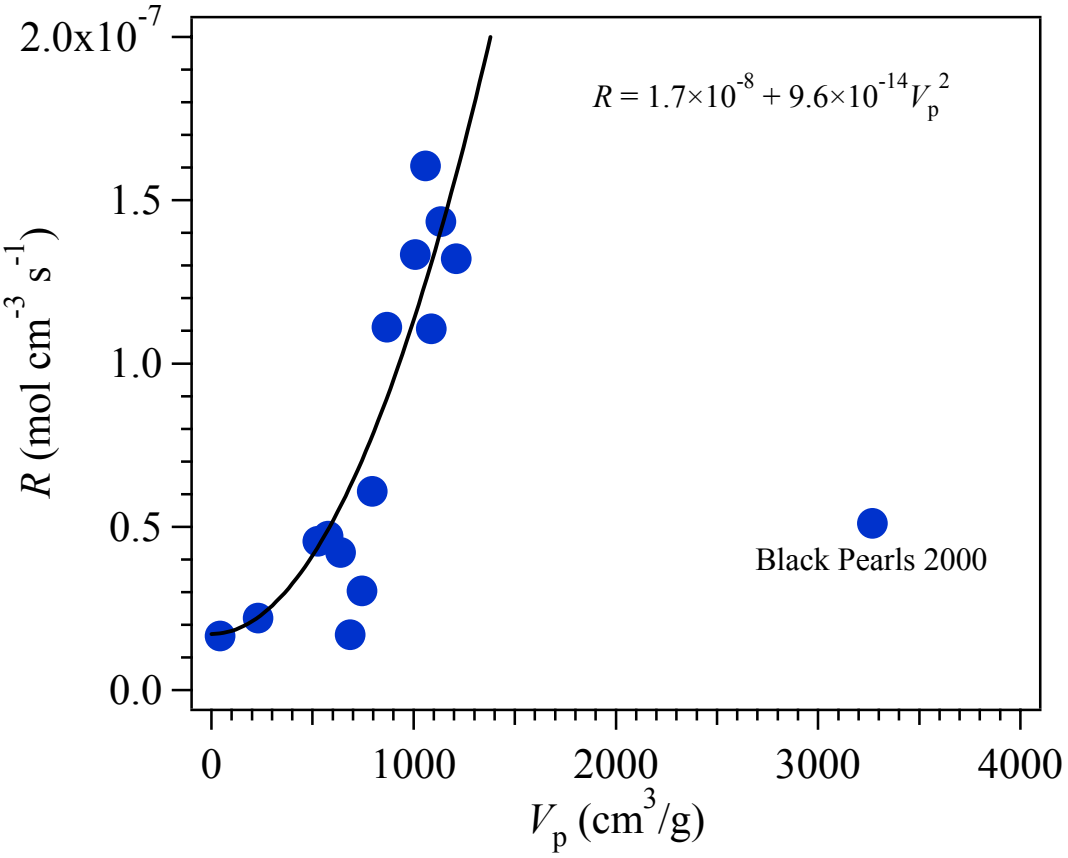

Figure 5.11. Effect of pore volume of various carbons on the initial rate of nitrobenzene reduction. Solid line is a fit of the data to a power law function.

Chapter 6.

Summary and Conclusions

The kinetics of the nitrobenzene reduction to aniline by hydrazine and the decomposition of hydrazine over carbons in refluxing *iso*propyl alcohol solutions were investigated. The results presented in this thesis confirm previous results[1,12] that carbons catalyze both reactions, although with different activities. Both reactions exhibited well-known behaviors for heterogeneous catalysis.

The kinetics of the hydrazine decomposition over carbons exhibited a change of reaction order from first order at low concentrations of hydrazine to zero order at high concentrations. The observed kinetics may be explained using the Langmuir adsorption isotherm to derive the overall rate equation on the assumption that the nondissociative chemisorption of hydrazine is the slow step in the reaction mechanism. A reaction is then postulated to occur where an adsorbed hydrazine molecule reacts with a hydrazine molecule in the liquid phase to form two molecules of ammonia and an adsorbed *cis*-diimide (N_2H_2) on the carbon surface. The overall reaction then proceeds with the reaction between neighboring diimide molecules on the carbon surface, forming nitrogen that then desorbs and one hydrazine molecule which remains adsorbed on the carbon surface. This is the same catalytic mechanism proposed for metals such as iridium and rhodium.

The kinetics of the nitrobenzene reduction to aniline by hydrazine exhibited a pronounced order change from a fractional positive value at low nitrobenzene concentrations to a fractional negative order at high nitrobenzene concentrations. The observed kinetics may be explained by assuming that the slow step is a Langmuir-

Hinshelwood type reaction where an adsorbed nitrobenzene molecule reacts with an adsorbed hydrazine molecule to yield phenylhydroxylamine. Our kinetic results do not allow us to differentiate between catalytic processes where molecules adsorbed either side by side or at distant sites. In the latter case, the electron transfer is expected to occur through the carbon solid.

Both the hydrazine decomposition reaction and the nitrobenzene reduction by hydrazine may be surface-controlled reactions. This conclusion is based on the aforementioned variation of the reaction order with reactant concentrations, the lack of dependence of the reaction rates with stirring and the proportionality between the reaction rates and the catalyst mass. All these behaviors are characteristics of surface-controlled reactions. The nitrobenzene reduction reaction may be, in part, controlled by pore diffusion as determined by the almost linear relationship between the reaction rates and the external surface area and pore volume of the carbon catalysts. Further studies are needed to determine the validity of this assumption.

Comparison of the physicochemical properties of the carbon catalysts and kinetic studies showed that the structure and the nature of the carbon surface play a role in the catalysis. For instance, the reaction rate increased linearly with the surface area of carbon blacks, non-activated charcoals, graphite and weakly basic activated carbons. Both reactions are enhanced by the presence of acidic surface groups on the carbon surface. The effect of acidic surface groups on the reactants' adsorption can be understood by assuming that hydrazine molecules are adsorbed by interactions between their lone electron pairs with partially unfilled π bands of the carbon surface. The π electrons of the basal planes are attracted and localized by the acidic surface groups in the carbon edges.

The effect of oxygen surface groups is further evidenced by the linear relationship between the oxygen content of carbons and the reaction rates at low oxygen content. Acidic activated carbons are an exception to this trend due to changes in the relative concentration of the relevant oxygen surface groups for constant total oxygen contents.

Our hypothesis that carbon catalyzes both nitrobenzene reduction by hydrazine and hydrazine decomposition reactions in the same way that metals do appears to have been supported by our kinetic studies. However, more work needs to be done to account for possible factors influencing the results, such as the production of extra gases during the reactions.

Chapter 7.

Future Work

We have postulated a mechanism for hydrazine decomposition where both nitrogen atoms in the nitrogen molecule produced come from the same N_2H_4 molecule. It is thus of interest to check a possible redistribution of nitrogen atoms by using ^{15}N label and, more precisely, by studying the hydrazine decomposition reaction of equimolar mixtures of nitrogen-15 labeled hydrazine ($H_2{}^{15}N\text{-}{}^{15}NH_2$) and normal hydrazine ($H_2{}^{14}N\text{-}{}^{14}NH_2$). Mass spectrometric analysis (for mass numbers 28, 29 and 30) of the nitrogen gas resulting from this reaction can be used to determine whether randomization of molecular nitrogen (i.e., $^{15}N\text{-}{}^{15}N$ and $^{14}N\text{-}{}^{14}N$ do not exchange) does occur in the nitrogen product. For example, if there is no randomization at all the decomposition of an equimolar mixture of $H_2{}^{15}N\text{-}{}^{15}NH_2$ and $H_2{}^{14}N\text{-}{}^{14}NH_2$ should give an equimolar mixture of $^{14}N_2$ and $^{15}N_2$, whereas a complete randomization should lead to the following distribution:

$[^{14}N_2] = 25\%$;

$[^{15}N_2] = 25\%$;

$[^{14}N^{15}N] = 50\%$.

Previous ^{15}N-labeled hydrazine decomposition investigations reveal a lack of scrambling in some cases, namely, on supported rhodium[187] and supported iridium[185] in the liquid phase, on supported iron in the gas phase,[219] and even in thermal decomposition in a quartz or glass vessel.[220] Conversely, scrambling was observed during hydrazine oxidation over several electrocatalysts.[187,221,222] The only experiments found in the literature on ^{15}N-labeled hydrazine decomposition in the liquid phase[185,187] were performed over catalyst in the form of pellets and without stirring of the hydrazine

solution. Besides, the authors used a small sample (1 mole) of ^{15}N enriched hydrazine in the presence of a large excess of normal hydrazine (65.3 or 122.3 moles). These observations suggest that these experiments may have not been done properly. Unfortunately, ^{15}N enriched hydrazine is very expensive.

As mentioned before, our results on the nitrobenzene reduction by hydrazine can also be explained by an electrochemical mechanism. It was suggested that here the carbon catalyst acts as an electron conductor. It accepts electrons from adsorbed hydrazine and donates them to adsorbed nitrobenzene and its reduced intermediates. One or more tests should be applied to check that the catalysis does indeed proceed by electrochemical mechanism. The experimental tests of the electrochemical model are provided by a combination of kinetic and electrochemical experiments:

(a) Comparison of the observed kinetics (with respect to reaction rate and reaction orders) of heterogeneous catalysis with that predicted from independent current-voltage curves of the two redox couples individually at the same carbon surface. Moreover, judicious changes in the experimental conditions should alter the rate equations in a predictable way.[213]

(b) Comparison of the observed potential taken up by the carbon catalyst during heterogeneous catalysis with the electrochemically determined mixture potential at equal anodic and cathodic currents.[213]

(c) Carrying out a specially designed experiment in which the two reactants are in contact with the carbon catalyst but are separated from each other.[223,224] If reaction still takes place under these circumstances, it must do so via electron transfer through the carbon catalyst.

(d) Imposing upon the catalyst a potential equal to the equilibrium potential of one of the redox couples. This will stop the overall reaction.

(e) Measurement of the steady-state potential of the catalyst and of its polarization characteristics in the reaction mixture.

Many of the factors involved in the mechanisms proposed here are general to all carbon-catalyzed reactions and so will be broadly useful. The effect of the carbon surface functionality on the reactions remains to be explored. Three approaches are proposed. We have already observed that the rate of the reactions studied here increases as the oxygen content of the carbon catalyst increases. Standard Fourier transform infrared spectroscopy (FTIR) can be used to identify the oxygen functional groups present in the carbon catalysts to correlate them with catalytic ability, but it provides relatively little quantitative information. The technique has already been applied to carbon blacks.[225,226] X-ray photoelectron spectroscopy (XPS) can be used to determine the concentration of surface oxygen functionality for several of the most effective carbon catalysts. XPS is ideal for this use because it is a surface-sensitive technique that yields functional group populations and has already been applied to coals and chars, so its application to commercial carbons does not involve any technique development.[227] Surface oxides of carbons can be identified by their reaction (or failure to react) with bases and acids of different strengths. The procedure has been described and discussed earlier.[157] From this work it would be possible to tailor the carbon surface to achieve maximum catalysis.

It would be interesting to evaluate the prospects for producing premium carbon catalysts from commercial carbon precursors. This requires the study of the catalytic activity of, for example, anthracitic coals. This represents new markets, which in turn,

provides additional sales opportunities for coals. Anthracites have the highest electrical conductivity of any rank of coal; as the structure approaches that of graphite via heat-treatment, conductivity should also approach that of graphite. The heat-treating of anthracitic coals to various degrees to produce a sequence of samples ranging from the native anthracite to a nearly graphitic carbon provides a suite of samples in which conductivity will vary over several orders of magnitude.

If anthracites are able to catalyze these reactions, it would raise the possibility of using anthracite coal waste (culm) to develop catalysts for the reduction of nitroaromatics. This development would simultaneously represent a potential new market for this carbonaceous material and a means of removing culm from the environment. The low-coal-content waste material that remains after mining for anthracite coal is an extremely low cost feedstock. In fact, it may be possible to obtain credit via the Department of Environmental Protection for "remining" this material and getting it out of the environment. This waste causes air and water pollution problems, danger from waste pile fires, and is an aesthetic blight on the landscape. Currently, there are at least 800 million, and possibly billions, of tons of culm within the anthracite region of Pennsylvania. Such a project could look at converting anthracite waste in Pennsylvania into high-quality, environmentally friendly catalysts for an environmentally relevant reaction: the reduction of nitroaromatics.

Diesel engines are major contributors to the emission of toxic substances into the atmosphere.[228] These toxic substances are a vital concern nationwide due to human health and environmental effects.[229] For example, nitroaromatic compounds such as nitronaphthalenes—major components of diesel exhaust emissions—are potent mutagens

and carcinogens for humans.[230,231] Reductive transformation of nitroaromatic compounds into their corresponding aromatic amines could play a major role in the detoxification process of diesel exhaust emissions. Thus, such a project would aim to address the following environmental concerns:

(a) Removal of culm banks that have accumulated as a result of coal mining.

(b) Detoxification process of diesel exhaust emissions.

(c) Development of environmentally friendly catalysts.

The first concern would be addressed by showing experimentally that anthracite waste can be used as a catalyst in the reaction of nitroaromatic compounds with hydrazine. The demonstrated reduction of large nitroaromatic compounds, typical of diesel exhaust, would address the second concern. This represents an extension of our present work, which so far has looked only at nitrobenzene reduction. The third concern is being addressed by the general theme of this work, which is to replace expensive catalysts containing heavy metals with the much less expensive and safer carbon.

Unfortunately, due to the differences in the reaction conditions employed (i.e., temperature, initial concentrations, etc.), we cannot compare the reaction rates obtained in this study with those in previous studies on metal catalysts. It would be interesting to perform a systematic study on the performance of carbons compared to typical metal catalysts.

Even though, we are confident that mineral matter has a minor or none effect on the catalytic properties of the carbon used in this study, a comprehensive and more systematic study is needed on this issue. For instance, mineral matter content of the carbon can be reduced or eliminated by washing the carbon with HCl and HF to remove

trace metal impurities.

References

[1] J. W. Larsen, M. Freund, K. Y. Kim, M. Sidovar, and J. L. Stuart, "Mechanism of the carbon catalyzed reduction of nitrobenzene by hydrazine." Carbon **38** (5), 655 (2000).

[2] D. E. Weiss, "The catalytic properties of amorphous carbons." Proceedings of the 5th Conference on Carbon **1**, 65 (1962).

[3] J. W. Hassler, *Activated carbon*. (Chemical Publishing Co., New York, 1963).

[4] R. W. Coughlin, "Carbon as adsorbent and catalyst." Industrial & Engineering Chemistry, Product Research and Development **8** (1), 12 (1969).

[5] R. W. Coughlin, "Predicting the activity of carbon catalysts." Proceedings on the 4th International Congress on Catalysis **2**, 322 (1971).

[6] D. L. Trimm, in *Catalysis* (Royal Chemical Society, London, 1981), Vol. 4, Chap. 8.

[7] V. S. Tripathi and P. K. Ramachandran, "Carbon as catalyst." Defence Science Journal **35** (1), 115 (1985).

[8] H. Juntgen and H. Kuhl, in *Chemistry and Physics of Carbon*, edited by P. A. Thrower (Marcel Dekker, New York, 1989), Vol. 22, Chap. 2.

[9] K. C. Kalra, P. Katyal, and K. C. Singh, "Catalytic reactions of carbons." Journal of Scientific and Industrial Research **48** (4), 186 (1989).

[10] M. Spiro, "Catalysis by carbons of reactions in solution." Catalysis Today **7** (2), 167 (1990).

[11] L. R. Radovic and F. Rodriguez-Reinoso, in *Chemistry and Physics of Carbon*, edited by P. A. Thrower (Marcel Dekker, New York, 1997), Vol. 25, 243.

[12] J. W. Larsen, J. Jandzinski, M. Sidovar, and J. L. Stuart, "Carbon-catalyzed decompositions of hydrazine and hydroxylamine." Carbon **39** (3), 473 (2001).

[13] J. M. Austin, T. Groenewald, and M. Spiro, "Heterogeneous catalysis in solution. Part 18. The catalysis by carbons of oxidation-reduction reactions." Journal of the Chemical Society: Dalton Transactions (6), 854 (1980).

[14] Anonymous, "Carbon black: chemical profile." Chemical Market Reporter **261** (25), 35 (June 24, 2002).

[15] N. P. Cheremisinoff, *Handbook of industrial toxicology and hazardous materials*. (Marcel Dekker, New York, 1999).

[16] C. L. Mantell, *Carbon and graphite handbook*. (Interscience Publishers, New York, 1968).

[17] M. Pourbaix, *Atlas of electrochemical equilibria in aqueous solutions*. (Pergamon Press, New York, 1966).

[18] J. I. Kroschwitz, *Kirk-Othmer concise encyclopedia of chemical technology*, 4th ed. (Wiley, New York, 1999).

[19] S. J. Thomson and G. C. Webb, *Heterogeneous catalysis*. (John Wiley & Sons, Inc., New York, 1968).

[20] M. Spiro, in *Comprehensive chemical kinetics*, edited by R. G. Compton (Elsevier, New York, 1989), Vol. 28, Chap. 2.

[21] K. J. Laidler, *Chemical kinetics*, 3rd ed. (Harper & Row, New York, 1987).

[22] J. M. Thomas and William John Thomas, *Introduction to the principles of heterogeneous catalysis*. (Academic Press, New York, 1967).

[23] R. W. Coughlin and F. S. Ezra, "Role of surface acidity in the adsorption of organic pollutants on the surface of carbon." Environmental Science and Technology **2** (4), 291 (1968).

[24] P. Aggarwal, J. C. Kapoor, S. K. Kapoor, A. K. Bhalla, and R. C. Bansal, "Adsorption of nitrobenzene on activated carbon from dilute aqueous solutions." Indian Journal of Chemical Technology **3** (4), 187 (1996).

[25] J. M. Thomas and W. J. Thomas, *Principles and practice of heterogeneous catalysis*. (VCH, New York, 1997).

[26] P. H. Given and L. W. Hill, "Catalysis of the isomerization and polymerization of olefins on carbon blacks." Carbon **6** (4), 525 (1968).

[27] L. W. Hill, V. K. Acharya, and W. E. Wallace, Jr., "Carbon black catalyzed olefin isomerizations." Carbon **9** (2), 219 (1971).

[28] J. A. Meier and L. W. Hill, "Carbon black catalyzed olefin isomerization. I. Heterogeneous site model based on rate dependence on catalyst concentration." Journal of Catalysis **32** (1), 80 (1974).

[29] T. W. J. Taylor and E. M. W. Lavington, "The heterogeneous catalysis of stereoisomeric change in oximes." Journal of the Chemical Society, 980 (1934).

[30] T. W. J. Taylor and Sally Marks, "The conversion of alpha-benzil monoxime into the beta-oxime by animal charcoal." Nature **125**, 636 (1930).

[31] R. E. Pincock, W. M. Johnson, and J. Haywood-Farmer, "Carbon catalyzed organic reactions: racemization of 1,1'-binaphthyl by carbon surfaces." Canadian Journal of Chemistry **54** (4), 548 (1976).

[32] R. E. Pincock, W. M. Johnson, K. R. Wilson, and J. Haywood-Farmer, "Carbon catalyzed racemization of 1,1'-binaphthyl." Journal of the American Chemical Society **95** (19), 6477 (1973).

[33] L. G. Hutchins and R. E. Pincock, "Heterogeneous catalytic racemization of 4,4'-disubstituted 1,1'-binaphthyls by active carbons and by modified carbon catalysts." Journal of Organic Chemistry **45** (12), 2414 (1980).

[34] B. E. Douglas, "Racemization of tris(ethylenediamine)cobalt(III) ion in the presence of decolorizing carbon." Journal of the American Chemical Society **76**, 1020 (1954).

[35] W. C. Erdman, H. E. Swift, and B. E. Douglas, "The racemization of complex ions on activated carbon. II. The racemization of D-tris(ethylenediamine)cobalt(III) chloride and other complexes." Journal of Inorganic and Nuclear Chemistry **24**, 1365 (1962).

[36] F. P. Dwyer and A. M. Sargeson, "Catalytic racemization of tris-(ethylenediamine)cobalt(III) ion." Nature **187**, 1022 (1960).

[37] R. J. Mureinik and M. Spiro, "Heterogeneous catalysis in solution. Part 10. Racemization and reduction by solids of (+)589-tris(ethylenediamine)cobalt(III)." Journal of the Chemical Society: Dalton Transactions (23), 2480 (1974).

[38] R. J. Mureinik and M. Spiro, "Heterogeneous catalysis in solution. Part 12.

Racemization of (+)589-tris(ethylenediamine)cobalt(III) by a carbon black and kinetics of reacting systems involving racemization." Journal of the Chemical Society: Dalton Transactions (23), 2493 (1974).

[39] P. D. Totterdell and M. Spiro, "Heterogeneous catalysis in solution. Part 13. Kinetics of racemization in two immiscible phases with rapid exchange across the interface, illustrated by the racemization of (+)589-tris(ethylenediamine)cobalt(III) catalyzed by a carbon black." Journal of the Chemical Society: Faraday Transactions I **72** (6), 1477 (1976).

[40] G. H. Searle and E. Larsen, "The bis[di(2-aminoethyl)sulfide]cobalt(III) ion. Existence of only the unsymmetrical-facial geometric isomer and its optical resolution." Acta Chemica Scandinavica A **A30** (2), 143 (1976).

[41] A. Hammershoi and E. Larsen, "The stability of u-fac-bis[di(2-aminoethyl)sulfide]cobalt(III) and the charcoal-catalyzed racemization of the (-)D enantiomer in acidic solution." Acta Chemica Scandinavica A **32** (6), 485 (1978).

[42] F. P. Dwyer, F. L. Garvan, and A. Shulman, "Stereospecific influences in metal complexes containing optically active ligands. I. Some of the optical isomers of tris(propylenediamine)cobalt(III) ion." Journal of the American Chemical Society **81**, 290 (1959).

[43] W. C. Erdman and B. E. Douglas, "The racemization of complex ions on activated carbon. I. The racemization of potassium D-ethylenediaminetetraacetatocobaltate(III)." Journal of Inorganic and Nuclear Chemistry **24**, 1355 (1962).

[44] D. Sen and W. C. Fernelius, "Catalytic racemization of optically active complexes: Tris(ethylenediamine)cobalt(III), -platinum(IV), and -rhodium(III) halides." Journal of Inorganic and Nuclear Chemistry **10**, 269 (1959).

[45] Y. Y. Hoyano and R. E. Pincock, "Carbon catalyzed organic reactions: carbon promoted solvolysis of a phosphate ester derived from 1,1'-bi-2-naphthol." Canadian Journal of Chemistry **58** (2), 134 (1980).

[46] F. J. Waller, J. B. Appleby, and S. C. Webb, in *Chemical Industries*, edited by M. E. Ford (Marcel Dekker, Inc., New York, 2001), Vol. 82 (Catalysis of Organic Reactions), 169.

[47] B. R. Puri, S. Kumari, and K. C. Kalra, "Acidoid behavior of charcoal as a function of its oxygen complexes. VIII. Strength of charcoal acidoid." Journal of the Indian Chemical Society **49** (2), 127 (1972).

[48] P. S. Walton and M. Spiro, "Heterogeneous catalysis in solution. Part 4. Effect of solids on some organic substitution reactions." Journal of the Chemical Society B (1), 42 (1969).

[49] J. M. Austin, O. D. E. S. Ibrahim, and M. Spiro, "Heterogeneous catalysis in solution. Part 5. Catalysis by charcoal and silver iodide of the ethyl iodide-silver nitrate reaction." Journal of the Chemical Society B (6), 669 (1969).

[50] J. Bjerrum and E. Christensen, *Metal ammine formation in aqueous solution: theory of the reversible step reactions*. (P. Haase & Son, Copenhagen, 1941).

[51] J. C. Bailar, Jr. and J. B. Work, "The role of catalysis in the preparation and reactions of some Co(III) and Cr(III) ammines." Journal of the American

Chemical Society **67**, 176 (1945).

[52] R. J. Mureinik, "Carbon-catalyzed formation of hexamminecobalt(III) in solution." Journal of Catalysis **50** (1), 56 (1977).

[53] A. Tomita and Y. Tamai, "Catalytic effect of surface groups on carbon in the hydrolysis of a hexanitrocobaltate(III)." Journal of Colloid and Interface Science **36** (1), 153 (1971).

[54] A. Tomita and Y. Tamai, "Effect of surface groups of carbon on the adsorption and catalytic base hydrolysis of a hexaamminecobalt(III) ion." Journal of Physical Chemistry **75** (5), 649 (1971).

[55] T. G. Alkhazov, A. E. Lisovskii, Yu A. Ismailov, and A. I. Kozharov, "Oxidative dehydrogenation of ethylbenzene on activated carbons. I. General characteristics of the process." Kinetika i Kataliz **19** (3), 611 (1978).

[56] A. E. Lisovskii, A. I. Kozharov, Yu A. Ismailov, and T. G. Alkhazov, "Oxidative dehydrogenation of ethylbenzene on activated carbons. II. Study of the nonsteady-state activity of carbons." Kinetika i Kataliz **19** (4), 950 (1978).

[57] T. G. Alkhazov, A. E. Lisovskii, and T. K. Gulakhmedova, "Oxidative dehydrogenation of ethylbenzene over a charcoal catalyst." Reaction Kinetics and Catalysis Letters **12** (2), 189 (1979).

[58] G. C. Grunewald and R. S. Drago, "Oxidative dehydrogenation of ethylbenzene to styrene over carbon-based catalysts." Journal of Molecular Catalysis **58** (2), 227 (1990).

[59] M. F. R. Pereira, J. J. M. Orfao, and J. L. Figueiredo, "Oxidative dehydrogenation

of ethylbenzene on activated carbon catalysts. I. Influence of surface chemical groups." Applied Catalysis A: General **184** (1), 153 (1999).

[60] M. F. R. Pereira, J. J. M. Orfao, and J. L. Figueiredo, "Oxidative dehydrogenation of ethylbenzene on activated carbon catalysts 2. Kinetic modelling." Applied Catalysis A: General **196** (1), 43 (2000).

[61] M. F. R. Pereira, J. J. M. Orfao, and J. L. Figueiredo, "Oxidative dehydrogenation of ethylbenzene on activated carbon catalysts 3. Catalyst deactivation." Applied Catalysis A: General **218** (1-2), 307 (2001).

[62] A. Schraut, G. Emig, and H. Hofmann, "Kinetic investigations of the oxydehydrogenation of ethylbenzene." Journal of Catalysis **112** (1), 221 (1988).

[63] G. S. Szymanski and G. Rychlicki, "Importance of oxygen surface groups in catalytic dehydration and dehydrogenation of butan-2-ol promoted by carbon catalysts." Carbon **29** (4-5), 489 (1991).

[64] G. S. Szymanski and G. Rychlicki, "Catalytic conversion of 2-propanol on cation-substituted forms of oxidized carbon." Reaction Kinetics and Catalysis Letters **43** (2), 475 (1991).

[65] G. S. Szymanski and G. Rychlicki, "Catalytic conversion of propan-2-ol on carbon catalysts." Carbon **31** (2), 247 (1993).

[66] G. S. Szymanski, G. Rychlicki, and A. P. Terzyk, "Catalytic conversion of ethanol on carbon catalysts." Carbon **32** (2), 265 (1994).

[67] I. F. Silva, J. Vital, A. M. Ramos, H. Valente, A. M. B. do Rego, and M. J. Reis, "Oxydehydrogenation of cyclohexanol over carbon catalysts." Carbon **36** (7-8),

1159 (1998).

[68] V. N. Dubchenko and V. I. Kovalenko, "Chlorination of carboxylic acid anhydrides by carbon tetrachloride on activated charcoal." Zhurnal Prikladnoi Khimii **41** (11), 2568 (1968).

[69] V. N. Dubchenko and V. I. Kovalenko, "Transformation of carboxylic acid anhydrides in the gas phase on activated carbon." Zhurnal Prikladnoi Khimii **41** (9), 2048 (1968).

[70] V. N. Dubchenko, "Thermocatalytic reaction of carboxylic acids with carbon tetrachloride in the gas phase." Zhurnal Prikladnoi Khimii **46** (8), 1822 (1973).

[71] B. R. Puri, B. Kumar, and K. C. Kalra, "Studies in catalytic reactions of carbon. IV. Oxidation of hydrogen sulfide." Indian Journal of Chemistry A **9** (9), 970 (1971).

[72] M. Steijns and P. Mars, "Role of sulfur trapped in micropores in the catalytic partial oxidation of hydrogen sulfide with oxygen." Journal of Catalysis **35** (1), 11 (1974).

[73] R. Sreeramamurthy and P. G. Menon, "Oxidation of hydrogen sulfide on active carbon catalyst." Journal of Catalysis **37** (2), 287 (1975).

[74] O. C. Cariaso and P. L. Walker, Jr., "Oxidation of hydrogen sulfide over microporous carbons." Carbon **13** (3), 233 (1975).

[75] M. Steijns, F. Derks, A. Verloop, and P. Mars, "The mechanism of the catalytic oxidation of hydrogen sulfide. II. Kinetics and mechanism of hydrogen sulfide oxidation catalyzed by sulfur." Journal of Catalysis **42** (1), 87 (1976).

[76] M. Steijns, P. Koopman, B. Nieuwenhuijse, and P. Mars, "The mechanism of the catalytic oxidation of hydrogen sulfide. III. An electron spin resonance study of the sulfur catalyzed oxidation of hydrogen sulfide." Journal of Catalysis **42** (1), 96 (1976).

[77] B. R. Puri, D. D. Singh, and S. K. Verma, "Studies on catalytic reaction of carbon. Part VIII. Oxidation of hydrogen sulfide by air in the presence of active carbons." Indian Journal of Chemistry A **18A** (5), 388 (1979).

[78] W. O. Stacy, F. J. Vastola, and P. L. Walker, Jr., "Interaction of sulfur dioxide with active carbon." Carbon **6** (6), 917 (1968).

[79] T. Otake, S. Tone, Y. Yokota, and K. Yoshimura, "Kinetics of sulfur dioxide oxidation over activated carbon." Journal of Chemical Engineering of Japan **4** (2), 155 (1971).

[80] H. Komiyama and J. M. Smith, "Sulfur dioxide oxidation in slurries of activated carbon." AIChE Journal **21** (4), 664 (1975).

[81] E. Richter, "Carbon catalysts for pollution control." Catalysis Today **7** (2), 93 (1990).

[82] X. S. Zhao, G. Y. Cai, Z. Z. Wang, Q. X. Wang, Y. H. Yang, and J. S. Luo, "Influences of surface functional groups on catalytic activity over activated carbon catalysts for sulfur dioxide removal from flue gases." Applied Catalysis B: Environmental **3** (4), 229 (1994).

[83] M. N. Rao and O. A. Hougen, "Catalytic oxidation of nitric oxide on activated carbon." Chemical Engineering Progress Symposium Series **48** (Reaction Kinetics

and Transfer Processes), 110 (1952).

[84] H. Jüntgen, E. Richter, and H. Kühl, "Catalytic activity of carbon catalysts for the reaction of nitrogen oxides (NOx) with ammonia." Fuel **67** (6), 775 (1988).

[85] H. Jüntgen and H. Kühl, in *Chemistry and Physics of Carbon*, edited by P. A. Thrower (Marcel Dekker, New York, 1989), Vol. 22, Chap. 2.

[86] H. Kuhl, H. Baumann, H. Juentgen, P. Ehrburger, J. Dentzer, and J. Lahaye, "The importance of active surface area on the nitric oxide reduction with ammonia on carbon catalysts." Fuel **68** (1), 129 (1989).

[87] E. Richter, H. J. Schmidt, and H. G. Schecker, "Adsorption and catalytic reactions of nitric oxide and ammonia on activated carbon." Chemical Engineering and Technology **13** (5), 332 (1990).

[88] K. Yang and M. A. Johnson, "Novel carbon catalysis: oxidation in basic solution." Journal of Organic Chemistry **42** (23), 3754 (1977).

[89] Y. I. Pyatnitskii, G. I. Golodets, and T. G. Skorbilina, "Vapor-phase oxidation of o-xylene to phthalic anhydride on carbon." Kinetika i Kataliz **17** (3), 814 (1976).

[90] Y. I. Pyatnitskii, T. G. Skorbilina, and I. A. Tarkovskaya, "Catalytic vapor-phase oxidation of o-xylene on activated carbon." Kataliz i Katalizatory **19**, 41 (1981).

[91] A. Y. Lukomskaya, "Mechanism of the catalytic oxidation of o-xylene on active coals." Reaction Kinetics and Catalysis Letters **23** (1-2), 85 (1983).

[92] A. Y. Lukomskaya, I. A. Tarkovskaya, and V. V. Strelko, "Influence of chemical-composition of carbon catalysts on their adsorptive properties in catalytic-oxidation of ortho-xylene." Reaction Kinetics and Catalysis Letters **31** (2), 435

(1986).

[93] A. Tomita, S. Mori, and Y. Tamai, "Catalytic behavior of carbon on the oxidation of cyclohexene." Carbon **9** (2), 224 (1971).

[94] M. Voll and H. P. Boehm, "Catalytic hydrogen chloride oxidation on carbon black." Carbon **8** (1), 99 (1970).

[95] E. K. Rideal and W. M. Wright, "Low-temperature oxidation at charcoal surfaces. I. The behavior of charcoal in the absence of promoters." Journal of the Chemical Society **127**, 1347 (1925).

[96] E. K. Rideal and W. M. Wright, "Low-temperature oxidation at charcoal surfaces. III. The behavior of blood charcoal and the influence of temperature on the reaction rate." Journal of the Chemical Society, 3182 (1926).

[97] E. K. Rideal and W. M. Wright, "Low-temperature oxidation at charcoal surfaces. II. The behavior of charcoal in the presence of promoters." Journal of the Chemical Society, 1813 (1926).

[98] W. M. Wright, "Low-temperature oxidation at charcoal surfaces. IV. The active areas for different acids and their relative rates of oxidation." Journal of the Chemical Society, 2323 (1927).

[99] J. Barkauskas and A. Kareiva, "Investigation of n-hexane oxidation on the surface of activated charcoal." Reaction Kinetics and Catalysis Letters **53** (1), 7 (1994).

[100] G. Lemoine, "On some reactions effected by means of charcoal as a catalytic agent." Comptes Rendus **144**, 357 (1907).

[101] A. King, "Chemisorption on charcoal. VIII. Influence of temperature of activation of charcoal on (a) catalytic oxidation of salts and (b) catalytic decomposition of hydrogen peroxide." Journal of the Chemical Society, 1688 (1936).

[102] E. C. Larsen and J. H. Walton, "Activated carbon as a catalyst in certain oxidation-reduction reactions." Journal of Physical Chemistry **44**, 70 (1940).

[103] G. Brinkmann, "Chemical character and catalytic behavior of activated carbon." Angewandte Chemie **61**, 378 (1949).

[104] G. Brinkmann, "Catalytic reactions of active carbon." Kolloid-Zeitschrift **123**, 116 (1951).

[105] M. L. Studebaker, "Chemistry of carbon black and reinforcement." Rubber Chemistry and Technology **30**, 1400 (1957).

[106] V. A. Garten and D. E. Weiss, "Ion- and electron-exchange properties of activated carbon in relation to its behavior as a catalyst and adsorbent." Reviews of Pure and Applied Chemistry **7**, 69 (1957).

[107] A. S. Fomenko, I. L. Gankina, and T. M. Abramova, "Study of the mechanism of decomposition of hydrogen peroxide on activated carbon by the isotope method." Kinetika i Kataliz **2**, 732 (1961).

[108] R. N. Smith, A. J. Miles, and S. F. Watkins, "Carbon-catalyzed decomposition of hydrogen peroxide." Transactions of the Faraday Society **62** (9), 2553 (1966).

[109] B. R. Puri and K. C. Kalra, "Catalytic reactions of carbon. II. Catalytic decomposition of hydrogen peroxide." Indian Journal of Chemistry A **7** (2), 149 (1969).

[110] B. R. Puri and K. C. Kalra, "Decomposition of hydrogen peroxide in the presence of carbon blacks." Carbon **9** (3), 313 (1971).

[111] R. Davis, T. C. Lovelace, N. J. Martinez, and A. Millar, "Decomposition of peracids and their salts with activated carbon." Catalysis Letters **31**, 307 (1995).

[112] C. R. Walter, "Kinetics of ethylene chloride pyrolysis using a pumice catalyst." Journal of Chemical and Engineering Data **5**, 468 (1960).

[113] K. Okamoto, N. Tanaka, K. Adachi, and H. Shingu, "Catalytic dehydrochlorination of 1,2-dichloroethane on active carbon in the presence of some hydrocarbons." Bulletin of the Chemical Society of Japan **39** (7), 1522 (1966).

[114] J. J. Prinsloo, P. C. Van Berge, and J. Zlotnick, "Catalytic decomposition of 1,2-dichloroethane with activated carbon catalysts." Journal of Catalysis **32** (3), 466 (1974).

[115] M. Braden, W. P. Fletcher, and G. P. McSweeney, "Vulcanization of rubber by organic peroxides." Rubber Chemistry and Technology **28**, 190 (1955).

[116] B. R. Puri, V. K. Sud, and K. C. Kalra, "Studies in catalytic reactions of carbon. III. Catalytic decomposition of benzoyl peroxide." Indian Journal of Chemistry A **9** (9), 966 (1971).

[117] V. V. Kislykh and A. E. Sidel'nikov, "Decomposition of nitrous oxide in the presence of carbon." Kinetika i Kataliz **16** (3), 776 (1975).

[118] W. J. Snyder and D. Kunzru, "Effect of active carbon on the kinetics of polymerization of methyl methacrylate." Journal of Macromolecular Science:

Chemistry A **5** (2), 297 (1971).

[119] K. Ohkita, N. Tsubokawa, M. Noda, and M. Uchiyama, "Polymerization of N-vinylcarbazole initiated by carbon black surface." Carbon **15** (3), 194 (1977).

[120] K. Ohkita, M. Uchiyama, and H. Nishioka, "The polymerization of N-vinylcarbazole in the presence of carbon black." Carbon **16** (3), 195 (1978).

[121] N. Tsubokawa, N. Takeda, and K. Kudoh, "Carbon black as an initiator of cationic polymerization of isobutyl vinyl ether." Carbon **18** (2), 163 (1980).

[122] N. Tsubokawa, "Cationic polymerization of alpha-methylstyrene initiated by channel black surface." Journal of Polymer Science: Polymer Letters **18** (6), 461 (1980).

[123] N. Tsubokawa, N. Takeda, and A. Kanamaru, "The cationic polymerization of N-vinyl-2-pyrrolidone initiated by carbon black surface." Journal of Polymer Science: Polymer Letters **18** (9), 625 (1980).

[124] E. N. Shapatina, V. L. Kuchaev, B. E. Pen'kovoi, and M. I. Temkin, "Kinetics of the catalytic synthesis of phosgene." Kinetika i Kataliz **17** (3), 644 (1976).

[125] E. N. Shapatina, V. L. Kuchaev, and M. I. Temkin, "Kinetics of the catalytic synthesis of phosgene." Kinetika i Kataliz **18** (4), 968 (1977).

[126] E. N. Shapatina, V. L. Kuchaev, and M. I. Temkin, "Kinetics of phosgene synthesis at low chlorine concentrations." Kinetika i Kataliz **20** (5), 1183 (1979).

[127] W. J. Pope, "The preparation of sulfuryl chloride." Recueil des Travaux Chimiques **42**, 939 (1923).

[128] B. R. Puri, D. D. Singh, and S. K. Verma, "Studies in catalytic reactions of carbons: Part VII. Catalytic chlorination of toluene in presence of active carbons." Indian Journal of Chemistry A **16A** (12), 1026 (1978).

[129] B. R. Puri, D. D. Singh, N. C. Kaura, and S. K. Verma, "Studies in catalytic reactions of carbons. Part X. Catalytic chlorination of benzene and toluene at ambient temperature in the presence of activated carbons." Indian Journal of Chemistry A **19A** (2), 109 (1980).

[130] B. R. Puri, D. D. Singh, J. Chander, and L. R. Sharma, "Interaction of charcoal with chlorine water." Journal of the Indian Chemical Society **35**, 181 (1958).

[131] B. R. Puri, O. P. Mahajan, and D. D. Singh, "Interaction of charcoal with chlorine water. II." Journal of the Indian Chemical Society **37**, 171 (1960).

[132] M. Farcasiu, S. C. Petrosius, and E. P. Ladner, "Hydrodehydroxylation and hydrodehalogenation of substituted polycyclic aromatics using carbon catalysts." Journal of Catalysis **146** (1), 313 (1994).

[133] T. Sankarshana and M. B. Rao, "Catalytic dehydrochlorination of 1,1,2,2-tetrachloroethane." Indian Chemical Engineer **31** (1), 38 (1989).

[134] B. Neumann, W. Steuer, and R. Domke, "The conversion of bromine and hydrogen into hydrobromic acid in the presence of charcoal." Zeitschrift fur Angewandte Chemie **39**, 374 (1926).

[135] N. C. Jones, "The activation of halogen and carbon monoxide." Journal of Physical Chemistry **33**, 1415 (1929).

[136] G.-M. Schwab and F. Lober, "The halogen-transporting action of carbon."

Zeitschrift für Physikalische Chemie **A186**, 321 (1940).

[137] U. Hofmann and G. Ohlerich, "The surface chemistry of carbon." Angewandte Chemie **62**, 16 (1950).

[138] A. Clauss, H. P. Boehm, and U. Hofmann, "The adsorbing and catalytically effective surfaces of carbon blacks." Zeitschrift für Anorganische und Allgemeine Chemie **290**, 35 (1957).

[139] R. N. Smith, "The chemistry of carbon-oxygen surface compounds." Quarterly Reviews **13**, 287 (1959).

[140] E. Stumpp and W. Ruedorff, "Catalytic investigations on metal chloride-graphite compounds." Zeitschrift für Elektrochemie **66**, 648 (1962).

[141] B. R. Puri and K. C. Kalra, "Catalytic reactions on carbon. I. Catalytic combination of hydrogen and bromine." Indian Journal of Chemistry A **5** (12), 638 (1967).

[142] B. R. Puri and K. C. Kalra, "Carbons as catalysts for combination of hydrogen and iodine." Chemistry & Industry (50), 1810 (1969).

[143] Y. Uemichi, Y. Kashiwaya, A. Ayame, and H. Kanoh, "Formation of aromatic hydrocarbons in degradation of polyethylene over an activated carbon catalyst." Chemistry Letters (1), 41 (1984).

[144] B. S. Greensfelder, H. H. Voge, and G. M. Good, "Catalytic and thermal cracking of pure hydrocarbons. Mechanisms of reaction." Industrial & Engineering Chemistry **41**, 2573 (1949).

[145] M. Farcasiu and C. Smith, "Modeling coal liquefaction: Decomposition of 4-(1-

naphthylmethyl)bibenzyl catalyzed by carbon black." Energy & Fuels **5** (1), 83 (1991).

[146] M. Farcasiu, C. M. Smith, E. P. Ladner, and A. P. Sylwester, "Carbon materials - activity and selectivity in hydrocracking reactions." Preprints of Symposia - American Chemical Society, Division of Fuel Chemistry **36** (4), 1869 (1991).

[147] M. Farcasiu and S. C. Petrosius, "Heterogenous catalysis: mechanisms of selective cleavage of strong carbon-carbon bonds." Preprints of Symposia - American Chemical Society, Division of Fuel Chemistry **39** (3), 723 (1994).

[148] R. Burshtein, "Exchange between light and heavy hydrogen on charcoal." Acta Physicochimica U. R. S. S. **8**, 857 (1938).

[149] M. J. Rossiter, R. N. Smith, and J. R. Ludden, "The carbon-catalyzed hydrogen-deuterium exchange reaction." Journal of Physical Chemistry **67** (12), 2541 (1963).

[150] K. F. Bonhoeffer, A. Farkas, and K. W. Rummel, "Heterogeneous catalysis of the para-hydrogen conversion." Zeitschrift fur Physikalische Chemie **B21**, 225 (1933).

[151] J. Turkevich and J. Laroche, "Catalytic activity of a graded set of charcoals for hydrogen-deuterium equilibration and ortho-parahydrogen conversion and electron spin resonance." Zeitschrift fur Physikalische Chemie **15**, 399 (1958).

[152] M. Kodomari, Y. Suzuki, and K. Yoshida, "Graphite as an effective catalyst for Friedel-Crafts acylation." Chemical Communications (16), 1567 (1997).

[153] H. Shulman and E. Keinan, "Catalysis of the Kemp elimination by natural coals." Organic Letters **2** (23), 3747 (2000).

[154] E. F. G. Barbosa and M. Spiro, "Joint homogeneous and heterogeneous catalysis: a new synergistic effect." Journal of the Chemical Society: Chemical Communications (13), 423 (1977).

[155] R. M. Martin-Aranda, M. L. Rojas Cervantes, A. J. Lopez-Peinado, and J. D. Lopez-Gonzalez, "Alkaline carbons as base catalysts: alkylation of imidazole with alkyl halides." Journal of Molecular Catalysis **85**, 253 (1993).

[156] F. J. Weigert, "Carbon catalyzed polymethylbenzene dealkylation." Journal of Molecular Catalysis **85** (2), 229 (1993).

[157] H. P. Boehm, E. Diehl, W. Heck, and R. Sappok, "Surface oxides of carbon." Angewandte Chemie **76** (17), 742 (1964).

[158] B. R. Puri, in *Chemistry and Physics of Carbon*, edited by P. A. Thrower (Marcel Dekker, New York, 1970), Vol. 6, 191.

[159] D. Rivin, "Surface properties of carbon." Rubber Chemistry and Technology **44** (2), 307 (1971).

[160] H. P. Boehm, "Some aspects of the surface chemistry of carbon blacks and other carbons." Carbon **32** (5), 759 (1994).

[161] J. Klausen, S. P. Troeber, S. B. Haderlein, and R. P. Schwarzenbach, "Reduction of substituted nitrobenzenes by Fe(II) in aqueous mineral suspensions." Environmental Science and Technology **29** (9), 2396 (1995).

[162] N. V. Sidgwick, *The organic chemistry of nitrogen*. (Clarendon Press, Oxford, 1967).

[163] A. Furst, R. C. Berlo, and S. Hooton, "Hydrazine as a reducing agent for organic

compounds (catalytic hydrazine reductions)." Chemistry Reviews **65** (1), 51 (1965).

[164] B. H. Han, D. H. Shin, H. R. Lee, and B. H. Ro, "Reduction of aromatic nitro compounds with hydrazine catalyzed by activated zinc-copper." Bulletin of the Korean Chemical Society **10** (3), 315 (1989).

[165] B. H. Han and D. G. Jang, "Montmorillonite-catalyzed reduction of nitroarenes with hydrazine." Tetrahedron Letters **31** (8), 1181 (1990).

[166] B. H. Han, D. H. Shin, and S. Y. Cho, "Graphite catalyzed reduction of aromatic and aliphatic nitro compounds with hydrazine hydrate." Tetrahedron Letters **26** (50), 6233 (1985).

[167] M. K. Park, D. G. Jang, and B. H. Han, "Reduction of aromatic nitro compounds with hydrazine in the presence of sodium nitrate-carbon." Bulletin of the Korean Chemical Society **12** (6), 709 (1991).

[168] T. F. Stepanova and O. F. Ginzburg, "Use of oxidized SKT and BAU carbons as catalysts during the reduction of aromatic nitro compounds by hydrazine hydrate." Zhurnal Prikladnoi Khimii **46** (5), 1159 (1973).

[169] R. V. Rothenburg, "Performance of hydrazine hydrates in the removal of nitro-, nitroso- and isonitroso-groups." Chemische Berichte **26**, 2060 (1893).

[170] A. L. Endrey and T. A. Reilly, "Reduction mechanism of aromatic nitro compounds." Proceedings of the Annual Power Sources Conference **22**, 91 (1968).

[171] T. Hirashima and O. Manabe, "Catalytic reduction of aromatic nitro compounds with hydrazine in the presence of iron(III) chloride and active carbon." Chemistry

Letters (3), 259 (1975).

[172] P. M. G. Bavin, "The preparation of amines and hydrazo compounds using hydrazine and palladized charcoal." Canadian Journal of Chemistry **36**, 238 (1958).

[173] L. Holleck and R. Schindler, "Polarographic behavior of aromatic nitroso compounds." Zeitschrift fur Elektrochemie **60**, 1138 (1956).

[174] A. Furst and R. E. Moore, "Reductions with hydrazine hydrate catalyzed by Raney Nickel. II. Aromatic nitro compounds to intermediate products." Journal of the American Chemical Society **79**, 5492 (1957).

[175] C. Nishihara and H. Shindo, "Reduction of nitrobenzene in aqueous alkaline solution at a silver electrode. Observation by SERS, RRDE and UV absorption." Journal of Electroanalytical Chemistry and Interfacial Electrochemistry **202** (1-2), 231 (1986).

[176] A. Cyr, P. Huot, J. F. Marcoux, G. Belot, E. Laviron, and J. Lessard, "The electrochemical reduction of nitrobenzene and azoxybenzene in neutral and basic aqueous methanolic solutions at polycrystalline copper and nickel electrodes." Electrochimica Acta **34** (3), 439 (1989).

[177] A. Cyr, P. Huot, G. Belot, and J. Lessard, "The efficient electrochemical reduction of nitrobenzene and azoxybenzene to aniline in neutral and basic aqueous methanolic solutions at Devarda copper and Raney nickel electrodes: electrocatalytic hydrogenolysis of nitrogen-oxygen and nitrogen-nitrogen bonds." Electrochimica Acta **35** (1), 147 (1990).

[178] W. J. Plieth, in *Encyclopedia of electrochemistry of the elements*, edited by A. J. Bard (Marcel Dekker, New York, 1979), Vol. 8, 321.

[179] E. W. Schmidt, *Hydrazine and its derivatives: preparation, properties, applications*, 2nd ed. (Wiley-Interscience, New York, 2001).

[180] H. W. Schiessl, "Hydrazine - rocket fuel to synthetic tool." Aldrichimica Acta **13** (2), 33 (1980).

[181] L. F. Audrieth and B. A. Ogg, *The chemistry of hydrazine*. (John Wiley & Sons, New York, 1951).

[182] L. F. Audrieth and W. L. Jolly, "Catalytic decomposition of highly concentrated hydrazine by Raney nickel." Journal of Physics & Colloid Chemistry **55**, 524 (1951).

[183] C. F. Sayer, "The heterogeneous decomposition of hydrazine. Part 1: Kinetics of the liquid phase decomposition on a supported iridium catalyst." Technical Report No. RPETR688 (Rocket Propulsion Establishment, Westcott, Oct. 1968).

[184] C. F. Sayer, "The heterogeneous decomposition of hydrazine. Part 2: Use of N15 as a tracer to study the decomposition of hydrazine on the Shell 405 catalyst." Technical Report No. RPETR6910 (Rocket Propulsion Establishment, Westcott, Dec. 1969).

[185] C. F. Sayer, "The decomposition of hydrazine on the shell 405 catalyst." Technical Papers of the AIAA 6th Propulsion Joint Specialist Conference, Paper 70606 (1970).

[186] C. F. Sayer, "The heterogeneous decomposition of hydrazine. Part 4: Kinetics of

the decomposition of liquid hydrazine on a supported rhodium catalyst." Technical Report No. RPETR7116 (Rocket Propulsion Establishment, Westcott, Nov. 1971).

[187] K. M. C. Davis and C. F. Sayer, "Heterogeneous decomposition of hydrazine. 1. On a supported rhodium catalyst." Journal of the Chemical Society: Faraday Transactions I **68** (10), 1884 (1972).

[188] C. F. Sayer, "The heterogeneous decomposition of hydrazine: Part 5: Kinetics of the decomposition of liquid hydrazine on a supported ruthenium catalyst." Technical Report No. RPETR721 (Rocket Propulsion Establishment, Westcott, Jan. 1972).

[189] C. F. Sayer, "The heterogeneous decomposition of hydrazine. Part 6: Kinetics of the decomposition on supported palladium and platinum catalysts." Technical Report No. RPETR31 (Rocket Propulsion Establishment, Westcott, Nov. 1974).

[190] S. Tanatar, "Catalysis of hydroxylamines and hydrazine." Zeitschrift fur Physikalische Chemie **40**, 475 (1902).

[191] S. Tanatar, "Catalysis of hydrazines." Zeitschrift fur Physikalische Chemie **41**, 37 (1902).

[192] A. Gutbier and K. Neundlinger, "Catalysis of hydrazine by platinum black." Zeitschrift fur Physikalische Chemie **84**, 203 (1913).

[193] G. V. Vitvitskaya and G. B. Grabovskaya, "Catalytic decomposition of hydrazine over platinized carbon in an alkaline solution." Journal of Applied Chemistry **42** (10), 2091 (1969).

[194] S. Huenig, H. R. Mueller, and W. Thier, "Decomposition of diimine." Angewandte Chemie **75**, 298 (1963).

[195] S. Fouche, J. C. Goudeau, and M. L. Bernard, "Kinetic study of the catalytic decomposition of liquid hydrazine in a constant volume static reactor." Journal de Chimie Physique et de Physico-Chimie Biologique **71** (10), 1275 (1974).

[196] M. Spiro and A. B. Ravno, "Heterogeneous catalysis in solution. Part 2. The effect of platinum on oxidation-reduction reactions." Journal of the Chemical Society, 78 (1965).

[197] J.-B. Donnet, R. C. Bansal, and M.-J. Wang, *Carbon black: science and technology*, 2nd. ed. (Marcel Dekker, Inc., New York, 1993).

[198] Special Blacks Division, "Carbon blacks for specialty applications." Technical Report No. S-136 (Cabot Corporation, Billerica, MA, Apr. 2003).

[199] R. C. Bansal, J.-B. Donnet, and F. Stoeckli, *Active carbon*. (Marcel Dekker, Inc., New York, 1988).

[200] S. Lowell and J. E. Shields, *Powder surface area and porosity*, 3rd ed. (Chapman & Hall, New York, 1991).

[201] S. J. Gregg and K. S. W. Sing, *Adsorption, surface area, and porosity*, 2nd ed. (Academic Press, New York, 1982).

[202] F. Stoeckli and F. Kraehenbuehl, "The external surface of microporous carbons, derived from adsorption and immersion studies." Carbon **22** (3), 297 (1984).

[203] A. Seidell and W. F. Linke, *Solubilities: a compilation of solubility data from the periodical literature*, 4th ed. (Van Nostrand, Princeton, 1958).

[204] J.A. Dean and N. A. Lange, *Lange's handbook of chemistry*, 11th ed. (McGraw-Hill, New York, 1973).

[205] B. Wang and X. Cao, "The anodic oxidation of hydrazine on glassy carbon electrode." Electroanalysis **4** (7), 719 (1992).

[206] X. Cao, B. Wang, and Q. Su, "Anodic oxidation of hydrazine on glassy carbon electrodes in acetonitrile." Journal of Electroanalytical Chemistry **361** (1-2), 211 (1993).

[207] R. C. Cosser and F. C. Tompkins, "Heterogeneous decomposition of hydrazine on tungsten films." Transactions of the Faraday Society **67** (2), 526 (1971).

[208] B. R. Puri and R. C. Bansal, "Surface chemistry of carbon blacks. I. High-temperature evacuations." Carbon **1** (4), 451 (1964).

[209] N. V. Korovin and A. G. Kicheev, "Anodic oxidation of hydrazine on graphite." Elektrokhimiya **6** (9), 1330 (1970).

[210] S. Antoniadou, A. D. Jannakoudakis, and E. Theodoridou, "Electrocatalytic reactions on carbon fiber electrodes modified by hemin. II. Electro-oxidation of hydrazine." Synthetic Metals **30** (3), 295 (1989).

[211] P. Pouillen, A.M. Martre, and P. Martinet, "Electrochemical reduction of nitrobenzene in aqueous micellar solutions of various pH. Influence of the type of surfactant." Electrochimica Acta **27** (7), 853 (1982).

[212] I. Rubinstein, "Voltammetric study of nitrobenzene and related compounds on solid electrodes in aqueous solutions." Journal of Electroanalytical Chemistry and Interfacial Electrochemistry **183** (1-2), 379 (1985).

[213] M. Spiro and P. W. Griffin, "Proof of an electron-transfer mechanism by which metals can catalyze oxidation-reduction reactions." Chemical Communications (6), 262 (1969).

[214] J. Bénard and Y. Berthier, *Adsorption on metal surfaces: an integrated approach*. (Elsevier Scientific Publishing Co., New York, 1983).

[215] T. O. Pavela, "Hydrazine-platinum, a low-pressure hydrogen electrode." Suomen Kemistilehti **30B**, 240 (1957).

[216] G. Susbielles and O. Bloch, "Electrochemical study of the reaction of catalytic decomposition of hydrazine on platinum electrodes, in basic medium." Comptes Rendus de l'Académie des Sciences **255**, 685 (1962).

[217] S. Szpak, P. Stonehart, and T. Katan, "Electrode reactions of hydrazine in aqueous solutions." Electrochimica Acta **10** (6), 563 (1965).

[218] B. P. Nesterov and N. V. Korovin, "Anodic oxidation of hydrazine on smooth nickel in alkaline solution." Elektrokhimiya **2** (11), 1296 (1966).

[219] J. Block and G. Schulz-Ekloff, "Catalytic decomposition of nitrogen-15-labeled hydrazine on magnesium oxide-supported iron." Journal of Catalysis **30** (2), 327 (1973).

[220] A. Kant and W. J. McMahon, "Thermal decomposition of nitrogen-15-labeled hydrazine." Journal of Inorganic and Nuclear Chemistry **15**, 305 (1960).

[221] W. C. E. Higginson and D. Sutton, "Oxidation of hydrazine in aqueous solution. II. Use of N15 as a tracer in the oxidation of hydrazine." Journal of the Chemical Society, 1402 (1953).

[222] K. Arnolds, J. Heitbaum, and W. Vielstich, "Rupture of the nitrogen-nitrogen bond in the anodic oxidation and catalytic decomposition of hydrazine." Zeitschrift fur Naturforschung A **29** (2), 359 (1974).

[223] W. Jaenicke and F. Sutter, "Mechanism of photographic development with hydroquinone, Metol, and p-phenylenediamine." Zeitschrift für Elektrochemie **63**, 722 (1959).

[224] I. R. Jonasson and D. R. Stranks, "Heterogeneous catalyzed electron-exchange reactions. I. The thallium(I)-thallium(III) system." Electrochimica Acta **13** (5), 1147 (1968).

[225] P. L. Antonucci, L. Pino, N. Giordano, and G. Pinna, "A comparative analysis of structural and surface effects in the electrochemical corrosion of carbons." Materials Chemistry and Physics **21** (5), 495 (1989).

[226] N. Giordano, P. L. Antonucci, E. Passalacqua, L. Pino, A. S. Arico, and K. Kinoshita, "Relationship between physicochemical properties and electrooxidation behavior of carbon materials." Electrochimica Acta **36** (13), 1931 (1991).

[227] S. R. Kelemen, M. Afeworki, M. L. Gorbaty, and A. D. Cohen, "Characterization of organically bound oxygen forms in lignites, peats, and pyrolyzed peats by X-ray Photoelectron Spectroscopy (XPS) and Solid-State ^{13}C NMR methods." Energy & Fuels **16** (6), 1450 (2002).

[228] U.S. Environmental Protection Agency: Office of Transportation and Air Quality, "Diesel Exhaust in the United States." Report No. EPA420-F-02-048 (September

2002).

[229] G. M. Solomon, T. R. Campbell, T. Carmichael, G. R. Feuer, and J. S. Hathaway, "Exhausted by diesel: how America's dependence on diesel engines threatens our health." Natural Resources Defense Council Report (1998).

[230] E. T. Wei and H. P. Shu, "Nitroaromatic carcinogens in diesel soot: a review of laboratory findings." American Journal of Public Health **73** (9), 1085 (1993).

[231] M. Stiborova, "Nitroaromatic compounds: Environmental pollutants with carcinogenic potential for humans." Chemicke Listy **96** (10), 784 (2002).

Appendix A:

Nitrogen Adsorption Isotherms

V_{gas} = volume of N_2 gas adsorbed

P = N_2 equilibrium pressure

P_0 = N_2 saturated equilibrium vapor pressure

P/P_0 = relative pressure

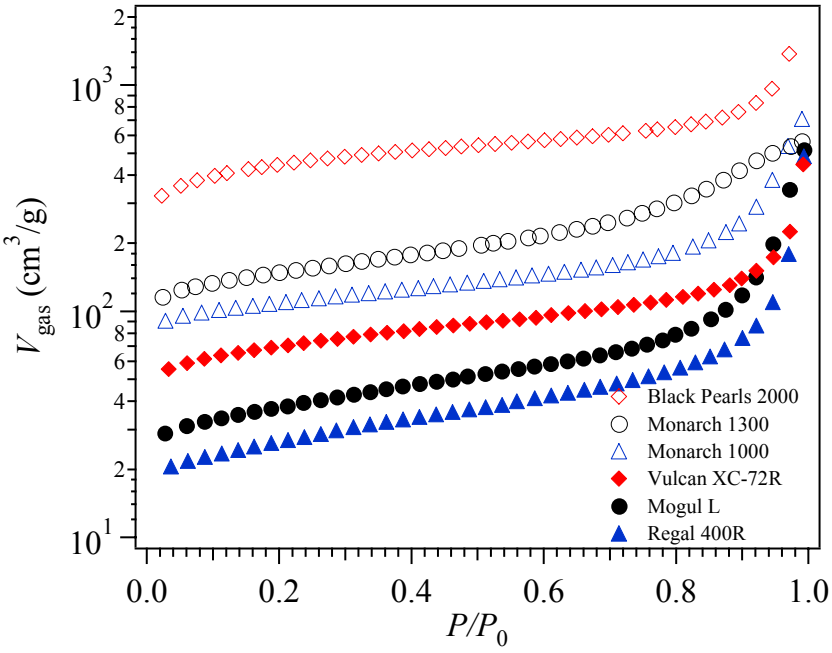

Adsorption isotherm of carbon blacks

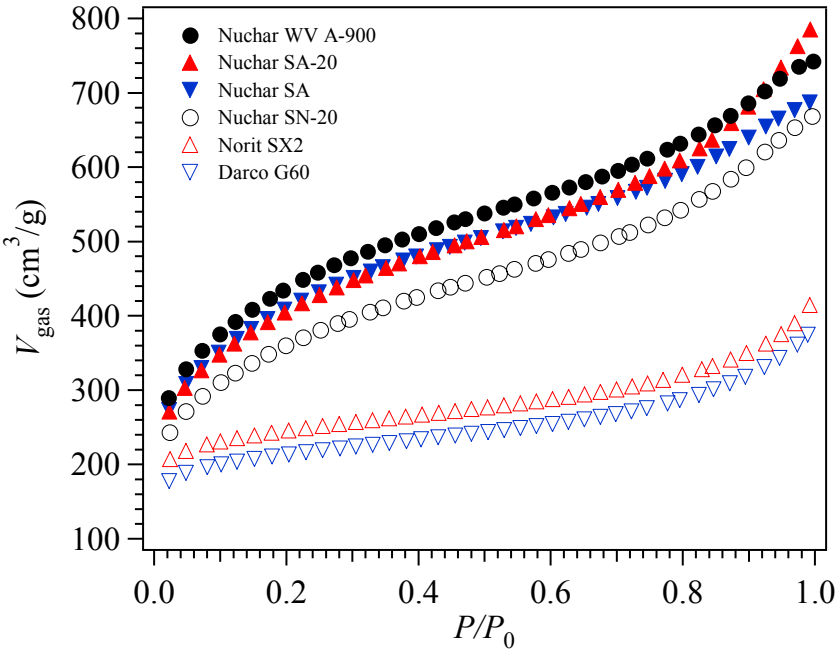

Adsorption isotherms of activated carbons

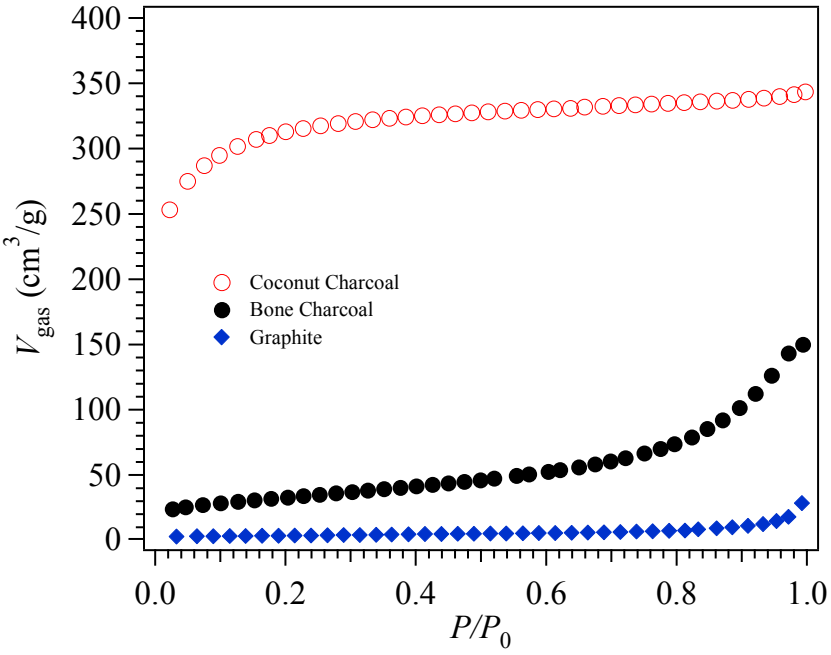

Adsorption isotherm of charcoals and graphite

Determination of the BET surface area

The weight of N_2 adsorbed is given by

$$W = \frac{V_{\text{liq}}}{\rho_{\text{liq}}},$$

where $\rho_{\text{liq}} = 0.807$ g/cm^3 is the liquid nitrogen density at 77 K, and V_{liq} is the volume of liquid N_2 adsorbed. The latter can be calculated from the moles of N_2 gas adsorbed, i.e.

$$\begin{aligned} V_{\text{liq}} &= n\overline{V} \\ &= \left(p\frac{V_{gas}}{RT} \right) \cdot \overline{V} \end{aligned}$$

Here, V_{gas} is the volume of N_2 gas adsorbed at standard conditions ($T = 273.15$ K, $p = 1$ atm), $R = 82.058$ cm^3·atm/mol·K is the universal gas constant, and $\overline{V} = 34.6$ cm^3/mol is the molar volume of liquid nitrogen.

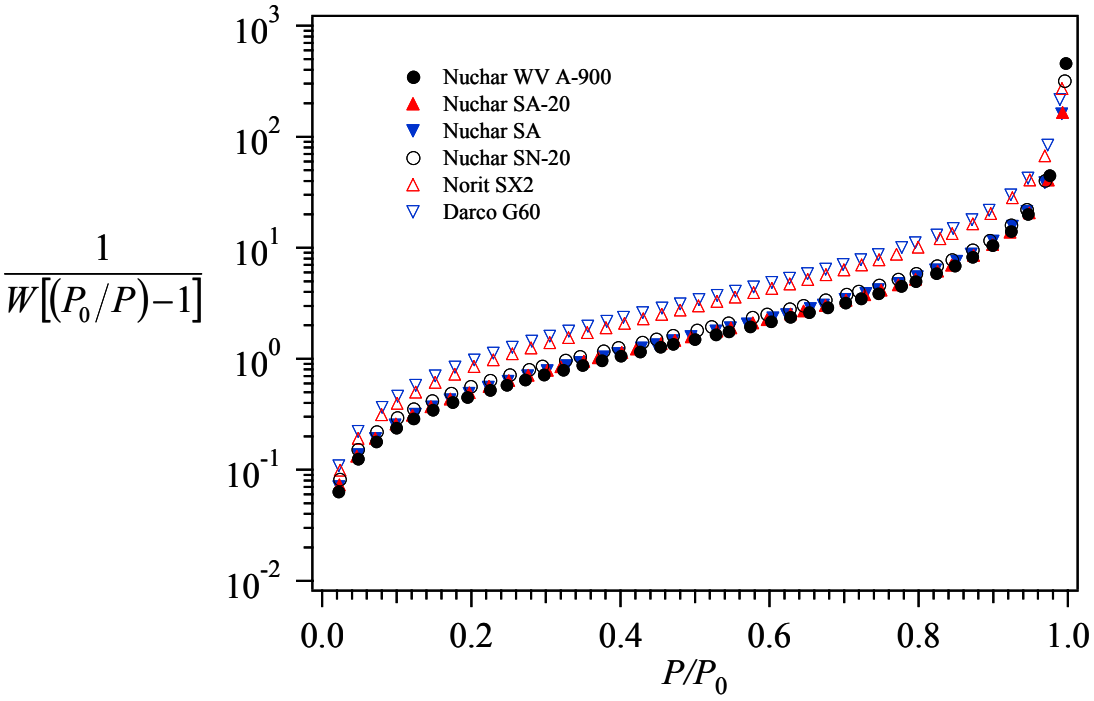

BET plots for activated carbons

BET surface area, S, is determined from a linear fitting of the BET plots in the range $0.05 < P/P_0 < 0.35$:

$$S = \frac{W_m \overline{N} A}{\overline{M}}$$

where $A = 16.2 \times 10^{-20}$ m^2 and $\overline{M} = 28.014$ g/mol are the cross-sectional area and the molecular weight of nitrogen, and $\overline{N} = 6.02214 \times 10^{23}$ mol^{-1} is the Avogadro number. The N_2 weight adsorbed in a monolayer is given by

$$W_m = \frac{1}{s + i}$$

where s and i are the slope and intercept of a BET plot.

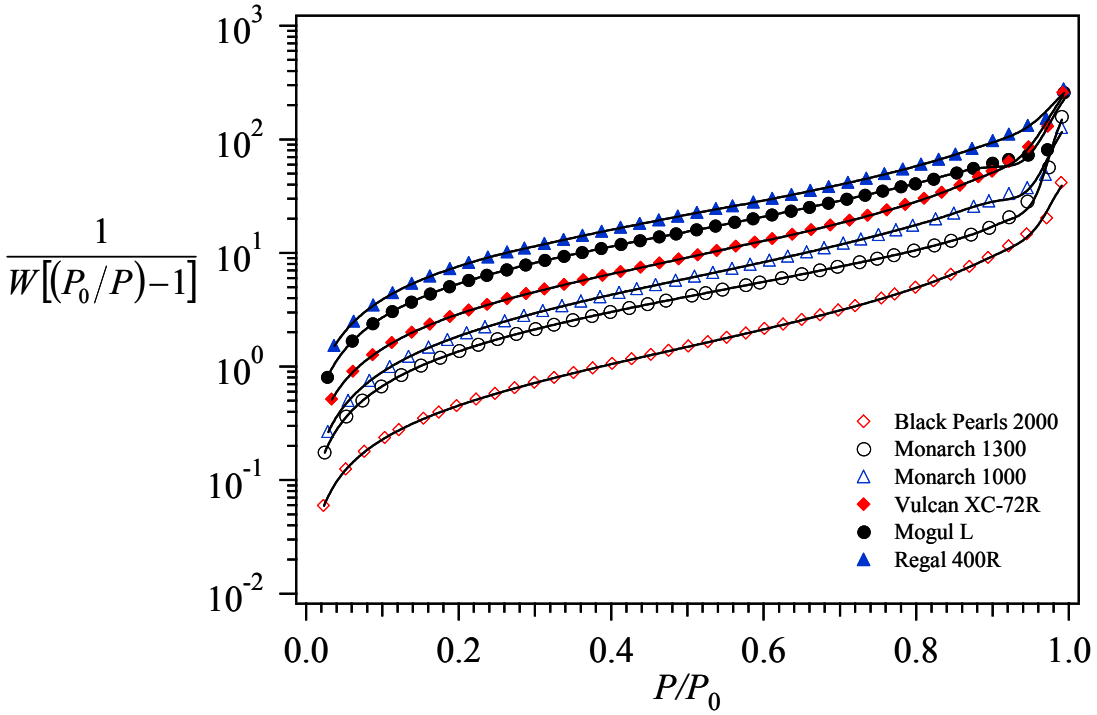

BET plots for carbon blacks

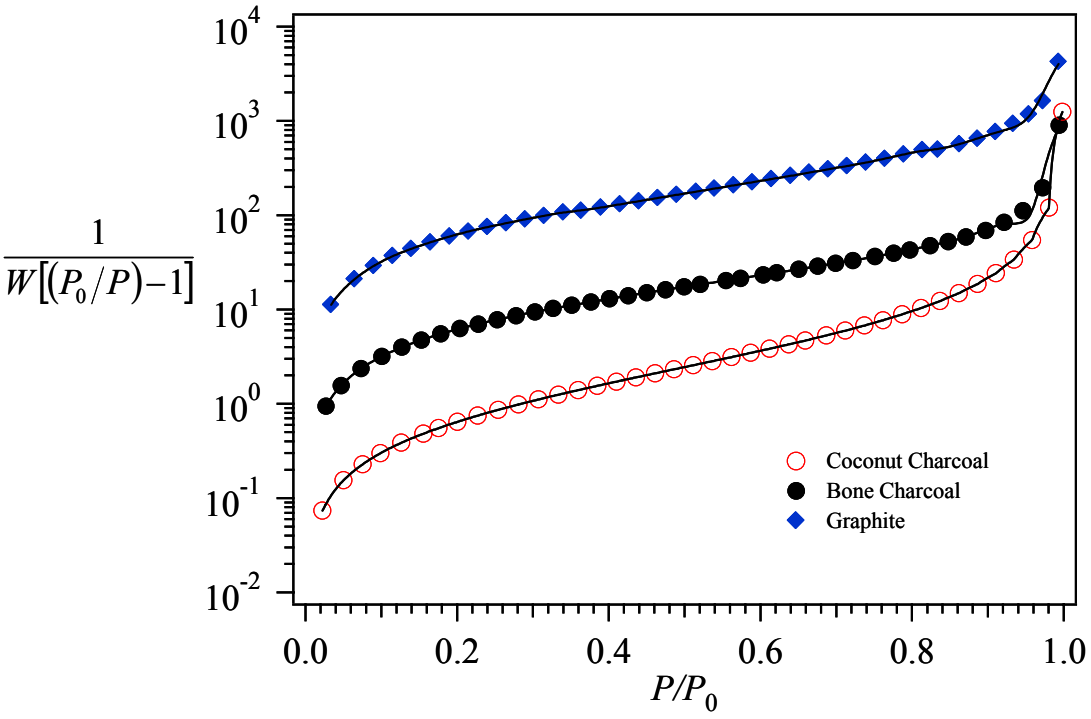

BET plots for charcoals and graphite

Determination of the external surface area: de Boer *t*-method

The determination of the external surface area is based on the *t*-curve, a plot of *t*, the statistical thickness, versus the relative pressure, P/P_0. The standard *t*-curve is expressed by the empirical de Boer equation:

$$t = \left(\frac{13.99}{\log P_0/P + 0.034} \right)^{\frac{1}{2}}$$

The calculated statistical thickness at various relative pressures is then used to replot the analysis isotherm as a *t*-curve, a plot of the volume of gas adsorbed versus *t*. Typical *t*-plots are shown below with the linear fitting to the upper linear portion. The external surface area is obtained from the slope of the upper linear portion of the *t*-plot, as follows

$$S_{\text{ext}} = \left(\frac{V_{\text{liq}}}{t} \right)_{\text{upper}} \times 10^4$$

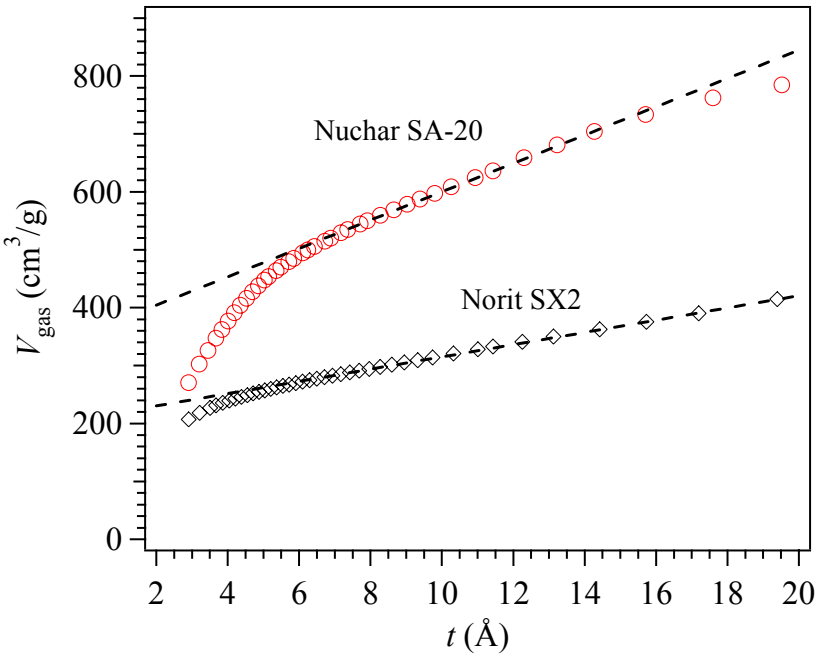

***t*-plot for selected activated carbons**

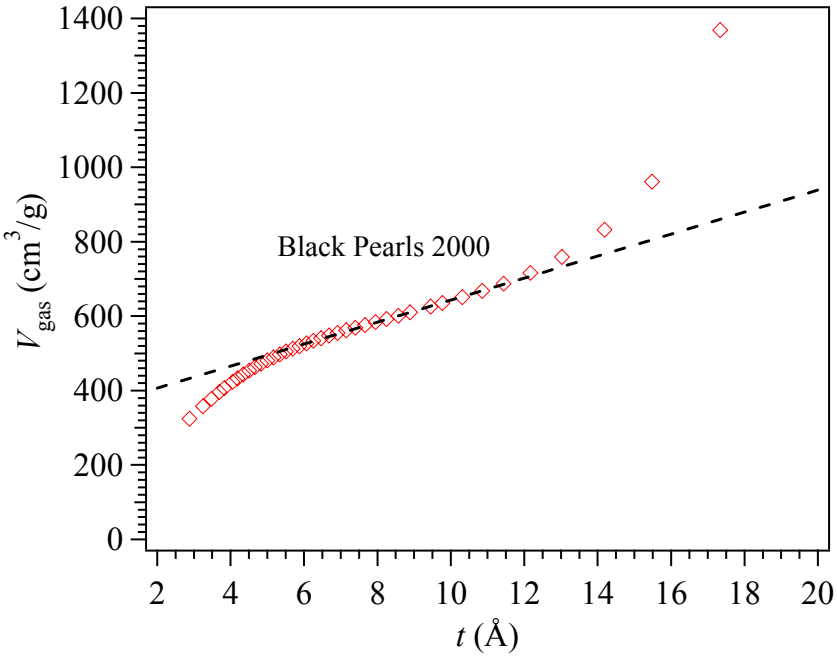

***t*-plot for a carbon black sample**

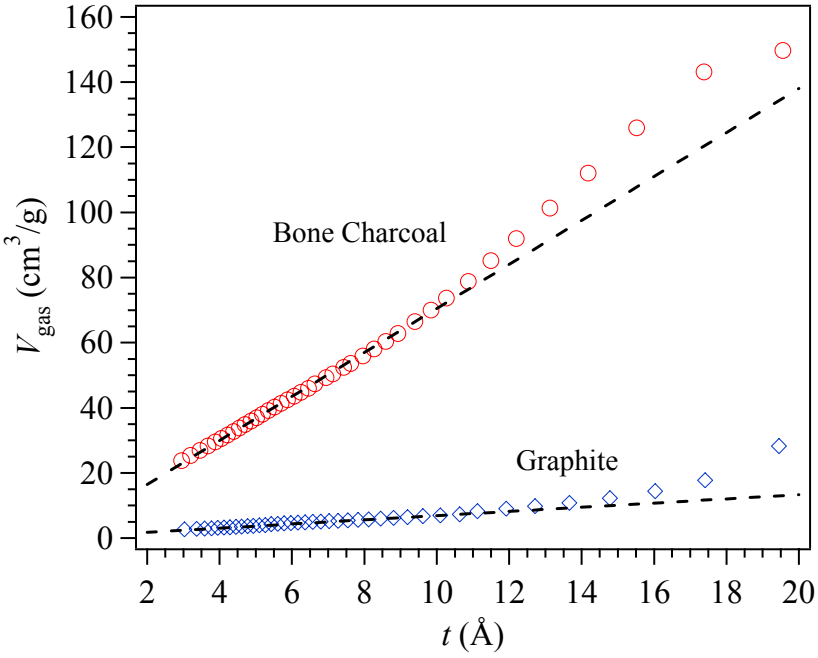

***t*-plot for a charcoal and graphite samples**

Appendix B:

Sample Calculations

1. Calculation of concentration of chemicals

The molarity (M) of a compound is calculated using the standard procedure,

$$M = \frac{n}{V_{\text{solution}}}$$

where n is the number of moles of solute and V_{solution} is the total volume of solution. The number of moles of solute is given by

$$n = \frac{\rho V_{\text{solute}}}{\overline{M}}$$

where ρ is the density, V_{solute} is the volume and $\overline{M}$ is the molecular weight of the solute.

A. For 0.8 mL of hydrazine (98.5 vol%) in 25 mL of solution

$$n = \frac{(1.028\ \text{g/mL})(0.8\ \text{mL})(0.985)}{32.04\ \text{g/mol}} = 0.025\ \text{moles}$$

$$M = \frac{0.025}{25\ \text{mL}} \times \frac{1000\ \text{mL}}{1\ \text{L}} = 1M$$

B. For 1.7 mL of nitrobenzene (99.5 vol%) in 25 mL of solution

$$n = \frac{(1.2037\ \text{g/mL})(1.7\ \text{mL})(0.995)}{123.11\ \text{g/mol}} = 0.017\ \text{moles}$$

$$M = \frac{0.017}{25\ \text{mL}} \times \frac{1000\ \text{mL}}{1\ \text{L}} = 0.68M$$

2. Calculation of the total volume of gas expected

To convert number of moles of gas to volume, we assume that either nitrogen or ammonia (at 0.967 atm, 25 ºC) behave as an ideal gas, so

$$V_C = n\overline{V}$$

where n is the number of moles expected and $\overline{V} = 25.30\ \text{L/mol}$ is the molar volume of the ideal gas.

A. From 0.025 moles of hydrazine in the reduction of nitrobenzene

$$V_C = (0.025\ \text{moles})(25.30\ \text{L/mol}) = 630\ \text{mL of } N_2$$

B. From 0.025 moles of hydrazine in the decomposition reaction

$$V_C = \frac{1}{3}(0.025\ \text{moles})(25.30\ \text{L/mol}) = 210\ \text{mL of } N_2$$

2. Calculation of the rate of reaction

The apparent rate of reaction (dV_g/dt) was calculated from the initial slope of the plot of volume of gas evolved with respect to time, as shown in the figure below. Additional approaches can be used with similar results: (a) volume of gas produced in certain unit of time at the beginning of the reaction (e.g., at 15 min of reaction time), and (b) graphical differentiation of the gas evolution plots. We assume that the traces of ammonia formed at the beginning of the reaction remained dissolved in the *iso*propanol solution. Thus, the gas evolved consisted of only nitrogen.

To convert apparent rate of reaction to reaction rate as expressed by Eq. (2.2), we assume that nitrogen (at 0.967 atm, 25 ºC) behave as an ideal gas, whose molar volume is $\overline{V} = 25.30\ \text{L/mol}$. The reaction rate (normalized by the total volume V of reaction mixture) is given by

$$R = \frac{1}{V\overline{V}\nu}\frac{dV_g}{dt}$$

where ν is the nitrogen coefficient in the balanced equation ($\nu = 1$ for the hydrazine

decomposition reaction, ν = 3 for the nitrobenzene reduction reaction)

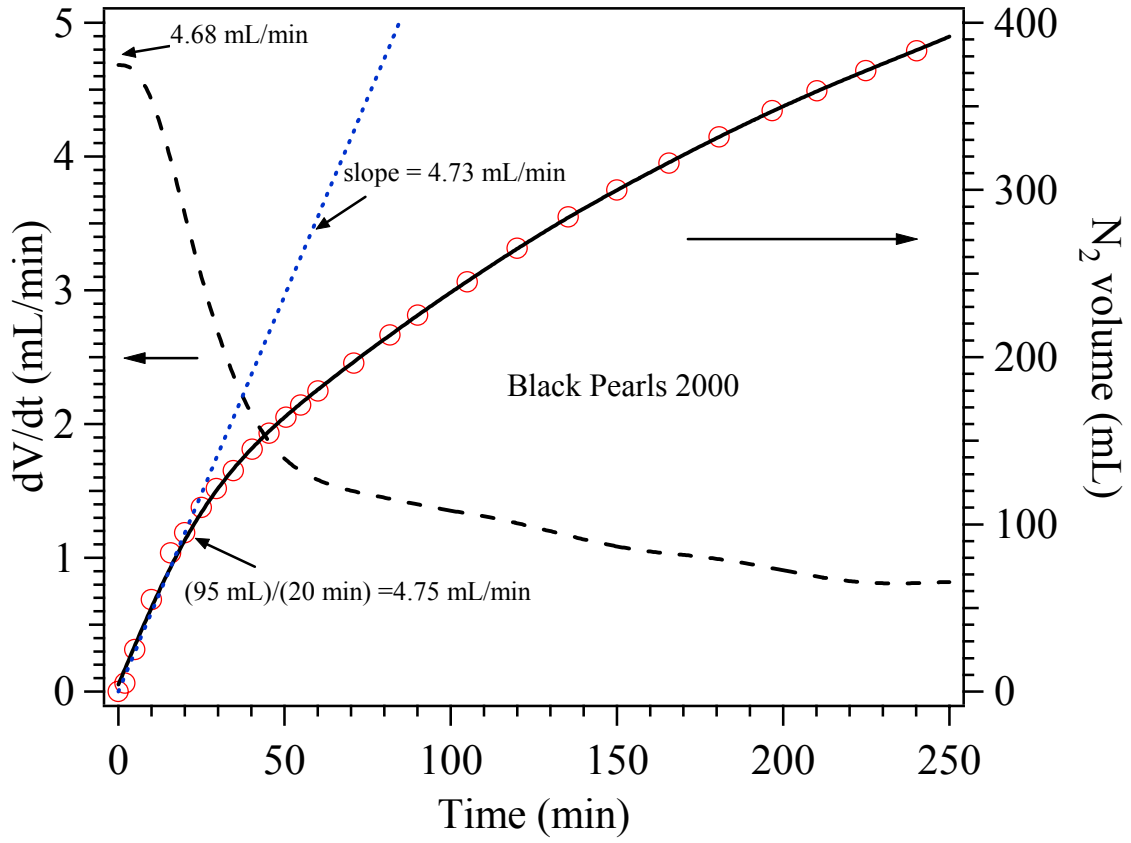

Typical determination of the reaction rate. Solid line represents the interpolation curve of the raw data. Dashed line represents the derivative of the interpolation curve. Short dashed line is the linear fitting of the first points of the gas evolution plot. Note that the slope of this line is very close to the derivative at $t = 0$ and the rate determined using the gas produced at 20 min.

Appendix C:

Igor Pro Curve Fitting

Igor's curve fitting capability is one of its strongest analysis features. The idea of curve fitting is to find a mathematical model that fits your data. The curve fit finds the specific coefficients which make that function match your data as closely as possible. Igor can fit to either built-in functions or user-defined functions. One creates a user-defined function by entering the function in the New Fit Function dialog. Very complicated functions may have to be entered in the Procedure window.

If we want to fit the data to a function of the form

$$R = \frac{k_a[a]}{1 + K_a[a]},$$

the user-defined fitting function used in our analyses has the following form:

Function Adsorption(w, x) : FitFunc

Wave w; Variable x

Variable r

r =w[0]*x/(1+w[1]*x)

return r

End

A typical example of the Curve Fitting Dialog is shown below

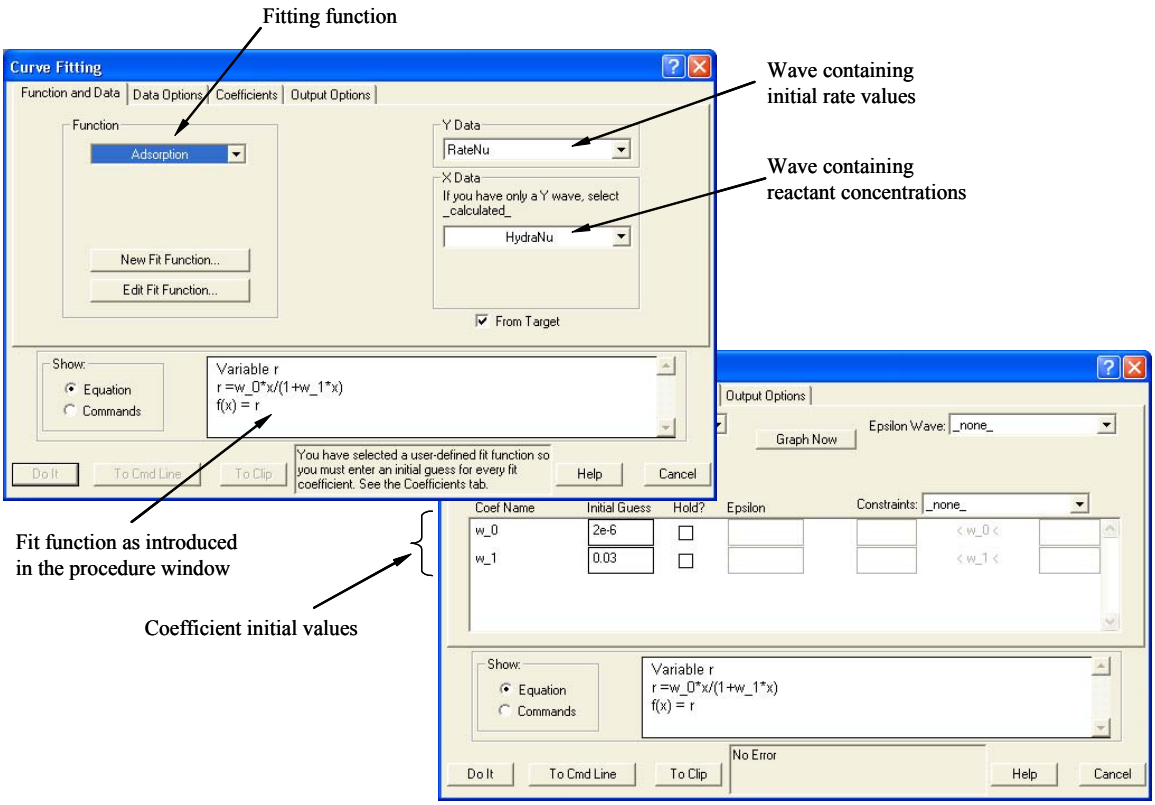
Fitting function
Wave containing initial rate values
Wave containing reactant concentrations
Curve Fitting
Function and Data
Data Options
Coefficients
Output Options
Function
Adsorption
New Fit Function...
Edit Fit Function...
Y Data
RateNu
X Data
If you have only a Y wave, select _calculated_
HydraNu
From Target
Show:
Equation
Commands
Variable r
r =w_0*x/(1+w_1*x)
f(x) = r
Do It
To Cmd Line
To Clip
You have selected a user-defined fit function so you must enter an initial guess for every fit coefficient. See the Coefficients tab.
Help
Cancel
Graph Now
Epsilon Wave: _none_
Coef Name
Initial Guess
Hold?
Epsilon
Constraints: _none_
w_0
2e-6
w_1
0.03
< w_0 <
< w_1 <
No Error
Fit function as introduced in the procedure window
Coefficient initial values

Synthetic Coal Tar Enamel Using Solvent Extraction

FINAL REPORT

Reporting Period
March 1, 2003 February 29, 2004

Report Prepared by

Peter G. Stansberry
Department of Chemical Engineering
College of Engineering and Mineral Resources
P. O. Box 6102
West Virginia University
Morgantown, WV 26506-6102

Report Issued
April 15, 2004

DOE Award Number DE-FC26-98FT40350

Other Contributors

Elliot B. Kennel and Lloyd Ford
Department of Chemical Engineering
College of Engineering and Mineral Resources
P. O. Box 6102
West Virginia University
Morgantown, WV 26506-6102

DISCLAIMER

ASTRACT

Producing a synthetic coal tar enamel proved to be both feasible and moderately successful. After characterizing a commercial grade coal tar enamel, a synthetic coal tar enamel was made using solvent extracted coal, heavy oil, bituminous coal and talc. The synthetic enamel was developed in a 1L autoclave reactor at temperatures up to 300°C with stirring at a rate of 1000rpm for digestion times up to 3 hours. The resulting synthetic enamel has properties that fall within most specifications of commercial grade coal tar enamel. The synthetic enamel had slightly higher volatile loss, very similar viscosity, and lower sulfur content than that of commercial enamel. Penetration values for the synthetic enamel generally were slightly lower, but were still within the specified range for commercial enamels. In cathodic disbonding, the synthetic enamel did not perform as well as the commercial product. It was demonstrated that synthetic enamel can be used as an adhesive for carbon foam-steel composites, and the bond strength to carbon foam can be adequate for some applications.

TABLE OF CONTENTS

LIST OF FIGURES

LIST OF FIGURES
(Continued)

Page

LIST OF TABLES

1 EXECUTIVE SUMMARY

Coal tar enamels suitable for wide-temperature or hot-applied applications are generally produced by digesting bituminous coal in pitch, heavy oil, and inorganic fillers. Sourcing of the pitch (and heavy oil) components is typically reliant on the byproducts recovered from metallurgical coke ovens. As such, because of the continuing decline of the byproduct coke oven industry in the United States, an alternative method for producing the pitch ingredient of coal tar enamel is timely.

Extraction of bituminous coal was used to produce a pitch-like material for testing in laboratory enamels. In all evaluations, the performance of the synthetic enamel was compared to a commercial product. Several synthetic enamel formulations with the coal extract were produced by digestion at 200°C, with resultant properties that varied in penetration behavior, viscosity, and volatility. However, optical microscopic examination of these enamels indicated that the digestion conditions were not severe enough to dissolve or digest the coal because the coal particles remained essentially unchanged. Therefore, other formulations were produced at 300°C and the samples again observed with the optical microscope. It appeared that preparation at 300°C produced partially dissolved coal particles very similar in appearance to commercial coal tar enamel.

One of the synthetic coal tar enamels was judged suitable for additional testing. In comparisons with the commercial product, the synthetic enamel had penetration values that, while lower than the commercial sample, were still within industrial specifications. Volatile content was similar to the commercial material as well, and the composition of the synthetic enamel did not contain any detectable organic compounds not already

evident in the commercial product. Additionally, the sulfur content of the synthetic enamel was only 0.18wt% and the commercial enamel was 0.46wt%.

Cathodic disbonding tests were conducted with enamel-coated steel coupons placed in an aqueous salt solution for four weeks under an applied potential of 1.5V. The synthetic enamel allowed significant corrosion to occur, possibly because of poor adhesion to the surface of the metal.

Resistance to moisture penetration of carbon foams coated with the synthetic and commercial enamels under ambient conditions was very good within the time constraints of the research project. Accelerated tests were devised in which the coated carbon foams were tested under pressurized water. These tests indicated that the synthetic enamel coating resisted water uptake more than the commercial coating initially, but after a longer period of time both behaved similarly.

Finally, the synthetic enamel was used as an adhesive in a steel-carbon foam composite with an encouraging degree of success. The enamel had a usable strength when subjected to a tensile test.

2 INTRODUCTION

Coal tar enamel is used as coatings for pipelines and other objects that need to be protected from environmental conditions. Since coal tar enamel is thermoplastic, it softens when heated for ease of application. After cooling, coal tar enamel hardens to form a flexible water and vapor-proof barrier. The desirable features of coal tar enamel include long lifetime during underground burial and resistance to salt water exposure and freeze-thaw cycles. Coal tar enamel has been, and continues to be, one of the most cost effective and forgiving corrosion mitigation coatings available.

Based on years of experience in real-world uses, coal tar enamel is preferred in certain applications to petroleum-based asphalt in barrier and cathodic protection applications. Unlike asphalt, which exhibits aliphatic characteristics, coal tar enamel is a stable complex of aromatic ring structures, which result in a denser and tighter molecular barrier. Thus, coal tar enamel is very stable, forming strong molecular associations that are difficult to disrupt.

Coal extraction is a well-known process for obtaining pitch-like materials. Coal extracts, being similar to the components in coal tar enamel, are also predominately comprised of aromatic hydrocarbons. Through control of extraction conditions, a wide range of low-ash, low-sulfur pitch-like products can be made from coal.

Currently, the pitch (and oil) component of coal tar enamel is obtained from the high-temperature carbonization of coal during the production of metallurgical coke. As such, the pitch used in enamel formulations is a byproduct similar to coal tar binder pitch. Because domestic coke production is expected to continue to decline, there are concerns about adequate sourcing. Thus being able to produce synthetic coal tar enamel via a new

approach is especially important considering the declining domestic production of coal tar pitch.

The specific objectives of this research were to 1) produce a coal extract as a surrogate for conventional coal pitch, 2) develop a synthetic coal tar enamel that closely matches a commercial product in penetration behavior, 3) compare the volatility of synthetic enamel to commercial product, 4) establish the upper sulfur content in the synthetic enamel at no more than 1wt%, 5) test the performance of the synthetic enamel with regards to cathodic protection, 6) determine the applicability of synthetic enamel as a vapor-barrier coating on carbon foam artifacts and, 7) fabricate a compliant seal between carbon foam and steel using a synthetic enamel and evaluate mechanical properties of the composite.

3 BACKGROUND

Coal tar enamels and coatings are a diverse family of materials. The diversity arises, in part, from the specifications and performance characteristics established by the customer. Figure 1 indicates some of the groups into which these materials are classified. Modern coal tar enamels are comprised of essentially four components: coal pitch, heavy coal tar distillate (heavy oil), coal, and inorganic fillers. Coal pitch in its own right is an effective water vapor barrier but suffers from brittleness and poor temperature susceptibility, while heavy oils sag and flow from surfaces at relatively low temperatures.

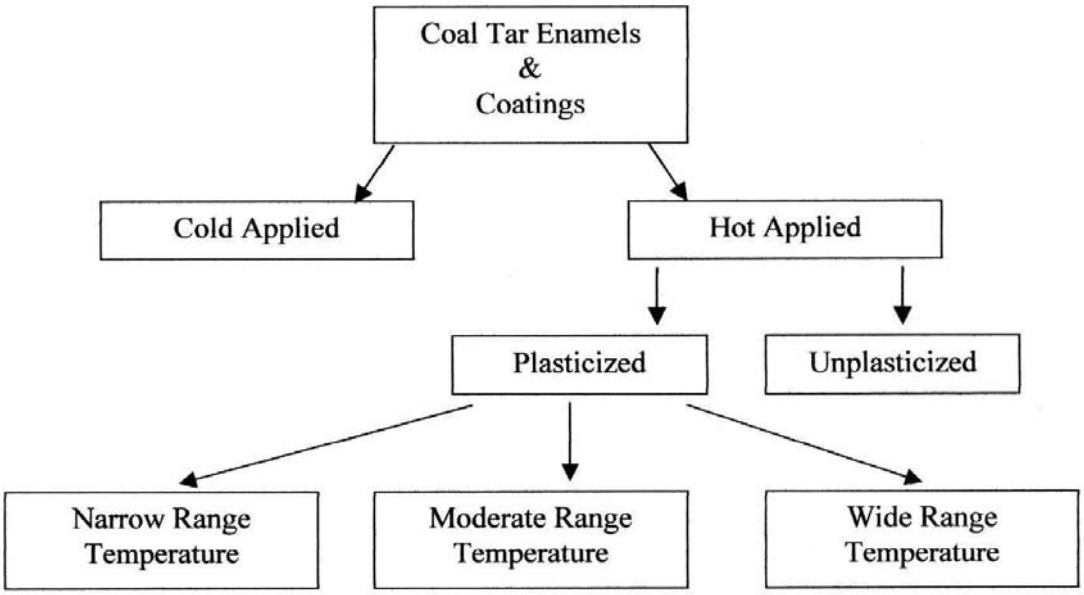

Figure 1. Categories of coal tar enamels and coatings.

The simplest method to reduce cold flow and to prevent sagging in enamels is to raise the softening point of the pitch by distillation. Chemical methods such as oxidation and dehydrogenation are optional treatments, but are rarely used. The addition of inorganic fillers to coal tars is quite effective in reducing brittleness and improving the mechanical properties of enamels. Further reduction in enamel brittleness, especially at low-temperature service, is achievable by digestion of bituminous coal in the pitch or oils. The digestion of coal results in enamels being "plasticized". Coal digests consist of mixing bituminous coal with coal pitch, heavy coal tar oil, or a combination thereof. Heating the mix below the thermal decomposition temperature of the coal, the pitch and oil partially dissolve the coal to form a "colloid" or "gel". The effectiveness of coal tar enamels can be attributed in large measure to the forces established between the solvent components, in this case pitch and oil, and the coal itself.

Development of coal tar enamel still remains a black art. The processes and ingredients used in enamel formulations that affect performance have evolved over many decades, if not centuries, through trail-and-error or cook-and-look methods. Ultimately, it is the result of extended field service that guides the manufacturer of coal tar enamel to produce a spectrum of specifications.

Laboratory studies of enamels made with charges of the same coal (18wt% VM), pitch (45°C softening point), and creosote oil have been previously reported.[1] Digestion took place in a stirred-batch mixer for 3 hours at 315°C. In Figure 2 are shown the effects of increasing coal content during digestion in *pitch* alone. There is about 3.8°C increase in softening point temperature for each percent increase in coal. Increasing the coal content makes the enamels more rigid, as evident by the penetration trends.

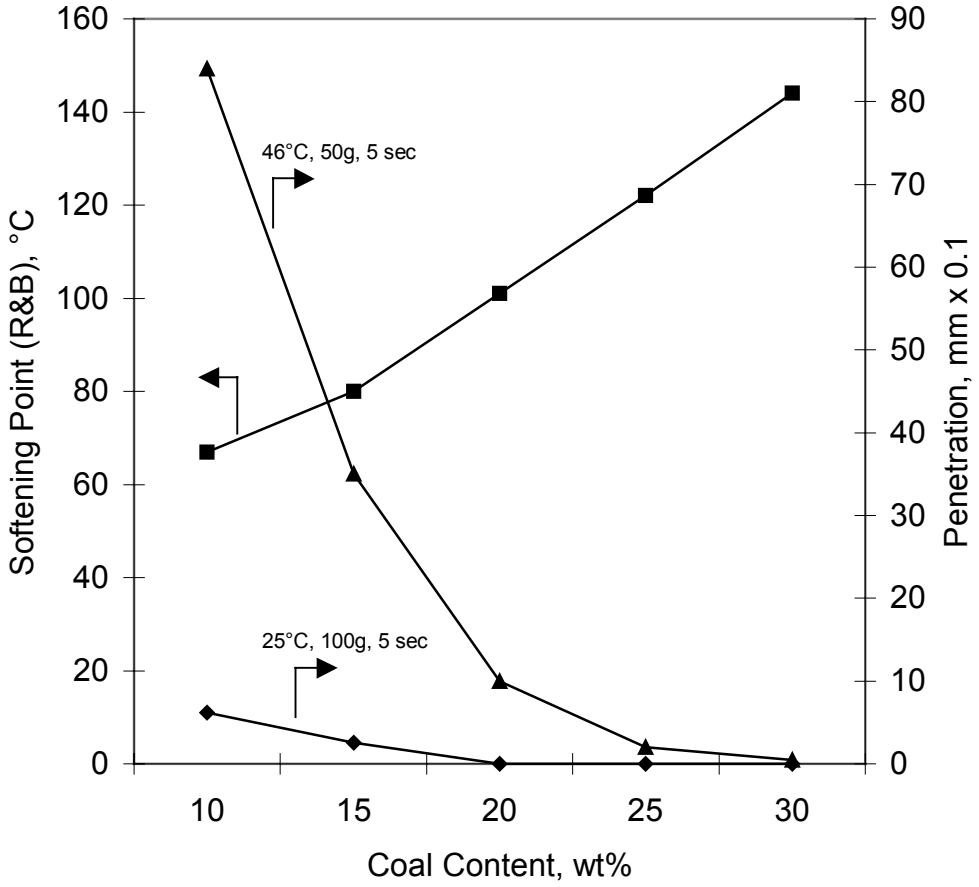

Figure 2. Effects of increasing coal content in pitch-alone digestion.[1]

The effects of digestion of coal in *oil* alone are indicated in Figure 3. Similar to the case involving only pitch, increasing the content of coal decreases softening point and penetration. Note that penetration behavior is much more pronounced because of the greater plasticizing power of the oil. Normally oil content is kept to a minimum, however, to reduce volatile emission during application and in service.

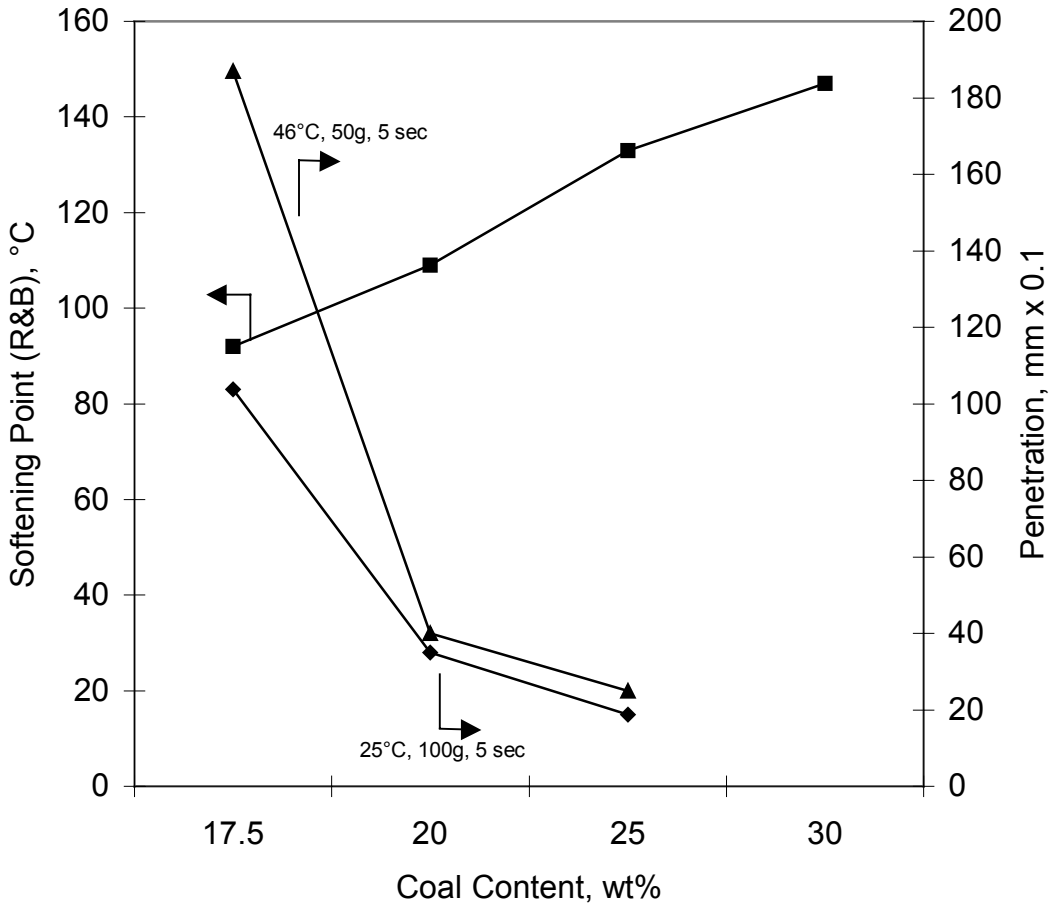

Figure 3. Effects of increasing coal content in oil-alone digestion.[2]

Several observations can be drawn from the results. The combination of coal and pitch alone produces enamels that are very hard and brittle. The enamels exhibit wide-temperature susceptibility as well, i.e., the 46 to 25°C penetration ratios are large. On the other hand, coal in oil alone produces high-softening point, but very soft enamels. An advantage in using oil over pitch is the narrow-temperature susceptibility, i.e., the 46 to 25°C penetration ratios do not change dramatically with softening point temperature. Interestingly, it was noted that the coal digested readily in the pitch but the oil required considerably longer processing time to complete its action on the coal. The effect agrees

with what is known about coal extraction processes in that condense aromatic molecules can extract or disperse large percentages of coal.[3-4]

Satisfactory enamels can be produced by combining separate pitch- and oil-digested coal together. For example, two enamels were prepared by digesting 25wt% bituminous coal in either pitch or oil. A composite was made by blending the separate enamels in a 50:50 ratio. As shown in Figure 4, penetration increases as the proportion of oil increases, as expected. Curiously, the softening point temperature for the blend is significantly lower than the softening point temperature of either individual enamel. This phenomenon is often encountered, demonstrating that many of the properties of enamels cannot be predicted based on simple mixing rules.

Normally, enamels are not made by combining separate pitch- and oil-digested coal because of the difficulty in controlling the characteristics of the blend. Once the amount of coal is determined and held relatively constant, the quantities of pitch and oil are manipulated until the desired softening point temperature and penetration are obtained. The results in Figure 5 are for enamels containing 33.3wt% coal digested in various proportions of pitch and oil. Similar to the results shown in Figure 4, the softening point temperature of coal digested in both pitch and oil is lower than in either coal liquid itself.

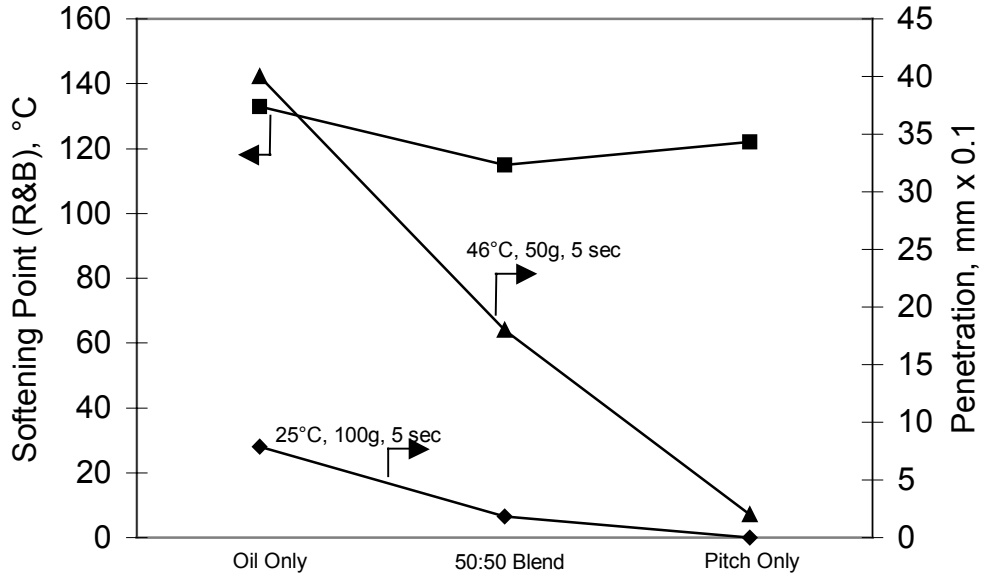

Figure 4. Effects of blending coal-digested enamels on softening point and penetration.[5]

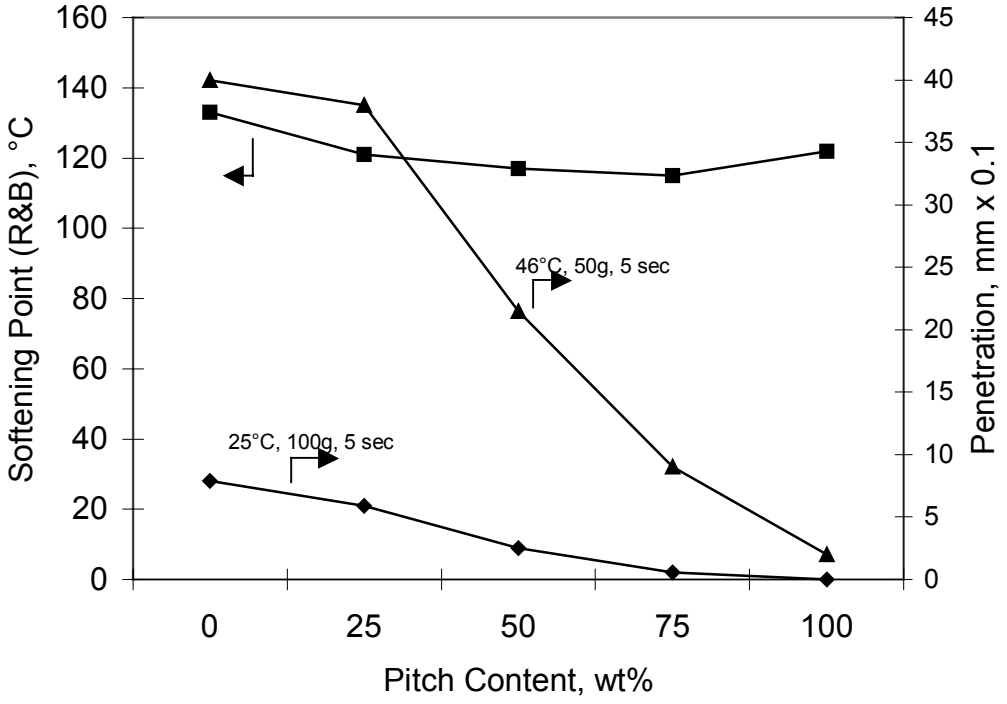

Figure 5. Effects of coal digestion in pitch and oil at constant coal content.[6]

Fillers are added to coal tar enamel to impart further reduction in brittleness and to increase mechanical strength. By far the most common fillers are pulverized talc and related minerals. These substances are nonabrasive and their foliated nature prevents settling in mixing and holding tanks. The characteristics of three fillers on enamel softening point temperature are shown in Figure 6. Note the relative insensitivity of softening point on the addition of talc.

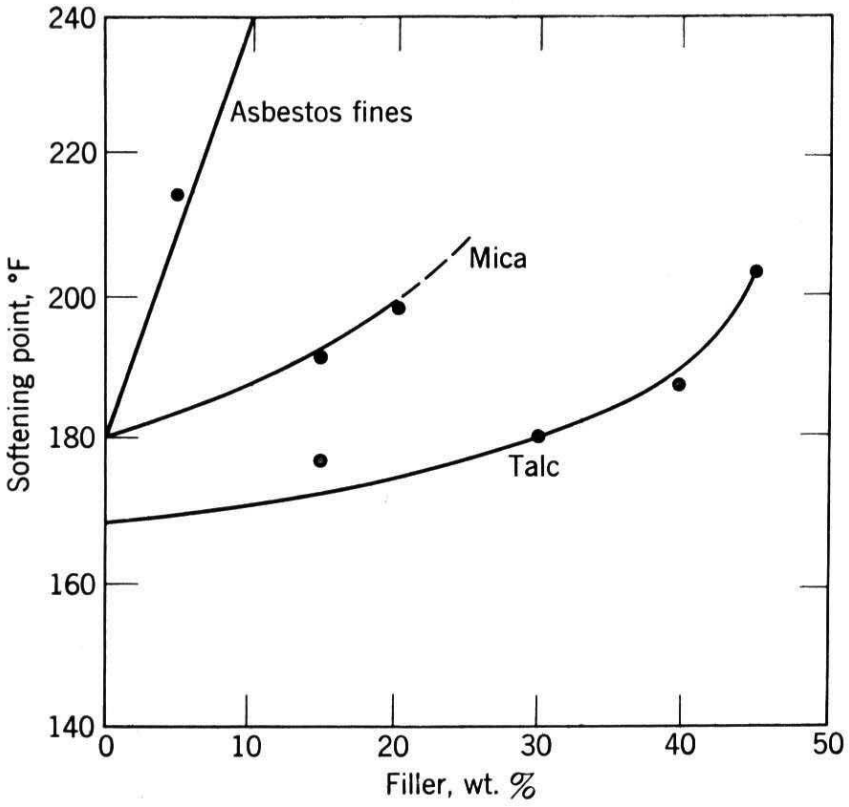

Figure 6. Effect of filler content on softening point temperature.[7]

4 EXPERIMENTAL

This research project focused on the development of synthetic coal tar enamel that would be categorized as a wide-range temperature product. Thus, the intent was to match the properties of synthetic coal tar enamel with those of commercial enamel as closely as possible.

4.1 Characterization of Commercial Coal Tar Enamel

A 5-gallon container of commercial coal tar enamel was obtained and subjected to testing to determine some if its gross properties. The test methods employed are shown in Table 1, and the average of duplicate measurements is shown in Table 2. The properties of the commercial coal tar enamel provided by the manufacturer are shown in Table 3.

Table 1. Test methods used to characterize coal tar enamel and pitches.

Determination	Test Method
Softening Point, °C	ASTM D3104
Toluene Insoluble (TI), wt%	Soxhlet Extraction
Pyridine Insoluble (PI), wt%	Soxhlet Extraction
Conradson Carbon Residue, wt%	ASTM D189
Ash Content, wt%	ASTM D2415
Viscosity, cP	Brookfield Viscometry

Table 2. Measured properties of commercial coal tar enamel.

Softening Point, °C	121.2
Toluene Insoluble, wt%	56.0
Pyridine Insoluble, wt%	53.4
Conradson Carbon Residue, wt%	60.5
Ash Content, wt%	30.0

Table 3. Manufacturer's specifications for coal tar enamel.

Measurement	Specification
Softening Point, °C	120 to 130
Ash Content, wt%	25 to 35
Application Temperature, °C	232 to 260
Penetration, 25°C, 100g, 5sec	2 to 9

The softening point temperature confirmed that this particular type of enamel is suited for hot-applied coatings. The high-temperature ash content of 30wt% indicates significant addition of inorganic fillers while the amount of pyridine and toluene insolubles suggests that the oil and/or pitch used in this formulation are highly soluble. The Conradson carbon residue is high, undoubtedly resulting from significant amounts of filler. The effect of temperature on viscosity of the coal tar enamel is shown in Figure 7, with a conventional coal tar binder pitch (110°C softening point) used for comparison.

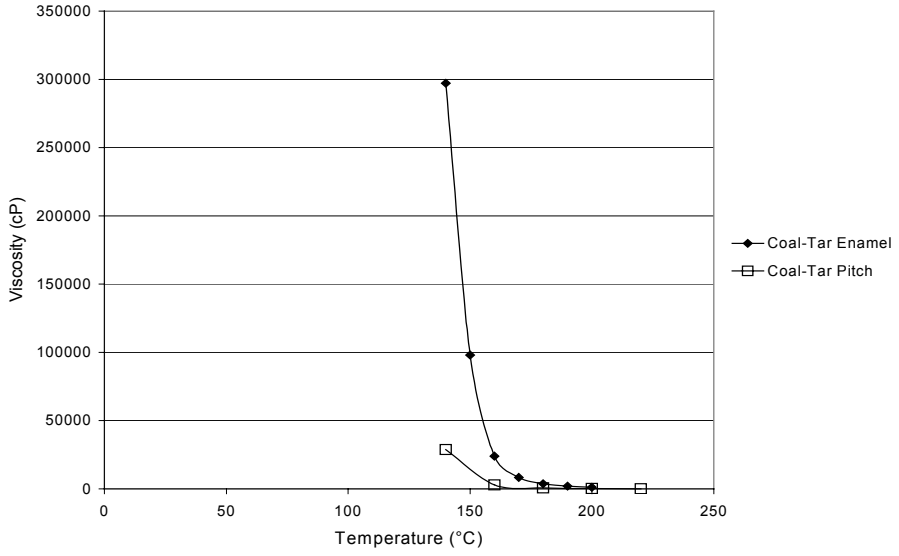

Figure 7. Effect of temperature on coal tar enamel viscosity.

4.2 Development of Coal-Extract Pitch

A West Virginia bituminous coal was extracted in tetralin and deashed by solvent extraction using N-methyl pyrrolidone as described elsewhere[8]. Characterization results of the feed coal are presented in Table 4 and properties of the coal-extract pitch are shown in Table 5.

Table 4. Basic characteristics of bituminous coal feed used in extraction.

Proximate (as received), wt%	
Moisture	0.82
Fixed Carbon	60.49
Volatile Matter	34.41
Ash	4.27
Petrographic Composition, vol%	
Vitrinite	71.4
Liptinite	5.5
Inertinite	21.7

Table 5. Characterization results of coal-extract pitch.

Softening Point, °C	130.5
Conradson Carbon, wt%	40.6
Ash Content, wt%	0.15
Density, g/cm^3	1.189
C/H Atomic Ratio	1.10

4.3 Development of Synthetic Coal Tar Enamels

As mentioned previously, coal tar enamels are made from bituminous coal, pitch, oil, and inorganic fillers. The bituminous coal used as the plasticizer is mined in West Virginia. Some of the basic characteristics of the coal are provided in Table 6. The oil, which is a coal tar distillate, was acquired from a commercial vender. The vender called the material “heavy oil,” which was a room temperature liquid containing about 1-2wt% insoluble solids. For some of the formulations the heavy oil was vacuum-distilled in

conventional laboratory glassware at 10mm Hg up to an end point of 250°C. The distillation was required to reduce volatility of the heavy oil. Talc (hydrous magnesium silicate, <350 mesh) was purchased from a chemical supply company and used as is.

Table 6. Characteristics of coal used as a plasticizer in synthetic enamels.

Proximate (dry basis), wt%	
Fixed Carbon	57.91
Volatile Matter	33.17
Ash	8.92
Petrographic Composition, vol%	
Vitrinite	74.6
Liptinite	5.0
Inertinite	16.1

Processing protocols were developed using a 1L-stirred autoclave by adding the appropriate proportion of feeds. The coal was dried and ground to a 150-mesh sieve top size. In all experiments, the total mass added to the vessel was held constant at 158g. Heat was applied until the mixture became sufficiently fluid after which the autoclave lid was bolted to the body. Stirring rate was 1000rpm and the reactor contents were brought to temperature and held there for 2 to 3 hours. After the coal digestion period, the reactor was opened and the contents poured into a metal pan to cool.

4.4 Determination of Pitch Volatility

The standard test of pitch volatility (ASTM D4893) stipulates that a sample of pitch must be placed into a preheated 350°C zone of a specific design. After 30 minutes the loss in mass is determined. For this research project, volatility was determined on a Leco thermoanlyzer by placing 1 to 2 grams of an enamel sample into a tared ceramic crucible. The sample was then placed into the instrument and brought to 350°C as rapidly as possible (about 20 to 25 minutes) and held at this temperature for thirty

minutes while monitoring weight changes. For an additional test, in order to ascertain weight loss at higher temperature, the sample was heated rapidly to 400°C and held at the higher temperature for 30 minutes while monitoring weight changes. The volatility tests were all conducted under a nitrogen blanket.

Select enamels were distilled in a Saybolt distillation flask. About 20g of sample were introduced into the flask and the bottom portion buried in sand for the even distribution of heat. Heat was applied by a gas burner to vaporize the volatile components, which were condensed and collected. The distillates were analyzed on a Saturn gas chromatograph/mass spectrometer (GC/MS) to determine composition.

4.5 Cathodic Disbonding Testing

A cathodic disbonding test was developed by modifying the ASTM G8-96 method. Steel coupons (3 ½ x 1 x ⅜ inches) were polished with fine abrasives to remove surface corrosion and dirt. The coupons were rinsed with de-ionized water and dried at 110°C, then wiped clean with acetone and dried again before coating with enamel. Coating was accomplished by first melting the enamel in a beaker to 250°C in an oven and quickly dipping the room-temperature steel coupon to a depth of about 2 inches. However, this procedure did not result in firm bonding of the enamel to the surface of the steel. Thus the test coupon was preheated to 250°C and then dipped twice into the 250°C molten enamel to form a smooth covering between 2 to 3mm in thickness. The adhesion using this approach appeared to be better than dipping the cold coupons into the molten enamel. Prior to the disbonding experiment, a circular holiday of about 6mm in diameter was made to expose some of metal surface to the salt solution.

A conductive, alkaline electrolytic solution was prepared by dissolving 1wt% each of the technical-grade salts, sodium chloride, sodium sulfate, and sodium carbonate, in de-ionized water. An imposed electrical potential of 1.5V was supplied by a potentiostat (BAS Power Module, model PWR-3) to the coupon at about 3mA for the duration of 4 weeks. At the end of the experiment the coupon was inspected visually for defects and the coating removed carefully to determine corrosion. Figure 8 is a schematic of the experimental set up.

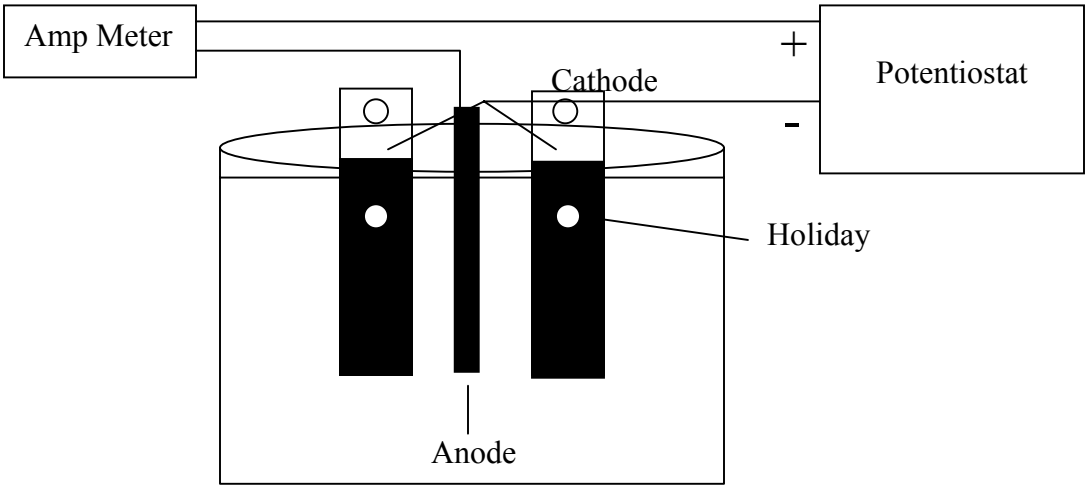

Figure 8. Schematic of cathodic disbonding experiment.

4.6 Carbon Foam Coatings and Metal Composites

4.6.1 Water Penetration of Enamel Coated Carbon Foam

Two pieces of carbon foam were cut into approximately 0.4 x 0.8x 0.5-inch rectangles. Coatings were made by first preheating both the enamel and foam to 250°C and then dipping the foam rapidly into the molten enamel two times and then allowing

them to cool to room temperature. The samples were submerged in a beaker of de-ionized water for a week and weighed to determine water weight gain.

The ASTM G9-87 procedure for determining water vapor requires several months to complete. Because of the time constraints of this research project, an accelerated water-penetration method was devised. The accelerated method was conducted under pressure. The coated carbon foam was inserted into a $50cm^3$ tubing bomb along with $25cm^3$ of de-ionized water. The reactor was pressurized with 500psig nitrogen. At various time intervals, the reactor was de-pressurized and the samples removed and allowed to air dry. After weighing to determine weight gain, the samples were reinserted the reactor and pressurized with nitrogen for another determination.

4.6.2 Carbon Foam/Steel Composite

Carbon foam/steel composites were produced using coal tar enamel as an adhesive. Two different types of composites were produced, one for tensile testing and the other for flexural testing via three-point bending. The steel for the tensile sample was 2.54cm 1018 carbon steel round stock machined into the shape shown in Figure 9. This particular shape was needed in order to secure the sample properly for testing. The grips are 0.4763cm thick and approximately 1.90cm to 2.50cm long. The foam was cut using a 3.18cm hole-saw that had the pilot bit removed.

Figure 9. Foam-steel composite for tensile test.

The enamel adhesive was heated to 250°C and allowed to become molten. The metal tabs were dipped into the enamel to coat and then were attached to the foam and allowed to cool. Tensile testing for the samples was done on an Instron tester.

The second type of composite, Figure 10, was made from automotive grade sheet metal cut into 2.54cm by 15.24cm sections and then attached to carbon foam 1cm thick by pouring some molten enamel onto the metal sheets and pressing the foam onto the enamel. The composite was then placed into the 250°C oven for approximately 1 minute to help set the enamel onto the foam.

This composite was tested using a three point bending method by modifying ASTM D790. Two pieces of the cut sheet metal, one set upon the other, and a tri-layer of sheet metal and packing foam cut to the same dimensions as the carbon foam, were used for comparison. The steel-packing foam-steel tri-layer was held together with rubber cement. This was done to allow for testing of objects of the same geometry. There were several differences between the method used and the ASTM standard, most notably the span to depth ratio was less than the 16:1 specified by ASTM D790. The composite had

a span to depth ratio of 6.89:1, while the sheet metal reference had a span to depth ratio of 60:1.

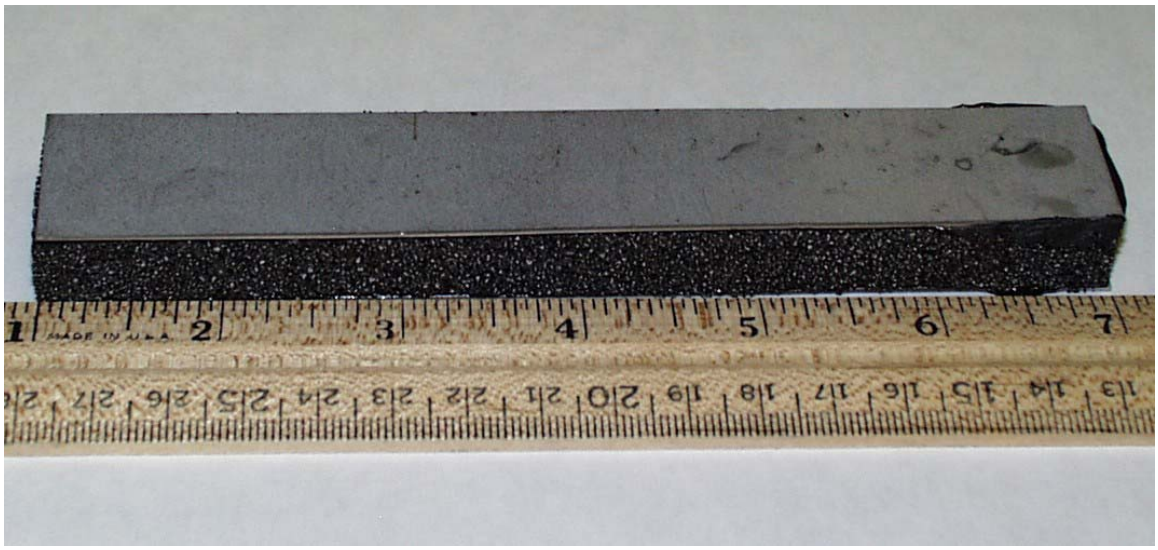

Figure 10. Foam-steel composite for flexural testing.

4.7 Other Characterization Testing Methods.

Penetration tests were conducted on a Humboldt H-1240 penetrometer following the ASTM method D5-97 at 22, 46, and 55°C under applied force of 50, 100, 150 and 200 grams for 5 seconds. Four penetration determinations were made at each temperature and the average penetration reported. Elemental analysis was accomplished on a ThermoQuest analyzer and the average of three determinations is reported. Select samples of enamels were embedded in plastic and polished following conventional procedures for examination by optical microscopy. Photomicrographs were taken on a Zeiss Axioskop reflected light microscope.

5 RESULTS AND DISCUSSION

5.1 Preparation and Characterization of Synthetic Enamels

A commercial coal tar enamel was used as the control material in all of the characterization and performance tests. Several synthetic enamels were produced by digestion of coal at 200°C. The formulations are summarized in Table 7 along with softening point temperatures.

Table 7. Synthetic coal-tar enamel formulations and softening point temperature.

	Component Concentration, wt%				
Sample ID	Coal	Coal Pitch	Oil	Talc	SP, °C
J025	20	31	33	15	87.0
J026	25	37	19	19	100.2
J028	18	27	41	14	83.6
J029	18	41	27	14	84.7
J030	25	19	37	19	107.2
J031	35	26	26	13	96.9
J032	18	27	28	27	58.7
J033	16	48	24	12	77.3
J034	0	40	40	20	Tacky
J036	44	22	22	11	113.7
J037	16	24	24	36	76.7
J038	31	46	0	23	135.1

The data in Table 7 indicate that the softening point temperature increased and the enamel became more brittle as the amount of coal was increased. When the amount of pitch was increased, a decrease of the softening point temperature resulted. As the amount of oil was increased, the softening point temperature decreased, and the enamel appeared to be less brittle.

A sample of the synthetic enamel was prepared for optical microscopy. Figure 11 compares the optical features of the commercial enamel with one of the synthetic enamels.

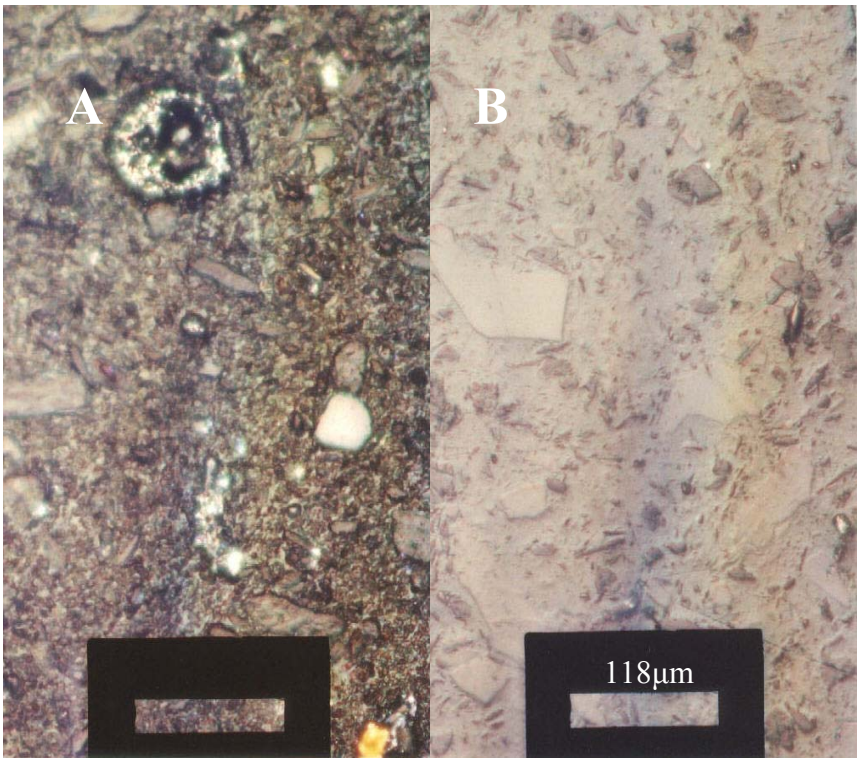

Figure 11. Optical photomicrographs of enamels: A, commercial coal tar enamel; B, synthetic enamel.

It was judged that the coal particles of the synthetic enamel were, for the most part, unchanged. The surface characteristics and particle shapes of the coal did not appear to be affected by digestion. This observation suggested the process temperature of 200°C was too low for the coal to be partially dissolved or digested. Thus the preparation temperature was raised to 300°C for two hours in order to digest the coal more fully, yet a low enough temperature to prevent complete thermal degradation of coal. All subsequent synthetic enamel formulations were prepared at the higher temperature.

Optical examination of these products confirmed that the morphology of the coal particles had been altered, becoming rounded and less distinct, as shown if Figure 12.

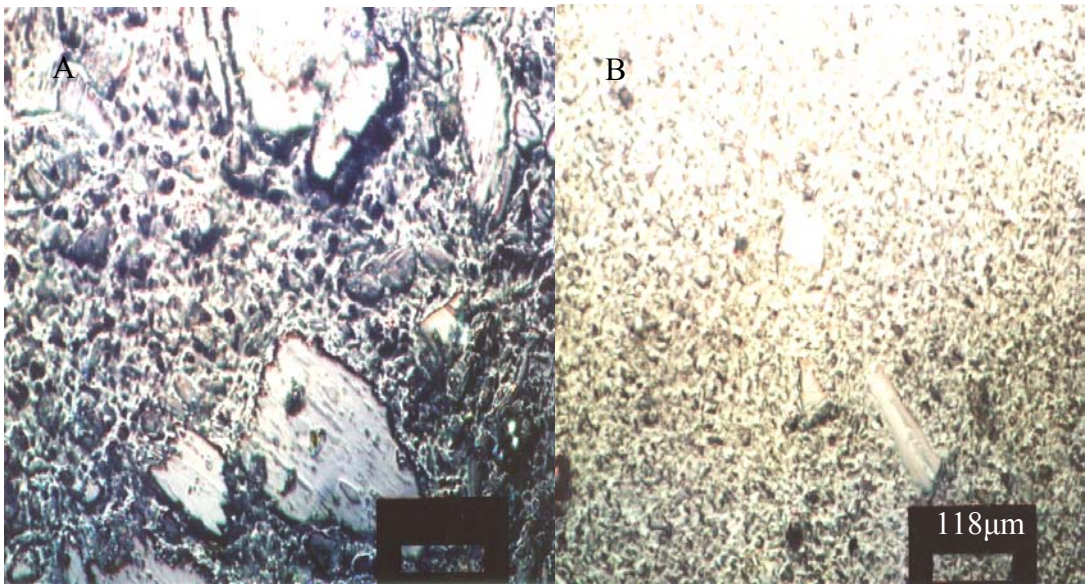

Figure 12. Photomicrographs of synthetic enamels: A at 200°C; B at 300°C

Table 8 shows the compositions of synthetic coal tar enamels that were prepared at 300°C. Figures 13 through 15 show the penetration behavior at 22, 46 and 55°C, respectively.

Table 8. Composition of synthetic enamels digested at 300°C.

	Component Concentration, wt%				
Sample ID	Coal	Coal Extract	Oil	Talc	SP, °C
J040	25	20	30	25	157.9
J041	25	15	35	25	138.1
J042	20	31	33	15	119.2
J044	20	10	42	28	126.0

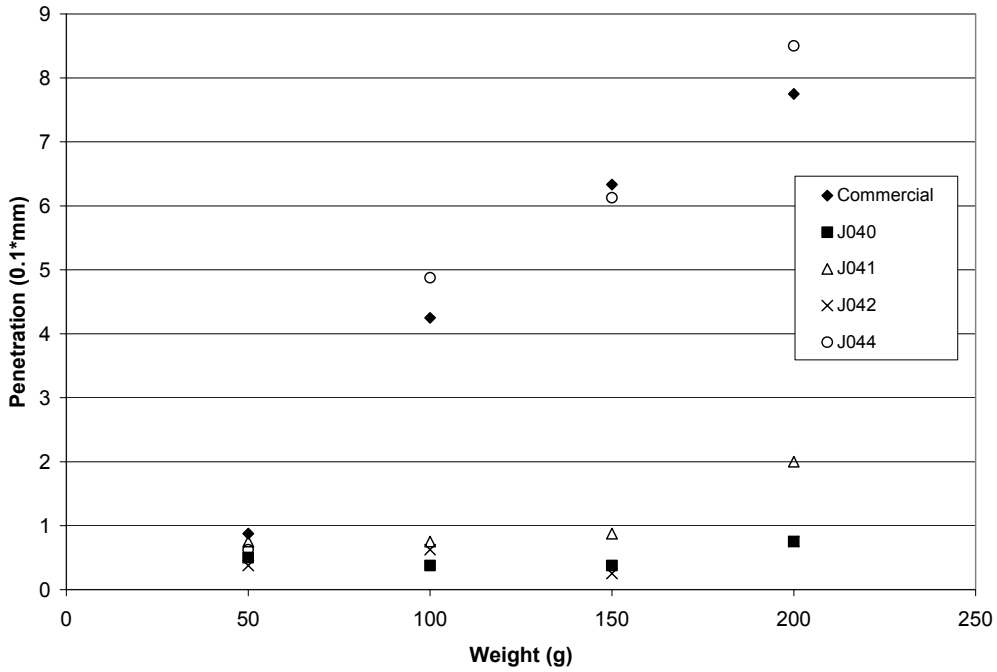

Figure 13. Penetration results at 22°C.

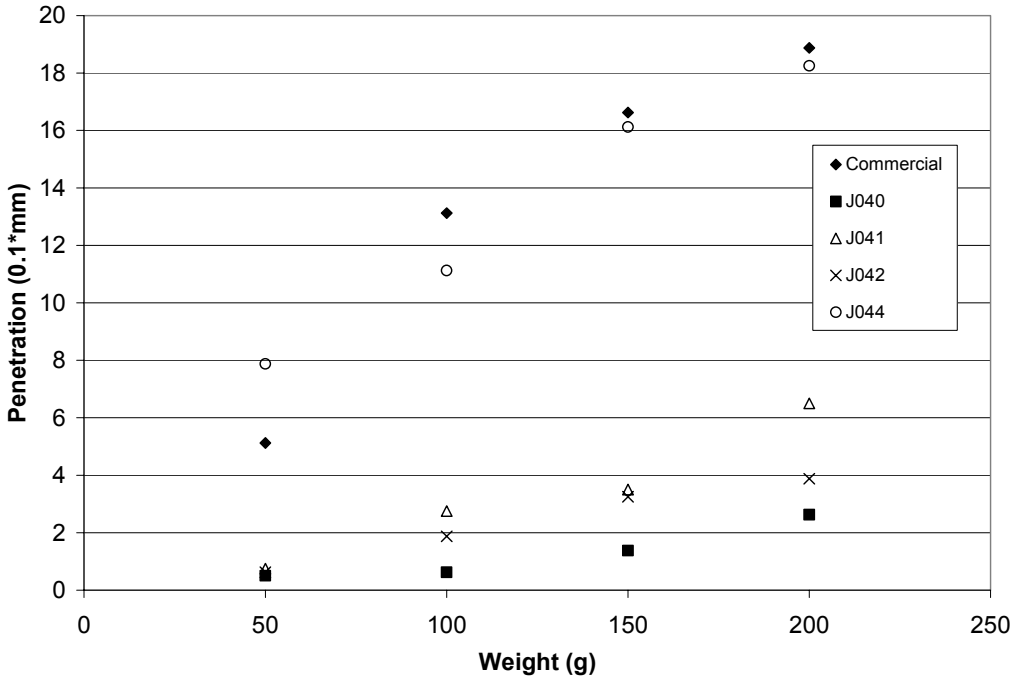

Figure 14. Penetration results at 46°C.

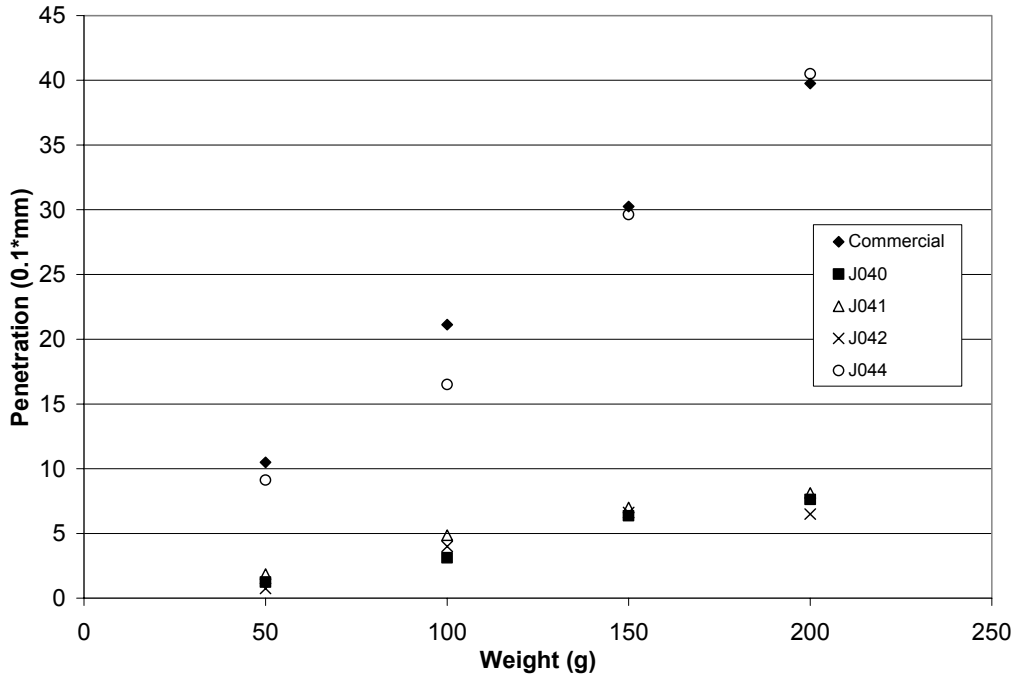

Figure 15. Penetration results at 55°C.

Formulations J040, J041, and J042 were relatively high in coal extract and low in heavy oil content. This combination produced synthetic enamels that were stiff and resistant to penetration when compared to the commercial material. Adjustments were made in the mix recipe (Table 8) to produce synthetic enamel J044. As can be seen, sample J044 behaved quite similarly to the commercial enamel in nearly all respects in terms of penetration.

Although the penetration performance of synthetic enamel J044 matches that of the commercial product very well, the volatile content of J044 was significantly higher, as shown in Figure 16. High volatility is undesirable because of safety concerns.

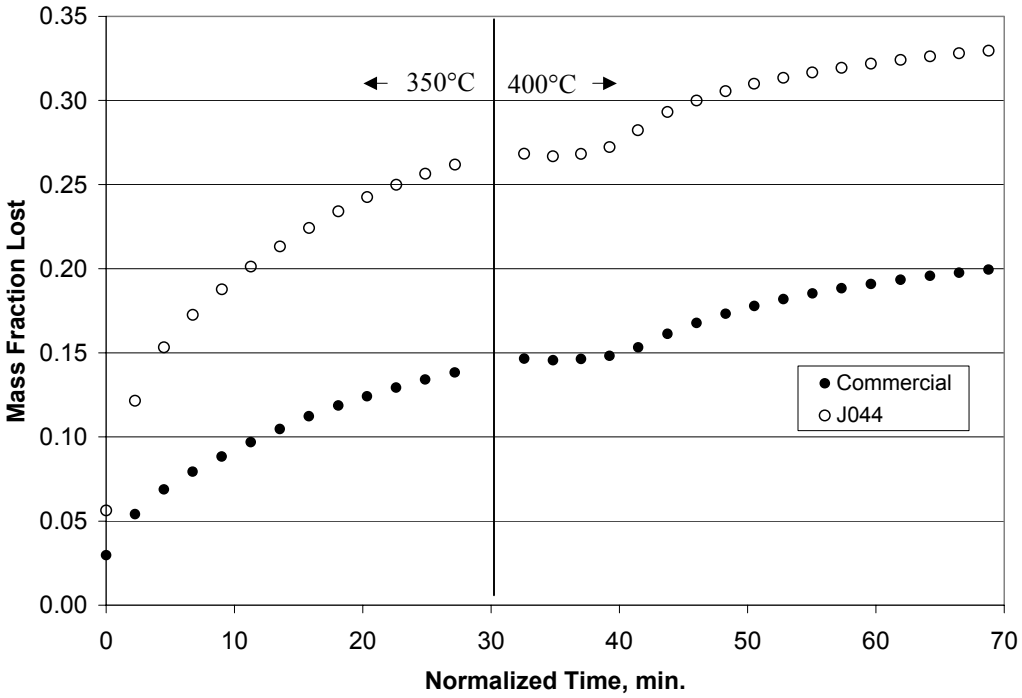

Figure 16. Volatility of sample J044 and commercial coal tar enamel.

It was concluded that the volatility of the synthetic enamel originated with the heavy oil. Thus, a couple of fomulations with similar composition were prepared with distilled heavy oil, as listed in Table 9, and digested at 300°C for 2 hours.

Table 9. Synthetic enamel formulations with distilled heavy oil.

	Component Concentration, wt%				
Sample ID	Coal	Coal Extract	Oil	Talc	SP, °C
*J044	20	10	42	28	126.0
J049	20	10	42	28	130.7
J056	20	10	42	28	126.7

* Prepared with undistilled heavy oil.

Although synthetic enamels J049 and J056 were prepared under similar conditions, the former exhibited penetration behavior more like the commercial enamel than the latter, as seen in Figures 17, 18, and 19. The reason is not known. Part of

reason might be attributed to the greater amount of volatile material in sample J046, as can be seen in Figure 20.

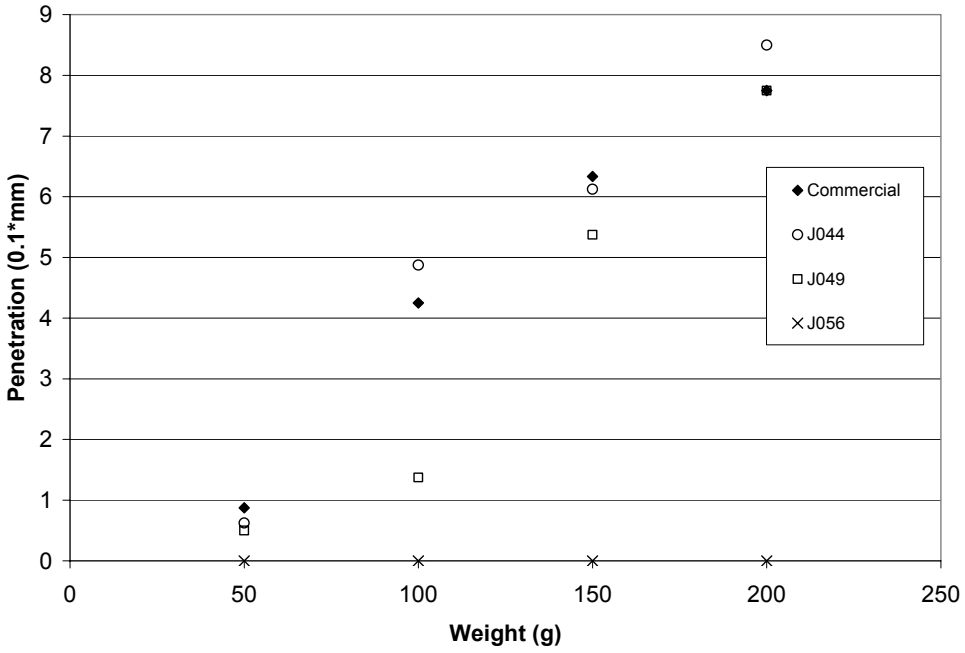

Figure 17. Penetration results at 22°C with formulations containing distilled heavy oil.

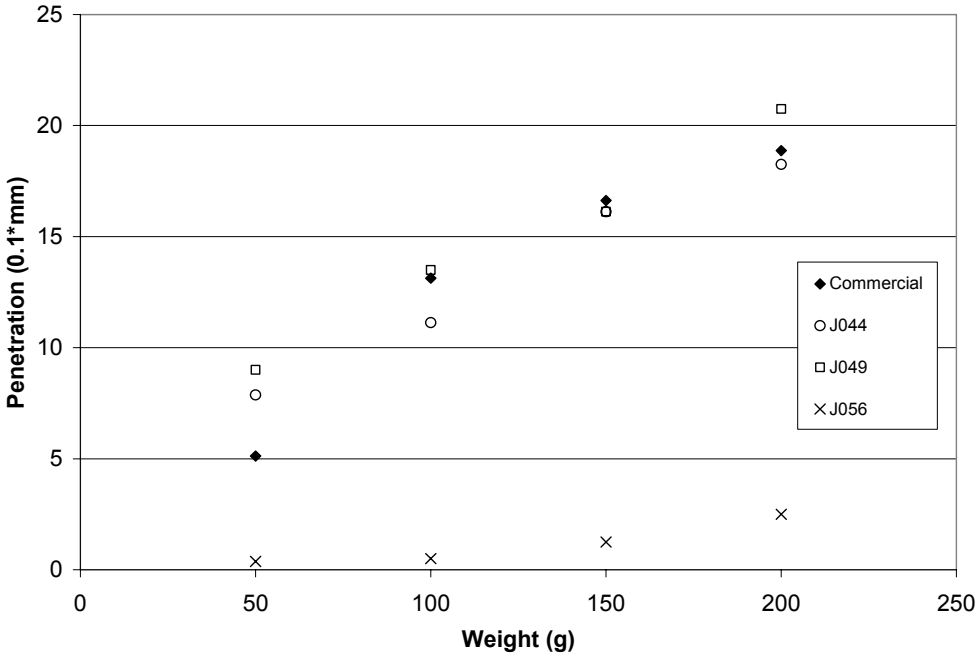

Figure 18. Penetration results at 46°C with formulations containing distilled heavy oil.

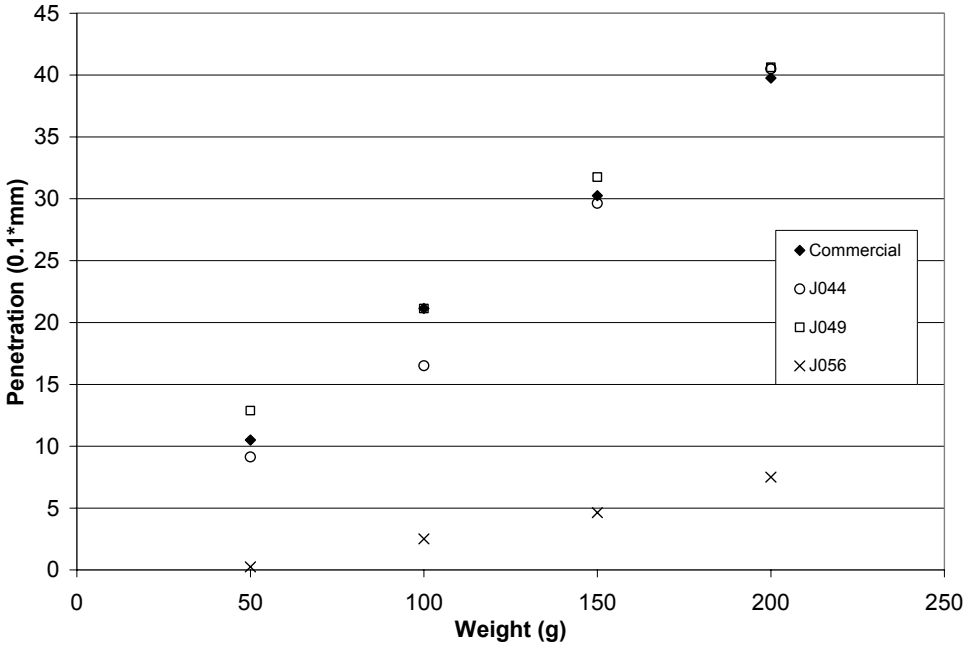

Figure 19. Penetration results at 55°C with formulations containing distilled heavy oil.

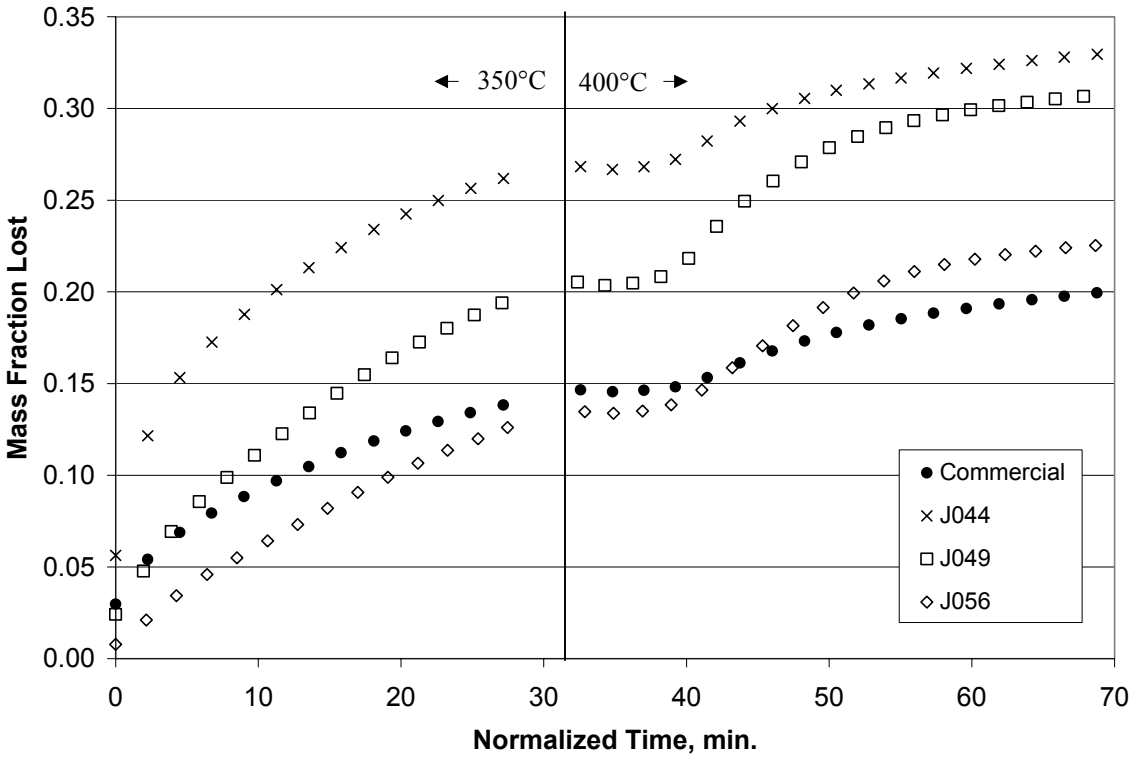

Figure 20. Volatility of samples prepared with distilled heavy oil.

Since the volatile content of J056 is less and J049 more than the volatile content of the commercial enamel, it was possible to make a blend of the two synthetic enamels in order to match the commercial product more closely. Thus, the synthetic enamels J049 and J056 were mixed in a 1:1 ratio at 200°C with the goal of making a blend that would match the commercial material in both penetration and volatility behavior. The blend is identified as sample J060. Penetration behavior of sample J060 (softening point 112.6°C) was less than the commercial enamel for all temperatures, as is evident in Figures 21, 22, and 23. Nonetheless, the volatile content of the blend was judged quite acceptable up to the test temperature of 350°C, as shown in Figure 24.

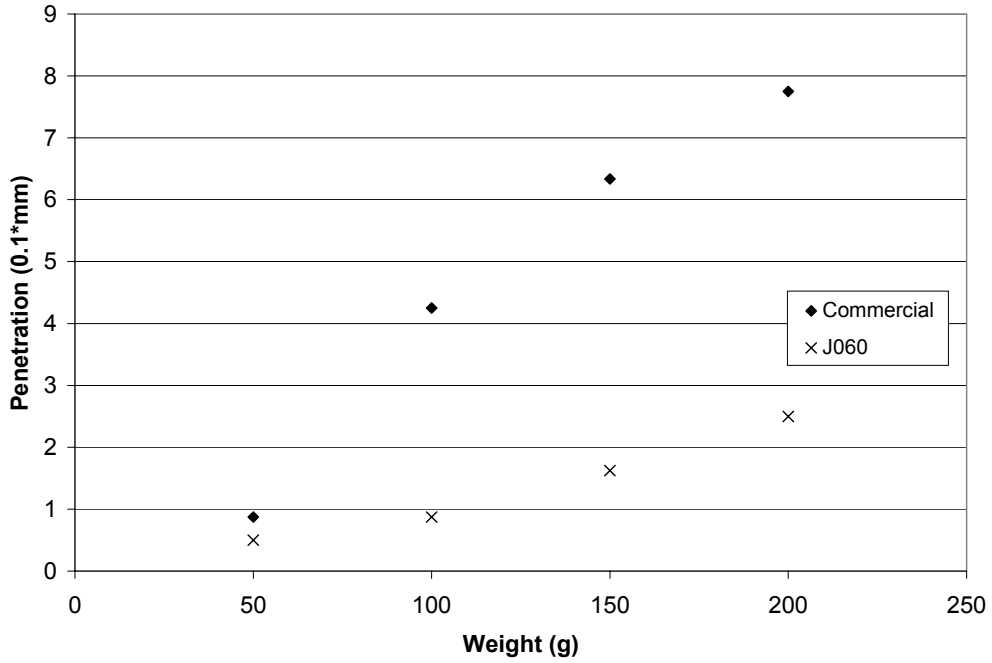

Figure 21. Penetration of synthetic enamel J060 at 22°C.

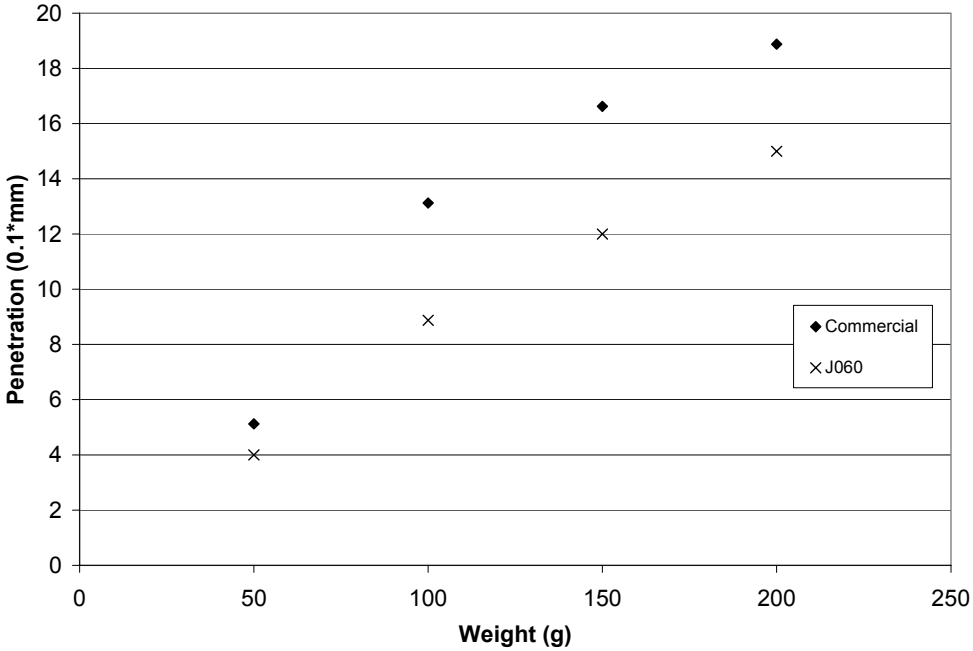

Figure 22. Penetration of synthetic enamel J060 at 46°C.

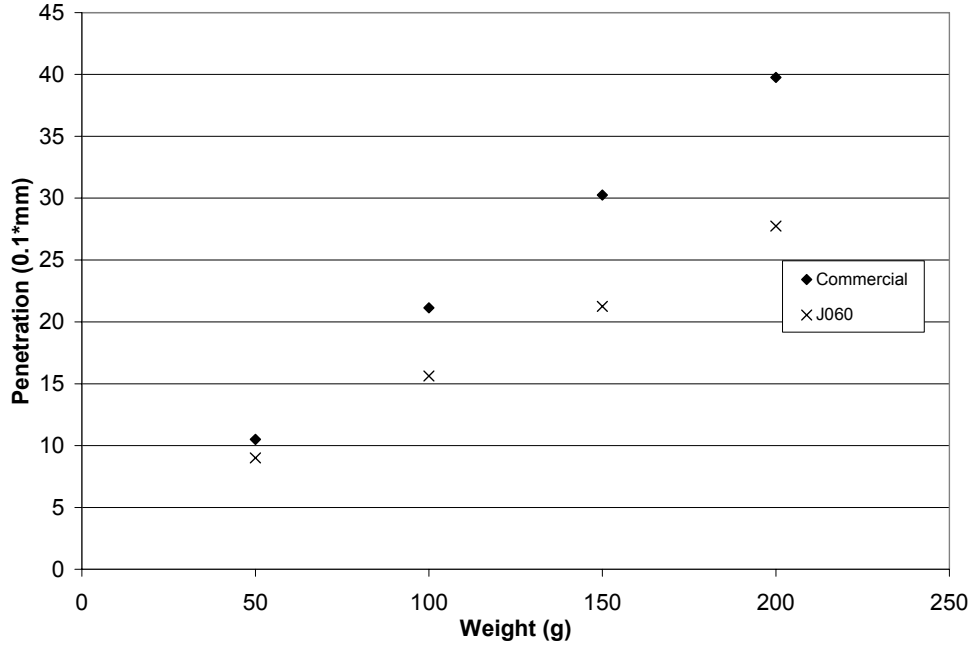

Figure 23. Penetration of synthetic enamel J060 at 55°C.

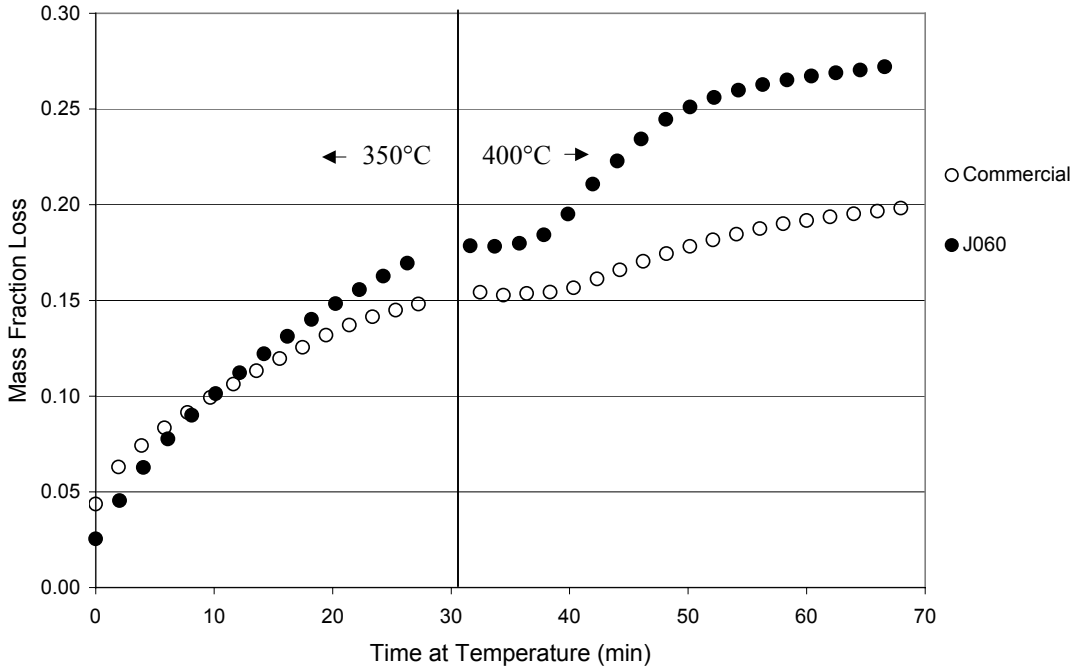

Figure 24. Volatility of sample J060 compared to commercial enamel.

In Figure 25 are shown the effects of temperature on the viscosity of sample J060 and the commercial enamel. The viscosity behavior of J066 is similar, except the synthetic pitch has a lower viscosity at the lower temperatures and somewhat higher viscosity at the higher temperatures compared with the commercial enamel control.

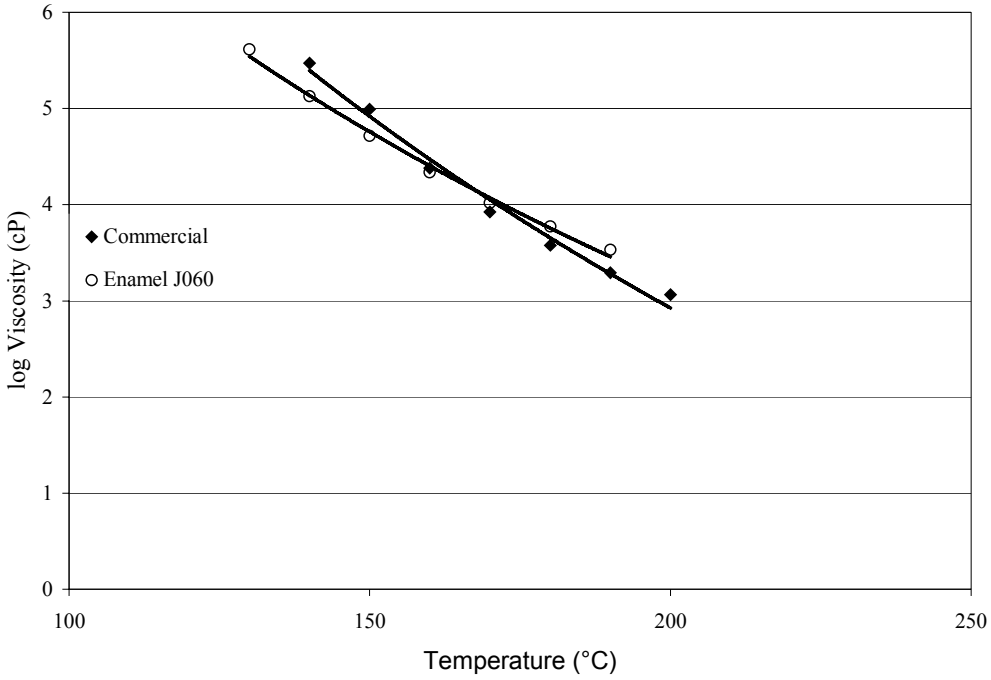

Figure 25. Effects of temperature on viscosity.

5.2 Testing of Synthetic Enamel J060 in Coating and Composite Applications

It was judged that synthetic enamel J060 was the best compromise attainable under the current research project. Consequently, synthetic enamel J060 was then used for the remaining tests related to coatings and composites.

5.2.1 Moisture Resistance

The enamel-coated carbon foam samples were prepared as described in section 4.6.1. After a week of immersion in water, neither the commercial nor the synthetic enamel-coated foam gained any weight. Thus both coated foams were able to resist water penetration under these conditions. The results of accelerated tests (conducted under pressure) are shown in Figure 26, where it can be seen that the synthetic enamel was more effective during the initial period of exposure to water under pressure.

However, both specimens behaved similarly after about an hour. The resistance of J060 during the initial period of the test might be related to its lower penetration numbers and volatile content.

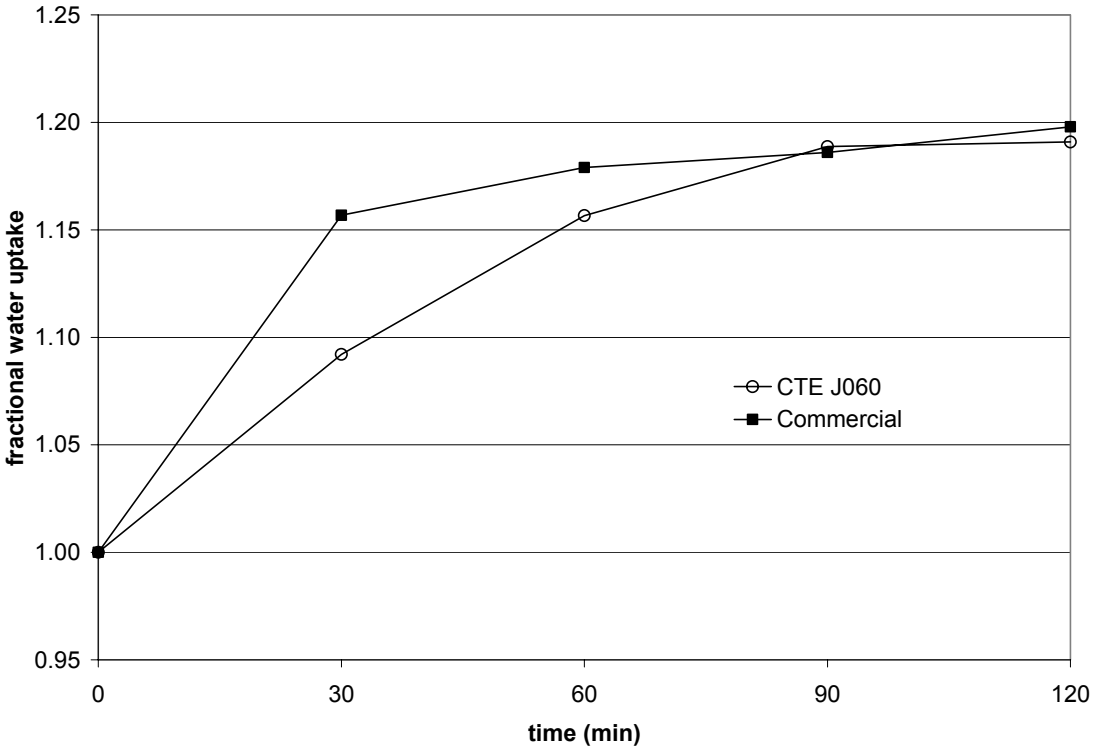

Figure 26. Water uptake of coated foam samples under pressure.

5.2.2 Identification of Organic Composition of Commercial and Synthetic Enamels.

The commercial enamel and synthetic enamel J060 were distilled as described in section 4.4. The condensed material was analyzed by gas chromatography/mass spectrometry, with the chromatographs shown in Figure 27. Both enamels were essentially comprised of the same volatile organic compounds, although the relative proportions were not the same. The synthetic enamel did not contain any measurable components that were not evident in the commercial enamel.

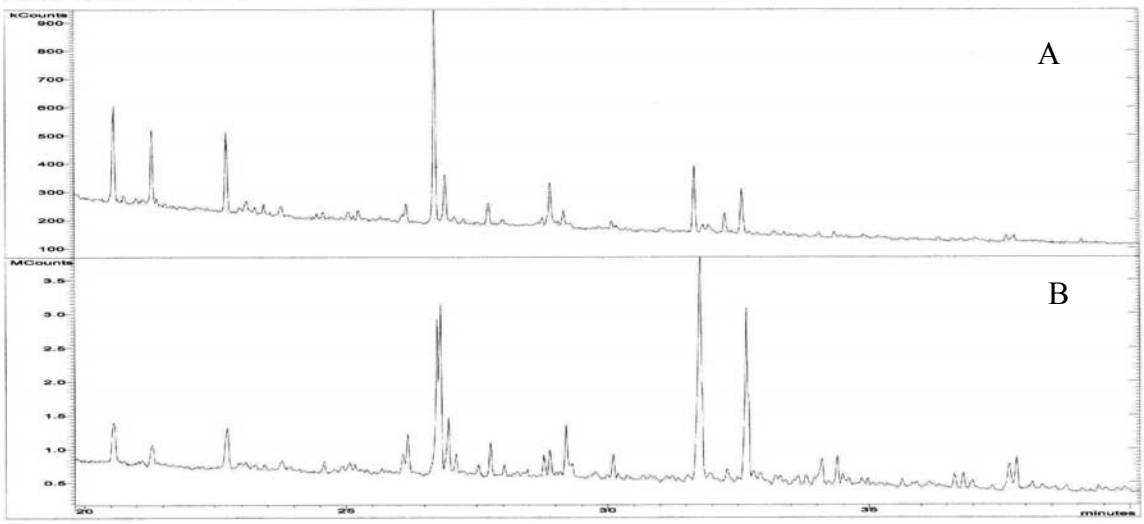

Figure 27. Gas chromatographs of enamel distillates: A, commercial enamel; B, synthetic enamel J060.

5.2.3 Results of Cathodic Protection

Visual inspection of the test coupons revealed no apparent disbonding of the coating from the surface of the metal. However, it was noticed that some "wicking" had occurred since there was a small amount of precipitated salts where the top portion where the enamel coating started. The coatings were removed carefully to reveal the nature of the metal surface underneath, as shown in Figure 28. The synthetic coating came off easily in single layers or pieces but the commercial enamel exhibited greater adhesion to the metal surface. The greater bonding of the commercial product was probably more effective in prohibiting corrosion than the synthetic material.

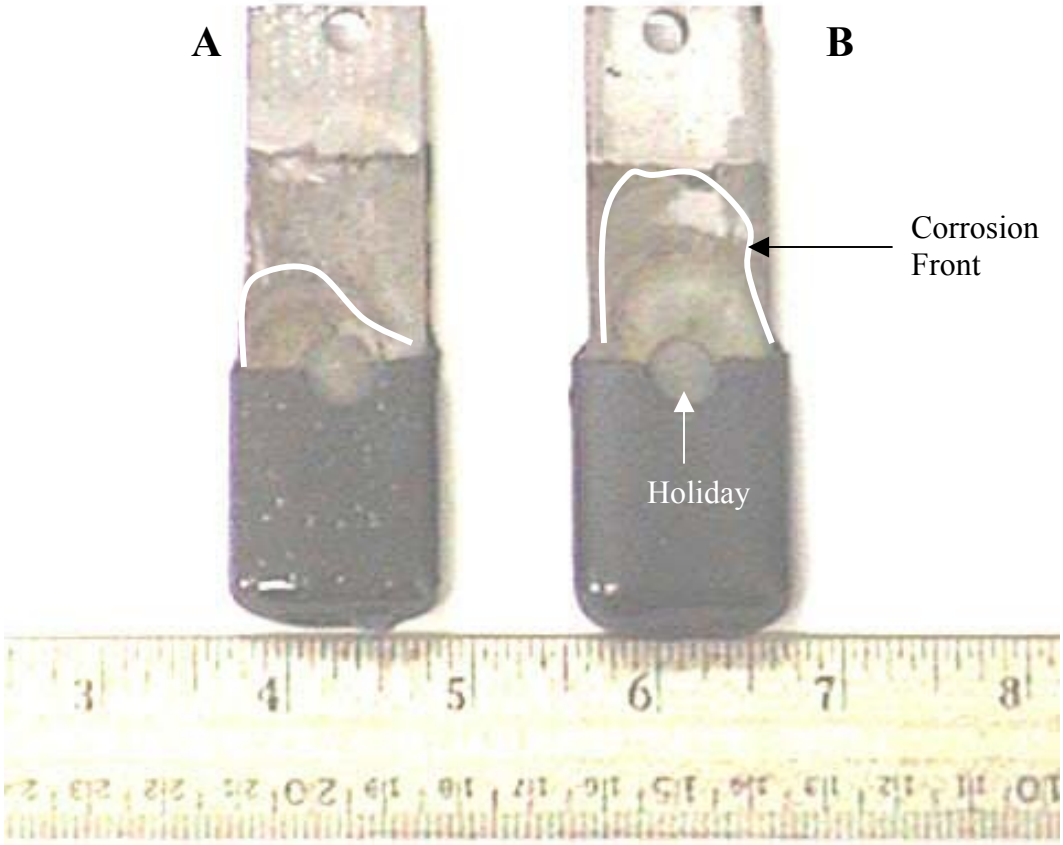

Figure 28. Comparison of cathodic disbonding between commercial enamel and J060: A, commercial enamel; B, synthetic enamel J060

5.2.4 Composite Testing and Evaluation

As discussed in Section 4.6.2, testing for all of the composite samples was performed on an Instron machine. The stress-strain curves shown in Figure 29 represent the result of the tensile test on the first composite type. The graph shows that the commercial enamel has a slightly higher tensile stress; however, the difference between the two is only about 100kPa. However, disbonding occurred at the enamel-metal surface and not at the enamel-foam surface. This is not surprising given the difference in surface area available to the enamel on the foam interface as opposed to the steel interface.

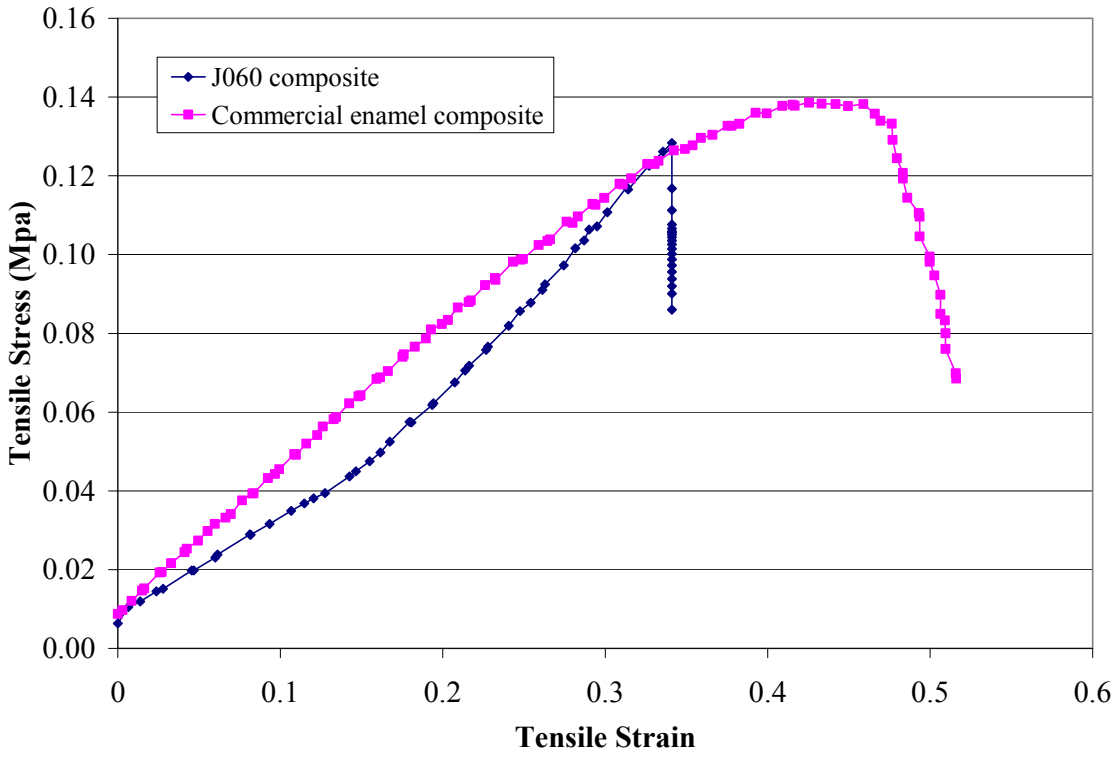

Figure 29. Stress-strain curve for tensile test

The results from the testing of the second composite type are shown in Figures 30 and 31. The most likely explanation for the low flexural stress of the composite in Figure 30 can be attributed to the relative weakness of the carbon foam when compared to steel. The carbon foam was simply crushed between the two pieces of sheet metal, whereas the steel physically bent. In essence, difference in the strength between the carbon foam composite and the steel plates turned the 3-point bend test into a distributed load test. However, Figure 31 shows that it did indeed take more force to get the same displacement out of the carbon foam composite than out of either the steel plates or the packing foam-steel tri-layer.

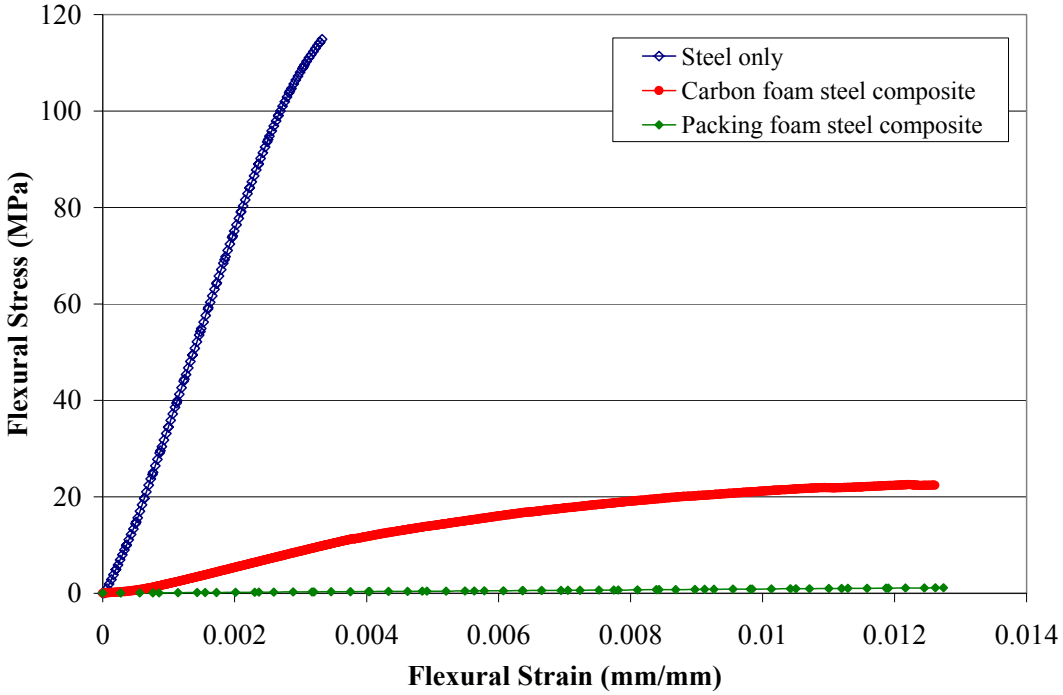

Figure 30. Flexural properties for foam-steel composite

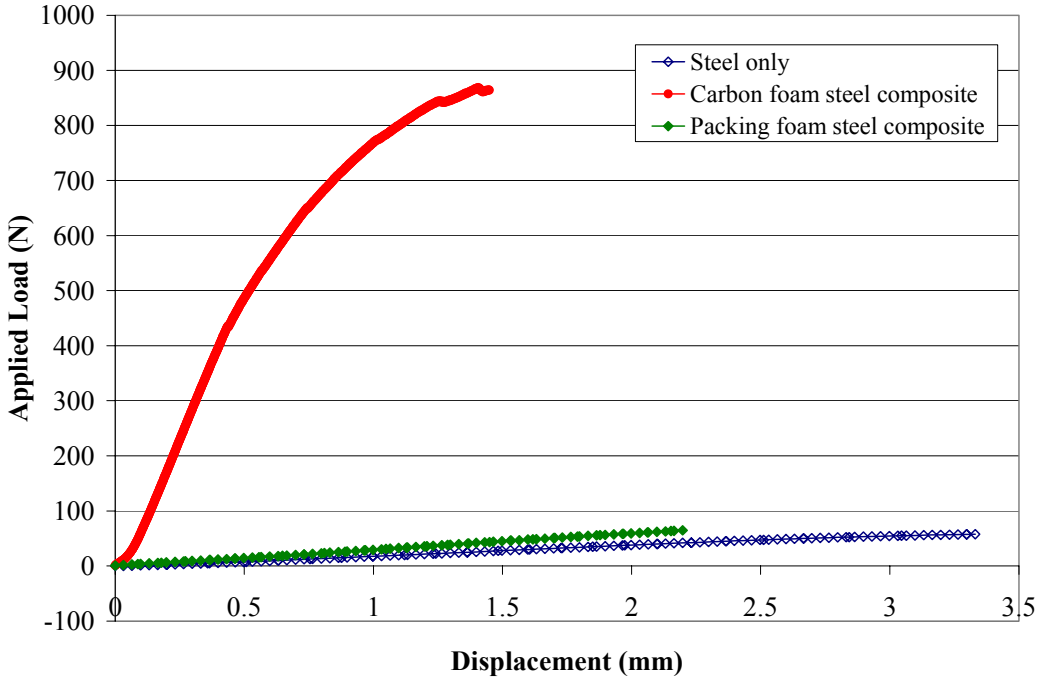

Figure 31. Loading diagram for three-point bending test

6 CONCLUSIONS

In the creation and production of synthetic coal tar enamel using solvent extraction, many interesting findings have been made. It is possible to produce coal tar enamel out of a solvent extracted pitch and commercial grade heavy oil. The results of that synthetic coal tar enamel produce properties that are within the specifications of commercial grade coal tar enamel, for the most part. The volatility of the synthetic is slightly higher than that of commercial enamel, but is not so much higher that it would not be usable. Penetration values, while lower than those of the commercial enamel available, were still within in range of standard, commercial grade enamel. Cathodic disbonding tests show that there are still improvements to be made to the synthetic coal tar enamel, but overall, given the difference in the timeframe used to develop commercial grade enamel and the timeframe used to develop synthetic enamel, the results are quite impressive. Also, it has been shown that enamel can be used as an adhesive for carbon foam-steel composites, and the bond strength to carbon foam is quite usable.

7 REFERENCES

[1] Whittier, F. "Pipeline Coatings" In: *Bituminous Materials: Asphalts, Tars, and Pitches*, Vol. III, Chap. 10, pg. 300, Hoiberg ed., John Wiley & Sons, Inc., New York (1966).
[2] Whittier, F. "Pipeline Coatings" In: *Bituminous Materials: Asphalts, Tars, and Pitches*, Vol. III, Chap. 10, pg. 301, Hoiberg ed., John Wiley & Sons, Inc., New York (1966).
[3]Donath, E. E. "Hydrogenation of Coal and Tar" In: *Chemistry of Utilization, Supplementary Volume*, H. H. Lowry ed., Chap. 22, National Academy of Sciences-National Research Council, John Wiley & Sons, Inc., New York (1963).
[4]Clarke, J. W., Kimber, G. M., Rantell, T. D., and Shipley, D. E. "Reactivity of British Coals in Solvent Extraction" In: *Coal Liquefaction Fundamentals*, ACS Symposium Series 139, Chap. 6, Whitehurst ed., American Chemical Society, Washington, D. C. (1980).
[5] Whittier, F. "Pipeline Coatings" In: *Bituminous Materials: Asphalts, Tars, and Pitches*, Vol. III, Chap. 10, pg. 302, Hoiberg ed., John Wiley & Sons, Inc., New York (1966).
[6] Whittier, F. "Pipeline Coatings" In: *Bituminous Materials: Asphalts, Tars, and Pitches*, Vol. III, Chap. 10, pg. 303, Hoiberg ed., John Wiley & Sons, Inc., New York (1966).
[7] Whittier, F. "Pipeline Coatings" In: *Bituminous Materials: Asphalts, Tars, and Pitches*, Vol. III, Chap. 10, pg. 296, Hoiberg ed., John Wiley & Sons, Inc., New York (1966).
[8] Stansberry et al., DOE/CPCPC final report *Development of an All-Coal Anode, 2003.*